Oregon State University
Climatic Research Institute

ANALYSIS OF THE SURFACE HEAT BALANCE OVER THE WORLD OCEAN

Steven K. Esbensen
Principal Investigator

FINAL TECHNICAL REPORT

NASA Grant NSG 5308
1 December 1978 - 30 September 1981

Submitted to

The National Aeronautics and Space Administration
Goddard Space Flight Center
Laboratory for Atmospheric Sciences

December 1981

TABLE OF CONTENTS

1. Summary of Major Research Findings

The goal of our research over the past three years has been to contribute to the development of a definitive global climatology of the surface heat balance over the world ocean using a combination of satellite and conventional observed data. After careful development and testing of a method for estimating climatological sensible and latent heat fluxes (Appendix A), we constructed an atlas of the components of the surface heat balance over the global ice-free oceans (Appendix B) which may be regarded as updating the work of Budyko (1963) and his colleagues. During the course of our research, we reached a number of conclusions about the role that satellite data may play in improving the estimates of heat balance components in the near future. Our heat balance results and recommendations for the use of satellite data are briefly summarized below.

1.1 *Estimates of Climatological Latent and Sensible Heat Fluxes*

In the paper by Esbensen and Reynolds (1981) we have demonstrated that is is possible to estimate long-term monthly mean latent and sensible heat fluxes over the ocean to within the $\lesssim$20% relative accuracy of the bulk aerodynamic formulas, by using observations of the monthly mean surface wind speed and the monthly mean sea-air temperature and humidity differences. Even more remarkable is that it appears to be possible to make a useful estimate of the fluxes on a month-to-month basis from monthly averaged surface data. Both of these findings have important implications for the use of satellite data (see Section 1.3).

1.2 *An Atlas of the Surface Heat Balance*

Using a climatology of surface marine meteorological observations prepared by the National Climatic Center and the cloudiness atlas of Berliand and Strokina (1980) we have produced an atlas of the components of the surface heat balance over the global ice-free oceans (Esbensen and Kushnir, 1981). The atlas includes maps of the monthly mean distributions of the calculated heat budget components and of the basic variables used in the calculation. All the fields have a uniform spatial resolution and are presented on a 4° x 5° grid. Although the resolution of our data set is coarse, we find good agreement between our atlas results and several recent regional studies. Our estimates have the advantages of being global in extent and achieving approximate annual heat balance over the global oceans.

The atlas has already been useful in the development and analysis of a coarse resolution global ocean model at the Climatic Research Institute and we expect that it will continue to be useful as the institute staff begins to explore coupled ocean-atmosphere models. The gridded data set is available to other investigators in a very portable format on magnetic tape.

1.3 *Recommendations for the Use of Satellite Data*

We believe that it is now possible to clearly define the role of satellite data in improving climatological estimates of the components of the surface heat balance and in monitoring their interannual variability. We recommend the following:

a) High priority should be given to monitoring the monthly mean of the magnitude of the surface wind stress using satellite data. We believe that our results show that this information can be used directly in bulk aerodynamic formulas to determine the monthly mean sensible and latent heat fluxes to well within a relative error of ∿20% wherever those fluxes are significant.

b) High priority should be given to developing and deploying a robust buoy-satellite instrument system which measures three quantities - surface air temperature and humidity, and the sea surface temperature. This is particularly important over regions of the global oceans where ships-of-opportunity provide inadequate coverage and the associated space-time sampling errors can approach 50% (Weare and Strub, 1981).

c) High priority should be given to obtaining the monthly averaged surface radiation balance over the global oceans by fully utilizing existing satellite data. We believe that climatological estimates can be obtained by combining existing radiative flux data from satellites with surface meteorological data from ships and buoys. In this context we suggest that cloudiness data be viewed more as a by-product of the analysis rather than a primary input variable to empirical radiation formulas. (See Appendix B for examples of this type of formula.) Of the three recommendations, we believe that this step would be the most likely to lead to a significant quantitative improvement in the estimates of the net downward heat flux into the oceans.

2. Summary of Research Activities

The research summarized here was performed in collaboration with Dr. R. W. Reynolds[1] and graduate students Messrs. Y. Kushnir and E. I. Tollerud. We have received good support from the staff of the computing facility at the OSU Climatic Research Institute (CRI) and excellent secretarial and clerical support through CRI and the Department of Atmospheric Sciences.

In addition to the research activities at CRI, the results of our work have been presented at several scientific meetings including the Symposium on Empirical and Model-Assisted Diagnosis of Climate and Climate Change, 1979, Tbilisi, U.S.S.R., the Third Conference on Ocean-Atmosphere Interaction, 1980, Los Angeles, CA, and the Workshop on the Application of Existing Satellite Data to the Study of Ocean Surface Energetics, 1980, Madison, WI. At the Madison workshop, the Principal Investigator co-chaired the Working Group on Wind Stress and Heat Fluxes.

3. Continuing Research

The heat balance computations obtained under this grant are being analyzed and extended as part of the Climatic Research Institute's ongoing study of the dynamics of seasonal climate change. By combining the values of evaporation implicit in the latent flux estimates from the heat balance atlas shown in Appendix B with the precipitation data of Jaeger (1976), we have obtained climatological estimates of evaporation minus precipitation over

---

[1]Present affiliation: Climatic Analysis Center, NMC, NWS, NOAA, Washington, D.C. 20233.

the global oceans for the twelve calendar months. These estimates have been very useful in the analysis of water vapor transport in the OSU Atmospheric General Circulation Model. We are also proposing to extend the surface heat balance computation to land and ice covered areas of the earth under a continuing grant from the National Science Foundation since budgetary constraints within NASA have forced the termination of this grant.

4. Publications of Grant NSG 5308

S. K. Esbensen and R. W. Reynolds, 1981: Estimating monthly averaged air-sea transfers of heat and momentum using the bulk aerodynamic method. *J. Phys. Oceanogr., 11,* 457-465. (See Appendix A.)

S. K. Esbensen and Y. Kushnir, 1981: The heat budget of the global ocean: an atlas based on estimates from surface marine observations. Report No. 29 Climatic Research Institute, Oregon State University, Corvallis, Oregon, 27 pp. and 188 charts (in press). (See Appendix B.)

References

Berliand, T. G., and L. A. Strokina, 1980: *Global Distribution of the Total Amount of Cloudiness.* Hydrometeorology Publishing House, Leningrad, 71 pp. (in Russian).

Budyko, M. I., Ed., 1963: *Atlas of the Heat Balance of the Earth.* Akad. Nauk, SSSR, Prezidum. Mezhduvedomstvennyi Geofiz. Komitet., 69 pp. [Also, *Guide to the Atlas of the Heat Balance of the Earth,* Transl. by I. A. Donehoo, U.S. Weather Bureau, WB/T-106, Washington, D.C.].

Esbensen, S. K., and Y. Kushnir, 1981: The heat budget of the global ocean: an atlas based on estimates from surface marine observations. Report No. 29, Climatic Research Institute, Oregon State University, Corvallis (in press). (See Appendix B.)

Esbensen, S. K., and R. W. Reynolds, 1981: Estimating monthly averaged air-sea transfers of heat and momentum using the bulk aerodynamic method. *J. Phys. Oceanogr., 11,* 457-465. (See Appendix A.)

Weare, B. C., and P. T. Strub, 1981: The significance of sampling biases on calculated monthly mean oceanic surface heat fluxes. *Tellus, 33,* 211-224.

APPENDIX A

Estimating Monthly Averaged Sea-Air Transfers of Heat and Momentum Using the Bulk Aerodynamic Method

S. K. Esbensen and R. W. Reynolds

Reprinted from JOURNAL OF PHYSICAL OCEANOGRAPHY, Vol. 11, No. 4, April 1981
American Meteorological Society
Printed in U. S. A.

Estimating Monthly Averaged Air-Sea Transfers of Heat and Momentum Using the Bulk Aerodynamic Method

STEVEN K. ESBENSEN AND RICHARD W. REYNOLDS[1]

Climatic Research Institute, Oregon State University, Corvallis, OR 97331

(Manuscript received 15 August 1980, in final form 26 January 1981)

ABSTRACT

Air-sea transfers of sensible heat, latent heat and momentum are computed from 25 years of middle-latitude and subtropical ocean weather ship data in the North Atlantic and North Pacific using the bulk aerodynamic method. The results show that monthly averaged wind speeds, temperatures and humidities can be used to estimate the monthly averaged sensible and latent heat fluxes from the bulk aerodynamic equations to within a relative error of ~10%. The estimates of monthly averaged wind stress under the assumption of neutral stability are shown to be within ~5% of the monthly averaged non-neutral values.

1. Introduction

Estimates of the transfers of sensible heat, latent heat and momentum between the atmosphere and the oceans may provide important insight into the dynamics of interannual and decadal climate fluctuations. Sensible and latent fluxes combine with radiative fluxes to determine the major part of the net air-sea exchange. Momentum transfers play an important role in driving the ocean general circulation and particularly in determining the vertical structure of the upper ocean.

The first systematic evaluation of the sensible and latent heat transfers over the world ocean was performed by Budyko (1963). He computed long-term monthly mean values of the near-surface wind speed and of the air-sea temperature and humidity differences, and evaluated the fluxes by the well-known bulk aerodynamic formulas with constant transfer coefficients (see Section 2).

Budyko's method depends on the validity of the following two conditions:

1) The covariance of the wind speed with either the air-sea temperature difference or the air-sea humidity difference must be less than the product of their respective mean values (except for cases in which the fluxes are small). This condition was found to be satisfied in several important climatic regions of the world oceans for limited time periods by Malkus (1962), Budyko and Gandin (1966), Kraus and Morrison (1966) and Fissel *et al.* (1977).

2) The transfer coefficients for sensible heat and evaporation must not be strongly dependent on either wind speed or air-sea temperature and humidity differences for typical conditions over the oceans. Budyko (1974) concludes that the stability of the surface boundary layer, as parameterized by the bulk Richardson number, is almost neutral except in weak wind conditions. As we will show in subsequent sections, computations using recent developments in surface boundary-layer theory support Budyko's conclusion.

The first systematic evaluation of air-sea momentum transfers on a global basis was presented by Hellerman (1967). His computations were based on the bulk aerodynamic formulas with a drag coefficient for neutral surface boundary-layer conditions and wind data consisting of monthly-averaged wind roses with both wind direction and speed categories. The use of only one mean wind speed in each direction category of a monthly averaged wind rose leads to underestimates of the computed monthly averaged wind stress by 10–30% (see Hellerman, 1965).

Recently there has been considerable interest in updating the classical estimates of Budyko (1963) and Hellerman (1967). An excellent example of this type of work is Bunker's (1976) estimates of the surface heat balance over the Atlantic Ocean. The approach used by Bunker differs from the classical approach since he computed the turbulent fluxes for each simultaneous measurement of surface meteorological variables. The computed fluxes within a given month are then summed, and finally are divided by the total number of observations. While data processing technology has made Bunker's approach

[1] Present affiliation: Climatic Analysis Center, NMC, NWS, NOAA, Washington, DC, 20233.

0022-3670/81/040457-09$06.25

feasible, more than 30 million ship reports would have to be processed at the present time to obtain global estimates of the turbulent heat and momentum transports. The classical method clearly has a number of practical advantages which will be discussed further in our final section.

The main purpose of this paper is to provide a basis for determining to what extent the classical method of estimating turbulent fluxes of sensible and latent heat from monthly averaged surface meteorological variables can be used for studies of interannual and decadal climatic variability. A unique feature of our study is the systematic exploration of the effects of boundary-layer stability and of the physics of the air-sea interface on the estimates of the sensible and latent heat fluxes using recent developments in boundary-layer theory. We also will discuss the importance of stability effects for the estimates of air-sea momentum transfers. Computations will be based on data taken from ocean weather ships in the North Pacific and North Atlantic Oceans since these data are the best available long-term records of surface marine meteorological variables. In the final section, we will discuss the implications of our results for studies of climatic variability.

2. The bulk aerodynamic calculations

The well-known bulk aerodynamic formulas for the sensible heat flux H and the latent heat flux LE at the air-sea interface are

$$H = \rho c_p C_H V_a (T_s - T_a), \tag{1}$$

$$LE = \rho L C_E V_a (q_s - q_a), \tag{2}$$

where the variables V_a, T_a and q_a are the wind speed, temperature, and specific humidity of the air at a given height (z_a) which is within the surface boundary layer. The variables T_s and q_s are the sea surface temperature and the saturation specific humidity of air with temperature T_s and sea-level pressure p_s.[2] In this study we have used $z_a = 10$ m and approximated the potential temperature difference $(\theta_s - \theta_a)$ by $(T_s - T_a)$. The variable ρ is the average air density in the layer from the surface to z_a, c_p is the specific heat of air at constant pressure, and L is the latent heat of evaporation of water. The quantities C_H and C_E are the so-called transfer coefficients for sensible heat and evaporation, respectively.

To estimate the fluxes from Eqs. (1) and (2), the transfer coefficients must be determined. Although these coefficients may be determined in a completely empirical manner using regression analysis, boundary-layer similarity theory provides a rational, physically motivated way to minimize the dependence of C_H and C_E on empiricism. In particular, similarity theory allows the inclusion of the effects of the stability of the atmospheric surface boundary layer, the measure of stability being the Monin-Obukhov length L which is defined as

$$L = -\frac{(\tau/\rho)^{3/2}}{g\bar{T}_v^{-1}\overline{w'T_v'}}, \tag{3}$$

where τ is the magnitude of the surface wind stress (see Section 7), T_v is the virtual temperature, and g is the gravitational acceleration. Here the overbar indicates the Reynolds averaging of the product $w'T_v'$, where w is the vertical air velocity. Similarity theory also allows the effects of the roughness of the sea surface to be parameterized by a roughness length z_0.

We have chosen to evaluate the transfer coefficients using the method proposed by Liu *et al.* (1979) with the exception that we have neglected the difference between the "observed" sea surface temperature and the skin temperature of the water at the air-sea interface. The effects of boundary layer stability are included using the Businger-Dyer model (see Businger *et al.*, 1971, Dyer and Hicks, 1970). Also, the Liu *et al.* model determines the roughness length z_0 and the corresponding lengths for the profiles of temperature and specific humidity, z_T and z_q; the lengths are not assumed to be equal. There is no free convection limit for unstable conditions as considered by Deardorff (1972); however, calm conditions with large unstable air-sea temperature and humidity differences are rare over the oceans.

The dependence of C_H on wind speed and air-sea temperature differences computed by the Liu *et al.* method are shown in Fig. 1 for a relative humidity of 70%. For any given wind speed and temperature difference, C_H and C_E differ by less than 10% (see Liu *et al.*). However, at wind speeds < 10 m s^{-1} both C_H and C_E are strongly dependent on both wind speed and air-sea temperature differences. At wind speeds > 10 m s^{-1}, the stability of the boundary layer has very little effect on the transfer coefficients and the dependence on wind speed is weak.

The transfer coefficients proposed by Liu *et al.* (1979) agree well with those of Kondo (1975), and give a reasonable fit to the currently available data from the surface boundary layers of the ocean and atmosphere. As we will show in Sections 4 and 5, the conclusions of this study do not depend crucially on the choice of transfer coefficients. Although this may seem paradoxical to the reader given the importance of the transfer coefficients in obtaining reliable estimates of the fluxes, this study is concerned with the *methodology* of estimating monthly averaged and long-term climatological fluxes from the bulk aerodynamic equations. We believe our

[2] The variables V_a, T_s, T_a, q_s and q_a are all assumed to be averages over a time-scale at least as long as the lifetime of boundary-layer convective elements.

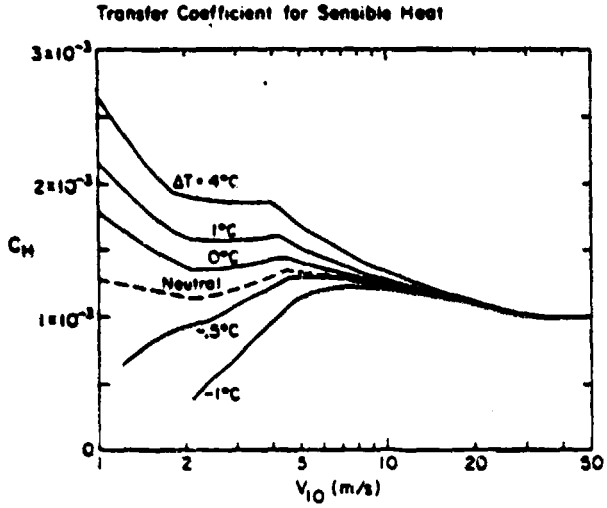

FIG. 1. The transfer coefficient for sensible heat from Liu *et al.* (1979) as a function of wind speed at 10 m above the sea surface for various air-sea temperature differences ($\Delta T = T_s - T_a$). The neutral surface boundary layer curve is also indicated. All curves assume a boundary-layer relative humidity of 70%.

conclusions concerning the method for obtaining flux estimates are valid for any physically reasonable choice of transfer coefficients.

3. Two estimation methods for monthly averaged heat fluxes

In this section we distinguish between the *sampling method* and the *classical method* for computing monthly averaged transfers of sensible and latent heat at the sea surface from the bulk aerodynamic equations. In the sampling method, fluxes are estimated from the sample means of H and LE in Eqs. (1) and (2) for a given calendar month and geographic area. These sample means are defined as

$$\bar{H} = \rho c_p \overline{C_H V_a (T_s - T_a)}, \tag{4}$$

$$\overline{LE} = \rho L \overline{C_E V_a (q_s - q_a)}, \tag{5}$$

where the averaging operation defined by the overbar is

$$(\bar{\ }) = N^{-1} \sum_{n=1}^{N} (\bar{\ })_n, \tag{6}$$

and N is the number of simultaneous measurements of T_a, q_a, T_s and V_a. It should be noted that ρ, c_p and L are not included in the averaging operation since these variations either play a negligible role in the surface flux estimates or can be incorporated using linear combinations of $\bar{H}$ and $\overline{LE}$ (e.g., Brook, 1978).

The classical method (see Budyko, 1963) uses the expressions

$$\hat{H} = \rho c_p \hat{C}_H \hat{V}_a (\hat{T}_s - \hat{T}_a), \tag{7}$$

$$\widehat{LE} = \rho L \hat{C}_E \hat{V}_a (\hat{q}_s - \hat{q}_a), \tag{8}$$

where $\hat{C}_H$ and $\hat{C}_E$ are obtained by substituting the sample means of T_a, T_s, q_a, q_s and V_a into the algorithm for C_H and C_E.

If measurements of surface meteorological variables are always simultaneous and dense in space and time, and if the resources for data processing are adequate, the sampling method provides the best estimate of the monthly averaged flux. However, for non-simultaneous and sparse data sets, the classical method may have both practical and theoretical advantages as discussed in Section 8.

4. Data

To quantitatively test the differences between the two methods, we have analyzed three-hourly marine meteorological observations from nine ocean weather ships. The study was limited to the 25-year period from 1948 to 1972 and the ships were selected to give good geographical coverage. Table 1 shows the ship positions and periods for which observations were available. The position of each ship also is shown in Fig. 2 with the ocean surface current regions from Sverdrup *et al.* (1942). As can be seen, the ships have sampled both eastern and western middle-latitude oceanic regions including the strong western boundary currents of the Kuroshio and Gulf Stream. Six of the ships have nearly continuous records for the entire 25-year period.

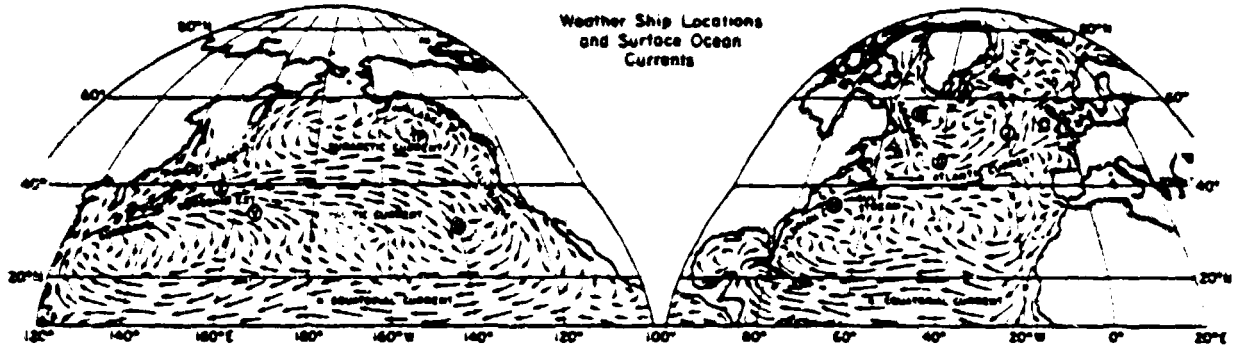

FIG. 2. Positions of ocean weather ships used in this study superimposed on ocean surface currents from Sverdrup *et al.* (1942).

TABLE 1. Ocean weather ship station data studied.

Station	Latitude	Longitude	Period studied
A	62°N	33°W	1942–71
B	56½°N	51°W	1948–72
D	44°N	41°W	1950–72
H	36°N	70°W	1950–54
J	52½°N	20°W	1951–71
N	30°N	140°W	1948–72
P	50°N	145°W	1950–72
V	34°N	164°E	1956–71
X	39°N	153°E	1948–53

We processed the data to eliminate any observations that were obviously in error or in which the weather ship was not within 1° of the position given in Table 1. We also eliminated data when simultaneous observations of wind speed, wind direction, sea level pressure, and air, sea and dew-point temperature were not available.

5. Long-term climatological estimates

In this section we see how closely the classical method approximates the sample mean of flux estimates from temporally dense observations taken within a given calendar month for a period of 10 to 20 years. The principal result is shown in Fig. 3 for January and July. The classical method agrees with the method of sample means to within a few percent in both summer and winter and in all climatological regimes of the subtropical and middle-latitude oceans which we have investigated. The only exceptions to this conclusion occur when the fluxes are small. However, when the fluxes are small, percentage comparisons are meaningless and Fig. 3 shows the agreement to be within a few Watts per square meter. From results not shown here, we reached the same conclusions using only nighttime observations. Thus, diurnal effects, whether they are real or instrumental do not lead to significant differences between the classical method estimates and the sampling method estimates.

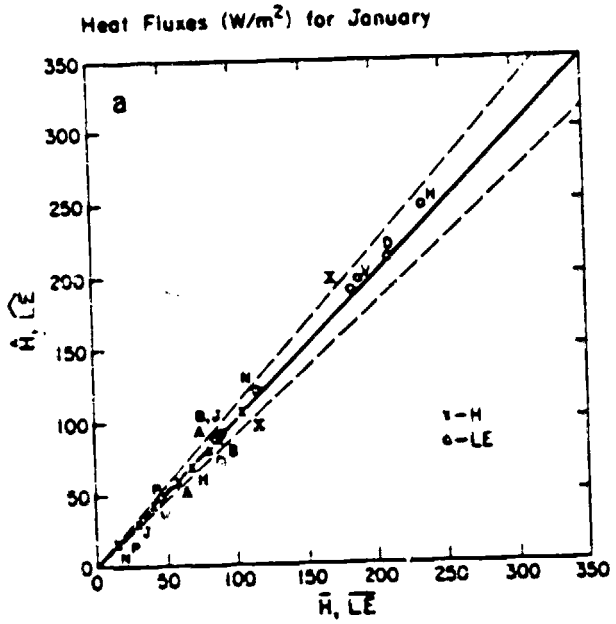

FIG. 3a. Climatological sensible and latent heat flux estimates for January for each ship computed by the sampling method (abscissa) and the classical method (ordinate). The dashed lines indicate relative errors of 10%. See text for details.

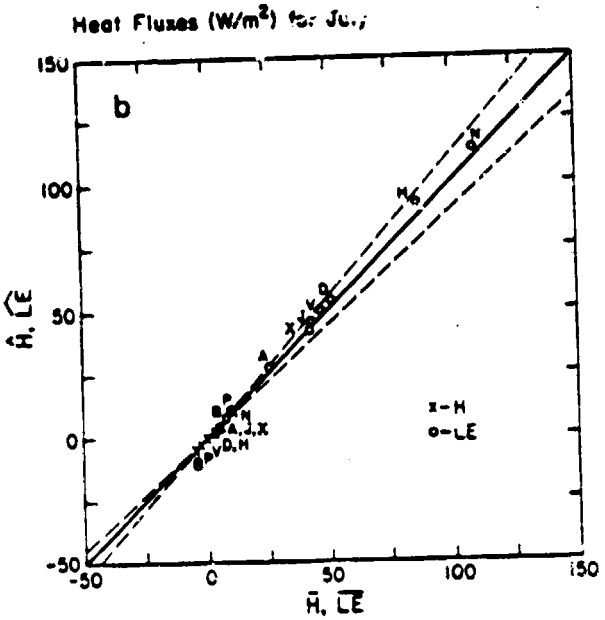

FIG. 3b. As in Fig. 3a except for July.

The authors believe the above conclusions are not likely to be changed by any physically reasonable choice of transfer coefficients. To demonstrate this point, the fluxes shown in Fig. 3 were recomputed with the assumption that sensible heat, water vapor and momentum are exchanged between the ocean and the atmosphere in the same manner. [Thus, in the Liu *et al.* (1979) algorithm, $z_T = z_q = z_0$.] As shown in Fig. 4, the transfer coefficient for sensible heat using this unrealistic assumption has an extreme dependence on wind speed. The curves for C_E are similar. The heat fluxes for January with this assumption are shown in Fig. 5. Again, the discrepancies between the classical method and the sample mean are only a few percent for the latent heat fluxes and about 10% or less for the sensible heat fluxes. This result implies that the difference between Budyko's (1963) flux estimates and Bunker's (1976) estimates for the Atlantic Ocean are due primarily to data availability, data reliability, and the use of different transfer coefficients. The differences are *not* due to the fact that Budyko chose the classical method and Bunker chose the sampling method.

A formal explanation for the agreement between

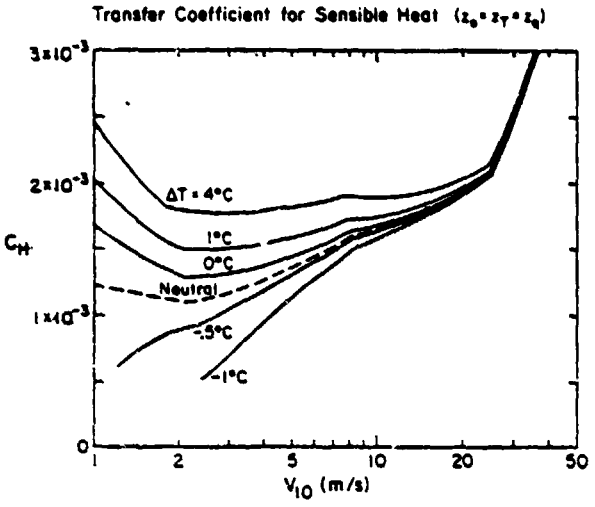

FIG. 4. Transfer coefficients from Liu *et al.* (1979) for which $z_0 = z_T = z_q$ (see also Fig. 1).

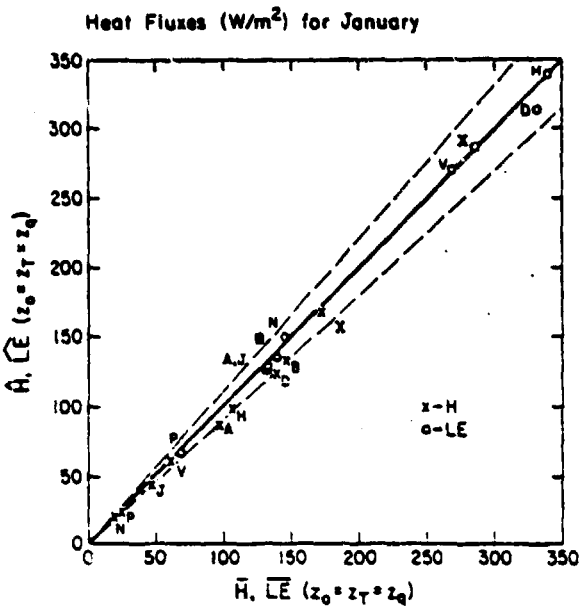

FIG. 5. Climatological sensible and latent heat fluxes as in Fig. 3a but computed with transfer coefficients for which $z_0 = z_T = z_q$.

the two methods of estimating the fluxes is obtained from an inspection of Table 2. First, as discussed in previous studies with constant transfer coefficients, the contribution of the $\overline{V_a'\Delta T'}$ and $\overline{V_a'\Delta q'}$ terms to the total flux is more than order of magnitude less than the contribution of the $\overline{V_a}\Delta\overline{T}$ and $\overline{V_a}\Delta\overline{q}$ terms except when the total fluxes are small. Second, the dependence of the transfer coefficients on the wind speed and air-sea temperature and humidity differences is small enough so that the remaining Reynolds-averaged terms involving C_H' and C_E' also are more than an order of magnitude less than the total fluxes. (Although not shown here, results from computations of the fluxes with $z_0 = z_T = z_q$ lead to similar conclusions.)

Finally, we consider the importance of including boundary-layer stability effects on long-term climatological estimates of the sensible and latent heat fluxes. The heat fluxes with the neutral transfer coefficients from Fig. 2 were recomputed using the sampling method, and Fig. 6 shows a comparison of these results with the stability-corrected sampling method results. The figure shows differences of ~10%. This result supports Budyko's (1974) conclusion which was reached using a bulk Richardson number as the stability parameter for the boundary layer.

TABLE 2. Terms in the Reynolds-averaged bulk aerodynamic equations for boundary-layer temperature and moisture fluxes at representative ship locations. The transfer coefficients of Liu *et al.* have been used.

	$\overline{C_H V_a \Delta T}$	=	$\overline{C_H}\,\overline{V_a}\,\Delta\overline{T}$	+	$\overline{C_H V_a' \Delta T'}$	+	$\overline{V_a C_H' \Delta T'}$	+	$\Delta\overline{T}\,\overline{C_H' V_a'}$	+	$\overline{C_H' V_a' \Delta T'}$
Temperature flux (10^{-2} m s^{-1} K)											
Ship D											
Jan	66.12		62.86		2.50		5.28		−3.35		−1.17
Jul	2.45		1.88		−1.03		2.44		0.01		−0.85
Ship N											
Jan	12.00		10.81		−0.56		2.40		−0.28		−0.37
Jul	8.37		6.50		0.45		1.52		0.05		−0.16
	$\overline{C_E V_a \Delta q}$	=	$\overline{C_E}\,\overline{V_a}\,\Delta\overline{q}$	+	$\overline{C_E V_a' \Delta q'}$	+	$\overline{V_a C_E' \Delta q'}$	+	$\Delta\overline{q}\,\overline{C_E' V_a'}$	+	$\overline{C_E' V_a' \Delta q'}$
Moisture flux (10^{-4} m s^{-1} g g^{-1})											
Ship D											
Jan	68.0		70.7		−0.1		1.9		−3.7		−0.8
Jul	16.4		16.5		−1.9		2.6		−0.0		−0.8
Ship N											
Jan	37.6		39.1		−1.4		1.2		−1.1		−0.2
Jul	35.3		35.2		−0.0		0.2		−0.1		−0.0

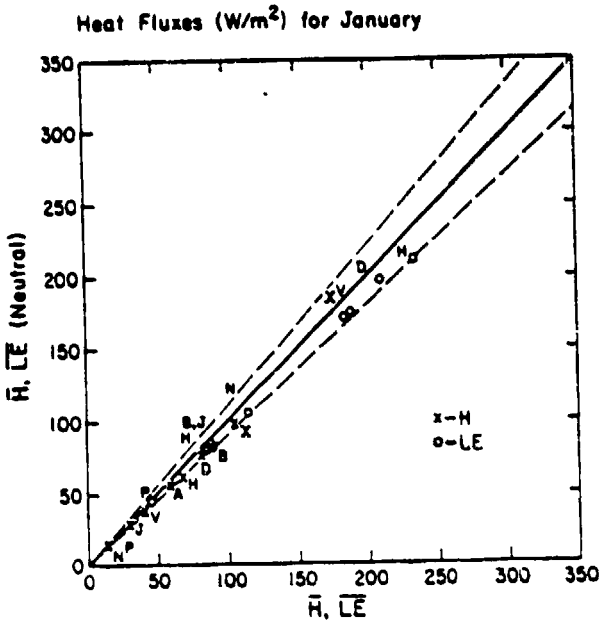

FIG. 6. Climatological sensible and latent heat fluxes as in Fig. 3a except that values along the ordinate are computed by the sampling method with neutral transfer coefficients.

6. Monthly averaged estimates

The results from the previous section suggest that the classical method also might be successful in monitoring the interannual variability of the sensible and latent heat fluxes. To examine this possibility we calculated the heat fluxes for each January and July

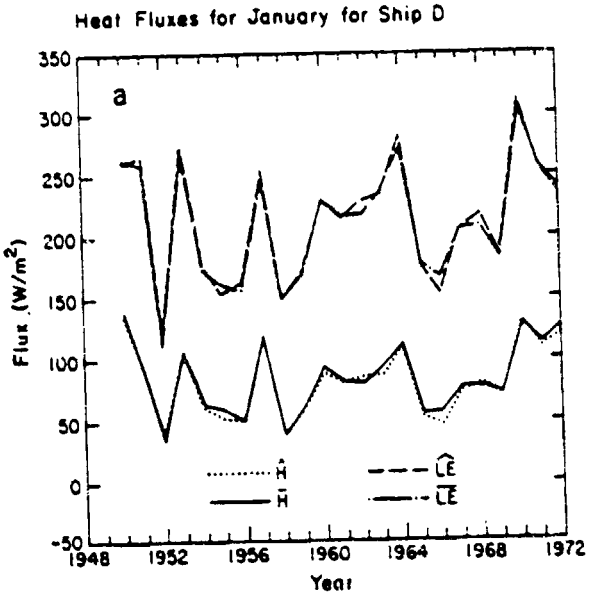

FIG. 7a. Monthly averaged sensible and latent heat fluxes computed by the sampling and classical methods for each January at Ship D.

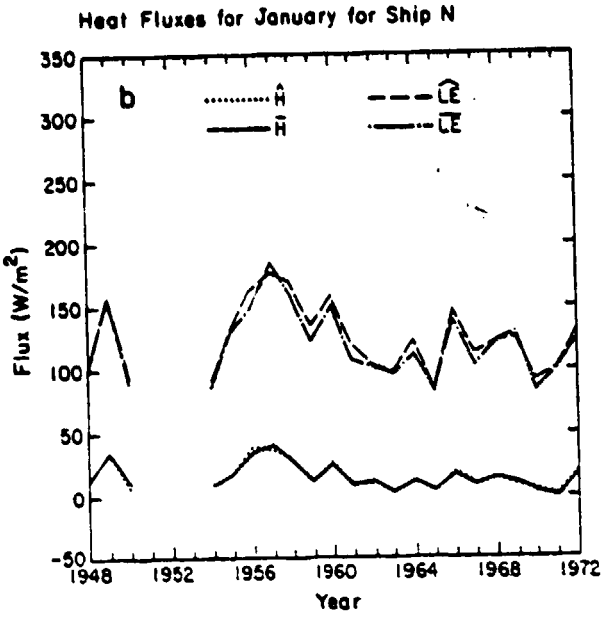

FIG. 7b. As in Fig. 7a except for Ship N.

at all the ocean weather ships using both the classical method and the sampling method. Since the results of the comparison are almost independent of the choice of month or ship, we have chosen to present only the January results at ships D and N representing significantly different heat flux regimes.

Fig. 7a shows the comparison for Ship D. Although the average heat fluxes are large (see Fig. 3), the interannual variability of the monthly averaged fluxes is also large. Despite the observed variability, the classical method still gives estimates of the heat fluxes which are within 10% of the values obtained by the sampling method. These results are consistent with the conclusions of Fissel *et al.* (1977) for Ship P; they performed cross-spectral analysis on a series of 2-year segments of data at Ship P with constant transfer coefficients and found that disturbances with periods of less than a month contributed only 10% of the biennially averaged sensible heat flux and only 5% of the biennially averaged latent heat flux.

The results in Fig. 7b for Ship N show that the interannual variability of the heat fluxes in subtropical regions also is well resolved by the classical method. The classical estimate of the latent heat flux is systematically higher than the sampling estimate, but still within 10%.

The comparisons in this section were based on the transfer coefficients shown in Fig. 1. However, we also computed the monthly averaged fluxes with the unrealistic transfer coefficients shown in Fig. 4. Since these coefficients have a stronger dependence on wind speed, the sampling and classical methods are not in such close agreement. However, the average

disagreement for the 25-year period was still <10%, and never exceeded 20% in any individual month.

Finally, we wish to point out that the transfer coefficients themselves are subject to uncertainties of ~20–30% (e.g., Pond *et al.*, 1974). In view of this uncertainty, the classical method is a practical and reliable alternative to the method of sample means. The uncertainty underscores the need for independent methods for obtaining the heat fluxes such as the budget approach of Oort and Vonder Haar (1976).

7. Climatological and monthly averaged wind-stress estimates

As discussed by Hellerman (1965) a wind rose with both direction and speed categories is necessary to accurately determine the wind stress. A similar result was obtained by Fissel *et al.* (1977). In this section we reexamine Hellerman's conclusion using the weather ship data and determine the effect of stability on the stress computation.

The wind stress vector τ can be determined from the bulk aerodynamic expressions

$$\left.\begin{aligned}\tau_x &= \rho C_D V_a u_x \\ \tau_y &= \rho C_D V_a u_y\end{aligned}\right\}. \qquad (9)$$

Here τ_x and τ_y are the east–west components and north–south components of τ, respectively; u_x and u_y are the components of the wind; and C_D is the drag coefficient for momentum. The Liu *et al.* (1979) algorithm was used to compute C_D. The behavior of C_D is similar to the behavior of C_H and C_E at wind speeds below 10 m s^{-1} but increases significantly at wind speeds larger than 10 m s^{-1}. As described in Liu *et al.* (1979) momentum can be transferred by pressure forces acting on the air as it flows over the waves as well as by frictional stresses at the surface. The transfer by pressure forces tends to be strongly dependent on wind speed. However, molecular diffusion is the only mechanism available for the sensible and latent heat fluxes at the air-sea interface. Thus, the dependence of C_H and C_E on wind speed tends to be less than the wind-speed dependence of C_D for moderate to strong winds.

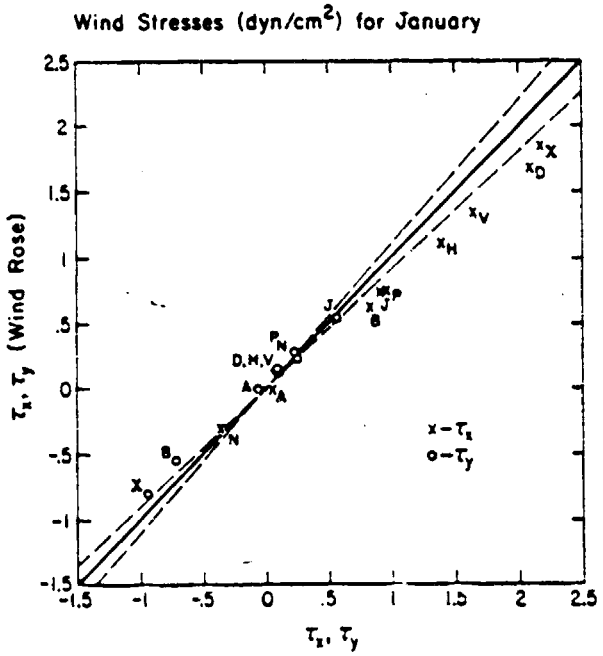

FIG. 8. Climatological wind stresses computed from the sampling method (abscissa) and a "direction-only" wind rose (ordinate). See also Fig. 3a.

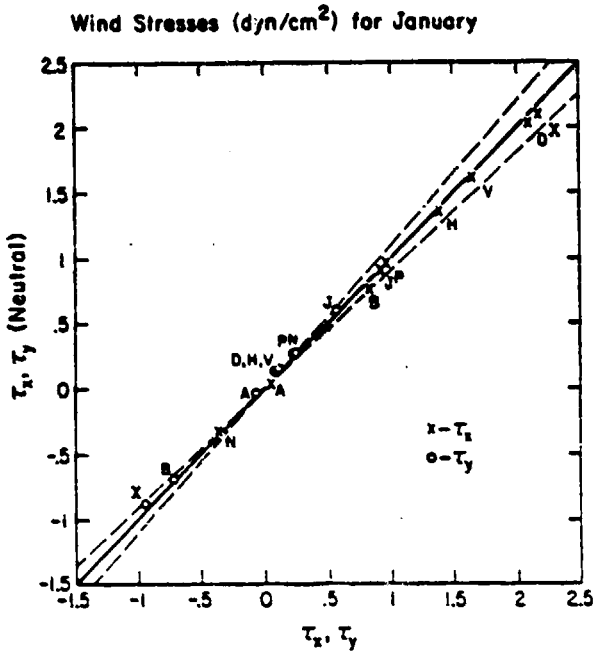

FIG. 9. As in Fig. 8 except that the ordinate indicates the wind stress computed from the sampling method with neutral coefficients.

Using the Liu *et al.* algorithm with the stability correction, we computed the climatological τ_x and τ_y at each weather ship using the sampling method with a wind rose with an average wind speed for each of the 16 direction categories. Fig. 8 shows that the "direction-only" wind rose consistently underestimates the wind stress when $|\tau_x|$ or $|\tau_y|$ is > 0.5 dyn cm^{-2}. This relative error can be as large as 25% (see τ_x for Ship B). Thus, Hellerman's wind rose conclusions for neutral coefficient wind stress also apply for stability corrected coefficients. Therefore, the wind stress should be computed either by the sampling method or by a wind rose with several speed categories for each direction.

To clarify the importance of stability we recomputed the wind stress with the sampling method for a neutral C_D. The results are shown for the climatological τ_x and τ_y in Fig. 9. The importance of

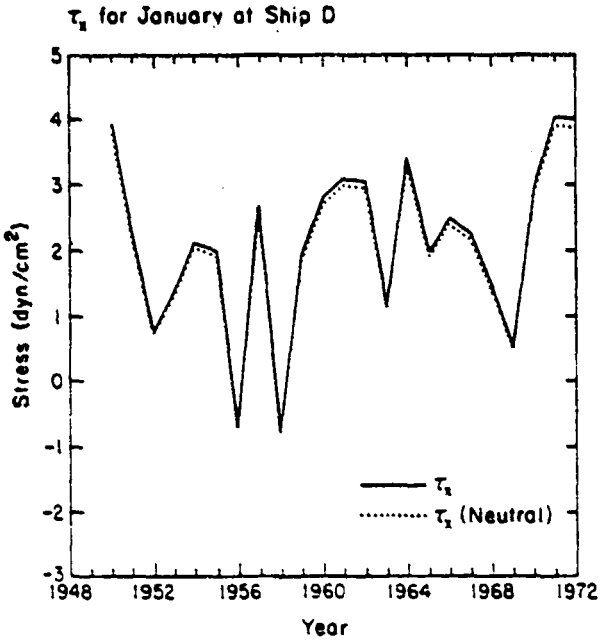

FIG. 10. Monthly averaged τ_x computed by the sampling method for stability corrected and neutral momentum transfer coefficients for each January at Ship D.

stability is small and affects the results by $<10\%$ except for small values of τ_x and τ_y. If we reexamine Fig. 6, we see that the effect of stability generally produces a smaller relative error for wind stress than for sensible and latent heat fluxes.

The effect of stability on τ_x and τ_y also was examined on an interannual basis for each ship for January and July, and was found to be small in each case. This comparison is shown in Fig. 10 for the January τ_x at Ship D. It is apparent that for many applications the atmospheric surface boundary layer may be considered to be neutral when computing wind stresses on time scales of one month or longer over the open ocean.

The small errors caused by the use of neutral coefficients can be further reduced by substituting monthly mean values of $(T_s - T_a)$ and $(q_s - q_a)$ into the transfer coefficient algorithms in place of the air-sea temperature and humidity differences at each observation time. Errors of less than a few percent are typical of the results found at every ship position.

8. Summary and discussion

We have shown that monthly averaged values of middle-latitude and subtropical surface marine meteorological data can be used in bulk aerodynamic formulas to obtain the monthly averaged surface fluxes of sensible and latent heat. These results confirm and extend the work of Budyko (1963) and his co-workers by including recent developments in boundary-layer similarity theory to give a more realistic representation of the physical processes which are important to air-sea transfers of sensible and latent heat.

Our results also confirm that neutral transfer coefficients give reliable wind stress estimates over the ocean. If greater reliability is desired, this is easily achieved through the use of monthly averaged air-sea temperature and humidity differences for the determination of the drag coefficient.

Similar results for heat flux and wind stress estimates should be obtained in tropical regions. Although this study does not include tropical marine data, our conclusions are valid for the small Bowen ratios (H/LE) and the moderate to low wind speeds which characterize large portions of the tropical oceans (see, e.g., Fig. 3b).

We believe that the classical method for using wind roses and monthly averaged state variables to estimate heat fluxes and wind stresses has advantages over computing weighted sample means, and that these may prove valuable in describing and monitoring interannual and decadal climate fluctuations:

1) Data processing requirements: The computational effort required to process monthly-averaged data from ship-of-opportunity and ocean weather ships is much less than the effort needed to process all the individual surface reports. Therefore, the revision of heat flux estimates with an improved transfer coefficient or updated mean field is a relatively simple task with the classical method.

2) Utilization of heterogeneous data: The classical method may provide a simple way of combining non-simultaneous data from a variety of observing platforms. For example, satellite data does not yet provide accurate estimates of the air-sea temperature and humidity differences, but may soon give useful information on the surface wind speed over the oceans. To compute monthly averaged heat fluxes using the sampling method, it would be necessary to interpolate these data sets in space and time while at the same time combining the satellite data with conventional data sets. On the other hand, the use of the classical method relaxes the restriction that the observations of wind-speed, temperature and humidity fields be simultaneous and thus provides a straightforward way to incorporate the satellite observations into the heat flux estimates.

Some additional lines of investigation are suggested by the results of this study. First, the excellent agreement between the classical method and the sampling method for monthly averages raises the question of what is the shortest time interval for which the conclusions hold. The study of Fissel *et al.* (1977) begins to give an answer for a limited region over the North Pacific but this type of work should be clarified and should be extended to other

regions. Second, it is possible that the classical method may provide a more reliable estimate of the heat flux when the number of observations is small. Since both the covariance and the correlations of V_a with either $(T_s - T_a)$ or $(q_s - q_a)$ are known to be relatively small, the nonlinearities in the flux estimates using the sampling method may lead to more statistical uncertainty in estimating the long-term average heat fluxes than the classical estimators. Finally, the effects of area averaging on the conclusions should be explored, particularly in regions of large gradients of surface parameters.

Acknowledgments. We would like to acknowledge the participation of Mr. E. I. Tollerud in background studies which led to this work. We would also like to acknowledge discussions with Drs. J. W. Deardorff, W. T. Liu and C. A. Paulson concerning the determination of the bulk aerodynamic transfer coefficients, and would like to thank Drs. Deardorff and Paulson for their comments on a draft of the manuscript. Mr. T. McCart assisted with the data processing tasks.

This research was supported primarily by a grant from the National Aeronautics and Space Administration (NSG 5308). Funds were also provided by the National Science Foundation under Grant ATM 77-26406-03.

REFERENCES

Brook, R. R., 1978: The influence of water vapor fluctuations on turbulent fluxes. *Bound.-Layer Meteor.*, 15, 481–487.

Budyko, M. I., Ed., 1963: *Atlas of the Heat Balance of the Earth*. Akad. Nauk SSSR, Prezidium. Mezhduvedomstvennyi Geofiz. Komitet., 69 pp. [Also, *Guide to the Atlas of the Heat Balance of the Earth*. Transl. by I. A. Donehoo, U.S. Weather Bureau, WB/T-106, Washington, DC.]

——, 1974: *Climate and Life*. Academic Press, 508 pp.

——, and L. S. Gandin, 1966: On determination of the turbulent heat exchange between ocean and atmosphere. *Meteor. Gidrol.*, 11, 15–25 [MGA 18.7–436].

Bunker, A. F., 1976: Computations of surface energy flux and annual air-sea interaction cycles of the North Atlantic Ocean. *Mon. Wea. Rev.*, 104, 1122–1140.

Businger, J. A., J. C. Wyngaard, Y. Izumi and E. F. Bradley, 1971: Flux-profile relationships in the atmospheric surface layer. *J. Atmos. Sci.*, 28, 181–189.

Deardorff, J. A., 1972: Parameterization of the planetary boundary layer for use in general circulation models. *Mon. Wea. Rev.*, 100, 93–106.

Dyer, A. J., and B. B. Hicks, 1970: Flux-gradient relationships in the constant flux layer. *Quart. J. Roy. Meteor. Soc.*, 96, 715–721.

Fissel, D. B., S. Pond and M. Miyake, 1977: Computation of surface fluxes from climatological and synoptic data. *Mon. Wea. Rev.*, 105, 26–36.

Hellerman, S., 1965: Computations of wind stress fields over the Atlantic Ocean. *Mon. Wea. Rev.*, 93, 239–244.

——, 1967: An updated estimate of the wind stress on the world ocean. *Mon. Wea. Rev.*, 95, 607–626 [see also Corrigendum, 1968, 96, 63–74].

Kondo, J., 1975: Air-sea bulk transfer coefficients in diabatic conditions. *Bound.-Layer Meteor.*, 9, 91–112.

Kraus, E. B., and R. E. Morrison, 1966: Local interactions between the sea and the air at monthly and annual time scales. *Quart. J. Roy. Meteor. Soc.*, 92, 114–127.

Liu, W. T., K. B. Katsaros and J. A. Businger, 1979: Bulk parameterization of air-sea exchanges of heat and water vapor including the molecular constraints at the interface. *J. Atmos. Sci.*, 36, 1722–1735.

Malkus, J. S., 1962: Large-scale interactions. *The Sea*, Vol. 1, M. N. Hill, Ed. Wiley-Interscience, 88–294.

Oort, A. H., and T. H. Vonder Haar, 1976: On the observed annual cycle in the ocean-atmosphere heat balance over the Northern Hemisphere. *J. Phys. Oceanogr.*, 6, 781–800.

Pond, S., D. B. Fissel and C. A. Paulson 1974: A note on bulk aerodynamic coefficients for sensible heat and moisture fluxes. *Bound.-Layer Meteor.*, 6, 333–339.

Sverdrup, H. U., M. W. Johnson and R. H. Fleming, 1942: *The Oceans*. Prentice-Hall, 1087 pp.

APPENDIX B

The Heat Balance of the Global Ocean: An Atlas Based on Estimates From Surface Marine Observations

S. K. Esbensen and Y. Kushnir

ABSTRACT

An atlas of the surface heat budget of the global ice-free ocean is presented. The atlas includes maps of the monthly mean distributions of the calculated heat budget components and of the basic variables used in the calculation. All the fields have a uniform spatial resolution and are presented on a regular 4°x5° grid.

To calculate the heat budget components, bulk formulas parameterizing the heat flux mechanisms were applied to monthly mean values of basic surface variables. The radiative fluxes were calculated using the bulk formulas documented by Budyko (1974), while the turbulent fluxes were calculated by the bulk aerodynamic method suggested by Liu *et al.* (1979). Data sources for the basic variables were a global climatology of surface marine meteorological observations prepared by the National Climatic Center and the Berliand and Strokina (1980) cloudiness atlas.

The results should be useful in ocean modeling and in a variety of diagnostic studies of the surface climate; all data presented are available in a computer compatible format.

1. Introduction

The annual cycle of the earth's climate clearly shows the important role of the oceans. By storing heat in the summer season and releasing it in the winter, and by transporting heat from areas of heat gain in the tropics to areas of heat loss at higher latitudes, the oceans moderate the climatic state of the atmosphere.

The energy sources for the ocean surface transport and storage are primarily the diabatic sources and sinks of heat at the ocean surface. These are the incoming solar radiation, the net loss by longwave radiation and sensible and latent heat fluxes. Budyko was first to conduct a study of the spatial and temporal structure of the oceanic heat balance on a global scale. Based upon bulk formulas obtained for this particular study, Budyko (1963) and his co-workers calculated the diabatic heating terms from available observations of basic surface variables such as temperature, wind, humidity and sea level pressure.

Since then many regional studies have been carried out by investigators using similar methods. Bunker and his co-workers (Bunker, 1976; Bunker and Worthington, 1976; and Bunker and Goldsmith, 1979) carefully constructed a relatively high resolution study of the heat balance of the North and South Atlantic Oceans. Their study supported the gross features revealed by Budyko's study and offered better estimates on the fine structure of the heat exchange patterns especially over the Gulf Stream and the North Atlantic. Bunker and his colleagues were also able to present local time series of the heat budget components.

Hastenrath and Lamb (1977, 1978 and 1979) have used long term 1°x1° latitude-longitude averages of surface marine observations to establish a monthly high resolution climatology of the heat budget over part of the tropical ocean. Hastenrath combined these studies with others to present the global aspects of the heat budget of the tropical ocean and atmosphere (Hastenrath, 1980).

Recently, Weare *et al.* (1981) studied the heat budget climatology over the tropical Pacific Ocean. They also addressed the problem of sampling errors inherent in using space and time averages of surface variables with the bulk formulas (Weare and Strub, 1981).

Following a completely different approach Oort and Vonder Haar (1976) addressed the question of the role of the oceans in the global heat budget and calculated meridional profiles of oceanic storage and northward heat transport over the northern hemisphere.

While a combination of these studies provides a representation of oceanic heat budget, the results are not readily available for use in model studies of the general oceanic and atmospheric circulations. The only data source particularly designed for this purpose is that by Schutz and Gates (1971, 1972, 1973 and 1974) compiled from Budyko's (1963) study containing the months of January, April, July and October. The major goal of this study to obtain a similar presentation for all twelve calendar months for use by the modeling community. To achieve this purpose a readily available global climatology of surface marine observations with a resolution of approximately 5x5 degrees was chosen and objectively checked and corrected. Bulk formulas were selected from the literature and a monthly climatology of the heat budget components was calculated over the entire ice free global ocean. These data and the climatology of basic surface variables are presented on a regular grid.

2. Climatology of Basic Variables

Budyko and his co-workers (Budyko, 1963) first utilized the so-called "classical method" for a comprehensive study of the global surface heat balance. Using monthly averaged atmospheric and oceanic data and bulk formulas they constructed the fields representing the spatial and temporal structure of the various components of the balance. Their approach has been well documented by Budyko (1974).

In this analysis we also use the classical method which allows the use of available surface climatological data. Two data sources were chosen: a global ocean climatology of marine observations prepared by the National Climatic Center (NCC), Asheville, North Carolina and an atlas of global cloudiness prepared by Berliand and Strokina (1980). In this section the data processing methods used in this study will be presented, followed by a brief discussion of the features revealed by the resulting fields.

2.1 *Data processing procedures*

2.1.1 The NCC climatology of marine surface observations

The main source of data for this study was prepared by NCC based upon various sources of marine surface observations contained in the TDF-11, Surface Marine Observation, data collection[1]. These data have long served as a basis for the preparation of numerous marine surface atlases. They were also used in the regional ocean-surface heat budget studies referred to in the introduction.

The specific climatology used here was prepared recently by NCC. The TDF-11 data were arranged into 1x1 degree Marsden sub-squares and time averaged to obtain monthly mean values of the observed variables. These were then averaged into 5x5 degree sub-squares which were suitable for the purposes of this study. Table 1 describes the basic variables included in the 5x5 degree NCC climatology.

The NCC 5x5 degree averages present climatological values which are assigned to the mean latitude and longitude of all observations within that square. This presentation may be thought of as an irregular grid which changes from month-to-month. The transformation of the original climatology onto a regular grid was the first stage in this study. The grid chosen was that of the OSU Oceanic and Atmospheric General Circulation Models (hereafter referred to as the OSU OGCM and AGCM). This is a rectangular latitude-longitude mesh with grid points located every 4 degrees in latitude and every 5 degrees in longitude[2]. Before starting the grid transformation procedure, land, inland sea basins and the monthly sea-ice covered ocean points were marked so they could be masked out during the transformation[3].

---

[1]The sources of data used in this collection, its contents and methods of quality control used during its assembly, are described in the Tape Deck TDF-11 Manual published by the National Climatic Center, Asheville, North Carolina, 1968.

[2]The latitude count starts at the south pole going northward and the longitude count at 180 longitude going eastward. Thus, there are 72 points on each of the 46 latitude circles, a total of 3312 grid points.

[3]We based the land-ocean classification upon that of the OSU AGCM (Schlesinger and Gates, 1979). Sea ice boundary for each month was based upon data from Alexander and Mohley (1976).

Table 1. Contents of NCC 5°x5° Climatology

Location Information:	(1) Marsden square number (2) 5°x5° sub-square number (3) Mean latitude and longitude of observations
Period:	Month of the year
Variable statistics:	(1) Superstructure icing potential (2) Wind rose statistics - Monthly force and percent frequency of wind from eight points of compass and percent frequency of calms (3) Scalar variable statistics - monthly means, standard deviations and number of observations for the following variables: (a) wind speed (b) sea level pressure (c) air temperature (d) wet bulb temperature (e) dew point temperature (f) sea surface temperature (g) air - sea temperature difference (h) wave height

The grid transformation was achieved by using a Gaussian space averaging technique similar to what is known as the Barnes (1964) objective analysis scheme. The new grid point value is a weighted average of all NCC "grid" values falling within a radius of ~1100 km around it. The weights depend only on the distances between the new grid point and the mean location in each 5x5 degree Marsden sub-square entering the calculation. The Gaussian averaging technique is nearly mean conserving and acts like a spatial filter. It was designed to uniformly suppress features with wavelengths shorter than ~1600 km.

During the interpolation procedure, values based upon less than 25 observations were immediately rejected, as were values located over the land and monthly sea-ice areas. A separate check was carried out on all values based upon 25 to 100 observations. If these deviated by more than a fixed amount from a value produced by a preliminary grid transformation, they were marked for rejection and a final transformation was then performed without them[4].

For each variable field a corresponding data density field was also constructed. This was achieved by treating the number of observations of that variable as a field value and transforming it to the 4x5 degree grid. Then, the base 10 logarithm of the interpolated value was calculated at every grid point. These data density fields are used as data reliability indicators.

The procedure described above was applied to 12 monthly sets of the following basic variables: sea level pressure, surface wind speed, sea surface temperature, sea - air temperature difference, air specific humidity and sea - air humidity difference[5]. Air temperature fields were constructed in a later stage from the monthly sea-surface temperature and sea - air temperature difference fields.

---

[4]The maximum allowed differences between NCC values and the new grid values were 2.5 m sec^{-1} for wind speed, 5 mb for pressure, 5°C for SST, 1°C for sea-air temperature difference, 3 g kg^{-1} for the humidity difference. NCC values were checked against the grid values after linearly interpolating from the grid to the NCC mean location of observations.

[5]Air specific humidity and sea-air humidity difference were calculated prior to interpolating from the NCC dew point temperature and sea surface temperature. Calculation was performed by using the Smithsonian (List, 1958) formulas for saturation vapor pressure.

Examination of the resulting filtered data fields revealed relatively small wavelength features located in areas of low data density. These probably resulted from sampling errors due to the original area and time averaging procedures. In an effort to obtain a more reasonable representation of the field we have applied additional smoothing to the fields in low data density areas. A special two dimensional Gaussian filter was designed which provided strongest smoothing in the zonal direction in lower data density areas. No smoothing was applied to areas where the data density indicators were larger then 2.7 (500 observations). This procedure improved the representation especially in the southern hemisphere high latitudes where most of the problems occurred. It did result though in very small amplitude $2\Delta x$ features on the borderlines between areas where smoothing was applied and those where it was not applied. It is recommended that the reader bear in mind the data density patterns when viewing or using the data fields.

2.1.2 Cloudiness data

The NCC climatology includes no cloudiness information and thus we had to use some other source of updated global cloudiness data. After comparing two such sources, Miller and Feddes (1971) and Berliand and Strokina (1980), we decided to use the latter because it was free of some local deficiencies that show up in Miller and Fedder's satellite study. Berliand and Strokina's data are also a more suitable input for the bulk radiation formulas which were designed for use with surface observations.

The Berliand and Strokina data are based on a variety of sources, from regular ground observation networks over land and ocean to satellite observations. These were all integrated and presented on a global rectangular 5x5 degree grid for each of the 12 months and are given both as figures and as tabulated values. The authors claim a better representation of the distributrion of cloudiness than achieved before, in particular over the ITCZ.

For the purpose of this study the Berliand and Strokina data were transformed to a 4x5 degree grid using the basic Gaussian averaging technique described in section 2.1.1.

2.1.3 Annual mean fields

After completing the grid transformation and smoothing stages, an annual mean field was calculated for each of the variables. This was done by simply averaging 12 values at each of the annually ice-free ocean grid points. A data reliability indicator for the annual mean fields was constructed from its minimum monthly value at each grid point with the exception of the cloudiness fields which were not assigned data density indicators.

2.2 *Data quality*

Before discussing the main features in the resulting basic variable fields it is important to address the subject of the data quality. This is affected by errors of two categories: observation errors and sampling errors.

The first category includes errors resulting from human factors and those resulting from instrumental limitations. Human errors most common in marine observations are those due to inadequate training and observational practice on behalf of the observers, and those introduced by the error susceptible communication links between the observer and the local climatic centers. Instrumental errors are commonly due to poor location of the instrument shelter or the sensors, and from the cruder instruments used on board merchant ships. These problems have been widely discussed in the open literature (see for example, Roll, 1965). The second category is associated with non-uniform spatial and temporal distributions of the observations as well as from an insufficient number of observations in the statistical sense (resulting in very broad confidence intervals). These errors and their effects on determination of a long term climatology of basic and derived variables were addressed and examined by Weare and Strub (1981). As indicated by their study, these result in both random and bias errors. The bias errors are larger in areas of strong spatial gradients and where the amplitudes of the diurnal and annual cycles are relatively large. The magnitudes of the biases also depend strongly on the number of observations used in the calculation of the climatological value. Weare

and Strub estimate that as far as basic variable climatology is concerned these errors are on the order of a few percent (and usually less than 10%).

The automated data handling procedures used in this study result in a plausible representation of the basic variable fields. Large scale oceanic and atmospheric features are generally well resolved over most of the global ocean area.

As indicated in section 2.1.1, field values over data-sparse areas should be viewed with some caution. In those areas some patterns show a considerable lack of time continuity. It should be noted, though, that only ocean areas south of about 50 S are seriously plagued by these features. We believe however, that these data are still adequate for heat budget studies on a global scale, in light of the uncertainties involved in estimating the heat fluxes from the semi-empirical bulk formulas.

The data fields were compared with other available climatologies[6] most of which based their marine climatology on the same TDF-11 data, though utilizing different data handling procedures and spatial resolutions. We found generally good agreement between these climatologies and ours. As a result of these comparisons we found that our automated data handling procedures performed well near the ocean - land boundaries.

2.3 *Discussion of basic variable fields in the atlas*

The basic variable fields constructed for the purpose of this heat budget study are presented in section 1 of the following atlas. Since the global distribution of these variables determines the global distribution of the heat budget components, it is important to examine the resulting fields for their agreement with other climatologies and for internal consistancy. This examination gives an indication of the inherent limitations in the quality and resolution of the heat balance components to be discussed later.

---

[6]The climatologies used were: Schutz and Gates (1971, 1972, 1973 and 1974), Alexander and Mobley (1974), Hastenrath and Lamb (1977), and the Bunker and Goldsmith (1979) data. Some common marine atlases were also used for comparisons in the various stages of the construction of the data handling routines.

2.3.1 Surface wind speed (Charts 1.1 to 1.13)

The monthly-averaged surface wind speed fields generally agree with the monthly averaged sea level pressure (see Charts 1.92 to 1.104). Regions of weak winds are generally associated with the centers of the sub-tropical highs and regions of strong winds with the zones of steep pressure gradients near the mean positions of the middle latitude quasi-stationary low pressure cells. The agreement deteriorates in the Southern Hemisphere south of 50°S. The wind fields also reveal the trade wind belts as zones of local maxima on both sides of the ITCZ trough. The annual cycle associated with the Indian monsoon over the Arabian sea is also shown.

2.3.2 Sea surface temperature (Charts 1.14 to 1.26)

In these fields the patterns are usually more smooth and consistent probably due to a smaller variability and a larger number of observations. The warm and cold ocean currents are indicated by zones of sharp temperature gradients and deep narrow troughs and ridges penetrating poleward along the continental boundaries. Strongest temperature gradients are associated with the Gulf and Kuroshio currents. These gradients show a marked annual cycle associated with the reduced horizontal temperature contrast during the summer months. Another belt of sharp temperature gradient is located over the Antarctic Ocean basin surrounding the Antarctic continent. It is more difficult to define seasonal variations in this region because of the lower data densities involved. Large amplitude equatorial features are seen in the eastern oceans. Here the annual cycle is also well represented by the shift of the equatorial maximum. The whole equatorial ridge especially the zone of warmest water over the Indian and Central West Pacific Oceans oscillates in position throughout the year. Finally, smaller scale features like the southward penetration of the Labrador current or the northward penetration of the Alaska current are also well defined.

2.3.3 Sea - air temperature difference (Charts 1.27 to 1.39)

The outstanding patterns in these fields are those associated with the large contrast between the winter continental air masses and the warm ocean surfaces on the western sides of the northern hemisphere ocean basins. Here the instability of the atmospheric boundary layer is maximum in December and is accompanied by strong horizontal temperature difference gradients. These figures reveal the stabilizing effects of the cold water currents to the north of the Gulf and Kuroshio. This is especially strong during summer when a stable air mass is created over the Labrador and Kamchatka currents. In general, the atmospheric boundary layer over the summer hemisphere is more stable than that of the winter hemisphere.

2.3.4 Air temperature (Charts 1.40 to 1.52)

These fields were constructed from the sea surface temperature and sea - air temperature difference fields and as such contain no additional information.

2.3.5 Air specific humidity (Charts 1.53 to 1.65)

The specific humidity of the air is strongly dependent on its temperature. This is shown by the strong similarity between these fields and the air and sea surface temperature fields. The spatial gradient in the humidity fields though smaller than in the temperature fields, are still directed from polar to equatorial regions. The strong zonal structure of these fields is slightly modified by troughs and ridges in the north-south direction associated with the oceanic circulations.

2.3.6 Sea surface - air specific humidity difference (Charts 1.66 to 1.78)

This variable is sometimes referred to as the evaporation potential. It is generally largest in the subtropical zones where subsiding dry air masses overlay relatively warm water surfaces. These zones usually extend over the southern branches of the warm Gulf and Kuroshio currents, except

during the northern hemispheric summer months when the surface boundary layer is relatively stable and its vertical humidity gradient less steep. The ITCZ minimum is enhanced over the cold upwelling regions of the eastern Atlantic and Pacific Oceans. These minima become especially sharp during the northern hemisphere summer months. Also noticeable are the strong horizontal gradients in the evaporation potential on the poleward boundaries of the middle latitude warm ocean currents. Some local features of interest are the maximum over the western coast of Central America persistent throughout the year which is associated with the local maximum in sea surface temperatures and the sea-sonal changes over the Arabian sea associated with the monsoon circulation.

2.3.7 Cloudiness (Charts 1.79 to 1.91)

These fields generally show maxima over the high latitudes and minima in the subtropics. The ITCZ is indicated by a local shallow ridge over the tropics, except for the tropical western Pacific where the cloudiness broadens to cover a large ocean area. Zones of marine fog and stratocumulus prevailing over the cold eastern ocean basins are well depicted. These also show stronger seasonal dependence than most other features. Overall, the cloudiness fields have a smoother appearance than the basic variables from the NCC climatology.

2.3.8 Sea level pressure (Charts 1.92 to 1.104)

The monthly averaged sea level pressure fields present the familiar patterns of the oceanic subtropical highs and the seasonal changes in their strength and location. In the Northern Hemisphere the Aleutian and Icelandic lows and their seasonal changes are also well depicted. Also indicated are the seasonal changes in sea level pressure over the Arabian Sea which are associated with the Indian Monsoon. In these coarse resolution fields the ITCZ appears as a broad and shallow pressure trough located over the tropics and migrating northward or southward with the seasons. Not so well represented are the pressure patterns over the southern hemisphere high latitudes. This is indicated primarily by lack of time

continuity of some of the patterns. These patterns are associatd with low data density and are usually confined to south of 50 S.

3. Ocean Heat Budget Climatology

The local monthly-averaged energy balance of the ocean's upper layer can be expressed as follows:

$$S = -DivF - F_W + F_S(1 - \alpha_W) - F_I - F_{LE} - F_H$$

where S is the layer-averaged rate of change of heat storage per unit area of the layer (storage term), DivF is the layer-averaged divergence of heat transported by the surface horizontal currents, and F_W is the downward heat transport through the lower boundary of the layer. The remaining terms are the diabatic sources and sinks of heat at the ocean surface: F_S is the incoming solar flux at the ocean surface reduced by the monthly mean surface albedo α_W, F_I is the net upward long-wave radiative flux, F_{LE} the upward latent heat flux, and F_H the upward sensible heat flux at the ocean-atmosphere interface. In constructing the monthly estimates of the diabatic terms, the classical approach first used by Budyko (1963) was taken, i.e., the monthly averaged fluxes were calculated from the monthly averaged values of the basic variables. The calculations were carried out on the 4x5 degree grid using the previously described climatology. The heat fluxes were calculated separ.tely at each grid point. All the fields that were based on variables taken from the NCC climatology were also assigned a data quality indicator. This is defined as the local minimum of all indicators associated with the input variables.

Estimating the diabatic heating sources will enable us to calculate the sum of the monthly storage and the flux divergence terms in the surface layer as a residual. When averaged annually and globally this sum should vanish, and an approximate balance should be achieved between the diabatic fluxes if we assume that the contribution of F_W is negligible.

3.1 *Estimating the components of the heat budget*

3.1.1 Incoming solar radiation

There are several methods presented in the literature which are intended to provide an estimate of the solar flux incident upon a horizontal surface at sea level. All of these consist of two parts: an estimate of the monthly averaged maximum available direct plus diffuse solar flux at sea level, which is dependent on latitude and season, and a factor which includes the effects of cloudiness. Of all the bulk formulas used for climatological studies, only that suggested by Berliand (1960) was designed for a comprehensive global study (Budyko, 1963), under the constraint of achieving a global heat balance.

The Berliand algorithm is described rigorously by Kondratyev (1969) and Budyko (1974). It is easy to apply and combines both parts of the estimate in a consistent manner. Although its clear sky formulation and cloudiness factor performances have been criticized by Reed (1977) and others based on observations at specific times and locations, we believe one should judge its performance as a whole over a wide range of conditions as indicated by Budyko (1974). In their tropical Atlantic study Hastenrath and Lamb (1978) used a different method to estimate F_S but their estimates were no more than a few percent away from those obtained by Bunker (1976) and Bunker and Goldsmith (1979) using Berliand's algorithm. Reed's (1977) suggested method was used by Weare and Strub (1981) with results 10% larger than those calculated here.

Berliand's formula as presented by Budyko (1974) is

$$F_S = Q_0[1 - (a + bn)n]$$

where Q_0 is the monthly averaged direct and diffuse maximum solar flux and is a function of latitude. n is the monthly averaged cloudiness (in fractions), b is a constant and a is a coefficient varying with latitude. The monthly values of Q_0 were compiled by Berliand from observations from various latitudinal zones and are given by Budyko (1974, Table 3). The coefficients a and b were also calculated by Berliand and are given in Budyko's book (a values are presented in Table 4 and b = 0.38).

To assess the amount of solar heating of the ocean surface one has to subtract the reflected part of the incoming solar flux. For that purpose Payne's (1972) albedo table for the Atlantic was used globally as suggested by Kukla and Robinson (1980).

3.1.2 Net long-wave radiation

Here again there is a large diversity and controvery in the literature as to how to construct a reliable estimate of the local flux. Most of the methods agree closely with that originally suggested by Brunt (1932) and later modified somewhat by Berliand and Berliand (1952). This method, as presented in Budyko (1974), was the only one used for a global comprehensive heat budget study. Again the formula consists of two main parts: an estimate for the cloud-free net IR lost per unit area and time by the ocean surface, and a cloudiness factor. The formulation of the cloudiness effect is the most controversial aspect and seems to be the main source for the differences between estimates obtained by different investigators.

Berliand and Berliand's formulation is a linearized version of the difference between the grey body fluxes of the ocean (upward) and atmosphere (downward). The downward atmospheric flux should be affected mainly by the amount of water vapor in the lower layers and the amount and type of cloudiness. In Berliand's formulation the net flux is given by:

$$F_I = \varepsilon\sigma T_a(p - q\sqrt{e})(1 - cn^\tau) + 4\varepsilon\sigma T_a(T_s - T_a)$$

where T_a and T_s are the monthly mean air and sea surface temperatures, e is the monthly averaged water vapor pressure at anemometer level (in mb), and n is the mean cloudiness (in fractions). ε is the emissivity of water (=0.97), σ is the Stefan-Boltzmann constant. p and q are constants (according to Berliand, equal to 0.39 and 0.05, respectively). c is a coefficient depending on latitude in order to account for the varying radiative properties of clouds at different latitudes; Berliand assumed a linear dependence on latitude and his values were used here (Budyko, 1974, Table 9). τ is a constant and was set equal to 2 in this study.

Simpson and Paulson (1979) found good agreement between estimates based on Berliand's form of Brunt's formula and observations under clear sky conditions. Weare and Strub (1981) used a different cloudiness factor while basically not changing other parts of Berliand's expression. Comparing their final results with ours we found that their annually averaged F_I values are smaller by 20 to 40%. Here again we decided to apply Berliand's formulation as a whole, for the same reasons as before, namely, comprehensiveness and design for global and long term studies.

3.1.3 Sensible and latent heat fluxes

The latent and sensible heat flux estimates were based upon the bulk aerodynamic formulas

$$F_H = \rho c_p C_H V_a (T_s - T_a)$$

and

$$F_{LE} = \rho L C_E V_a (q_s - q_a)$$

where ρ is the density of air, c_p the isobaric specific heat of air, and L the latent heat of evaporation[7]. V_a, T_a and q_a are the monthly averaged wind speed, temperature and specific humidity of air at anemometer level. T_s is the sea surface temperature and q_s the humidity of the layer of air close to the sea surface, assumed saturated at temperature T_s. C_H and C_E are the transfer coefficients for sensible and latent heat; these were calculated using the iterative method suggested by Liu *et al.* (1979), using the observed T_s for the "skin" temperature of the ocean. This method was tested by Esbensen and Reynolds (1981).

[7]Here ρ was calculated locally from the monthly mean pressure and virtual temperature. c_p and L were taken as constants equal to their value at 0 C.

3.1.4 Some general remarks

The bulk formulas used to calculate the diabatic fluxes are parameterizations of the physical mechanisms involved in the heat transfer process. As such they are approximations to the true flux values. The approximation errors are believed to be in the range of 10 to 20%. Such errors are larger than bias errors arising from irregular sampling of basic variables in time or space, as was shown by Weare and Strub (1981). Their studies indicate that the magnitudes of the bias errors are strongly dependent on the number of observations of the basic variables and the geographic location (through the local spatial gradients of the variables and the magnitudes of their diurnal and annual cycles). Weare and Strub estimate that such sampling errors as reflected in the heat flux estimates are about 10%.

3.2 *Discussion of results*

The result of the heat flux calculations are presented in part 2 of the atlas. These include monthly sets of the spatial distributions of the fluxes and the calculated residual identified as the net downward heat flux. For each month a net downward radiative flux ($F_S(1 - \alpha_W) - F_I$) is also presented. Based upon these monthly fields a set of zonal mean vs. time sections of the spatial distribution of the local annual mean (only for annually ice free grid points) are presented for each of the components. Finally, the annually averaged meridional profiles of the components are presented based on the monthly zonal mean values for each of the components.

3.2.1 Available solar heat flux (Charts 2.1 to 2.13)

These fields present the distribution of the net solar flux (including the albedo effect) at the ocean surface. This is dependent upon the latitudinal maximum solar zenith angle and the distribution of cloudiness, the latter determining its longitudinal structure. Thus we find maxima in available solar flux over the relatively cloud-free subtropics with the

annual maximum occuring during the northern hemisphere summer over the western coast of North Africa. The ITCZ can be identified as a narrow zone of local minimum but is sometimes obscurred by larger scale features. The seasonal changes result mainly from changes in the solar zenith angle and are shown as an increase in the flux values over the middle latitudes during the summer season and a decrease during winter. Seasonal changes also occur in the relative strength of the subtropical maximum in both sides of the equator.

3.2.2 Net upward long-wave flux (Charts 2.14 to 2.26)

Over the warm and relatively cloud-free subtropics the net IR fluxes reach maximum values. Other local maxima occur over the warm ocean currents in winter, where the ocean loses more than it gains in longwave radiation. The ITCZ is a zone of local minimum since the relatively cloudy sky and colder ocean surfaces result in increased downward radiation and reduced upward radiation simultaneously. The strongest annual cycle is observed over the warm ocean currents. Here factors like the decrease in ocean - air temperature contrast and a more humid atmospheric boundary layer result in a marked decrease in the net IR flux leaving the ocean surface during the summer months. These changes are strongest over the Gulf and Kuroshio currents but are also noticeable over the Antarctic Ocean. The seasonal changes over the tropical oceans are small.

3.2.3 Net downward radiative flux (Charts 2.27 to 2.39)

These are presented as another means of observing the contribution of radiative fluxes to the heat budget.

3.2.4 Latent heat flux (Charts 2.40 to 2.52)

The flux of latent heat associated with the evaporation process presents the largest heat sink for the ocean surface layer. It is a strong function of the evaporation potential $q_s - q_a$ but also depends on the wind speed and the stability of the lower part of the atmospheric boundary

layer. The major patterns and their annual cycles closely resemble those of the sea - air humidity difference fields (Charts 2.79 to 2.91). The major maxima occur over the subtropics and extend northward over the Gulf and Kuroshio currents. These ridges weaken during the northern hemisphere summer. Fluxes are relatively weak over most of the low latitude oceans because of the stability of the boundary layer and the weak surface winds. The major minima occur over the regions of upwelling in the eastern equatorial Pacific and Atlantic oceans. A local maximum exists over the Arabian sea during the summer Monsoon months. The largest annual changes occur over the warm ocean currents of the Northern Hemisphere.

3.2.5 Sensible heat flux (Charts 2.53 to 2.65)

The sensible heat flux is a strong function of the sea - air temperature difference and as such their spatial and temporal distributions are similar. In the global average sensible heat flux is the weakest heat sink for the surface layer. Large fluxes occur regionally over the Gulf and Kuroshio currents during the northern hemisphere winter and near the southern tip of Africa out over most ocean areas these fluxes are very weak and show little coherent spatial structure.

3.2.6 Net downward heat flux (Charts 2.66 to 2.78)

This residual of the diabatic heating terms is mostly influenced by the patterns of solar radiation and latent heat fluxes. Large heat losses are found over the warm water currents while strong gains exist over the cooler surfaces of the tropical oceans. On the average both hemispheres lose heat during the winter months and gain during summer. The annual mean field presents the part of the residual available for transport on an annual basis. This field of course shows the tropics as a heat source and the high latitudes as heat sinks. The largest sinks are found over the western boundary currents and the largest sources are found in the regions of strong equatorial and coastal upwelling. It is interesting to note that this study shows that on the average the southern atlantic ocean does not act like a sink but rather like a weak source of heat.

3.2.7 Zonal means vs. time sections (Charts 2.79 to 2.84)

These figures illustrate the seasonal changes of the heat budget components. Zonal averaging was done over ice-free points only.

3.3 *Concluding remarks*

To summarize the study we present the meridional profile of the annually averaged net downward heat flux and its global mean (Fig. 1). These lead to an average residual heat storage rate of 5.37 Wm^{-2}. This value indicates that the results comply with our preconceived notion of the existance of a global balance. Here we should remember that only ice-free points are included in this study[8]. It is most likely that the ocean heat loss to the ice covered ocean would tend to balance part of the computed storage rate over the open ocean. In any case the residual amount of heat distributed over a 1 km deep ocean would result in an annual temperature increase of ~0.05 C.

The meridional profiles of the heat budget components are presented in Fig. 1 and Table 2. The shape of the net downward flux profile agrees quite well with that presented by Budyko (1974, Table 19) and Hastenrath (1980). Table 3 presents the total ocean area vs. the ice-free ocean area in this data set.

Finally, we note that the boundary layer fluxes of sensible and latent heat are systematically smaller than those calculated by Budyko (1963) and Bunker (1976). However, we believe that the transfer coefficients adopted for this study give a more realistic description of the sensible and latent heat fluxes with changes in wind speed and boundary layer stability. It is also encouraging to note that approximate annual heat balance can be shown over the global oceans with the new formulation.

---

[8]The annual-average zonal mean values were calculated as follows:

$$\bar{Z} = \sum_{m=1}^{12} Z_m N_m \Big/ \sum_{m=1}^{12} N_m$$

where Z_m is the monthly zonal average taken over the ice-free ocean points only and N_m is the monthly number of ice-free ocean points in the same latitude belt.

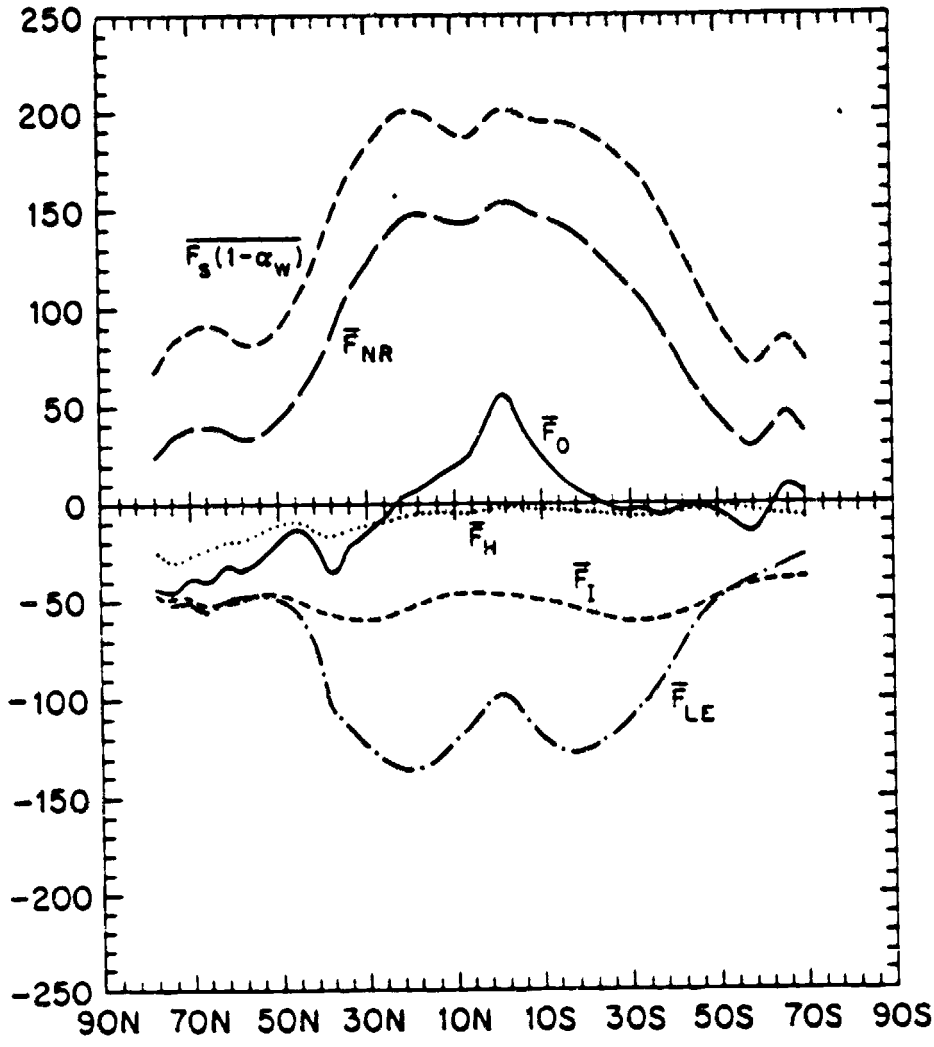

Fig. 1. Meridional profiles of the components of the ice-free ocean annual heat budget (in W m^{-2}). F_{NR} and F_Q stand for net radiative flux and net downward heat flux and the overbar for an average. Other symbols have the same meaning as in text.

Table 2. 10° zonal means of the components of the ice-free ocean annual heat budget (in W m^{-2}). F_O is the net downward heat flux. Other symbols have the same meaning as in text.

	$\overline{F_H}$	$\overline{F_{LE}}$	$\overline{F_I}$	$\overline{F_S(1-\alpha_W)}$	$\overline{F_{NR}}$	$\overline{F_O}$
80N-90N	***	***	***	***	***	***
70N-80N	29	50	46	81	35	-44
60N-70N	23	51	51	89	38	-36
50N-60N	16	48	48	83	35	-29
40N-50N	12	61	51	108	57	-16
30N-40N	14	113	58	160	102	-25
20N-30N	9	131	57	193	136	- 4
10N-20N	4	131	57	195	146	12
0 -10N	4	109	46	191	145	32
10S- 0	2	106	48	199	151	43
20S-10S	3	125	52	194	142	14
30S-20S	6	118	58	181	123	1
40S-30S	6	96	59	157	98	- 4
50S-40S	2	62	53	114	61	- 3
60S-50S	2	43	43	79	36	- 9
70S-60S	5	34	39	80	41	2
80S-70S	6	26	38	74	36	4
90S-80S	***	***	***	***	***	***
GLOBAL	6	98	51	160	109	5

Table 3: Total ocean area (1) and annually averaged ice-free ocean area (2) in 10° latitude belts in units of $10^{12}m^2$.

	(1)	(2)
80N-90N	3.207	0.000
70N-80N	7.074	1.881
60N-70N	4.491	3.512
50N-60N	10.214	9.620
40N-50N	14.065	13.955
30N-40N	18.796	18.796
20N-30N	24.083	24.083
10N-20N	30.743	30.743
0 -10N	34.837	34.837
10S- 0	34.338	34.338
20S-10S	33.356	33.356
30S-20S	30.634	30.634
40S-30S	31.991	31.991
50S-40S	30.735	30.735
60S-50S	25.424	23.982
70S-60S	17.236	7.364
80S-70S	4.126	0.102
90S-80S	0.000	0.000
GLOBAL	355.351	329.931

4. Summary

In this study the global ocean heat budget was estimated using bulk formulas and available climatologies of surface observations. The objective approach to the analysis renders such a global study simple and easy to update if additional data or improved formulas become available.

Recent developments in boundary layer theory were used for calculating the boundary fluxes of sensible and latent heat. This method leads to lower estimates of the fluxes when compared with previous studies, but an approximate global balance was achieved.

The bulk radiative formulas used were those suggested by Budyko and his colleagues during the preparation of their global study (Budyko, 1963). These have been seriously criticized in the open literature but none of the suggested alternatives have been subjected to a test of achieving a global balance against reasonable values of the turbulent fluxes. We believe that the radiative fluxes in this atlas are reasonable and that the next advance in determining the surface heat balance will not come from the improvement of the bulk radiative formulas for surface observations. Rather it remains the task of future studies to offer a direct and more accurate estimate of these fluxes through the full utilization of satellite information.

The fields of basic variables and heat budget components constructed during this study provide an easily accessible data source for scientists interested in boundary conditions for atmospheric and oceanic general circulations models or in evaluating model performance.

The complete data set presented in this report is available on a computer compatible tape from the Climatic Research Institute, Oregon State University, Corvallis, Oregon, 97331.

ACKNOWLEDGEMENTS

We would like to acknowledge Dr. Y.-J. Han for his review of this report and helpful discussions during the various stages of this project. We would also like to acknowledge the participation of Dr. R.W. Reynolds in developing the algorithms for calculation of the bulk aerodynamic coefficients and S.-W. Lee for his help in computing the solar radiation fields. All computations were performed at the Climatic Research Institute and the task was made much easier by the continuing help and support from the Institute staff: R. Mobley, W. McKie, S.-M. Heh and T. Spoering. Thanks also go to D. Ramey for typing the manuscript.

This research was supported primarily by two grants from the National Aeronautic and Space Administration (NSG 5308 and NSG 5353). Partial funding was also provided by the National Science Foundation under Grant ATM-8001702.

REFERENCES

Alexander, R.C., and R.L. Mobley, 1976: Monthly averaged sea surface temperatures and ice-pack limits on a 1° global grid. *Mon. Wea. Rev., 104*, 143-148.

Barnes, S.L., 1964: A technique for maximizing details in numerical weather map analysis. *J. Appl. Meteor., 3*, 396-409.

Berliand, M.E., and T.G. Berliand, 1952: Determining the net long-wave radiation of the Earth with consideration of the effect of cloudiness. *Isv. Akad. Nauk. SSSR Ser. Geofiz*, No. 1.

Berliand, T.G., 1960: Methods of climatological computation of total incoming solar radiation. *Meteorol. Gidrol., 6*, 9-12. MGA 12:1486.

Berliand, T.G., and L.A. Strokina, 1980: *Global Distribution of the Total Amount of Cloudiness*. Hydrometeorology Publishing House, Leningrad, 71 pp. (in Russian).

Brunt, D., 1932: Notes on radiation in the atmosphere. *Quart. J. R. Met. Soc., 58*, 389-420.

Budyko, M.I., Ed., 1963: *Atlas of the Heat Balance of the Earth*. Akad. Nauk, SSSR, Prezidum. Mezhduvedomstvennyi Geofiz. Komitet., 69 pp. [Also, *Guide to the Atlas of the Heat Balance of the Earth*, Transl. by I.A. Donehoo, U.S. Weather Bureau, WB/T-106, Washington, D.C.].

Budyko, M.I., 1974: *Climate and Life*. Academic Press, 508 pp.

Bunker, A.F., 1976: Computations of surface energy flux and annual air-sea interaction cycle of the North Atlantic Ocean. *Mon. Wea. Rev., 104*, 1122-1140.

Bunker, A.F., and R.A. Goldsmith, 1979: Archived Time-Series of Atlantic Ocean Meteorological Variables and Surface Fluxes. WHOI-79-3, Woods Hole Oceanographic Institution, Woods Hole, Mass., 28 pp.

Bunker, A.F., and L.V. Worthington, 1976: Energy exchange charts of the North Atlantic Ocean. *Bull. Amer. Meteor. Soc., 57*, 670-678.

Esbensen, S.K., and R.W. Reynolds, 1981: Estimating monthly averaged air-sea transfers of heat and momentum using the bulk aerodynamic method. *J. Phys. Oceanogr., 11*, 457-465.

Hastenrath, S., 1980: Heat budget of tropical ocean and atmosphere. *J. Phys. Oceanogr., 10*, 159-170.

Hastenrath, S., and P.J. Lamb, 1977: *Climatic Atlas of the Tropical Atlantic and Eastern Pacific Oceans*. University of Wisconsin Press, 105 pp.

Hastenrath, S., and P.J. Lamb, 1978: *Heat Budget Atlas of the Tropical Atlantic and Eastern Pacific Oceans*. University of Wisconsin Press, 104 pp.

Hastenrath, S., and P.J. Lamb, 1979: *Climatic Atlas of the Indian Ocean. Part 1. Surface Circulation and Climate. Part 2. The Oceanic Heat Budget*. University of Wisconsin Press, 104 pp.

Kondratyev, K. Ya., 1969: *Radiation in the atmosphere*. Academic Press, 912 pp.

Kukla, G., and D. Robinson, 1980: Annual cycle of surface albedo. *Mon. Wea. Rev., 108*, 56-67.

List, R.J., 1958: *Smithsonian Meteorological Tables*, 6th ed., Smithsonian Institution Press, Washington, D.C., 527 pp.

Liu, W.T., K.B. Katsaros and J.A. Businger, 1979: Bulk parameterization of air-sea exchange of heat and water vapor including molecular constraints at the interface. *J. Atmos. Sci., 36*, 1722-1735.

Miller, D.B., and R.G. Feddes, 1971: *Global Atlas of Relative Cloud Cover, 1967-70, Based on Photographic Signals from Meteorological Satellites*, U.S. Dept. of Comm., NOAA and U.S. Air Force, Air Weather Service (MAC), ETAC, Washington, D.C.

Oort, A.H., and T.H. Vonder Haar, 1976: On the observed annual cycle in the ocean-atmosphere het balance over the Northern Hemisphere. *J. Phys. Oceanogr., 6*, 781-800.

Payne, R.E., 1972: Albedo of the sea surface. *J. Atmos. Sci., 29*, 959-970.

Reed, R.K., 1977: On estimating insolation over the ocean. *J. Phys. Oceanogr., 7*, 482-485.

Roll, H.U., 1965: *Physics of the Marine Atmosphere*. Academic Press, New York, 426 pp. (Chap. 2).

Schlesinger, M.E., and W.L. Gates, 1979: Numerical simulation of the January and July global climate with the OSU two-level atmospheric general circulation model. Report No. 9, Climatic Research Institute, Oregon State University, Corvallis, 102 pp.

Schutz, C., and W.L. Gates, 1971: *Global Climatic Data for Surface, 800 mb, 400 mb: January*. R-915-ARPA, The Rand Corporation, Santa Monica, CA, 173 pp.

Schutz, C., and W.L. Gates, 1972: *Global Climatic Data for Surface, 800 mb, 400 mb: July.* R-1029-ARPA, The Rand Corporation, Santa Monica, CA, 180 pp.

Schutz, C., and W.L. Gates, 1973: *Global Climatic Data for Surface, 800 mb, 400 mb: April.* R-1317-ARPA, The Rand Corporation, Santa Monica, CA, 190 pp.

Schutz, C., and W.L. Gates, 1974: *Global Climatic Data for Surface, 800 mb, 400 mb: October.* R-1425-ARPA, The Rand Corporation, Santa Monica, CA, 192 pp.

Weare, B.C., and P.T. Strub, 1981: The significance of sampling biases on calculated monthly mean oceanic surface heat fluxes. *Tellus, 33,* 211-224.

Weare, B.C., P.T. Strub and M.D. Samuel, 1981: Annual mean surface heat fluxes in the Tropical Pacific Ocean. *J. Phys. Oceanogr., 11,* 705-717.

ATLAS OF THE HEAT BUDGET
OF THE ICE-FREE GLOBAL OCEAN:
PART I: BASIC SURFACE VARIABLES

THE BASIC VARIABLES(*)

	Chart Number												
	J	F	M	A	M	J	J	A	S	O	N	D	ANN
Surface Wind Speed	1.1	1.2	1.3	1.4	1.5	1.6	1.7	1.8	1.9	1.10	1.11	1.12	1.13
Sea Surface Temperature	1.14	1.15	1.16	1.17	1.18	1.19	1.20	1.21	1.22	1.23	1.24	1.25	1.26
Sea - Air Temperature Difference	1.27	1.28	1.29	1.30	1.31	1.32	1.33	1.34	1.35	1.36	1.37	1.38	1.39
Air Temperature	1.40	1.41	1.42	1.43	1.44	1.45	1.46	1.47	1.48	1.49	1.50	1.51	1.52
Air Specific Humidity	1.53	1.54	1.55	1.56	1.57	1.58	1.59	1.60	1.61	1.62	1.63	1.64	1.65
Sea - Air Specific Humidity Difference	1.66	1.67	1.68	1.69	1.70	1.71	1.72	1.73	1.74	1.75	1.76	1.77	1.78
Cloudiness	1.79	1.80	1.81	1.82	1.83	1.84	1.85	1.86	1.87	1.88	1.89	1.90	1.91
Sea Level Pressure	1.92	1.93	1.94	1.95	1.96	1.97	1.98	1.99	1.100	1.101	1.102	1.103	1.104

(*)Stippled areas are where the data density indicator is ≤ 2.7 (500 observations). The monthly sea-ice boundary is shown by a heavy line enclosing the shaded areas.

SURFACE WIND SPEED

1.1 January mean surface wind speed (m sec^{-1})

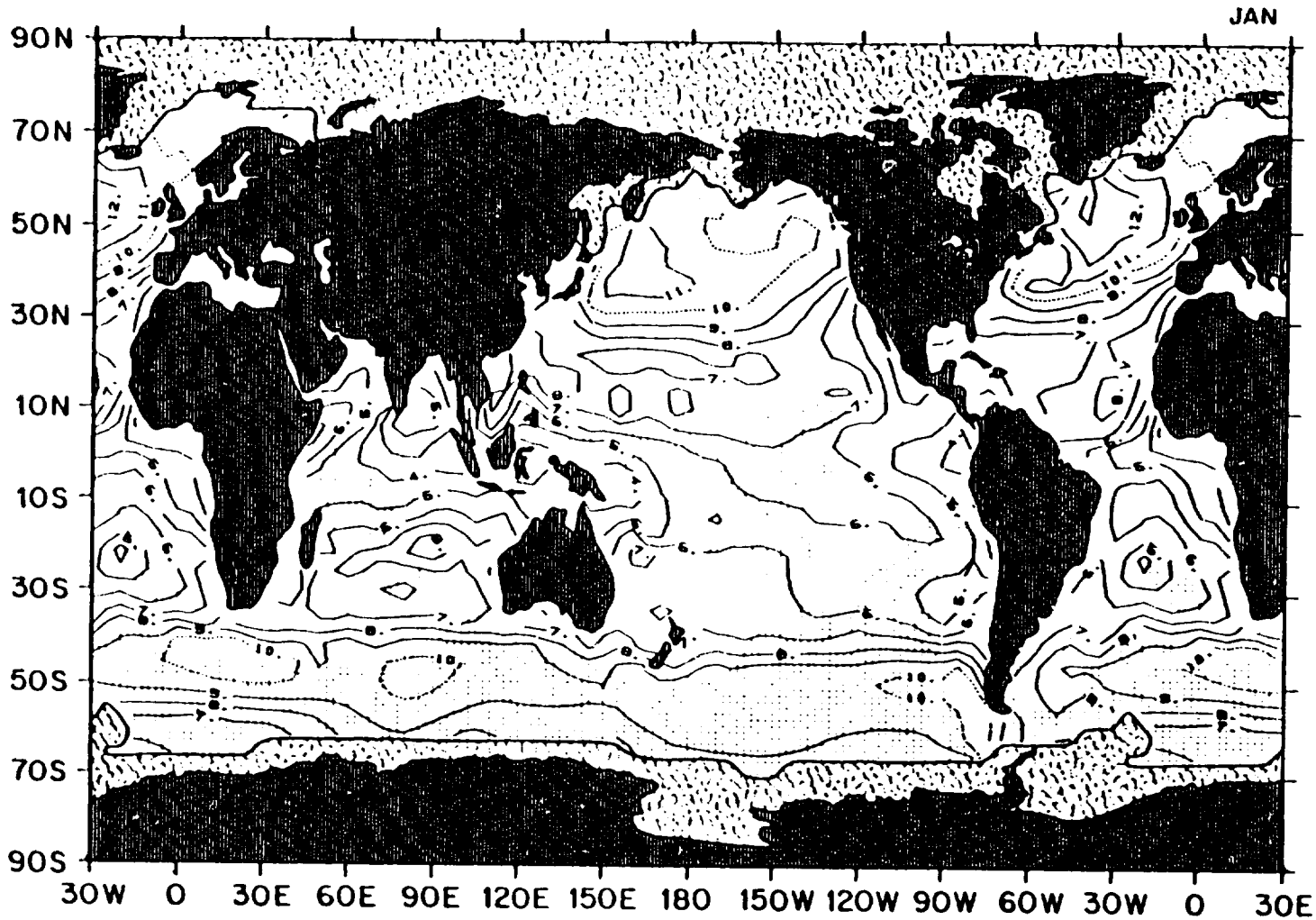

1.2 February mean surface wind speed (m sec^{-1})

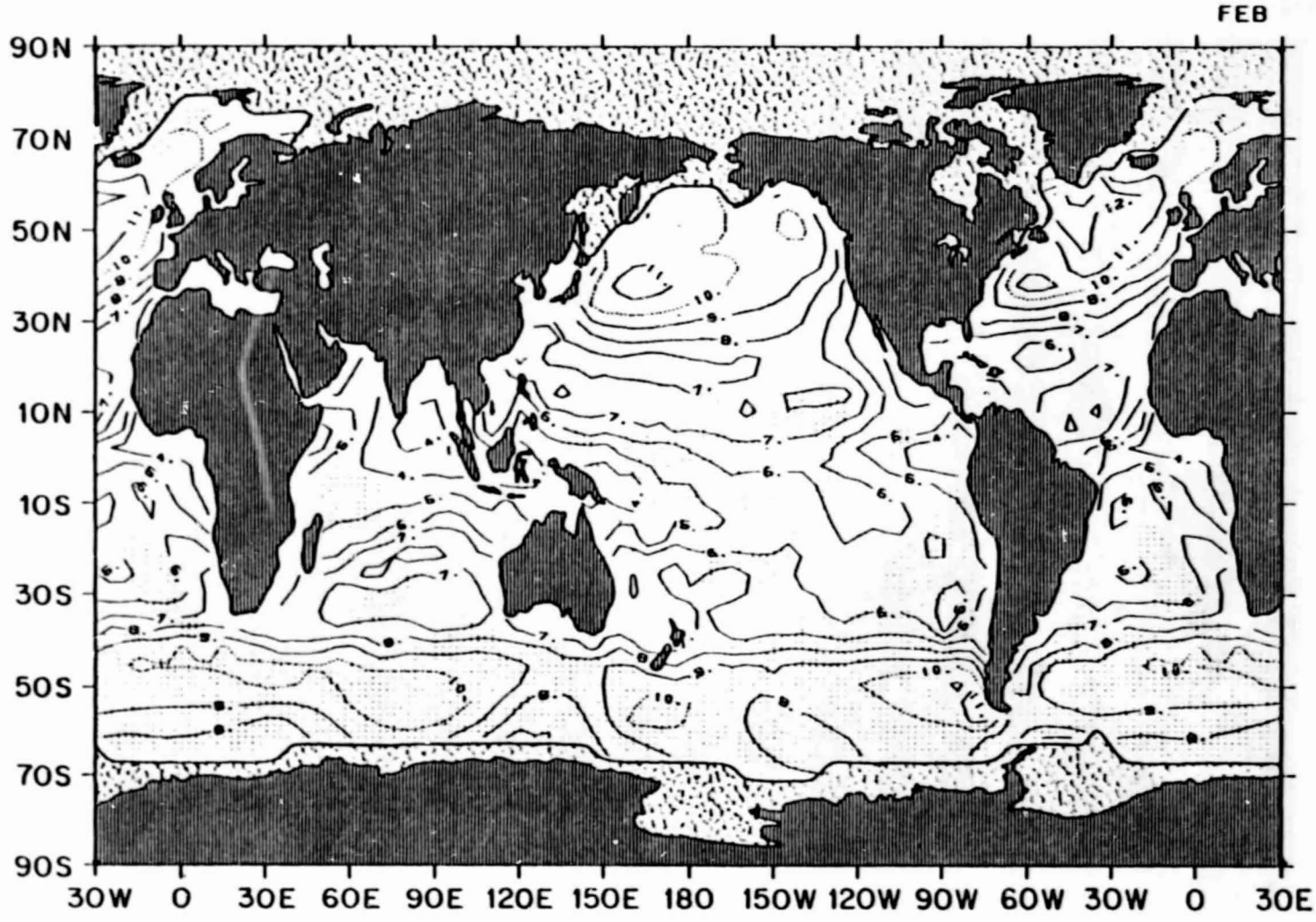

1.3 March mean surface wind speed (m sec^{-1})

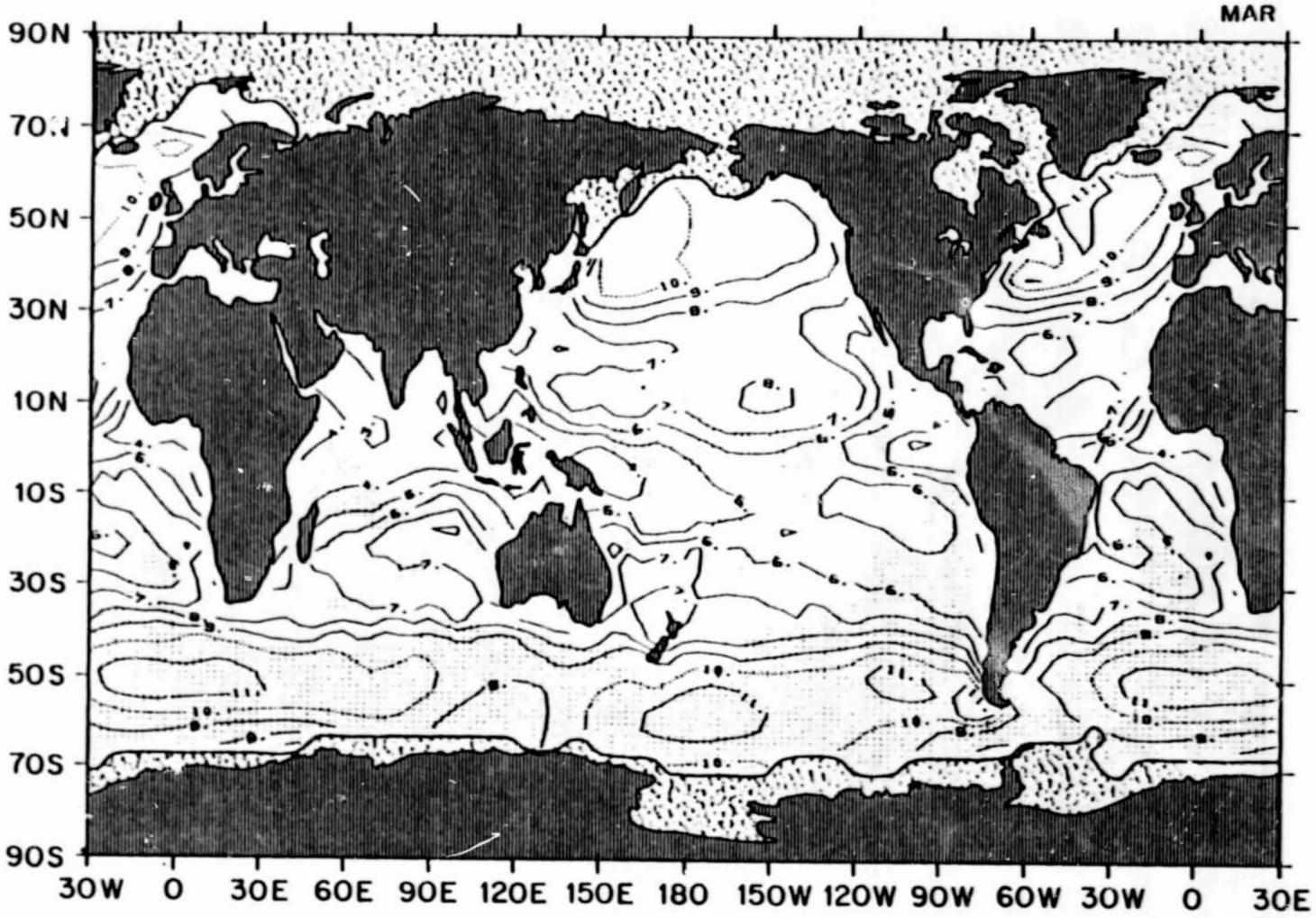

1.4 April mean surface wind speed (m sec^{-1})

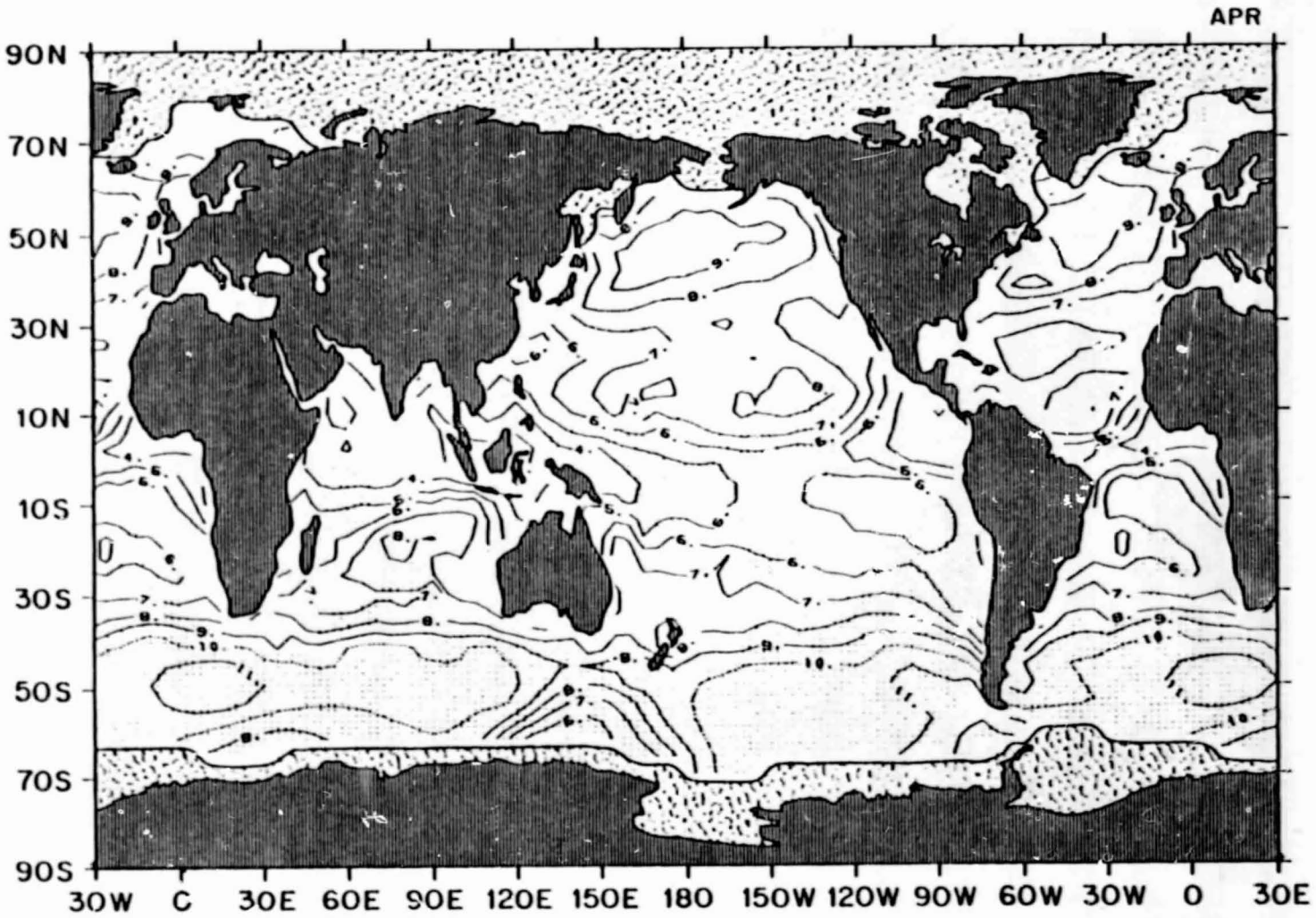

1.5 May mean surface wind speed (m sec^{-1})

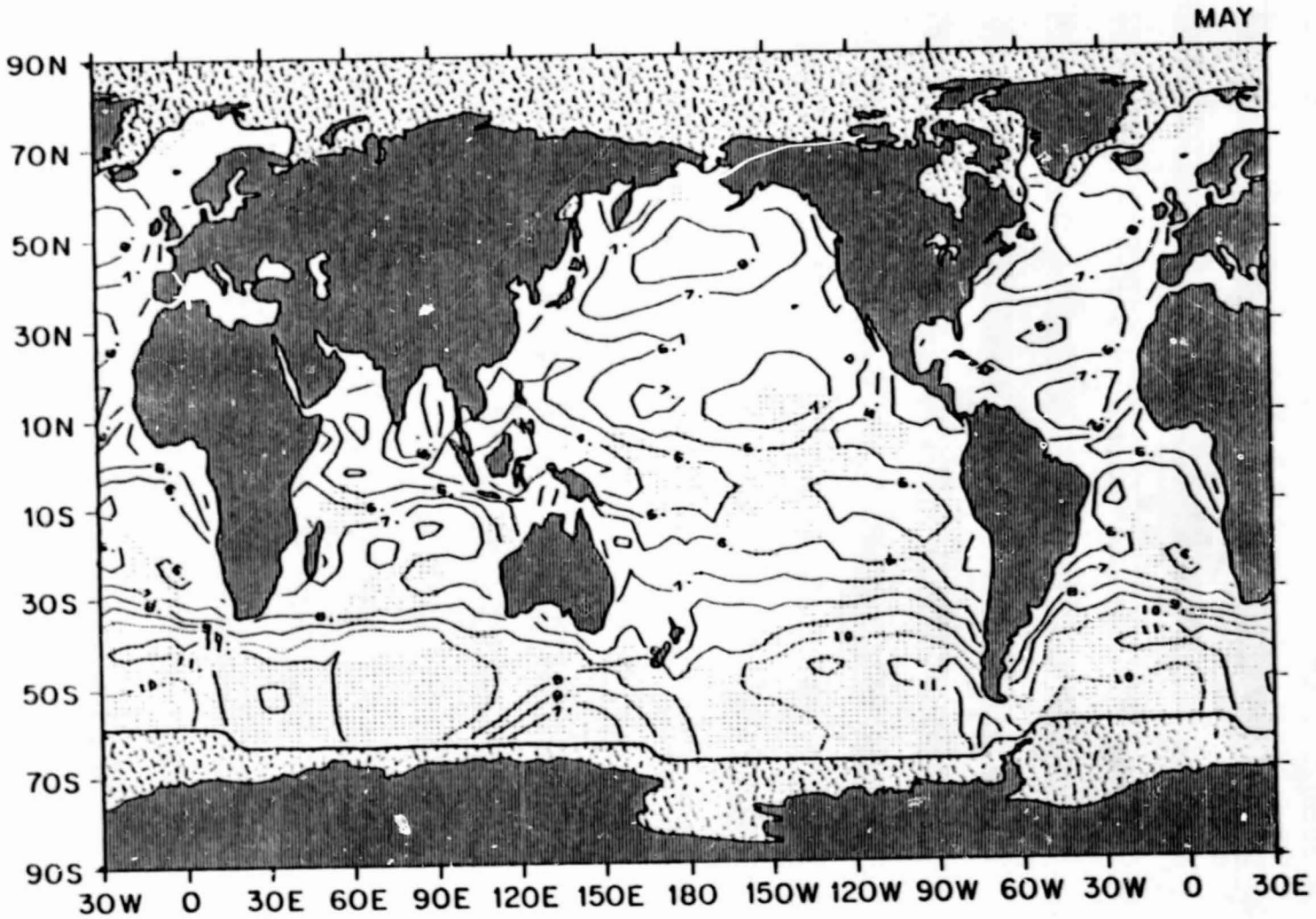

1.6 June mean surface wind speed (m sec^{-1})

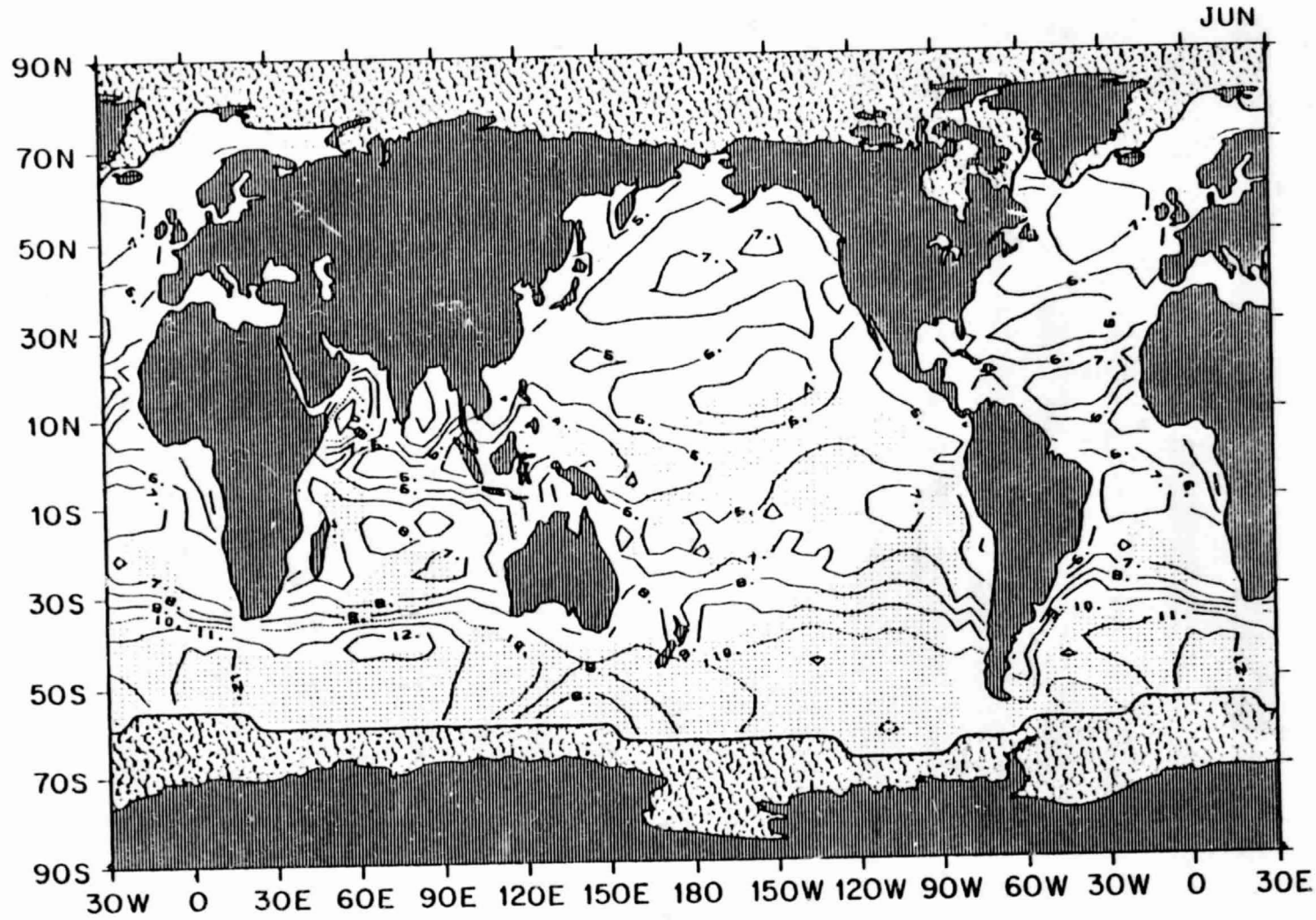

1.7 July mean surface wind speed (m sec^{-1})

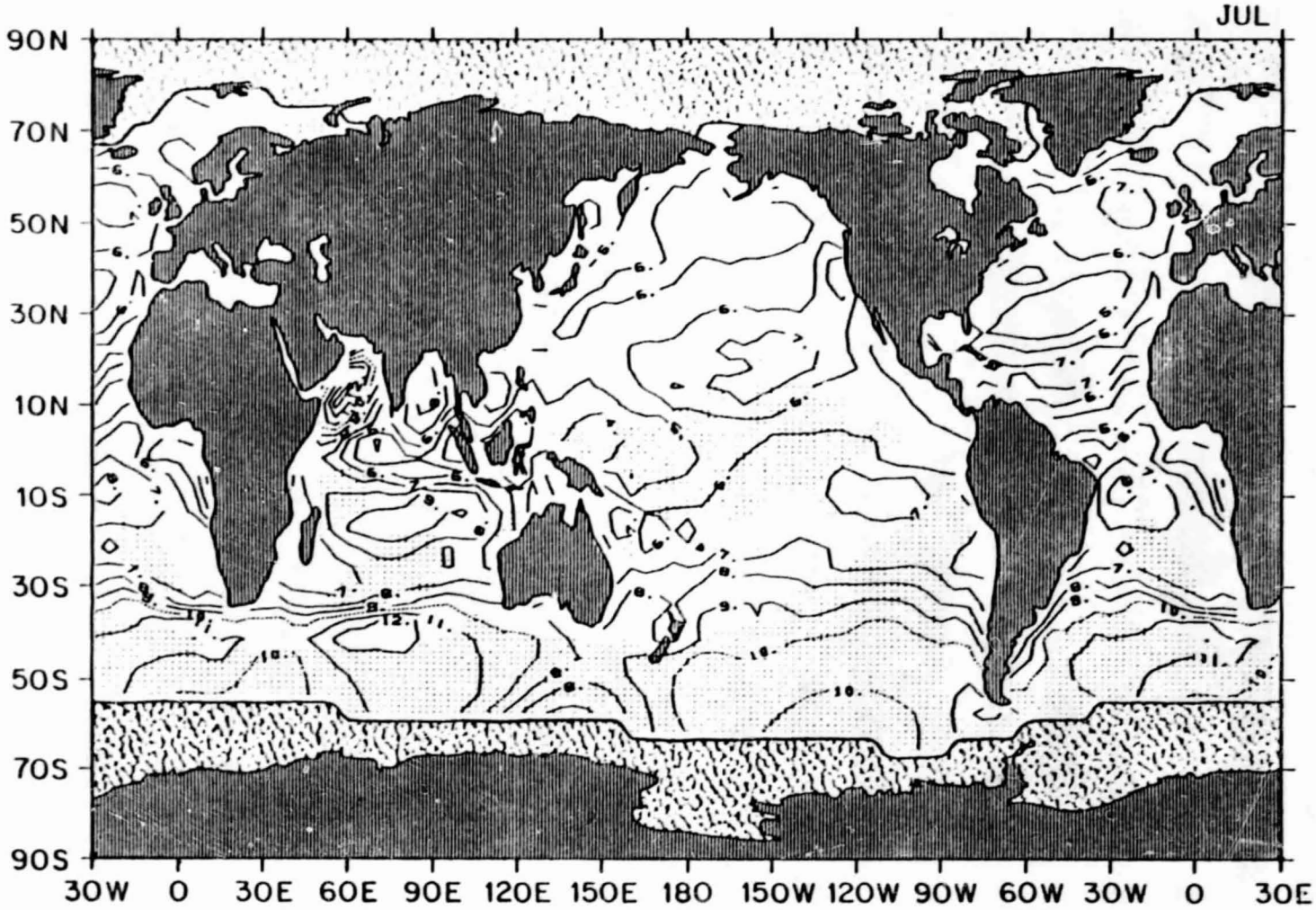

1.8 August mean surface wind speed (m sec^{-1})

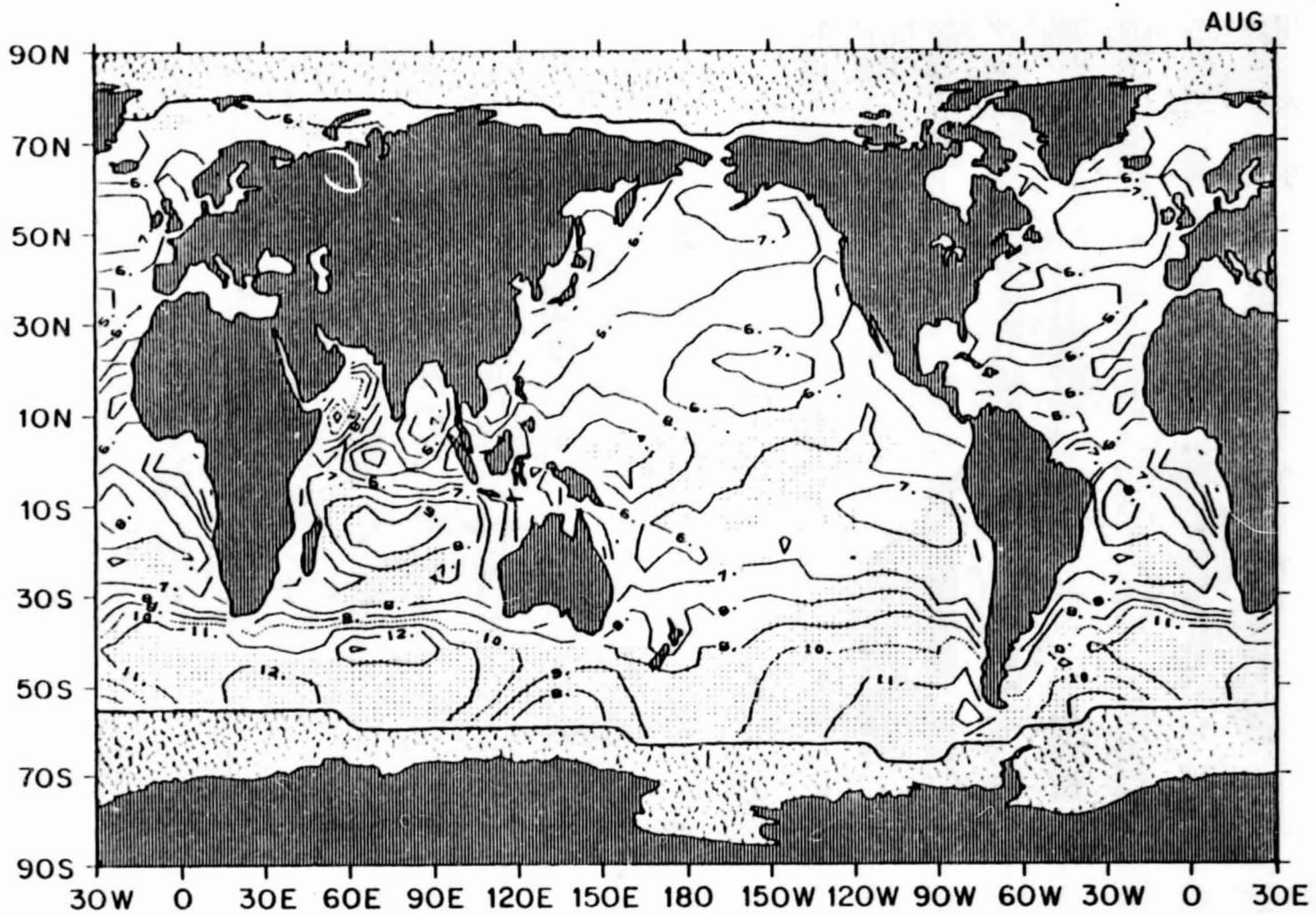

1.9 September mean surface wind speed (m sec^{-1})

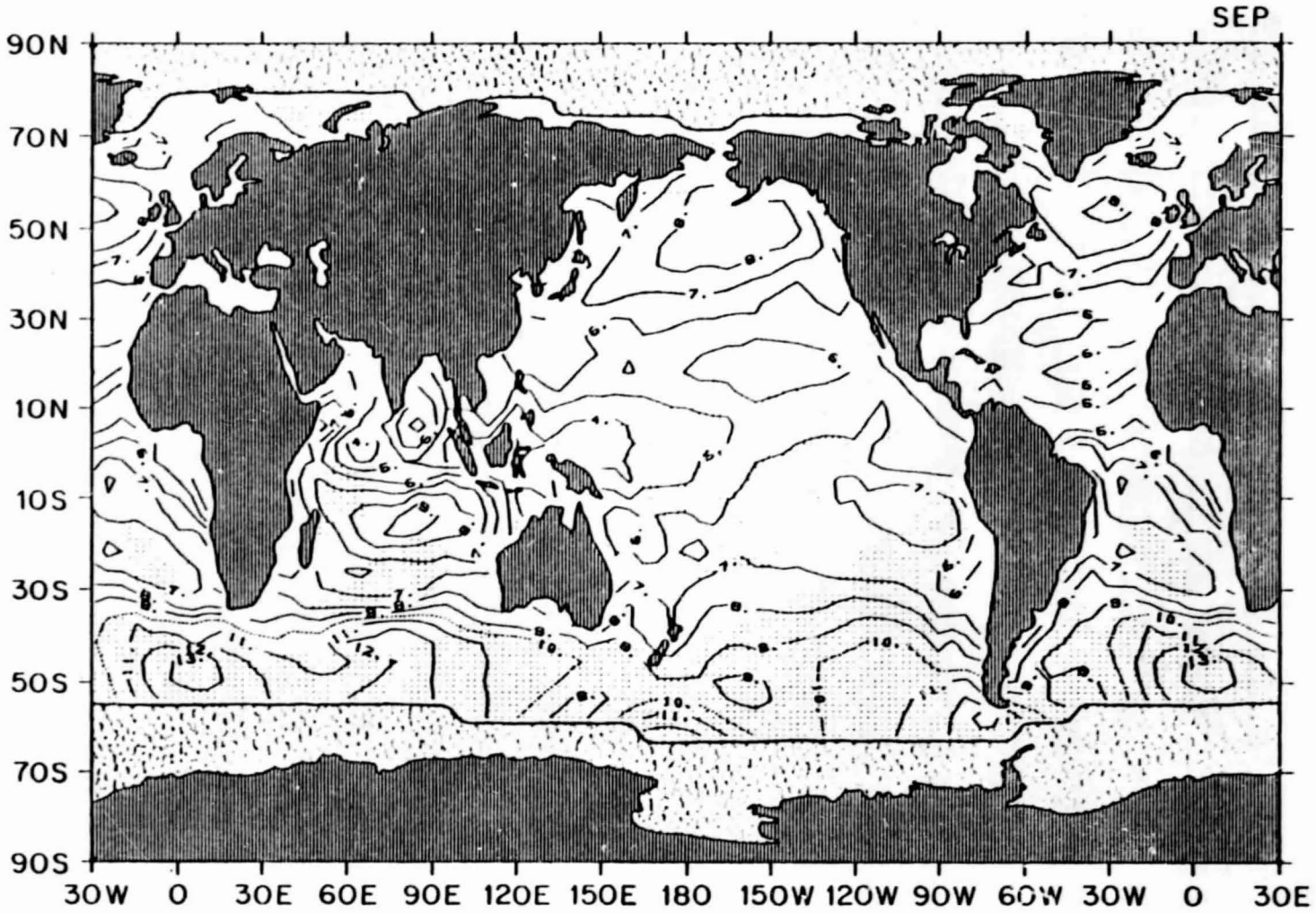

1.10 October mean surface wind speed (m sec^{-1})

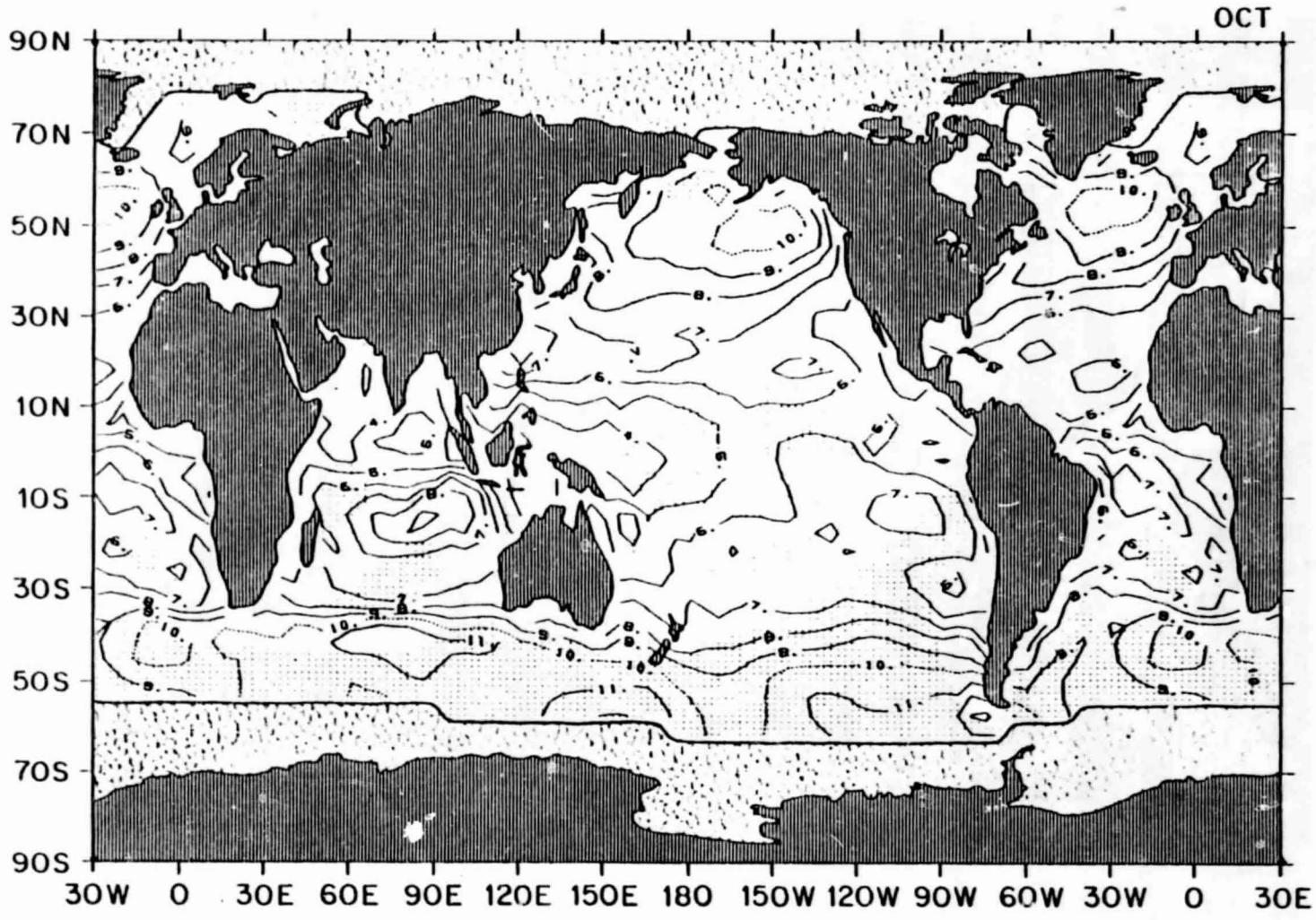

1.11 November mean surface wind speed (m sec^{-1})

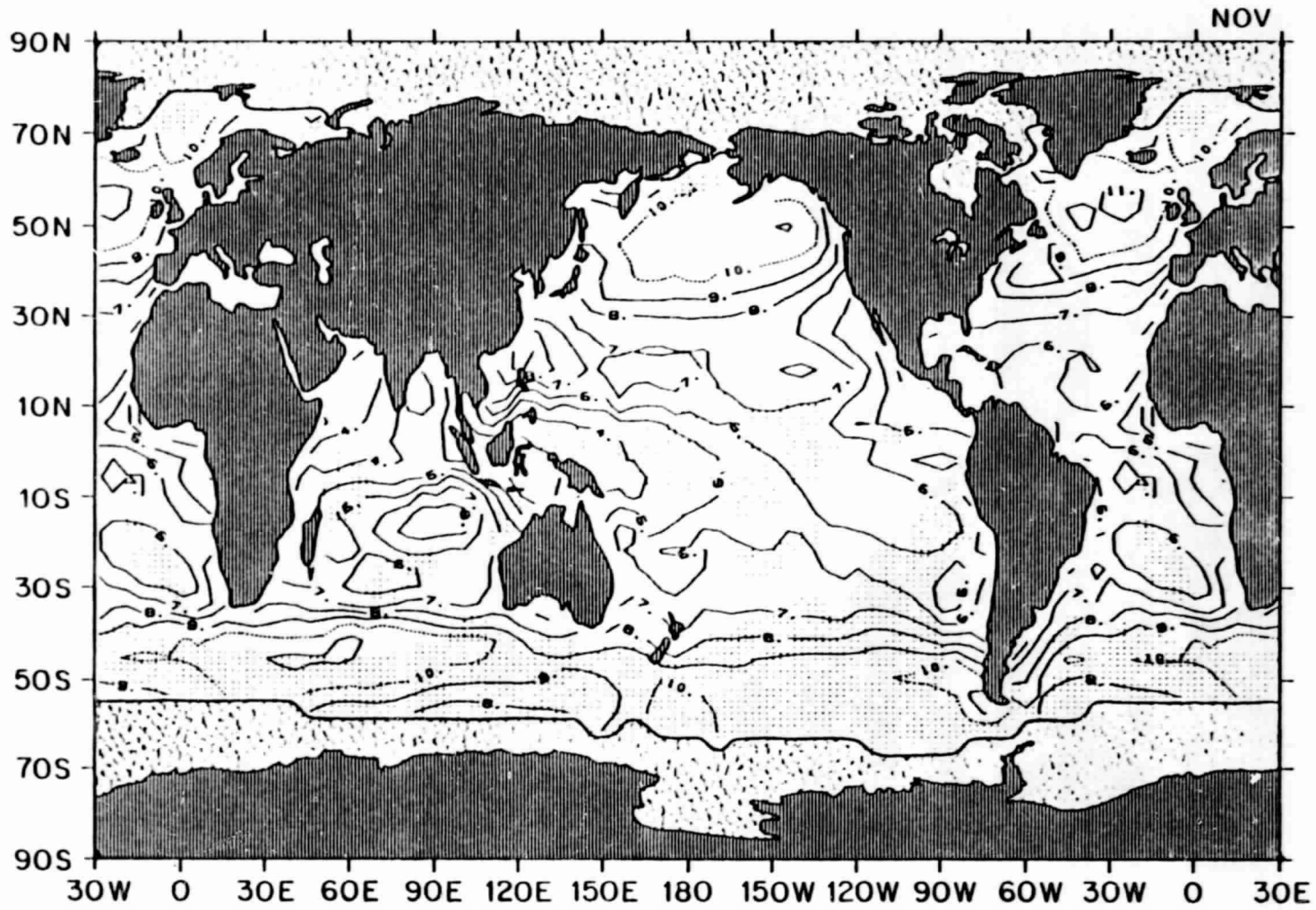

1.12 December mean surface wind speed (m sec^{-1})

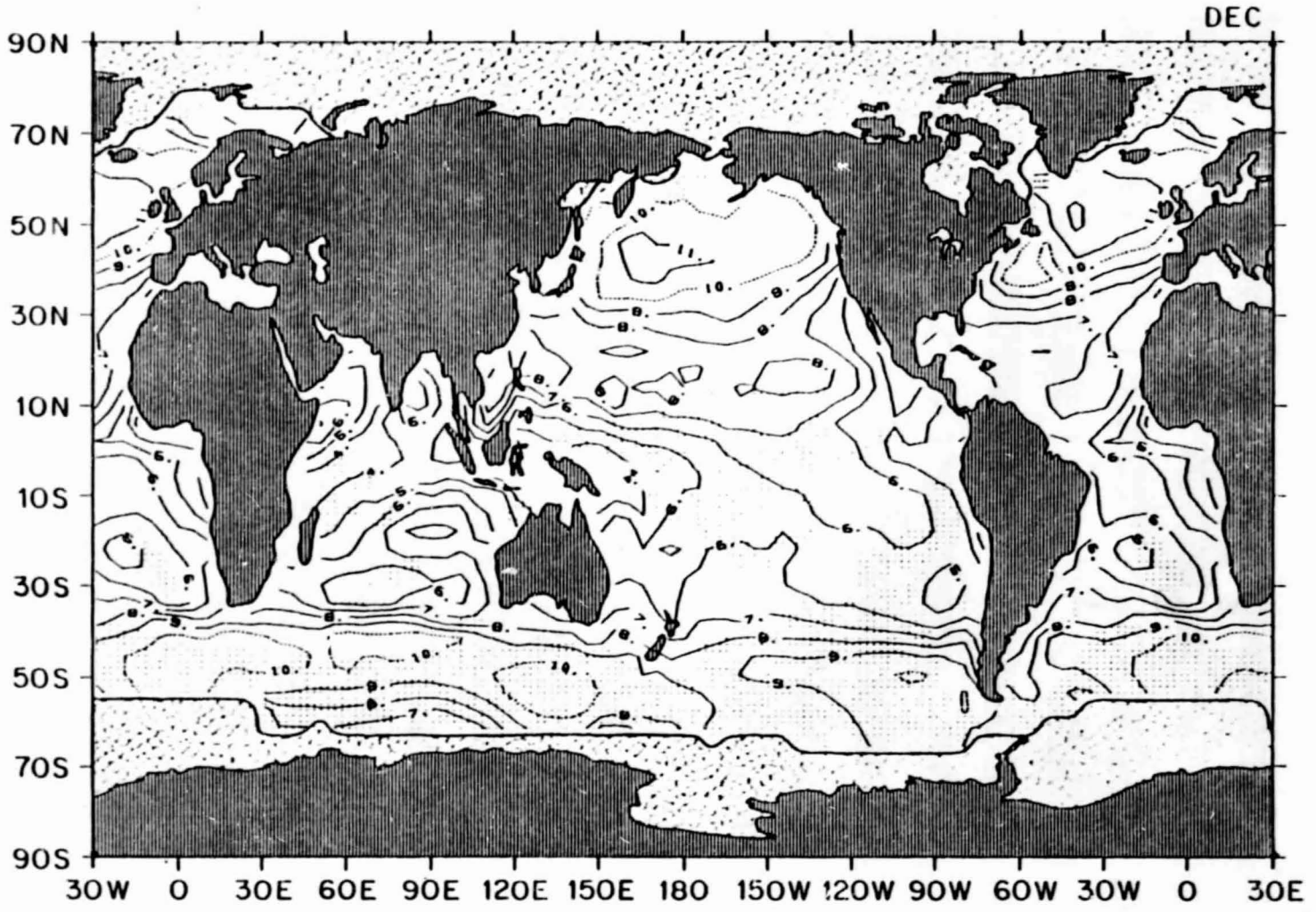

1.13 Annual mean surface wind speed (m sec-1)

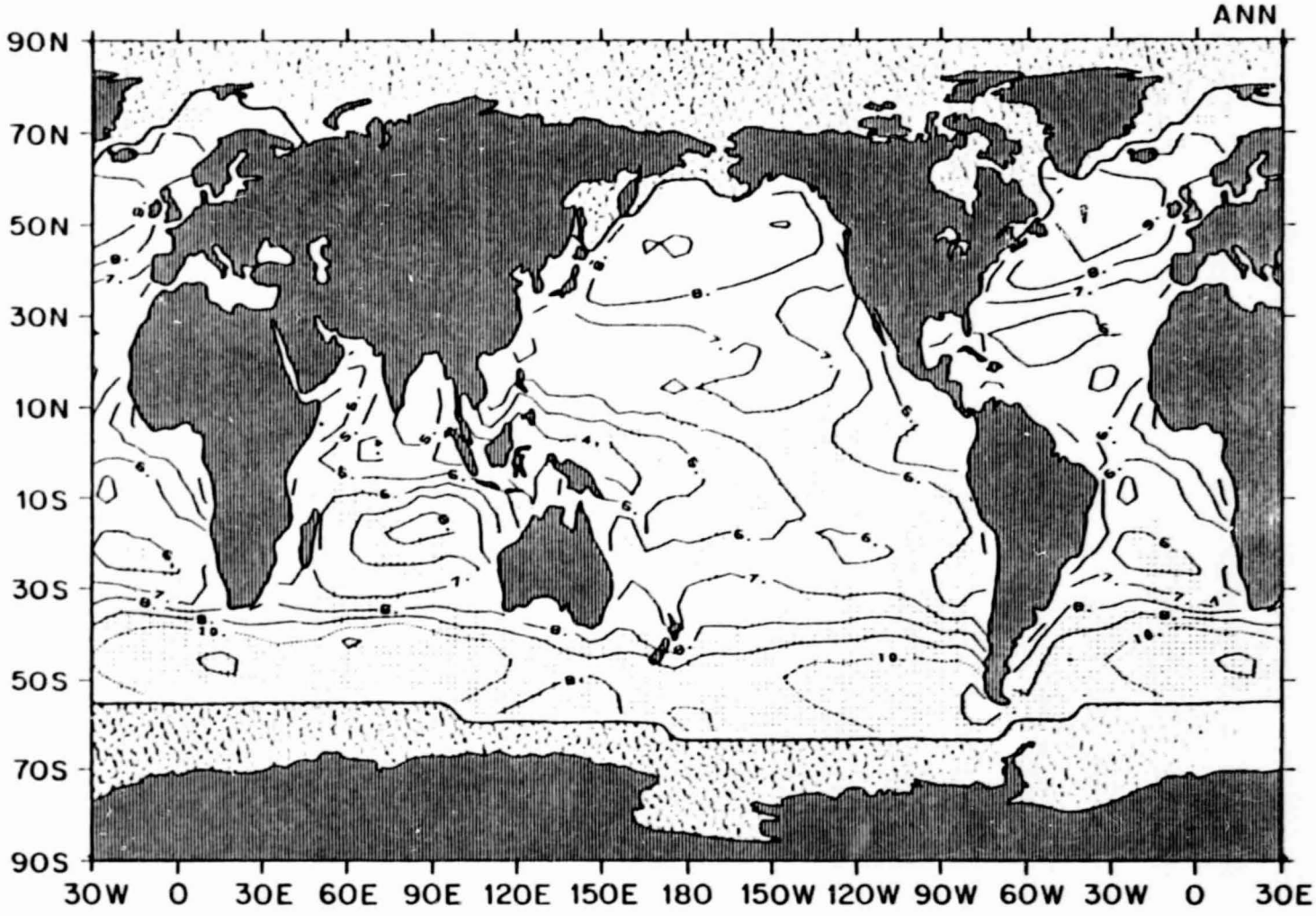

SEA-SURFACE TEMPERATURE

1.14 January mean sea-surface temperature (°C)

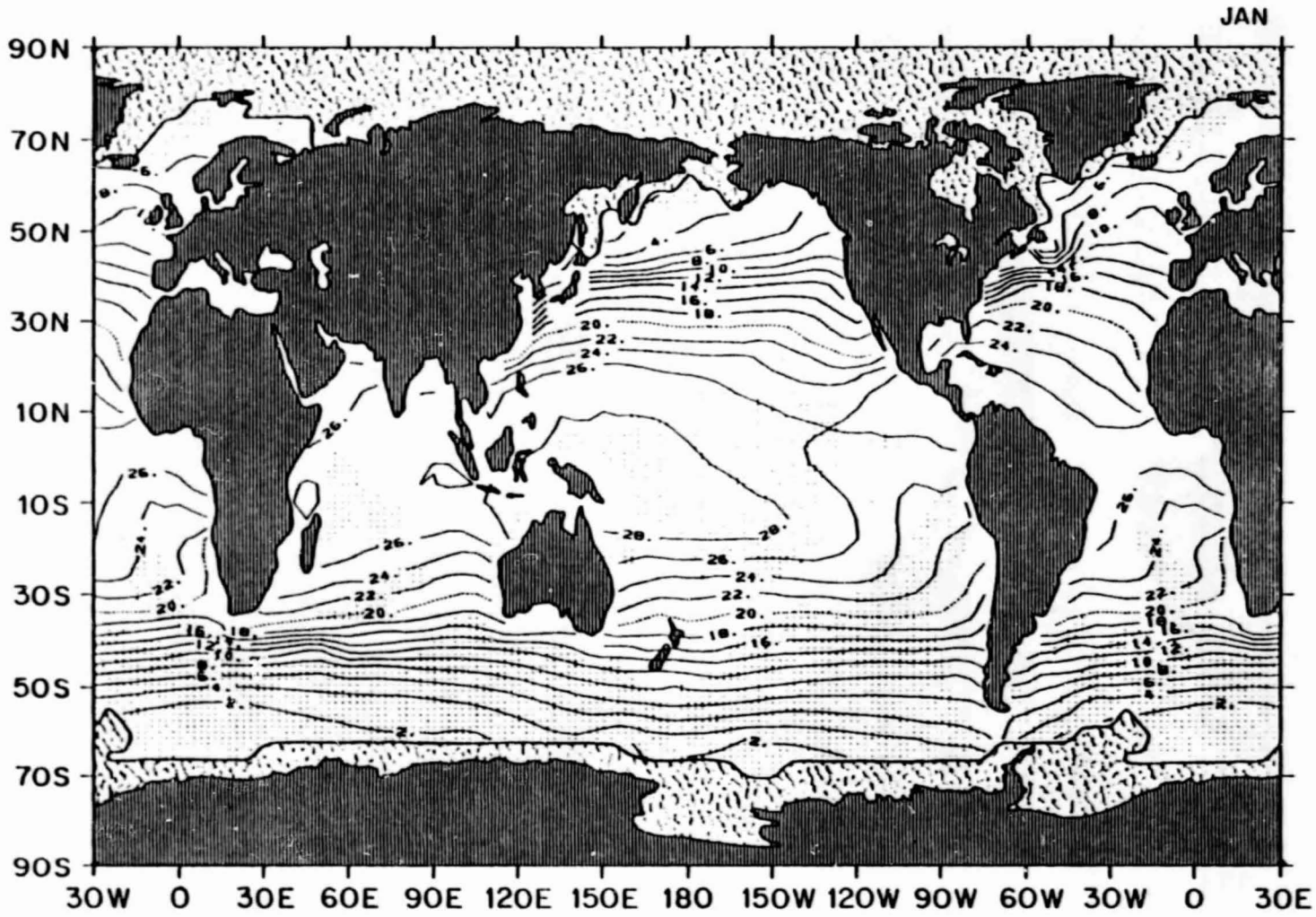

1.15 February mean sea-surface temperature (°C)

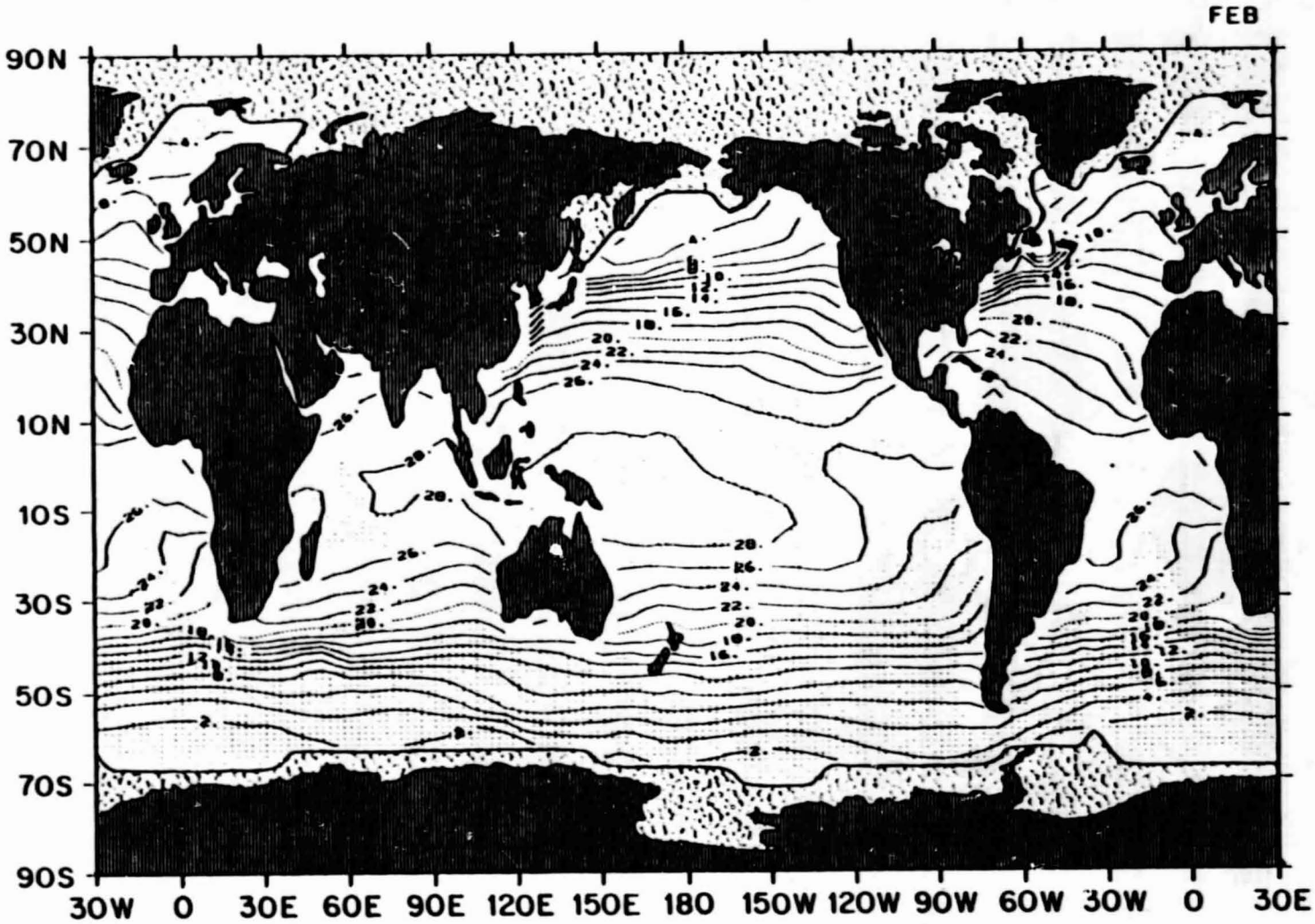

1.16 March mean sea-surface temperature (°C)

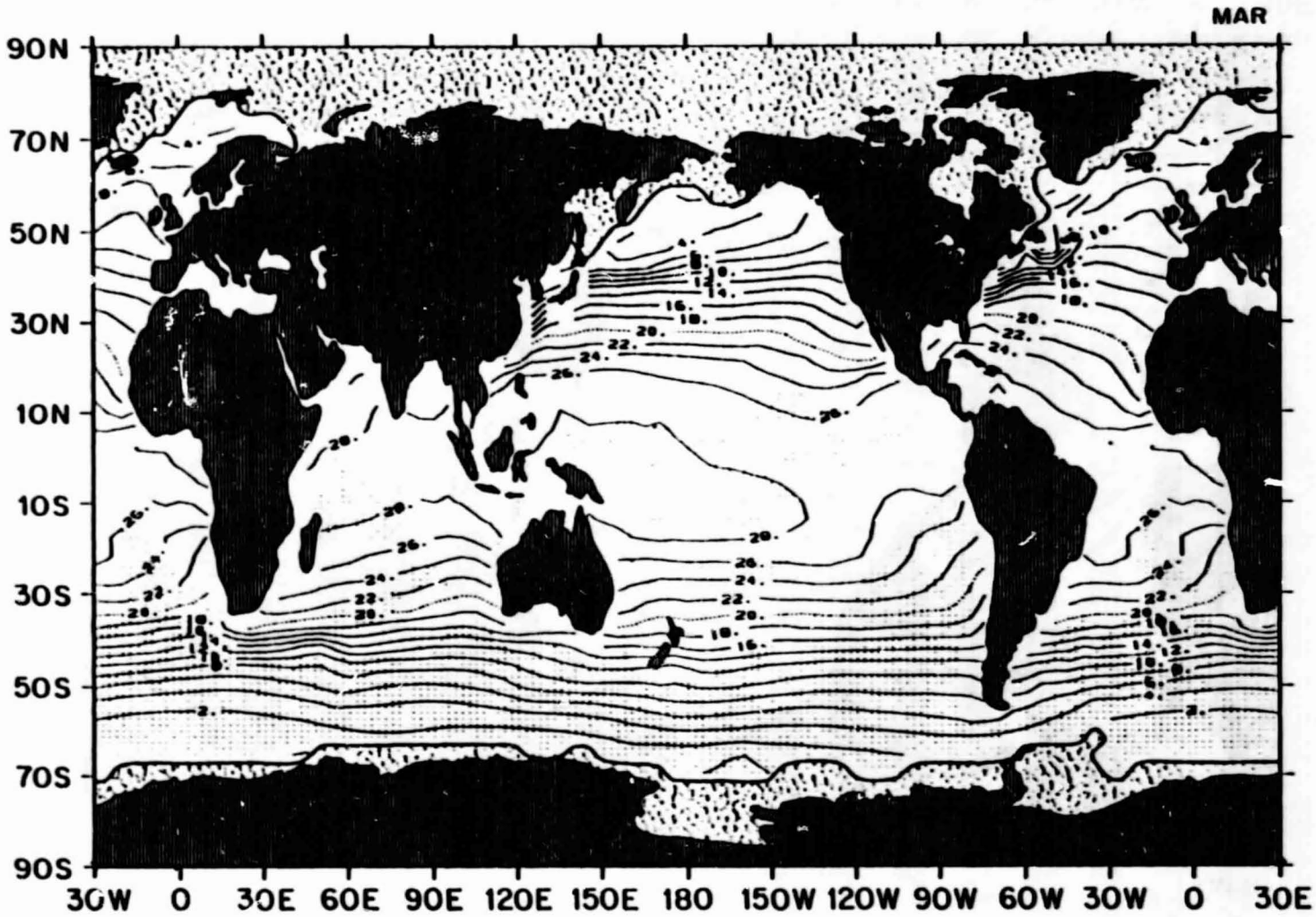

1.17 April mean sea-surface temperature (°C)

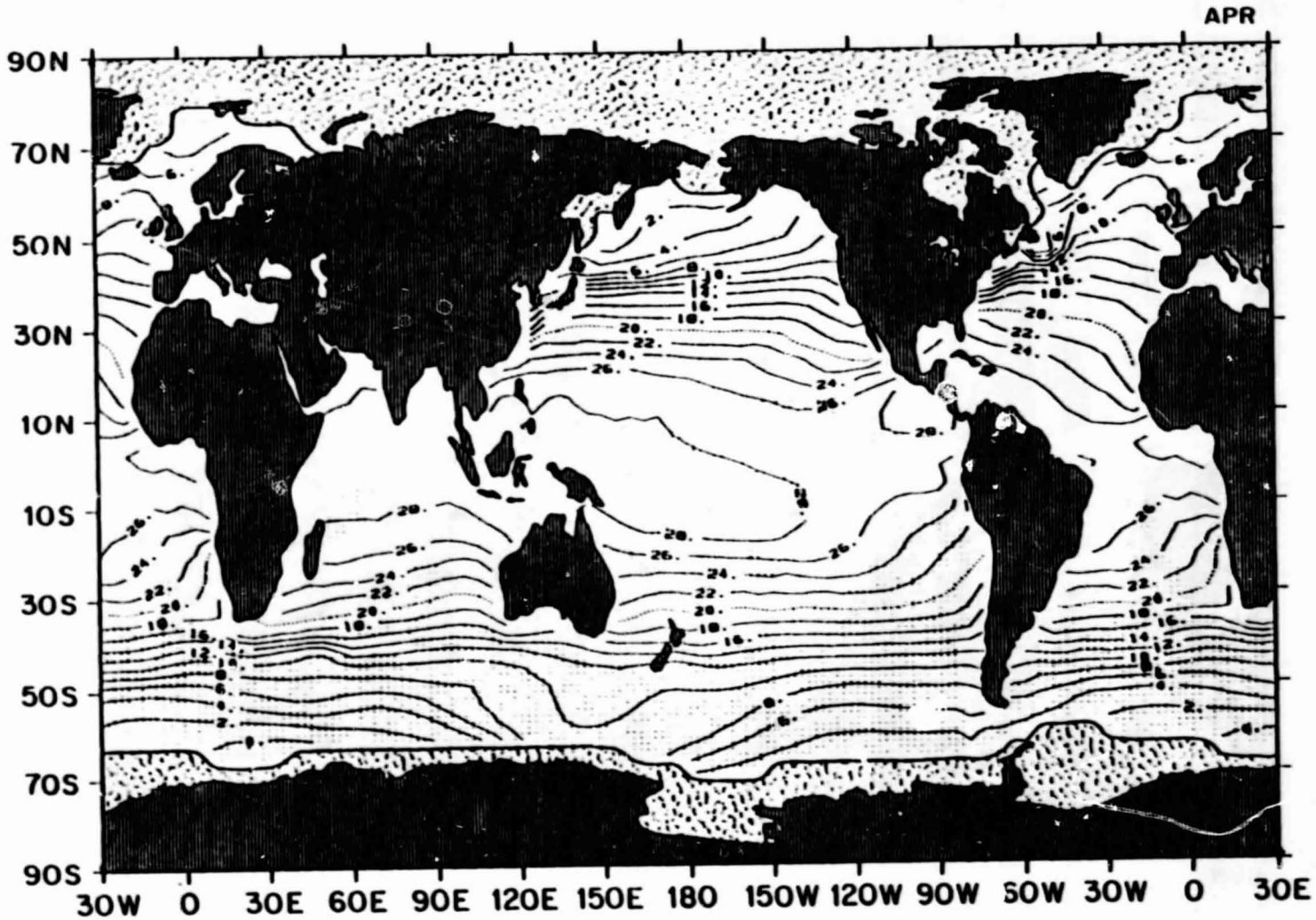

1.18 May mean sea-surface temperature (°C)

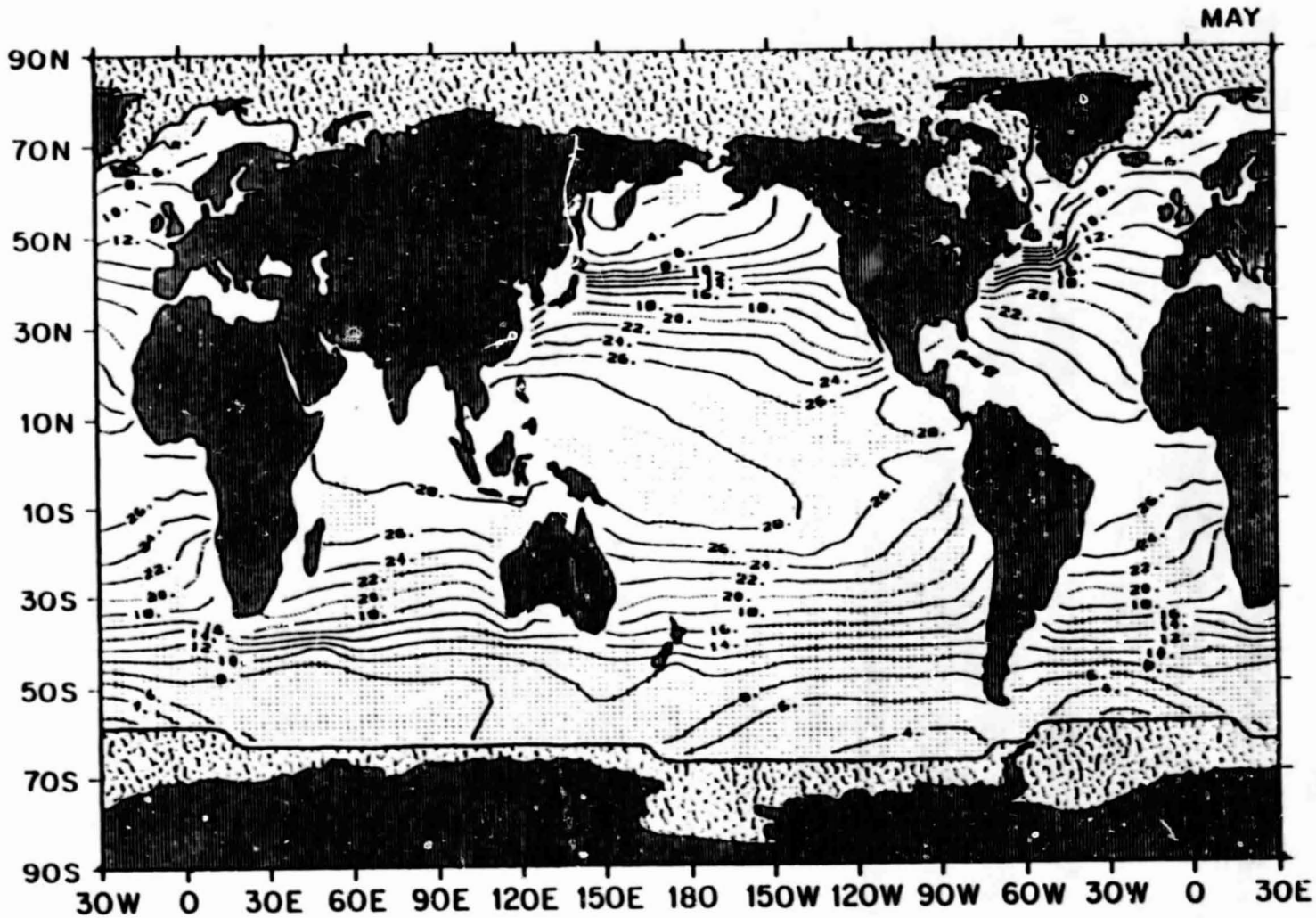

1.19 June mean sea-surface temperature (°C)

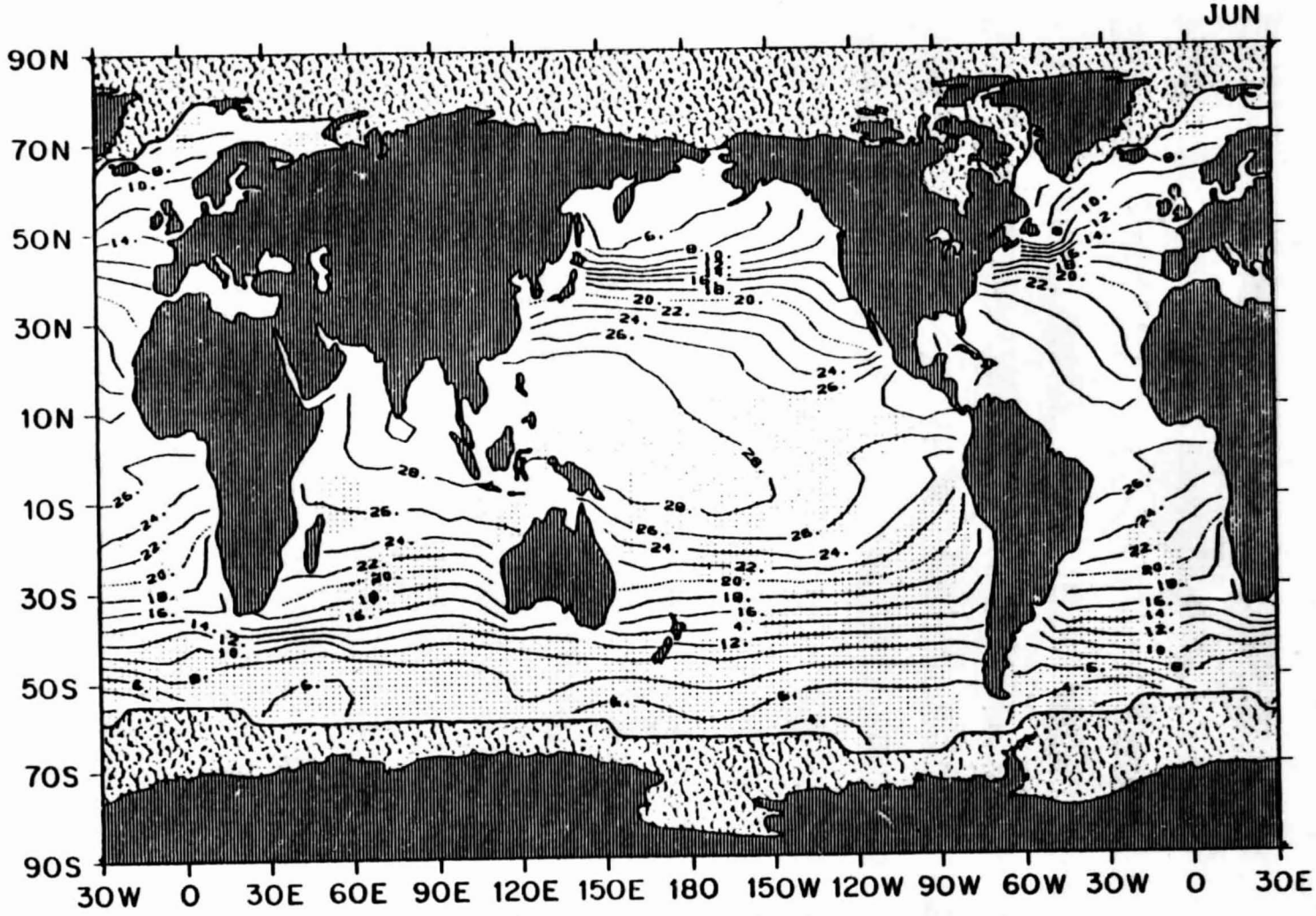

1.20 July mean sea-surface temperature (°C)

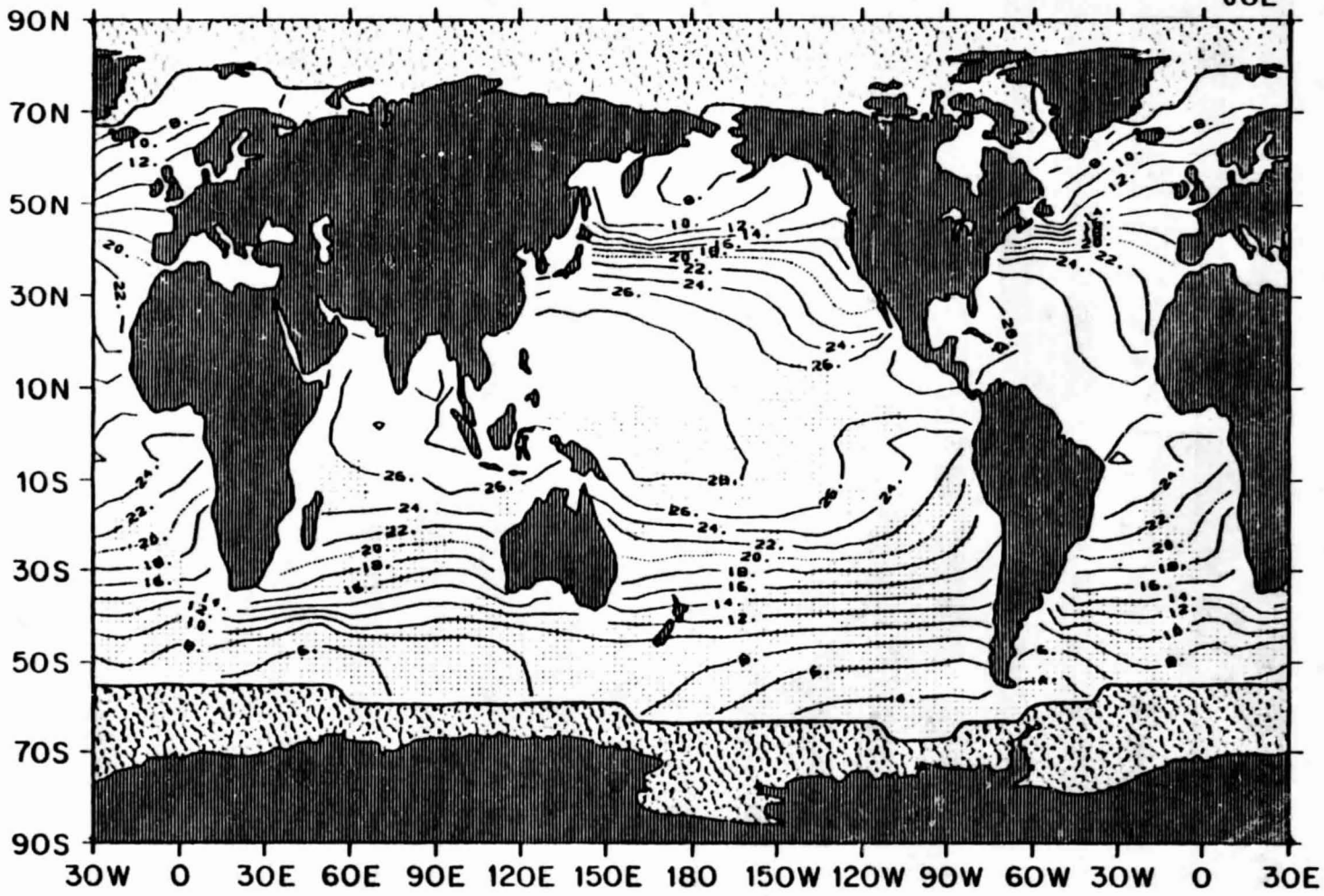

1.21 August mean sea-surface temperature (°C)

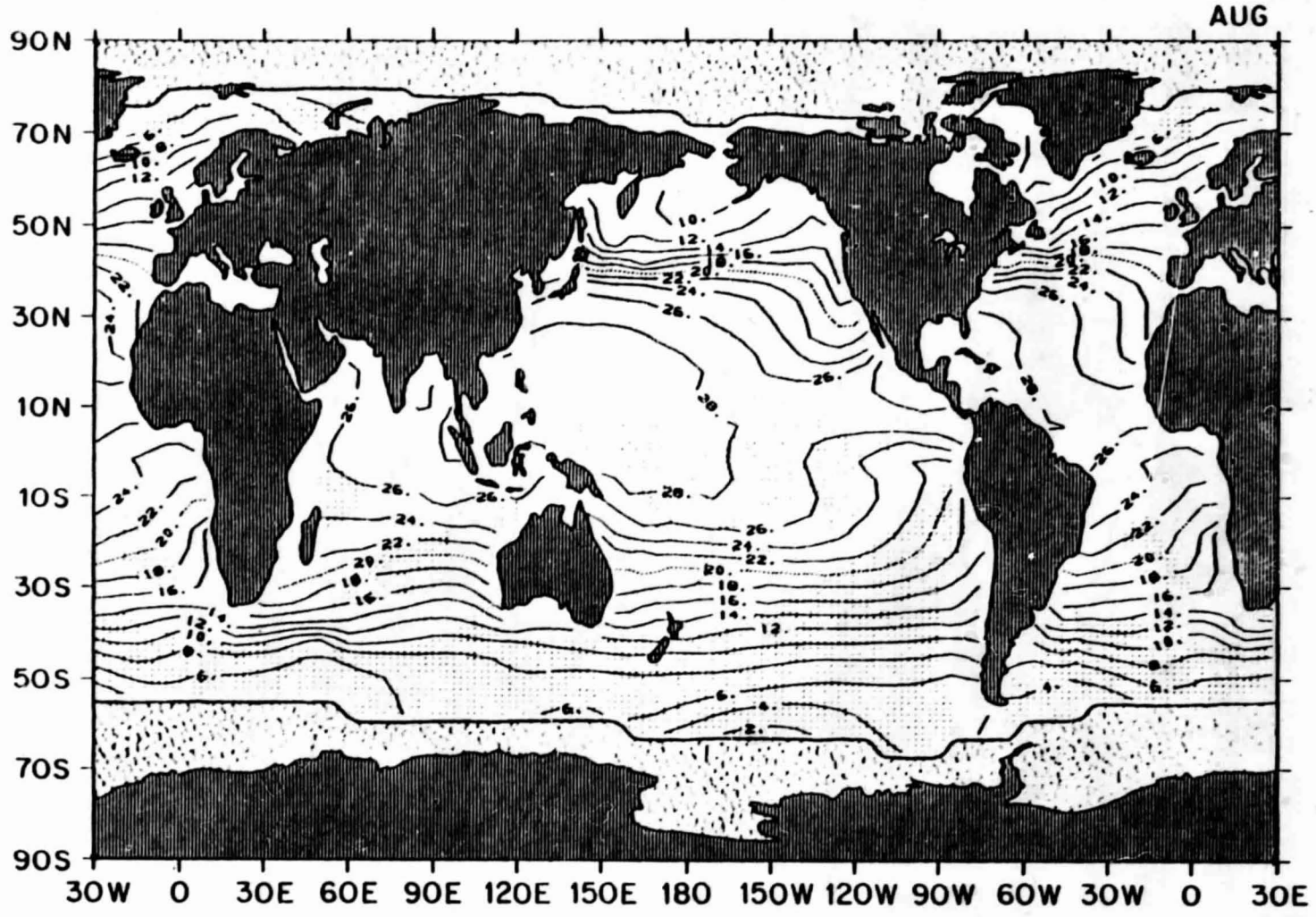

1.22 September mean sea-surface temperature (°C)

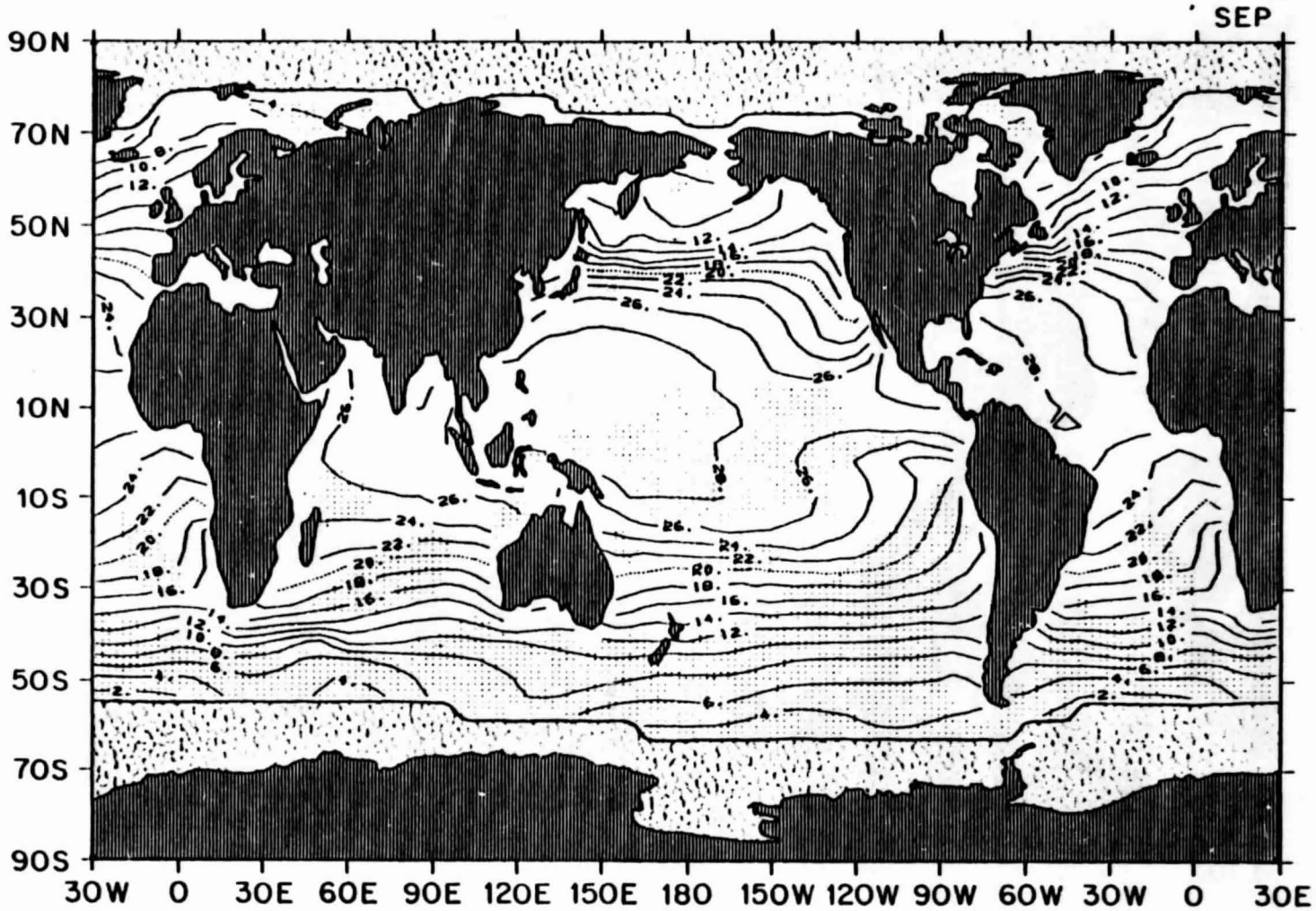

1.23 October mean sea-surface temperature (°C)

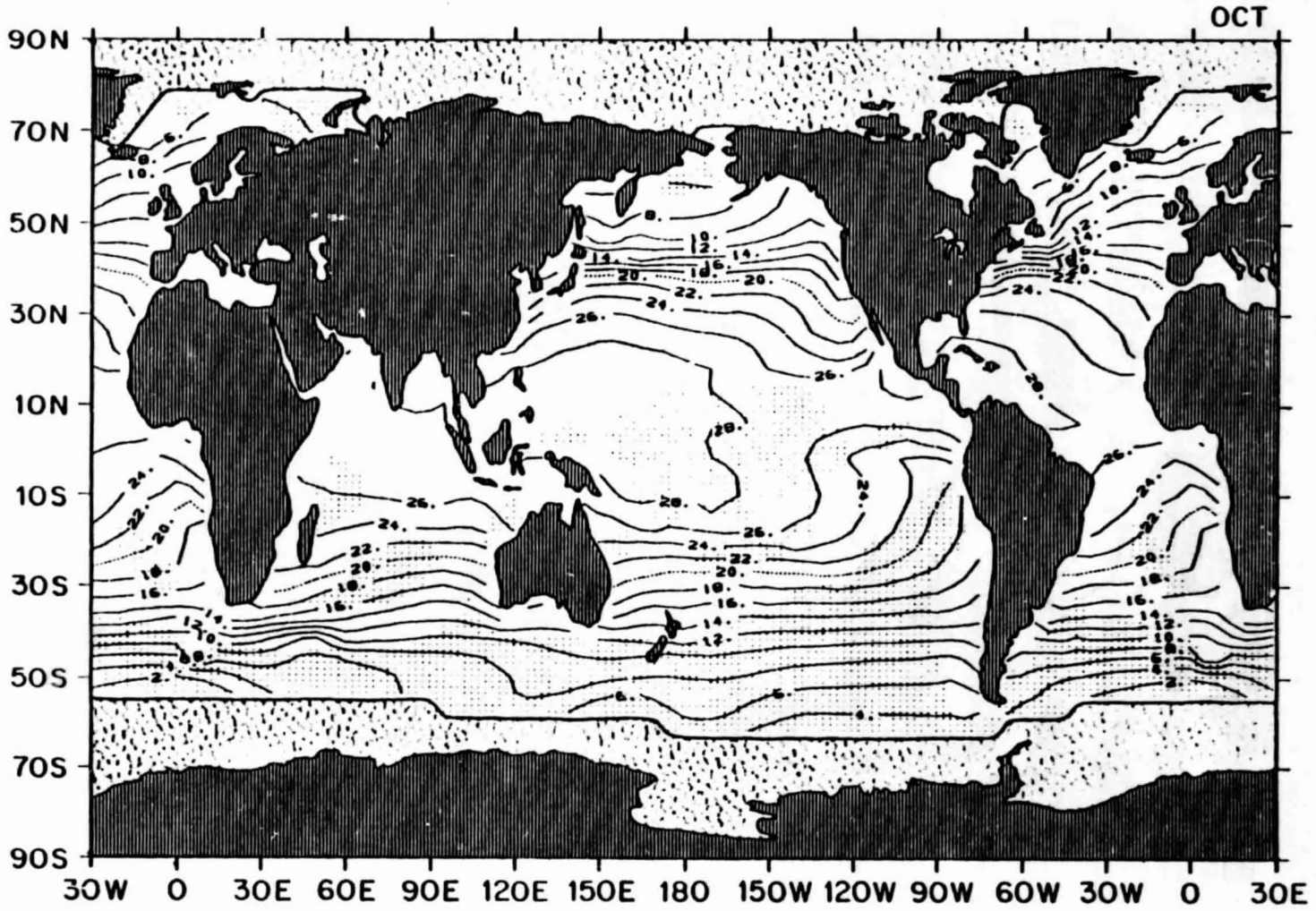

1.24 November mean sea-surface temperature (°C)

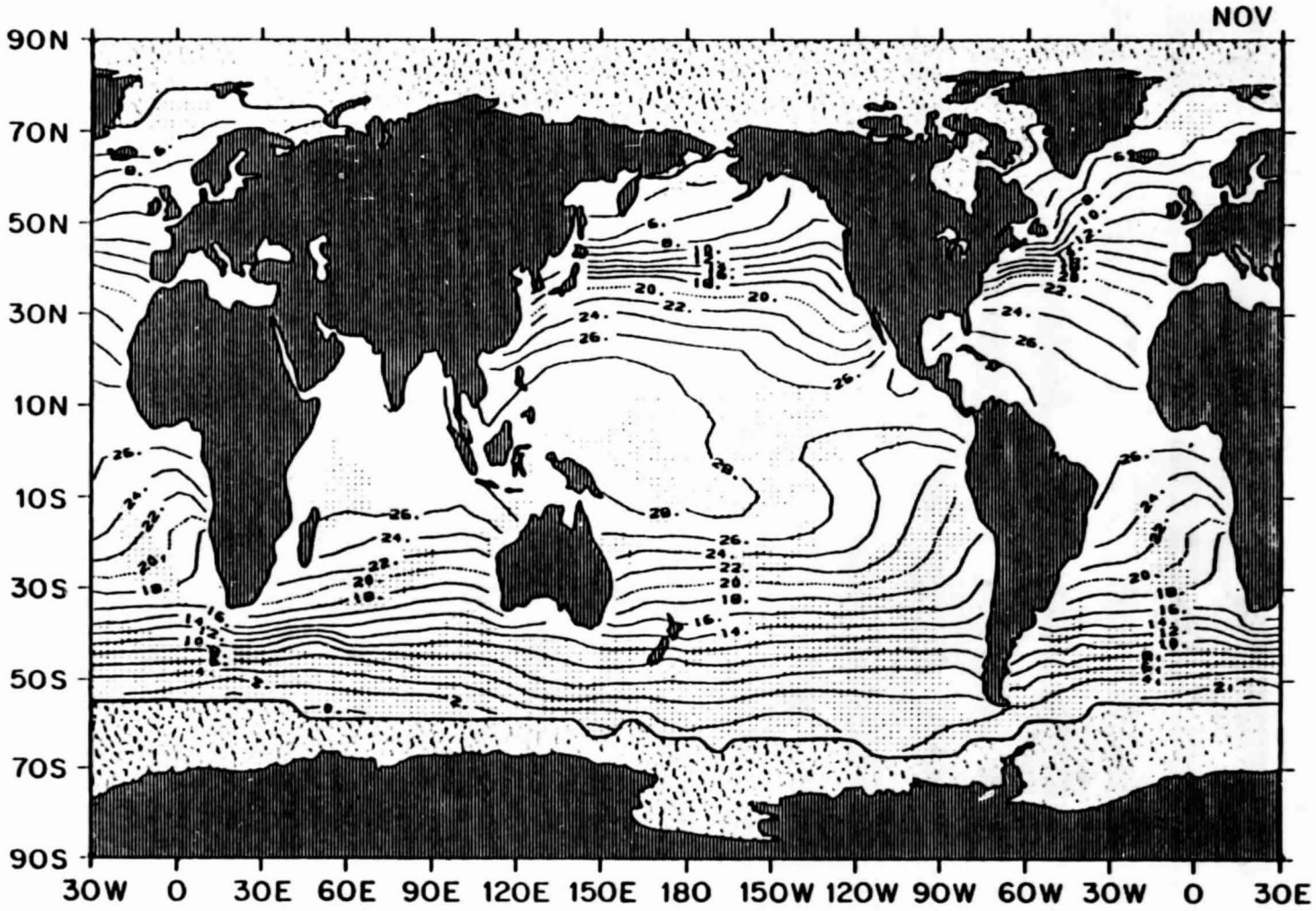

1.25 December mean sea-surface temperature (°C)

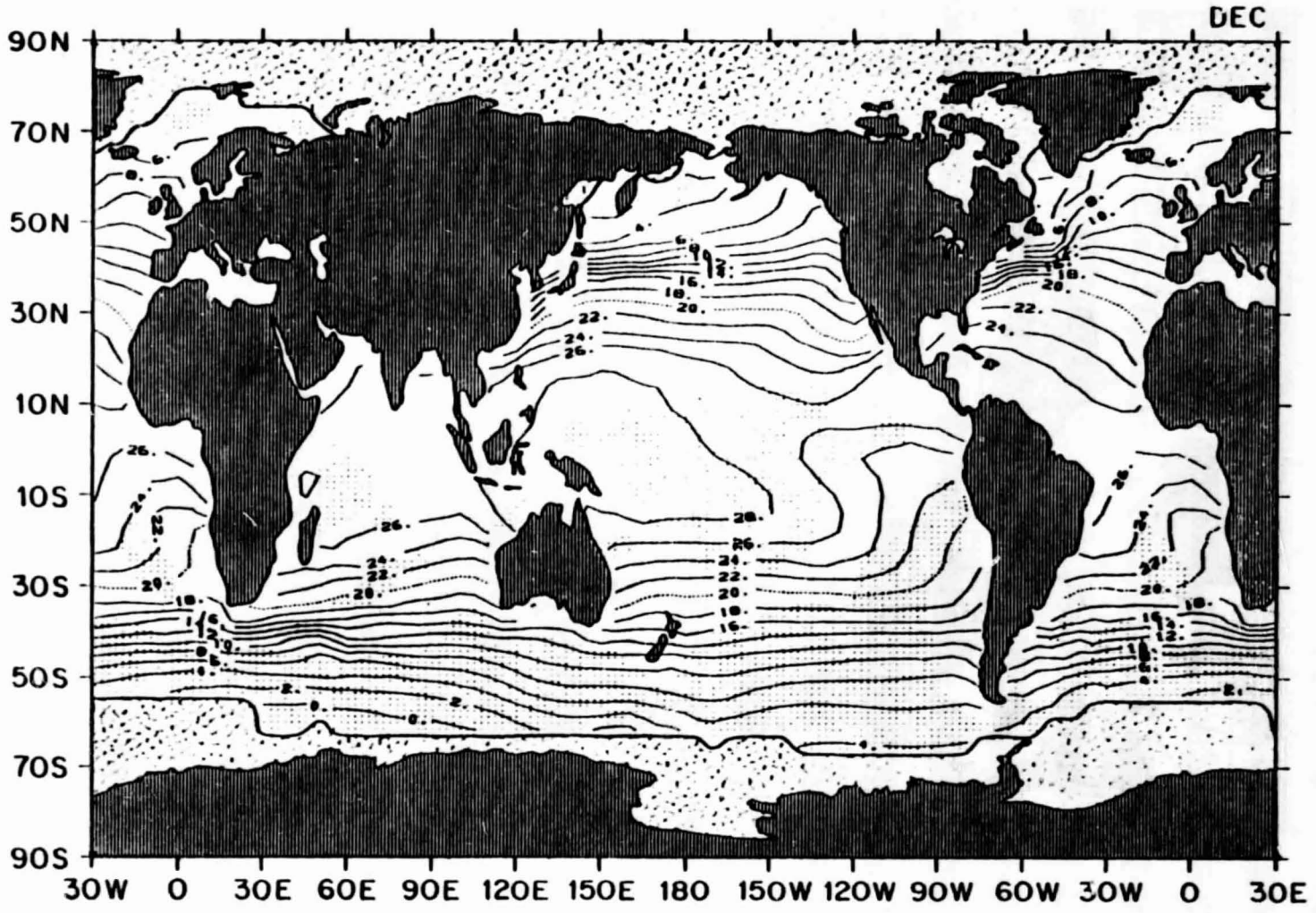

1.26 Annual mean sea-surface temperature (°C)

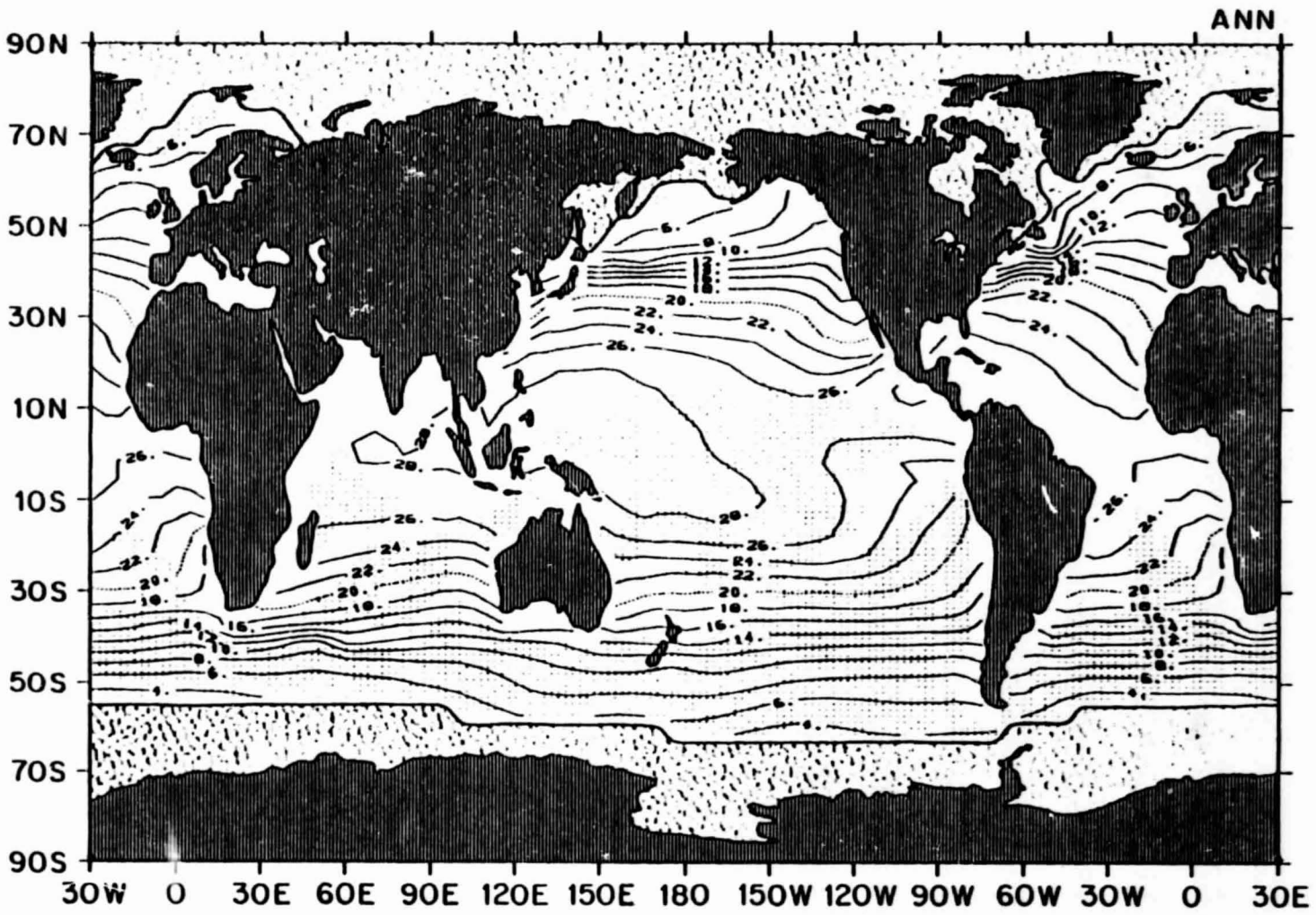

SEA - AIR TEMPERATURE DIFFERENCE

1.27 January mean sea - air temperature difference (°C)

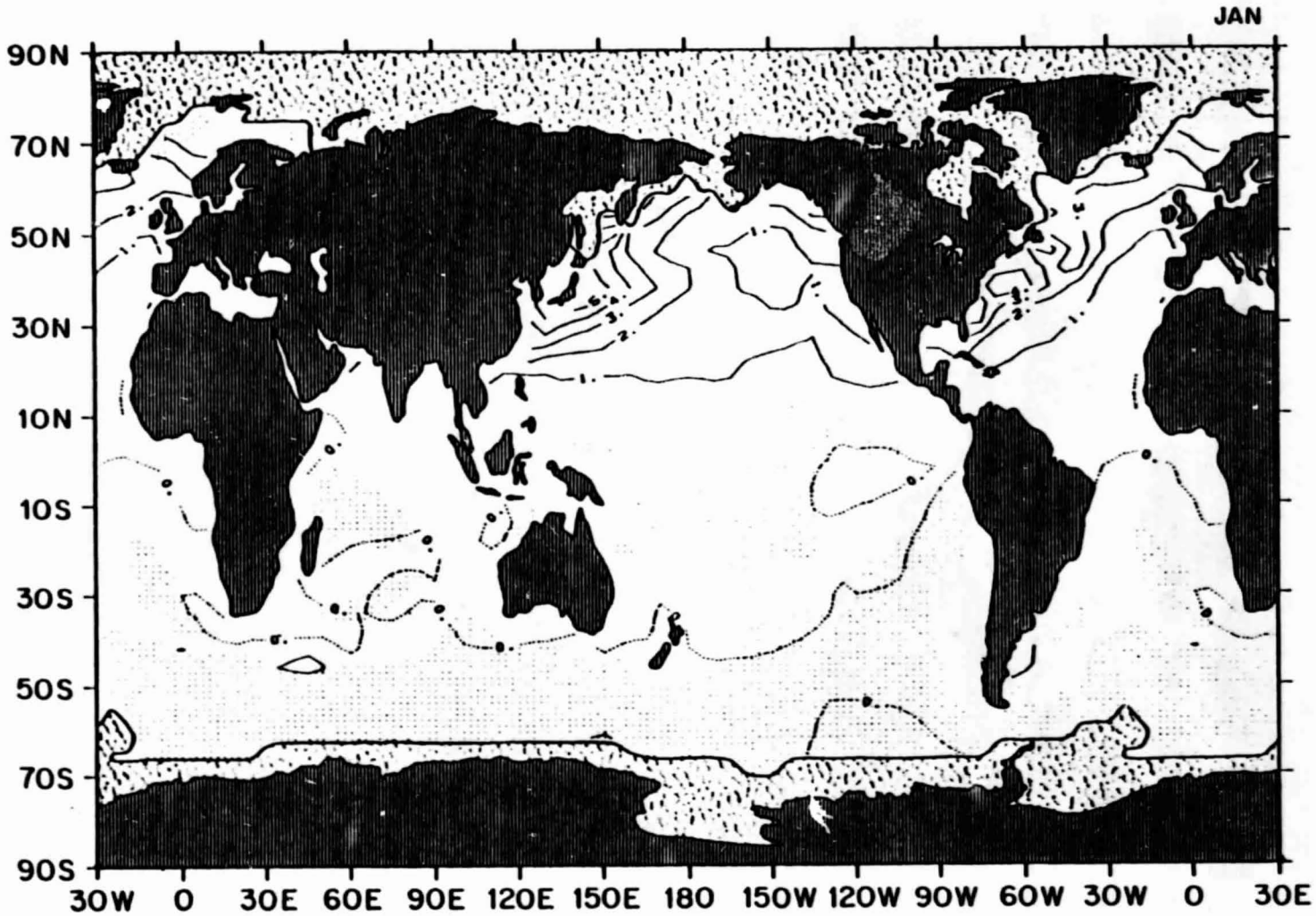

1.28 February mean sea - air temperature difference (°C)

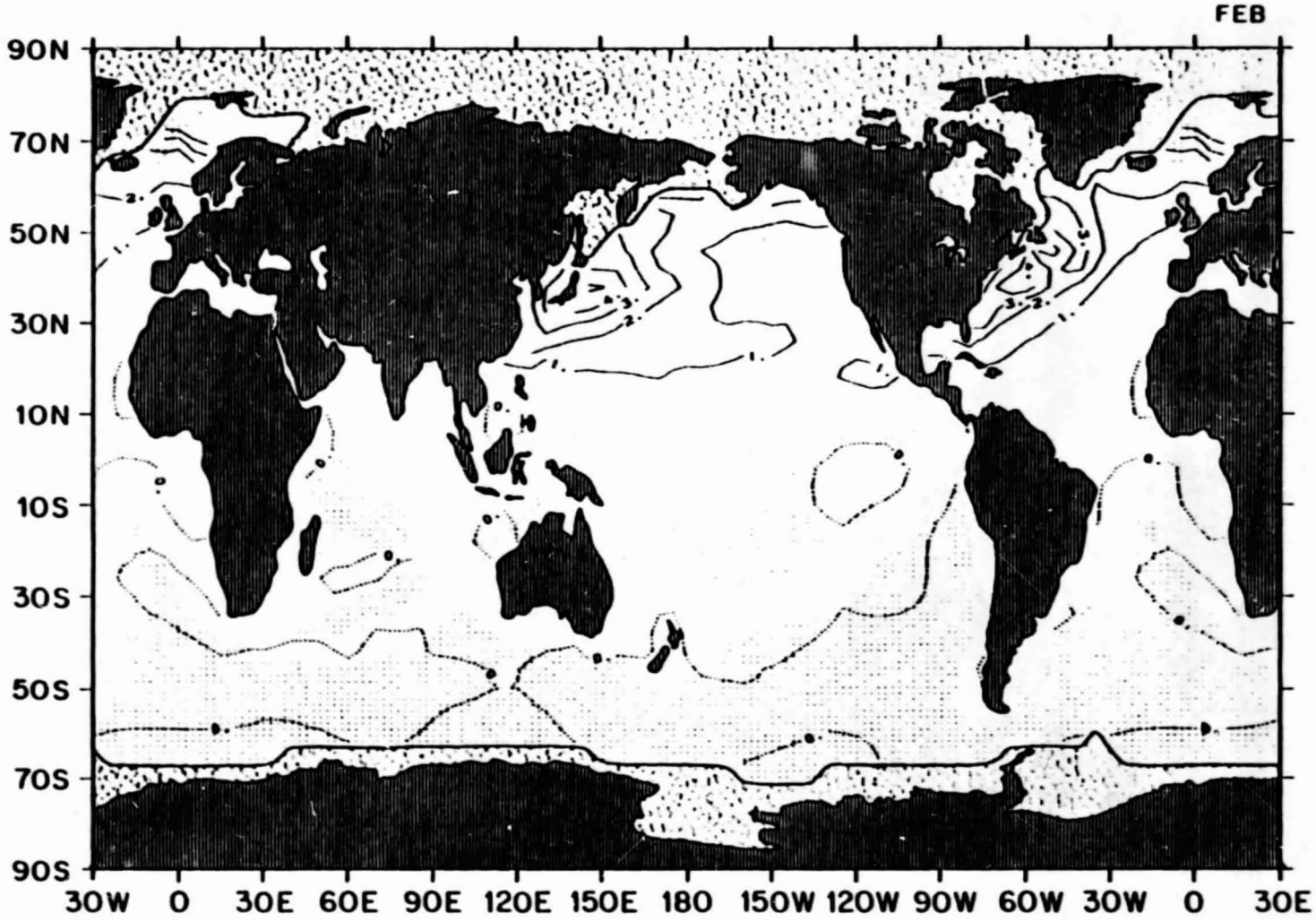

1.29 March mean sea - air temperature difference (°C)

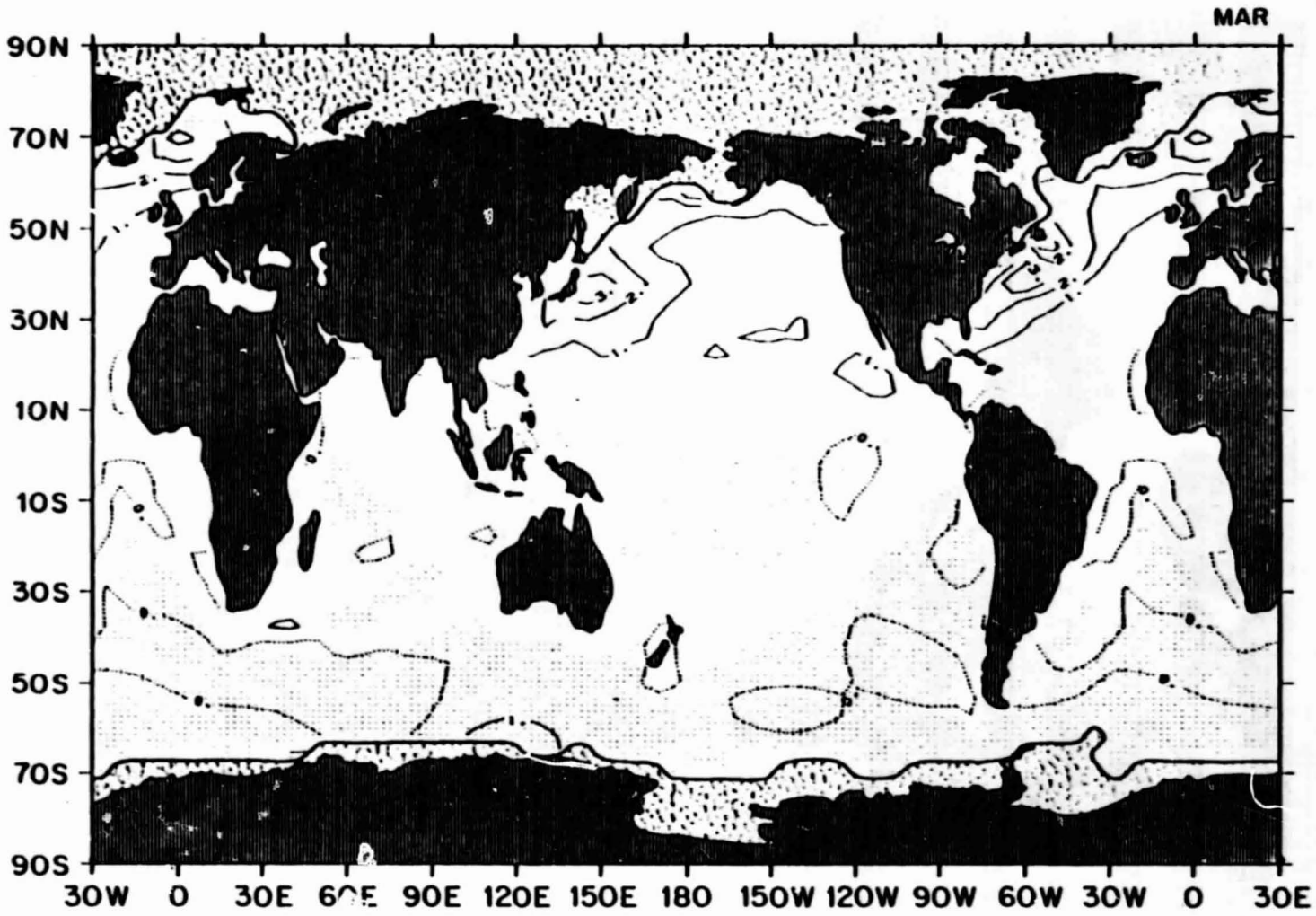

1.30 April mean sea - air temperature difference (°C)

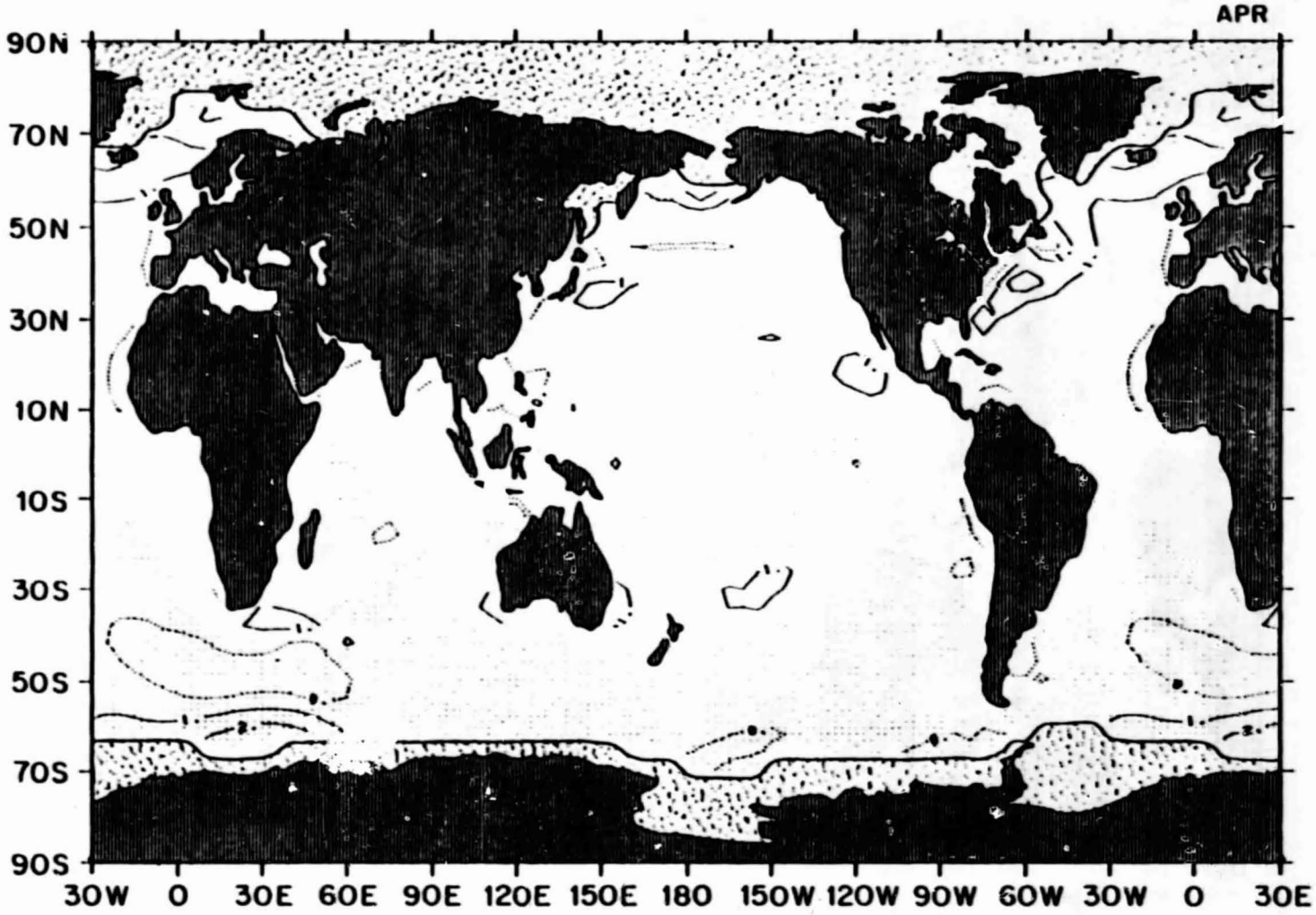

1.31 May mean sea - air temperature difference (°C)

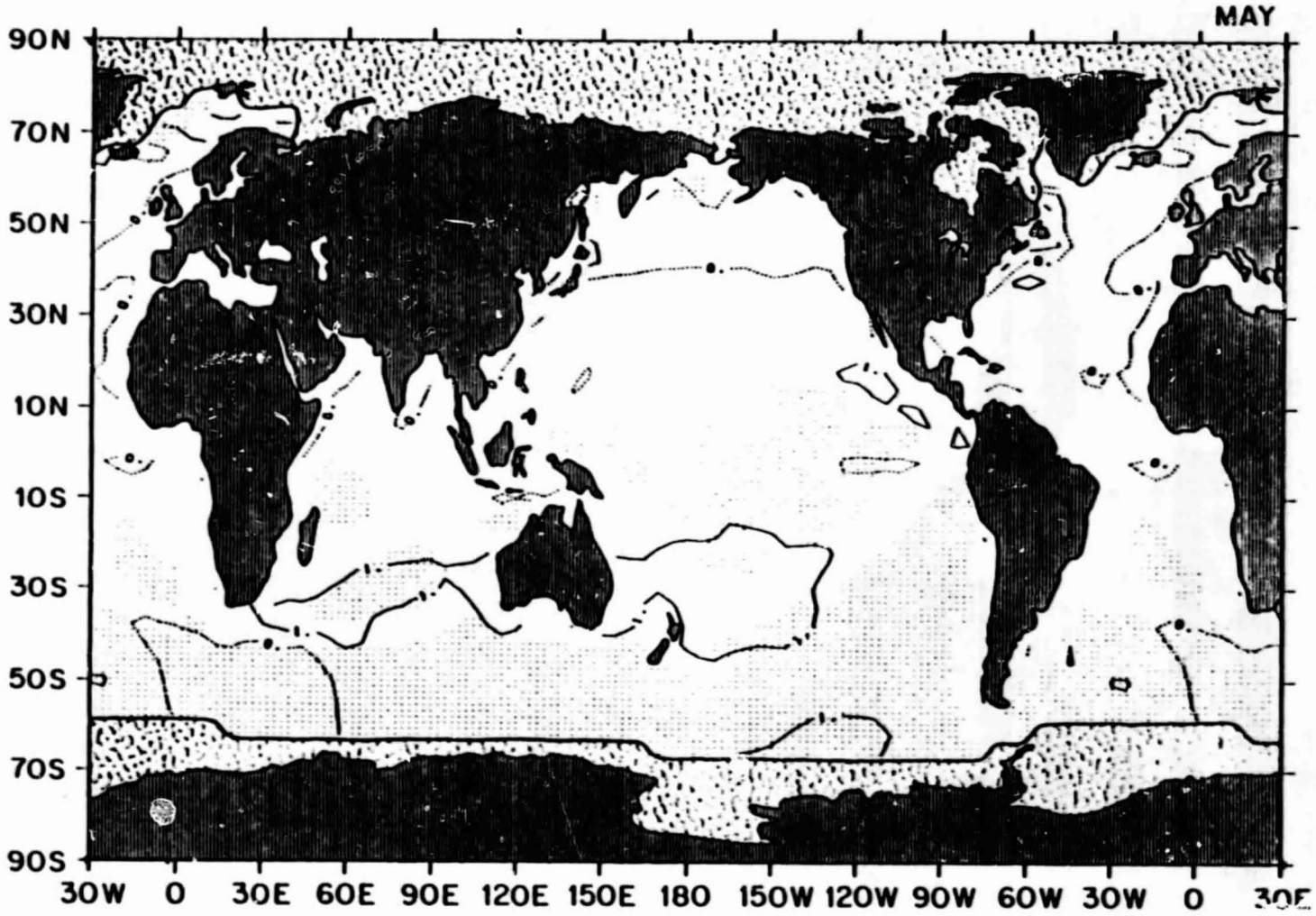

1.32 June mean sea - air temperature difference (°C)

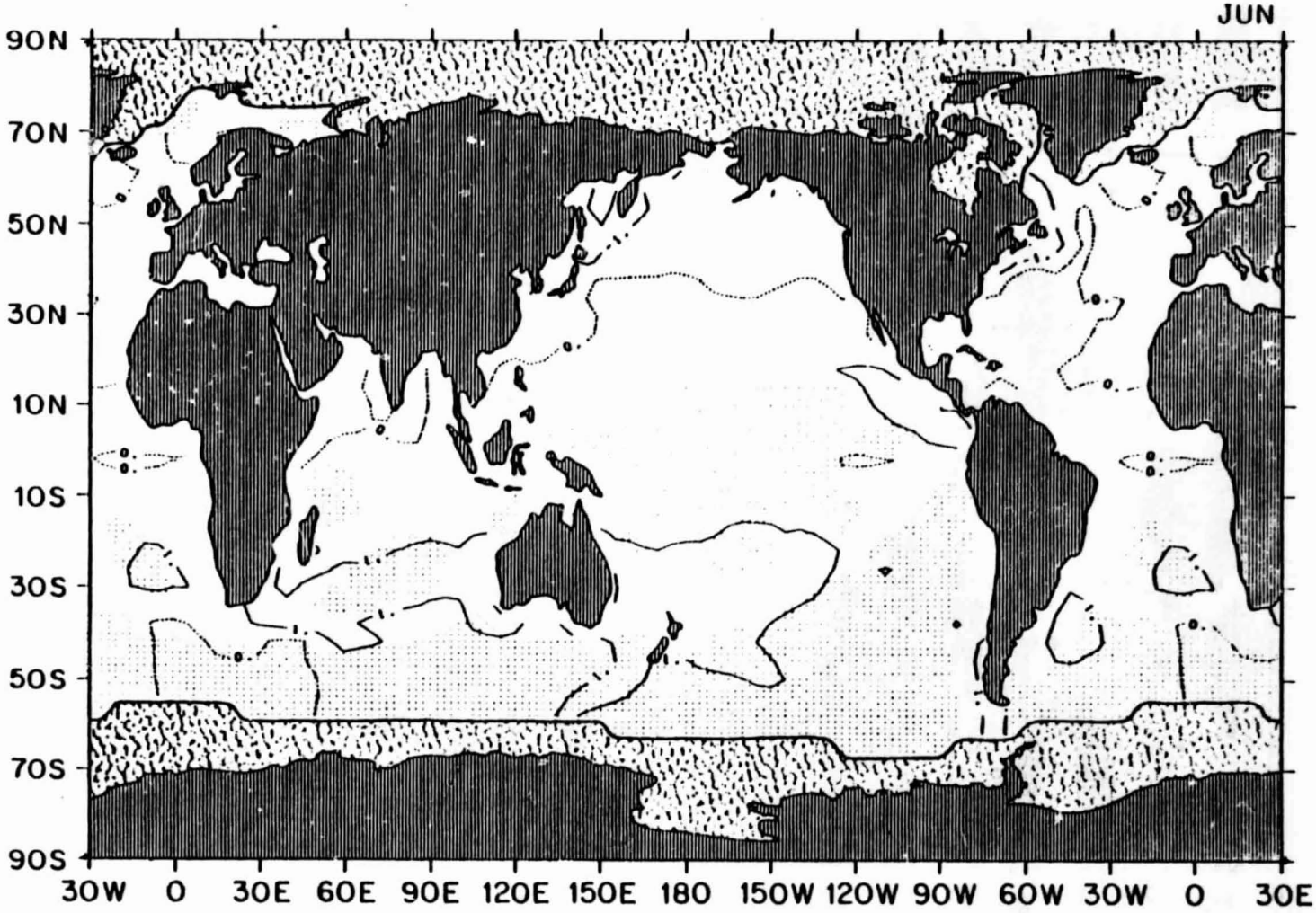

1.33 July mean sea - air temperature difference (°C)

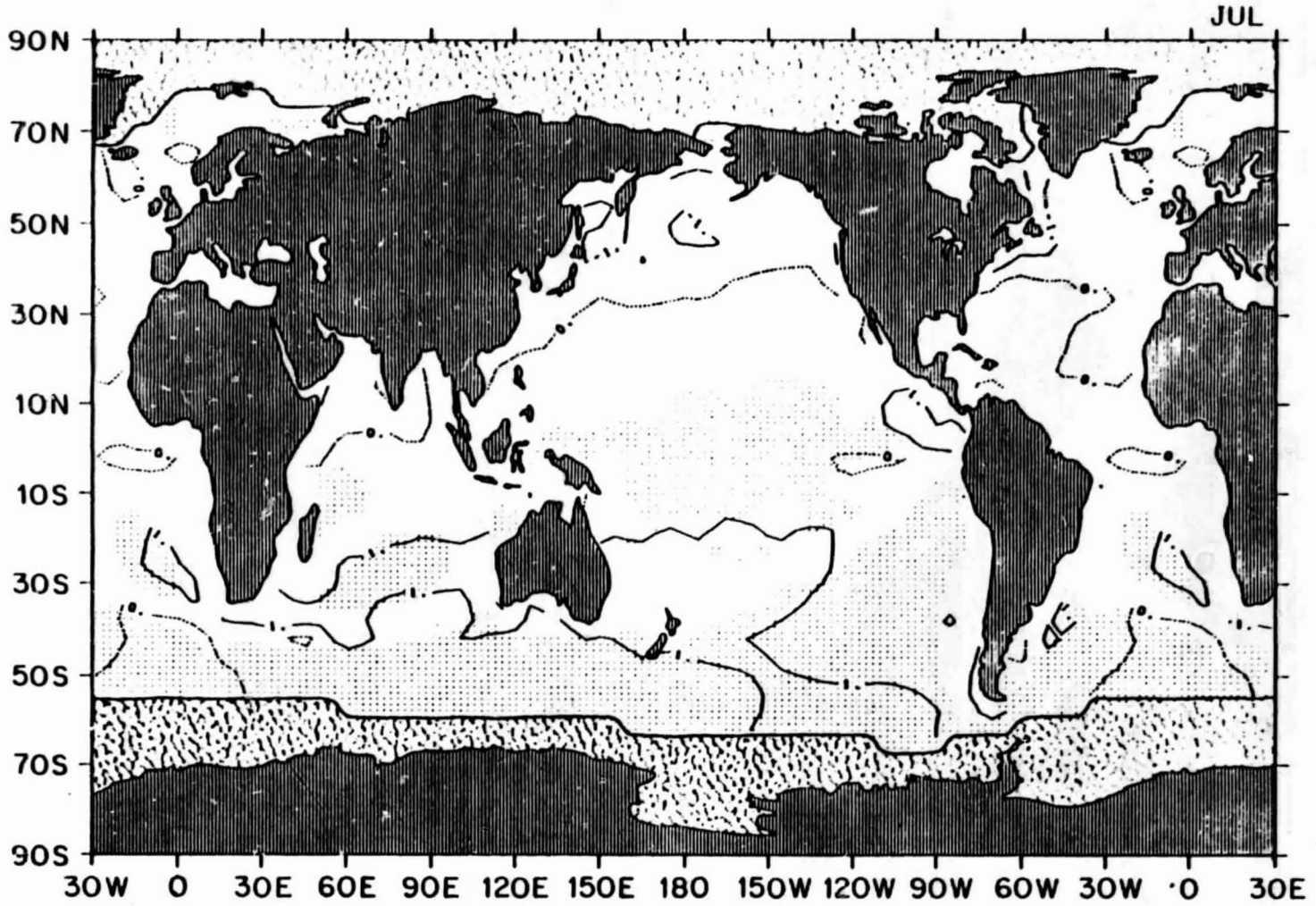

1.34 August mean sea - air temperature difference (°C)

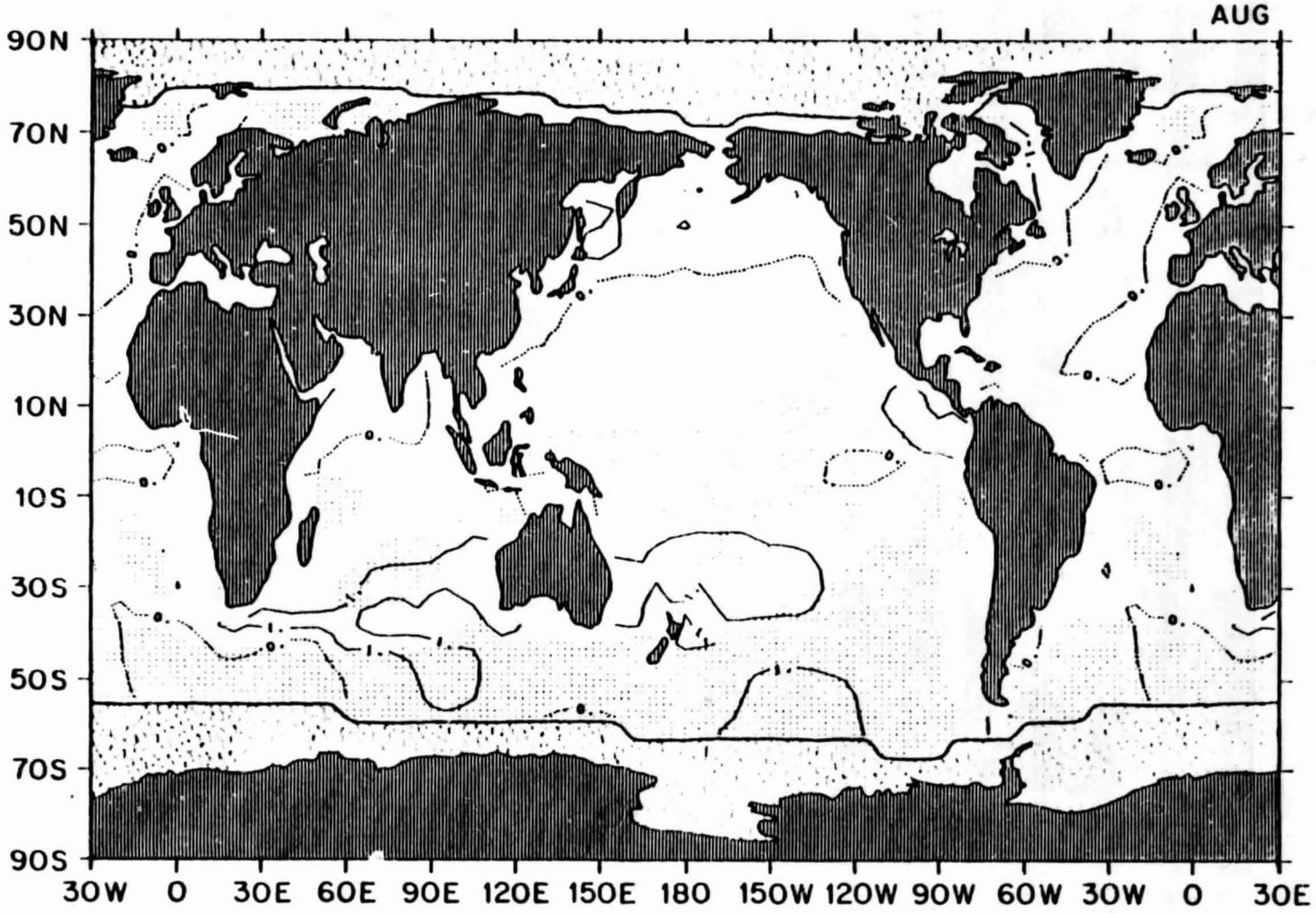

1.35 September mean sea - air temperature difference (°C)

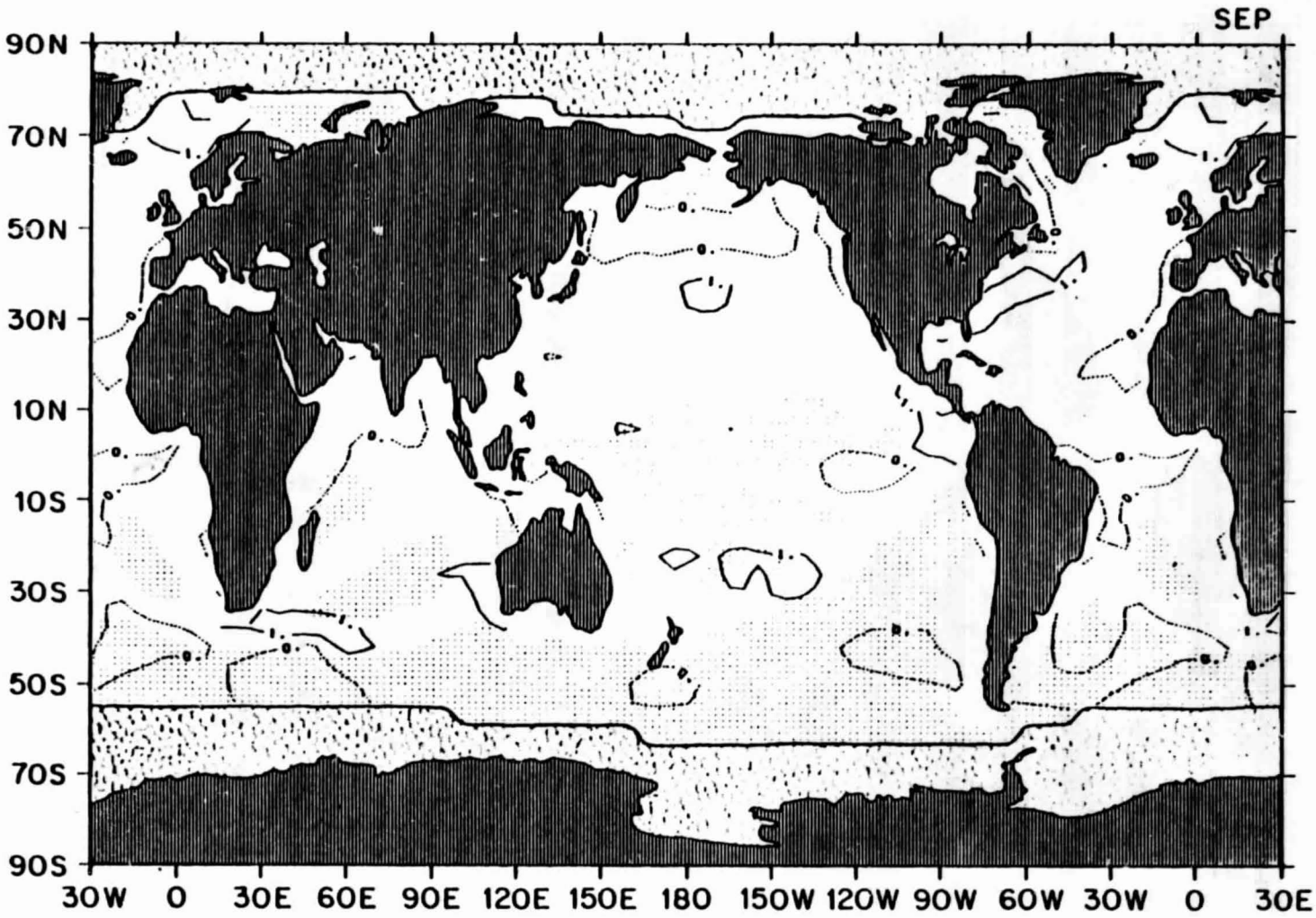

1.36 October mean sea - air temperature difference (°C)

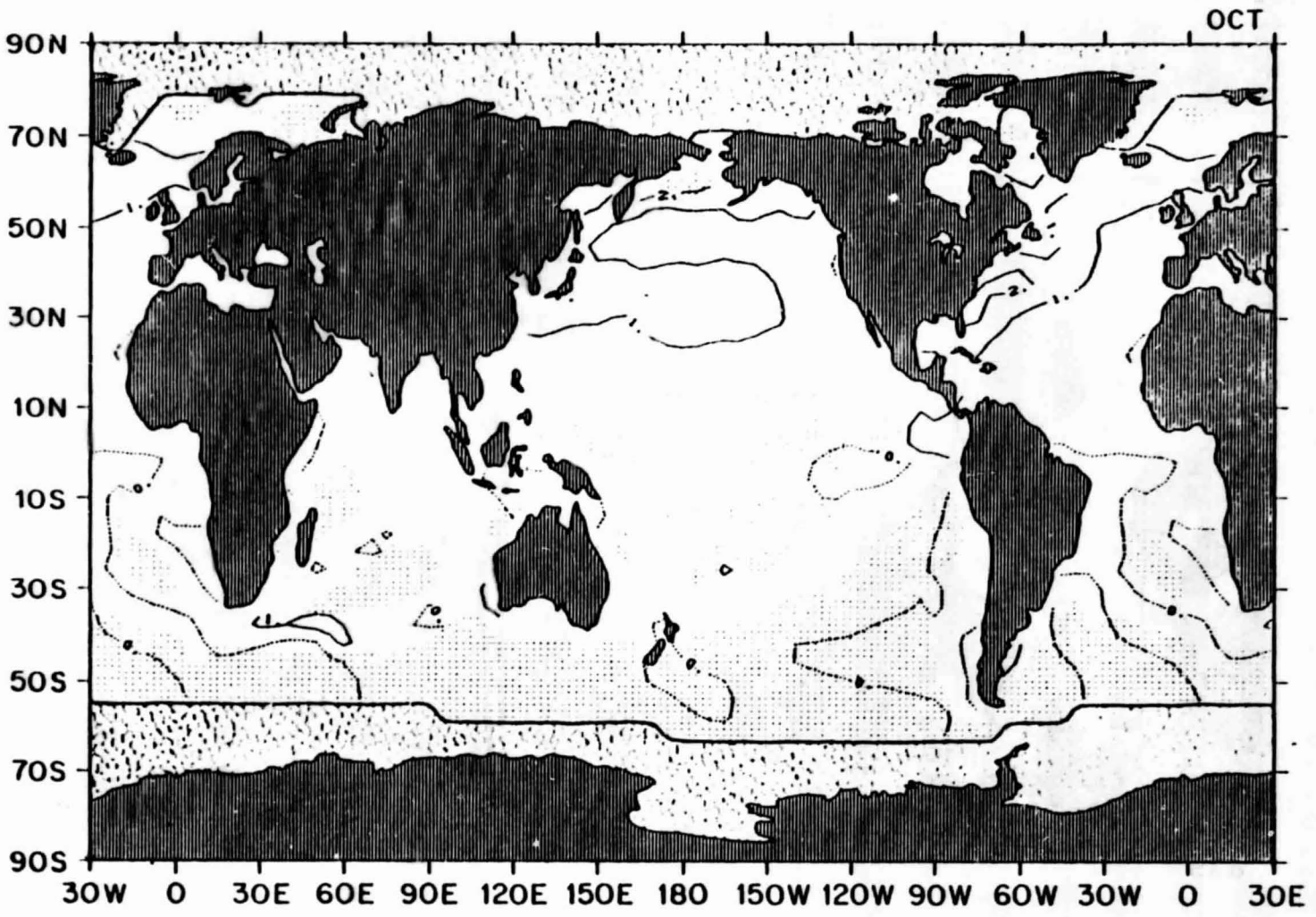

1.37 November mean sea - air temperature difference (°C)

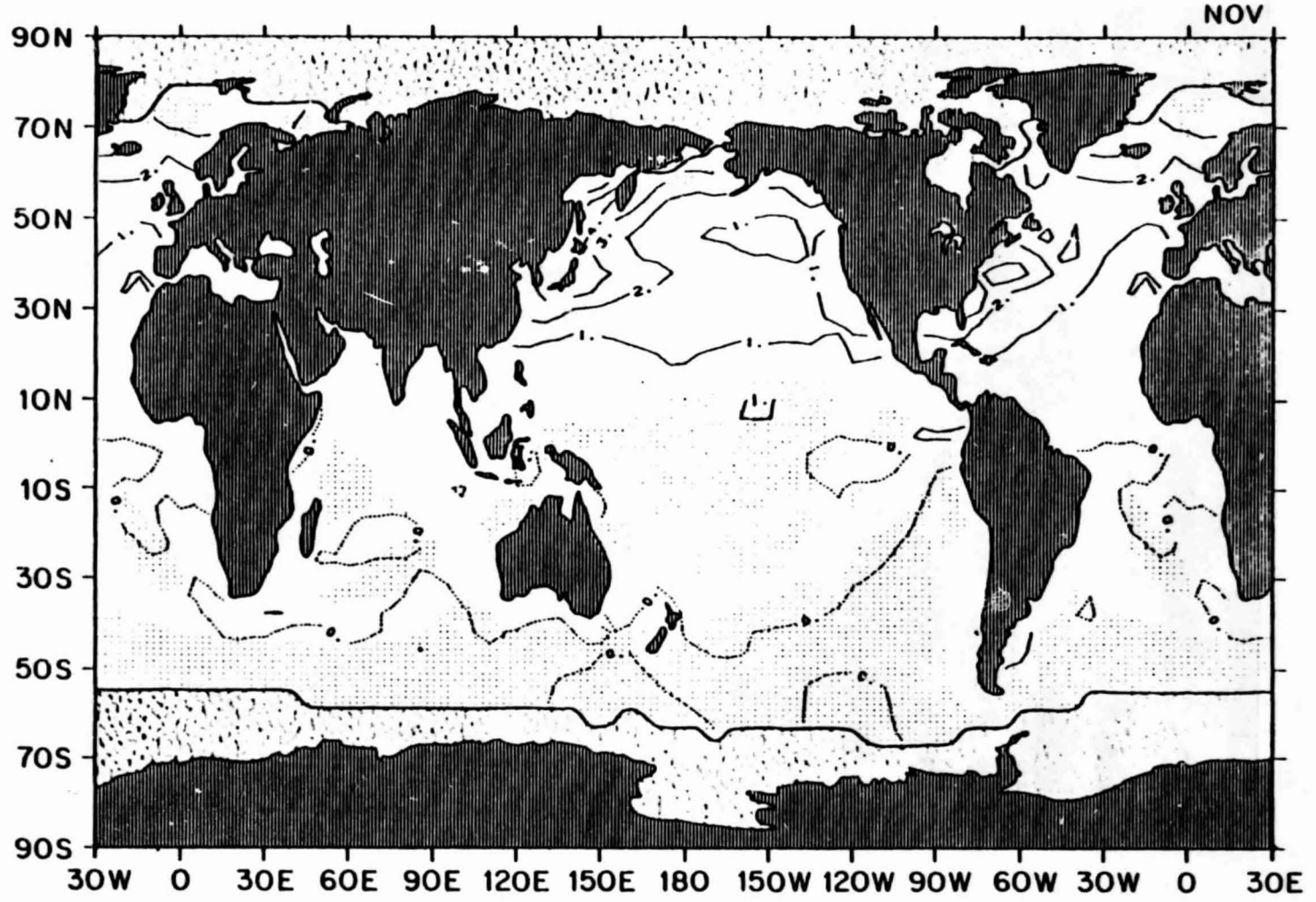

1.38 December mean sea - air temperature difference (°C)

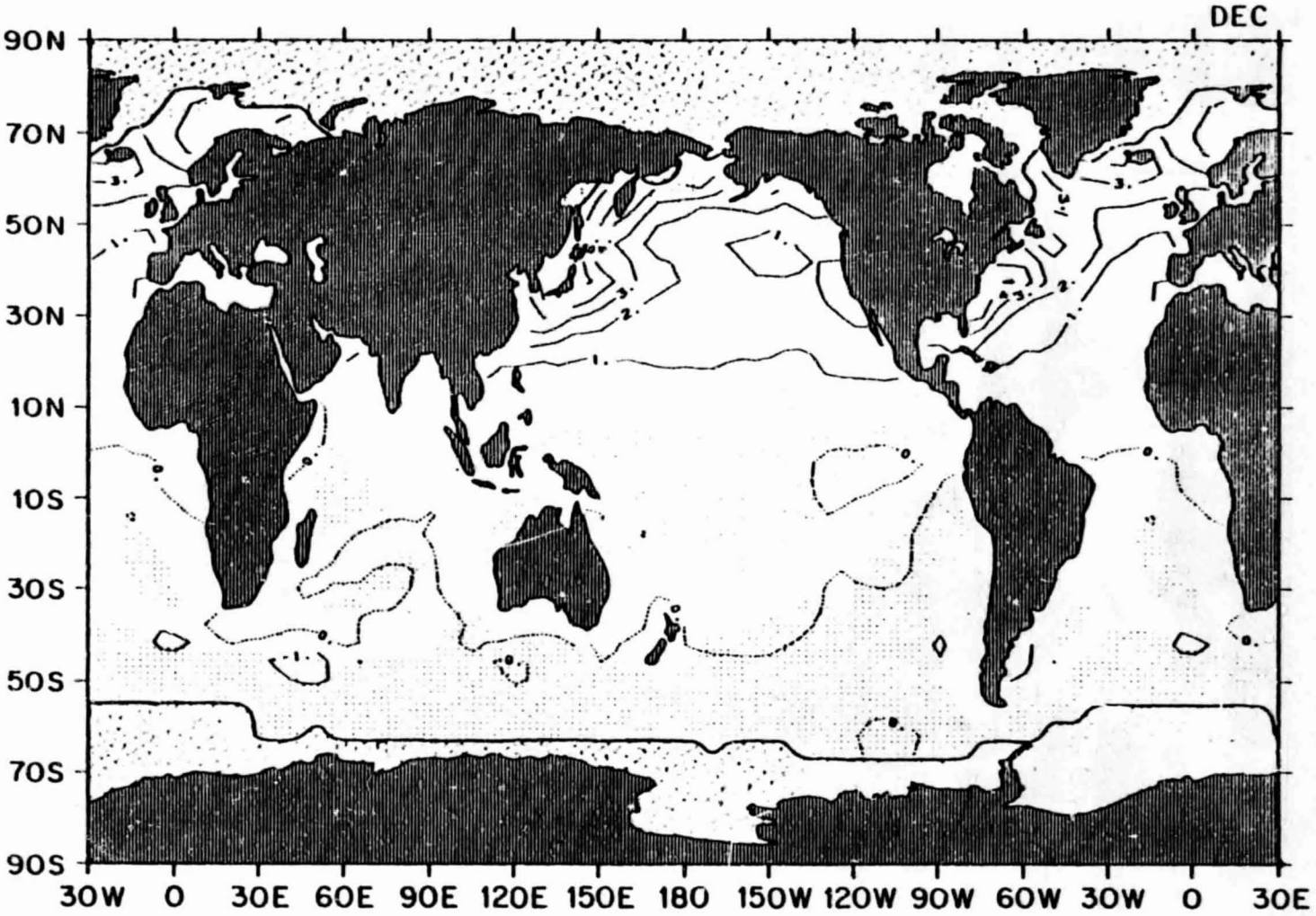

1.39 Annual mean sea - air temperature difference (°C)

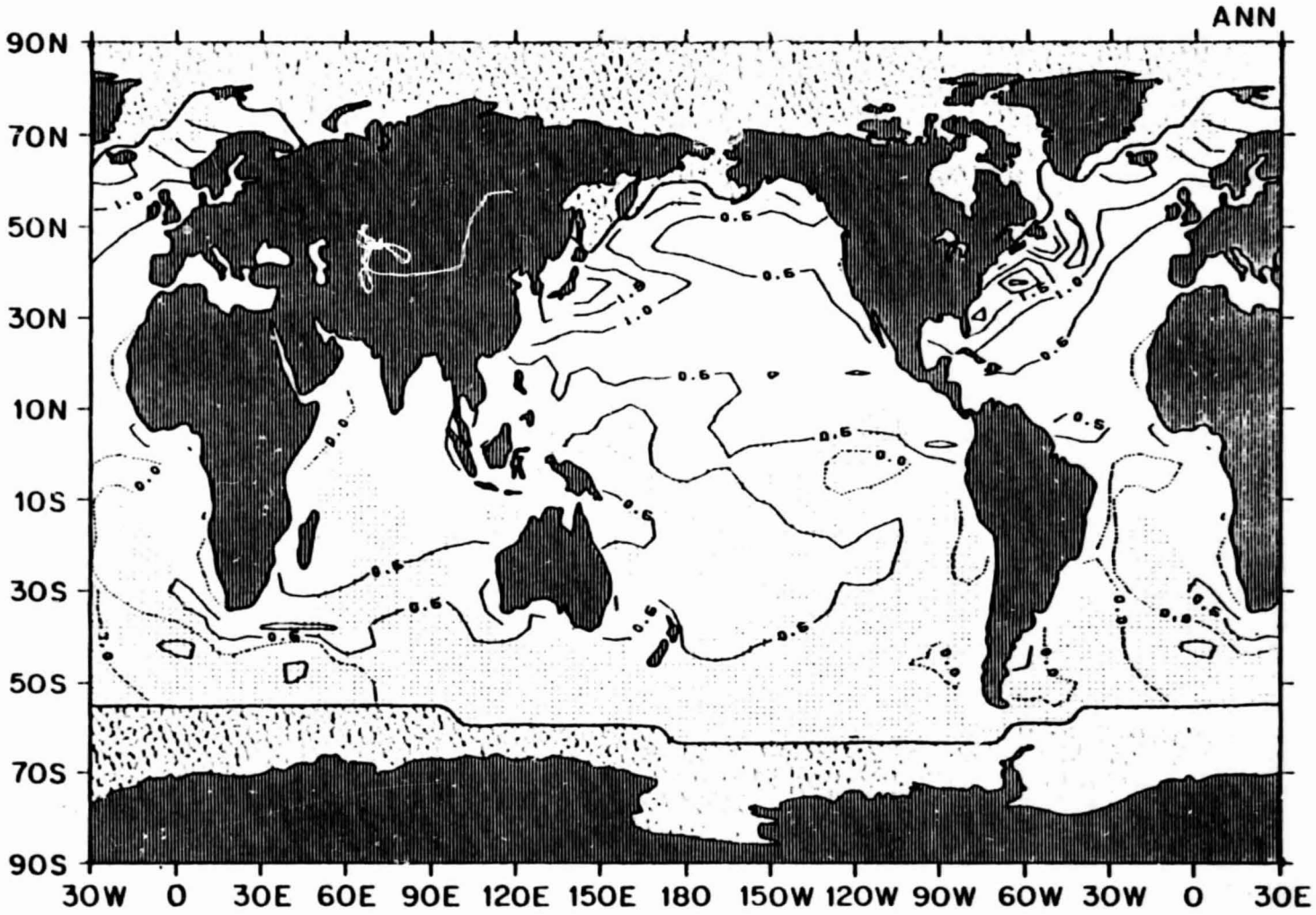

AIR TEMPERATURE

1.40 January mean air temperature (°C)

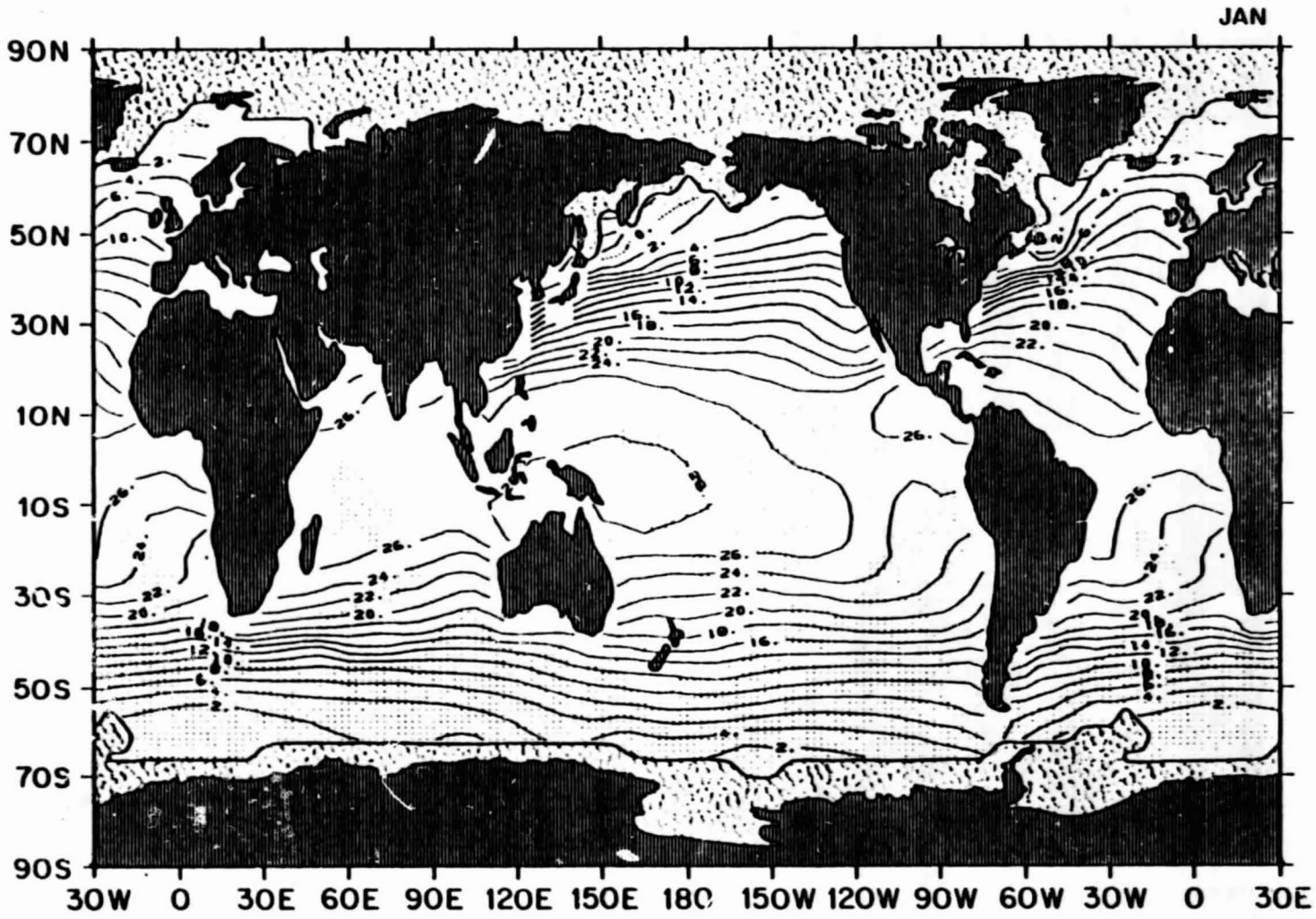

1.41 February mean air temperature (°C)

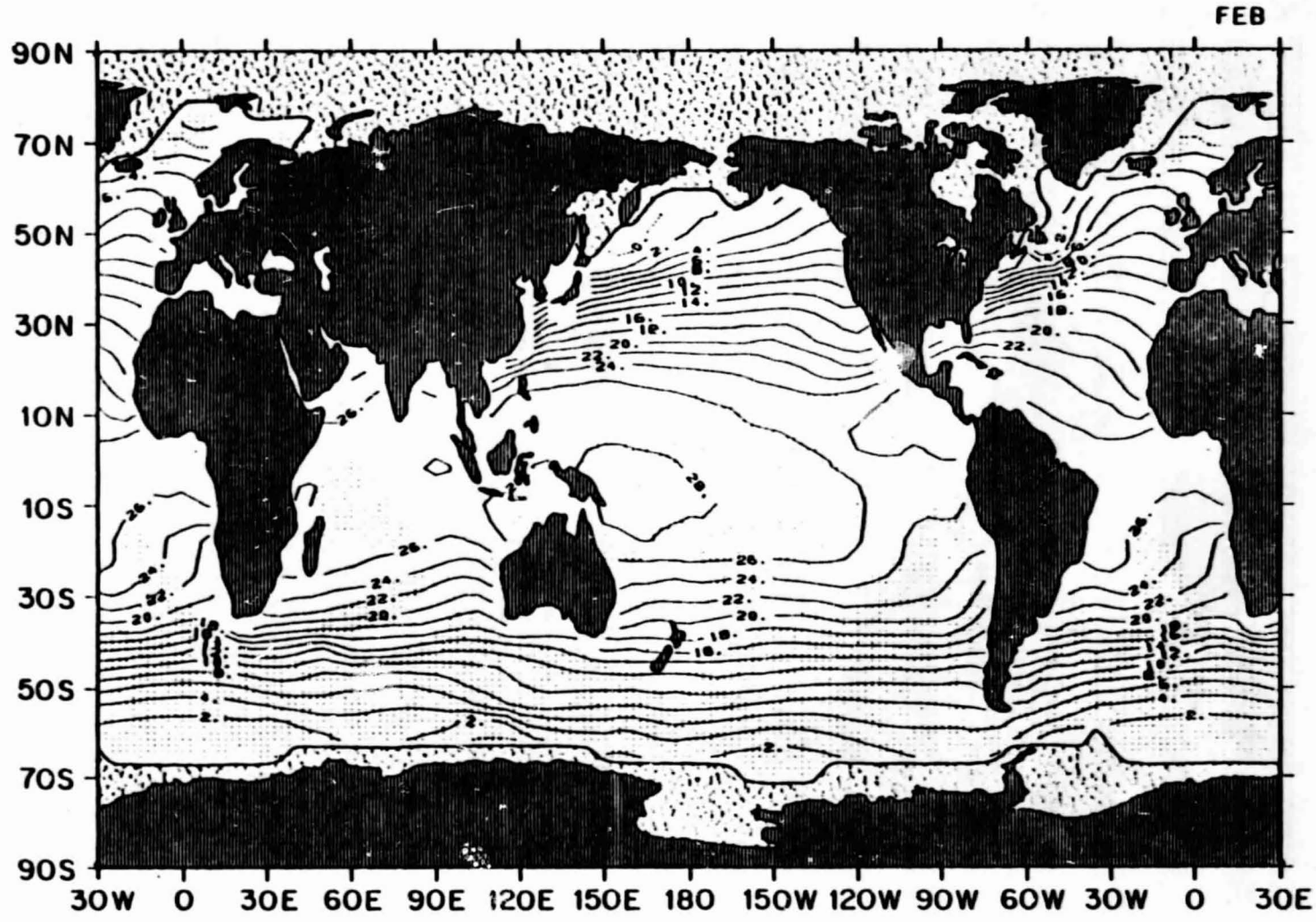

1.42 March mean air temperature (°C)

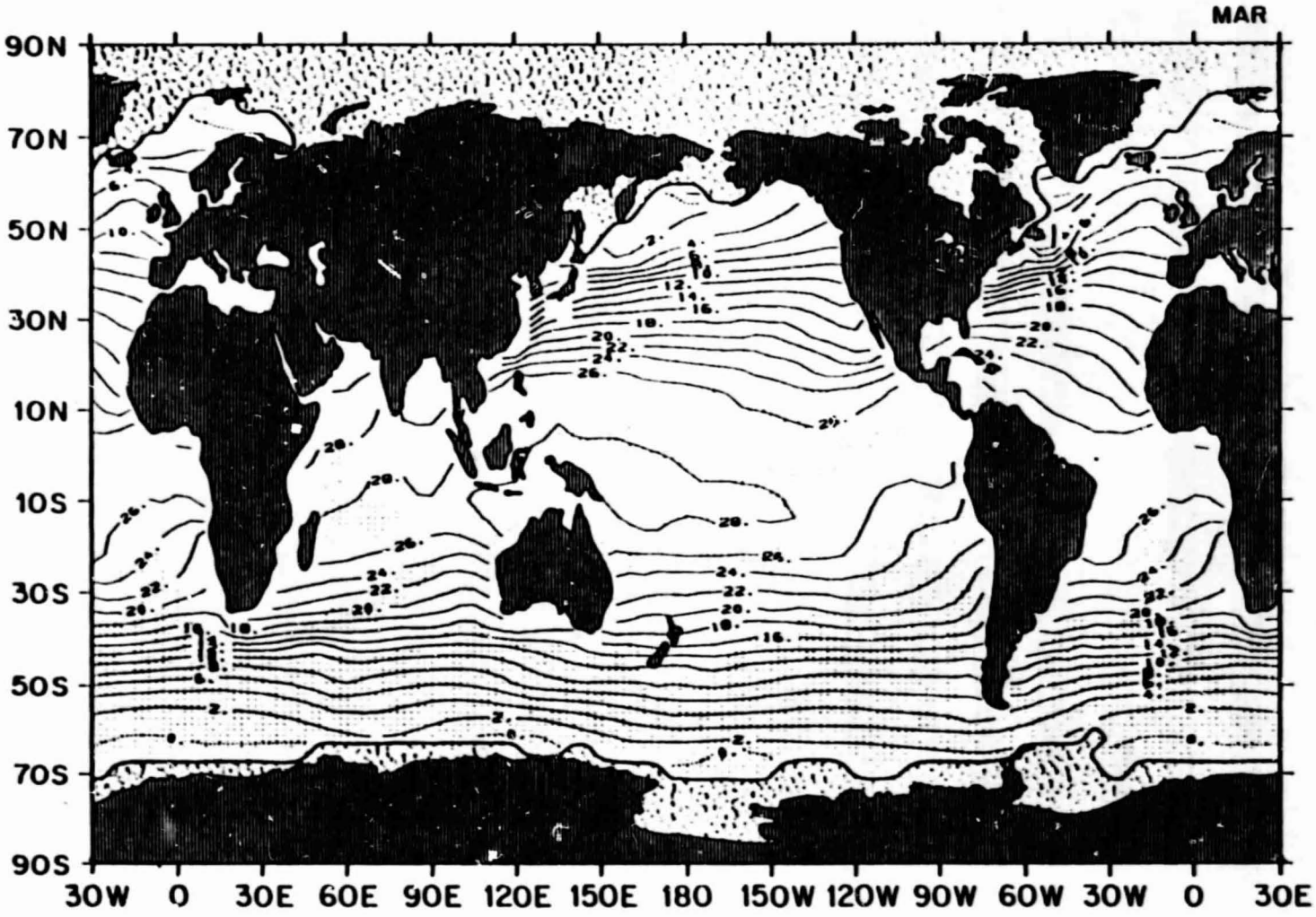

1.43 April mean air temperature (°C)

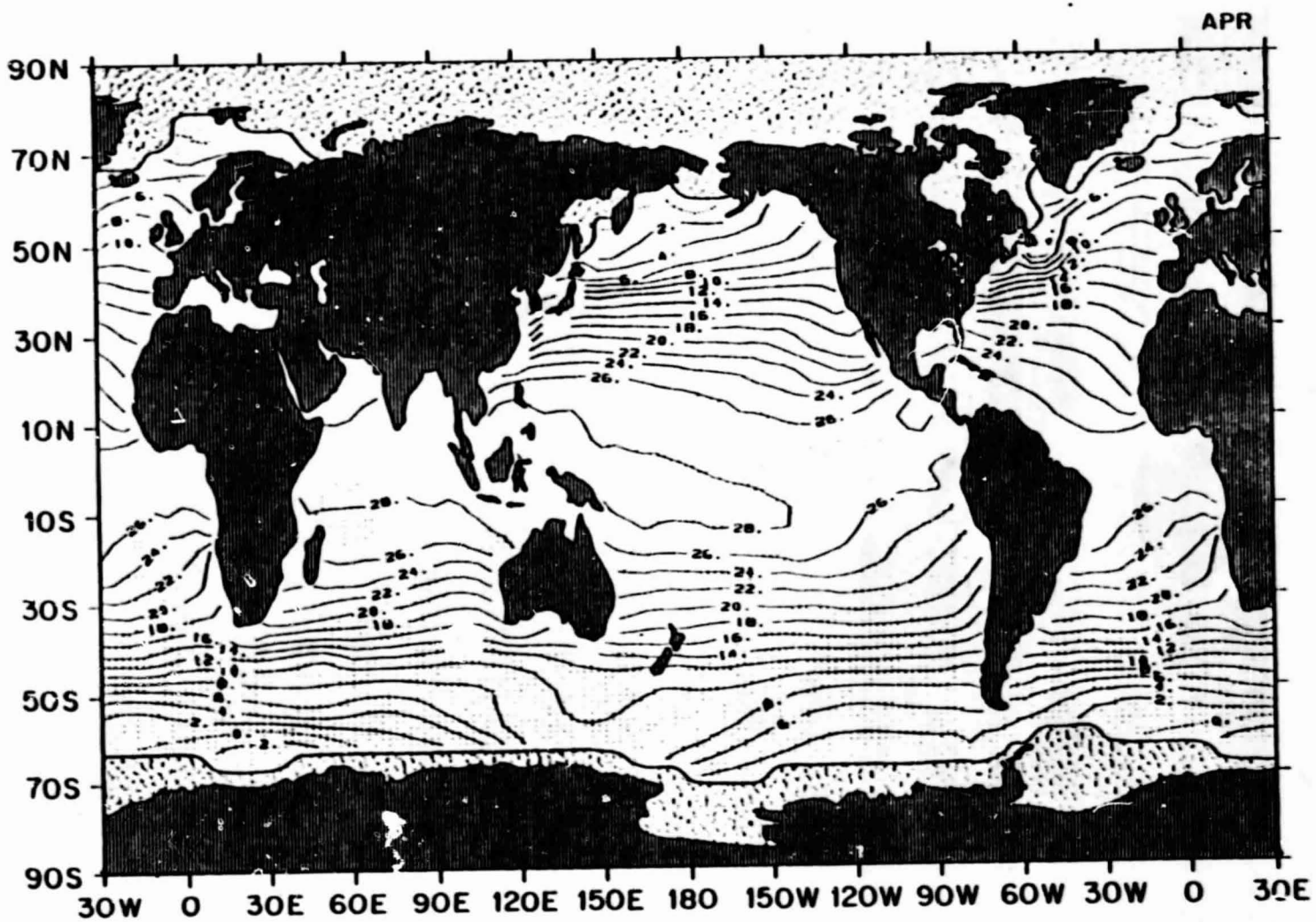

1.44 May mean air temperature (°C)

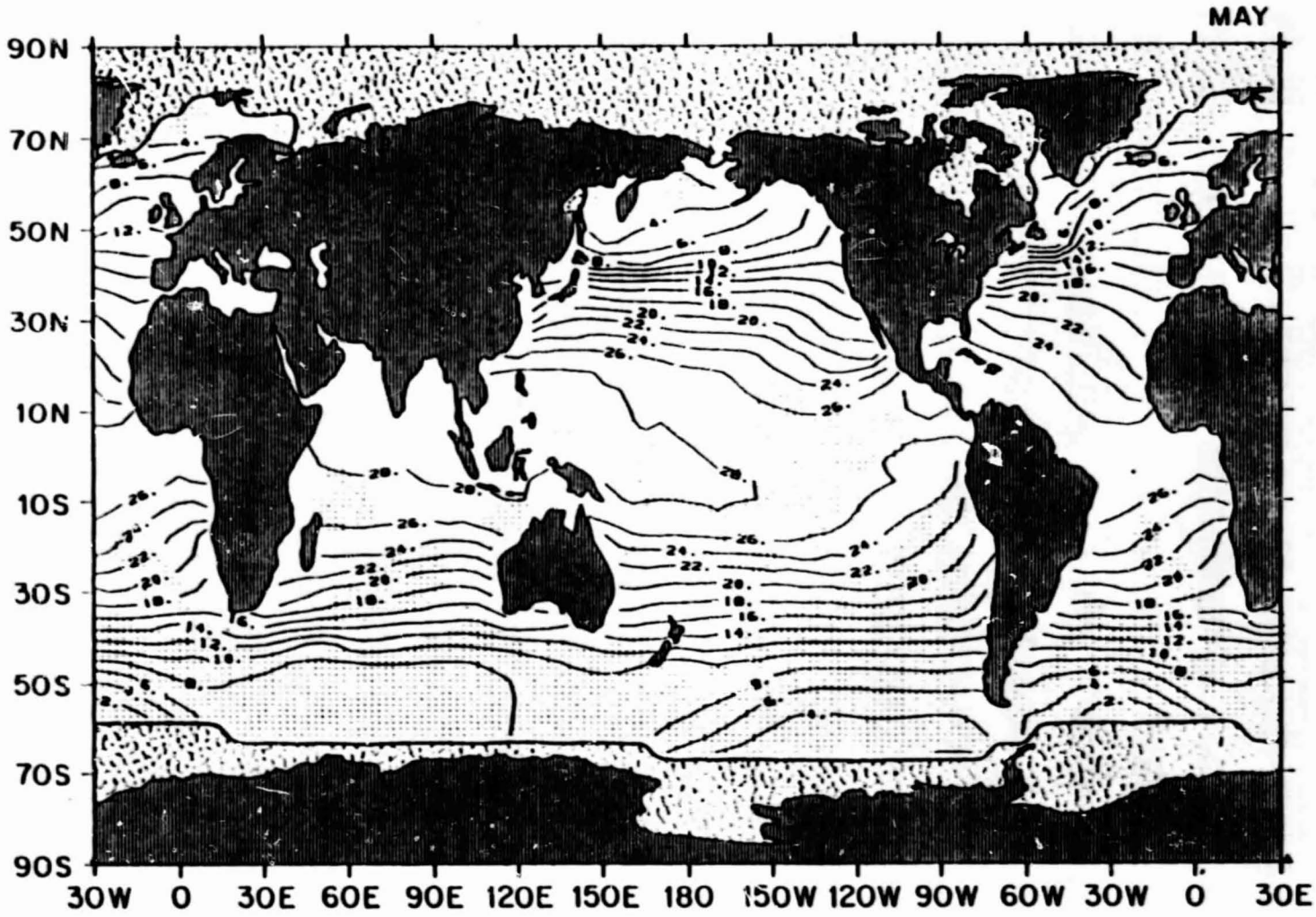

1.45 June mean air temperature (°C)

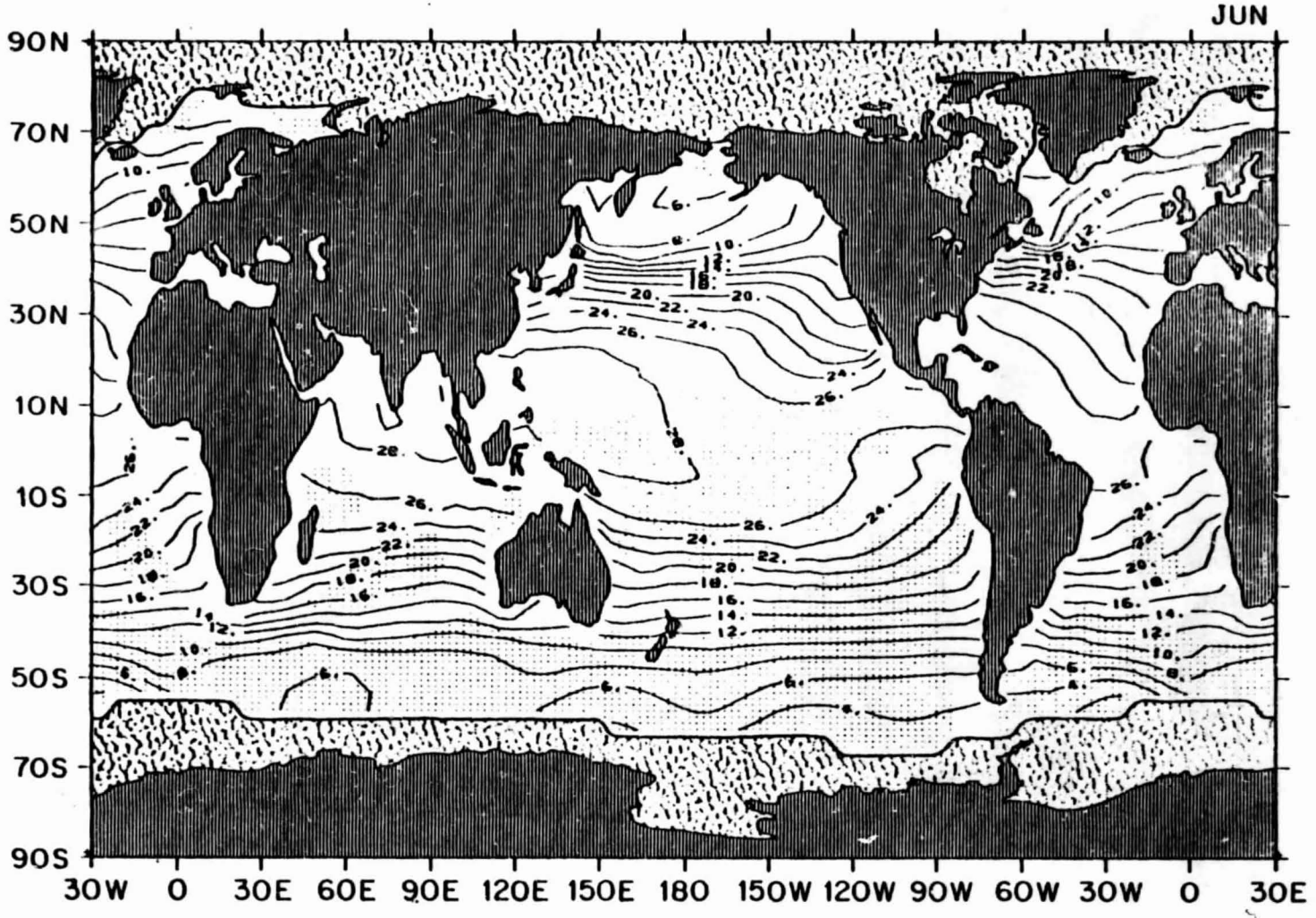

2-7

1.46 July mean air temperature (°C)

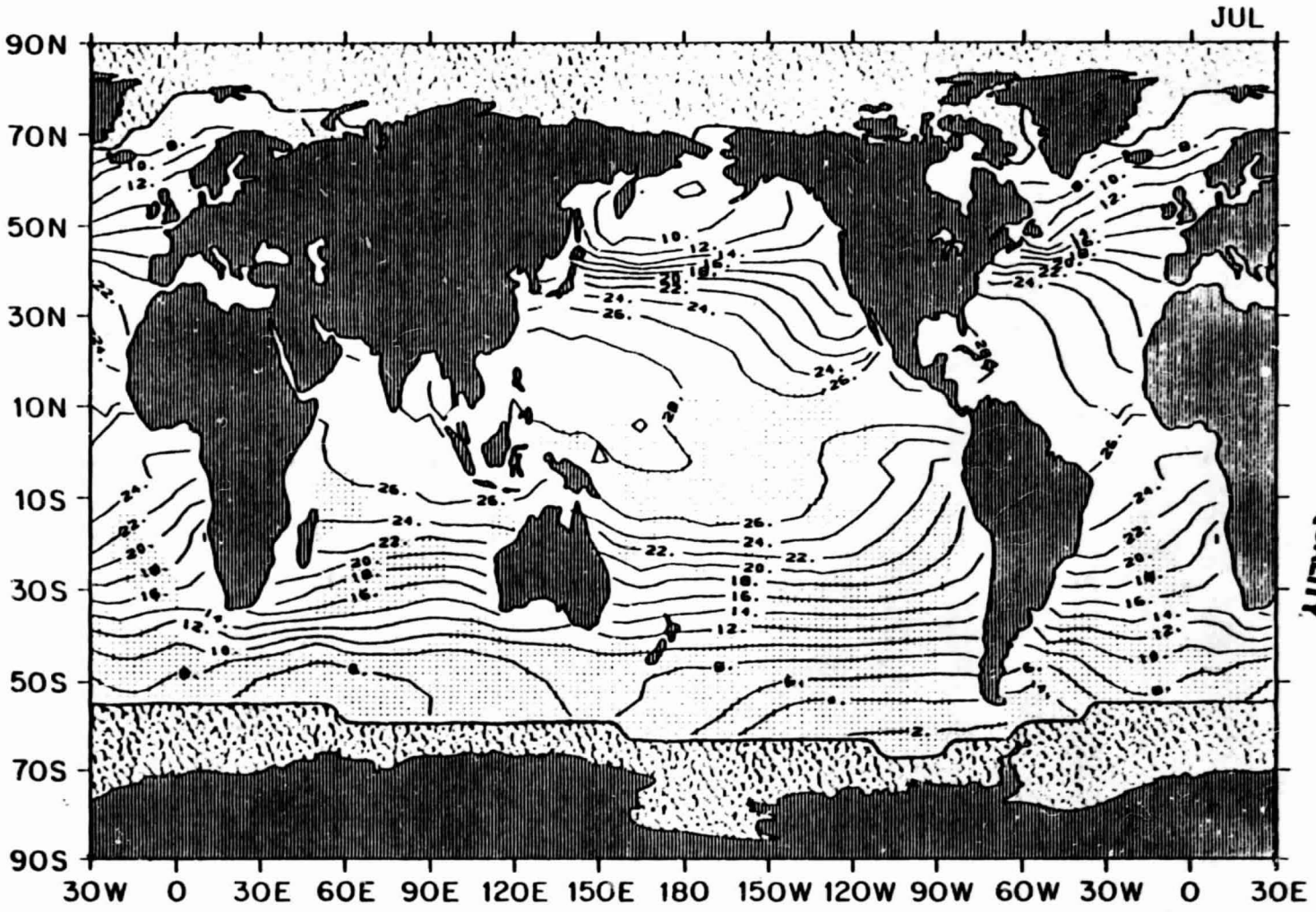

1.47 August mean air temperature (°C)

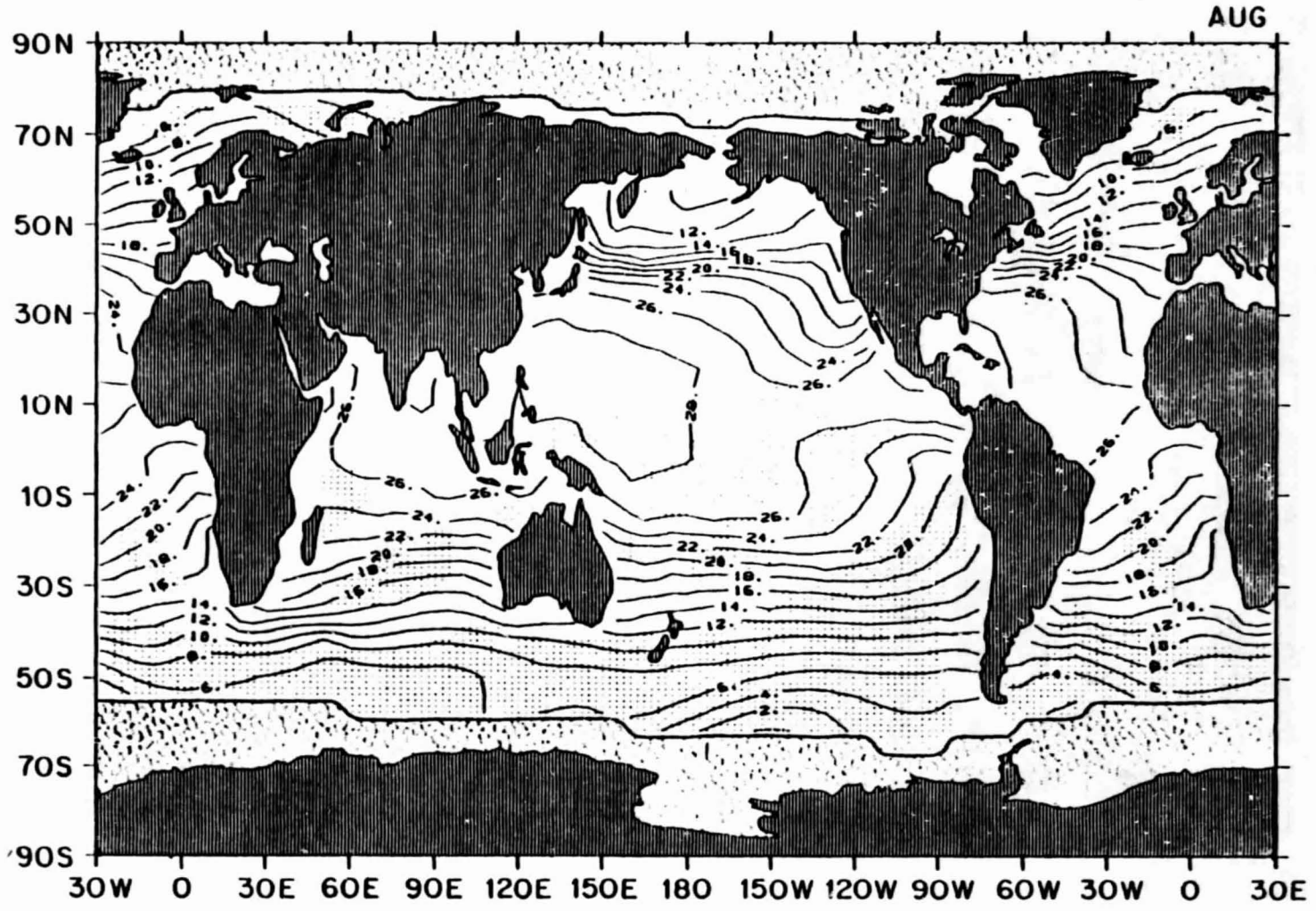

1.48 September mean air temperature (°C)

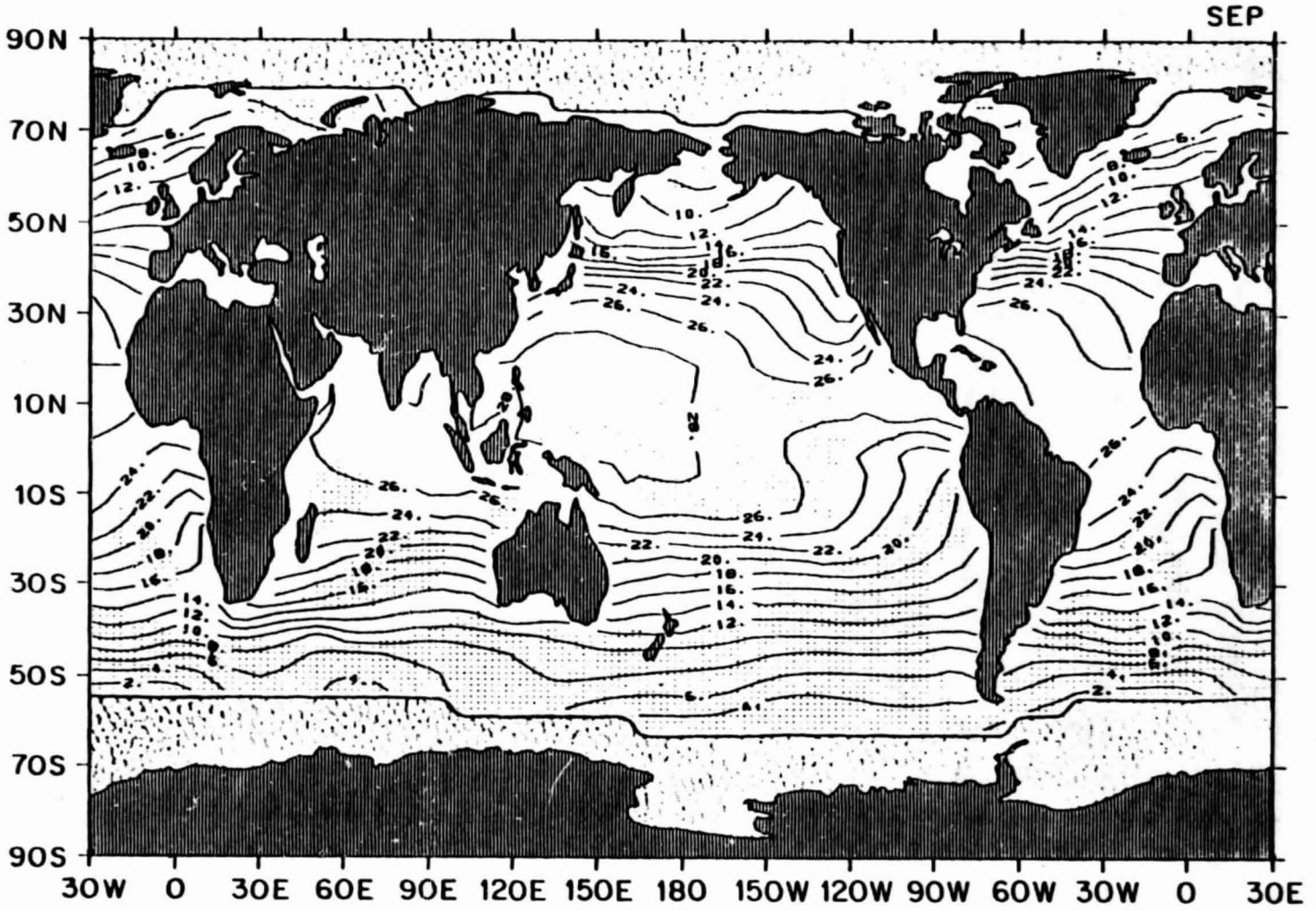

1.49 October mean air temperature (°C)

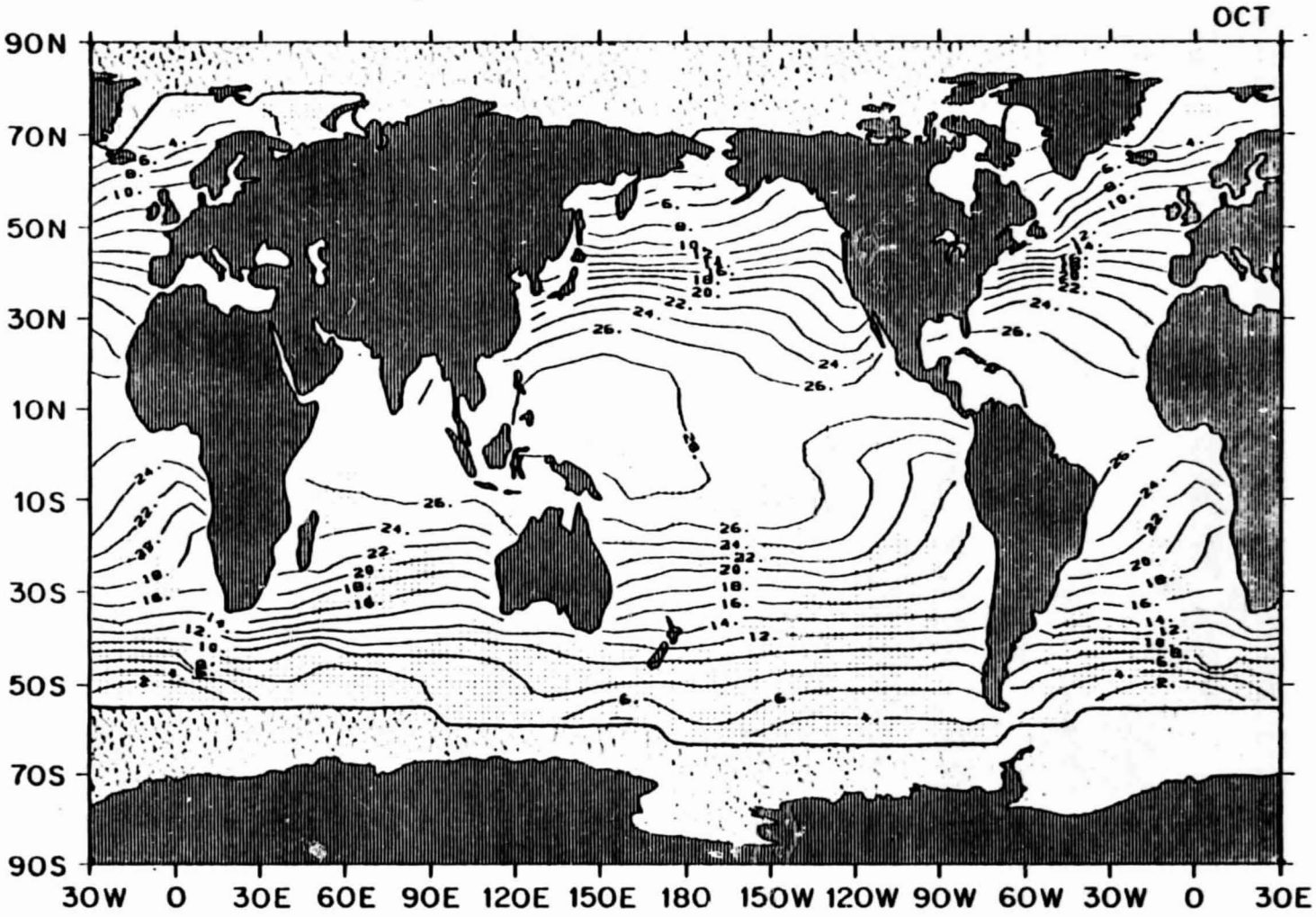

1.50 November mean air temperature (°C)

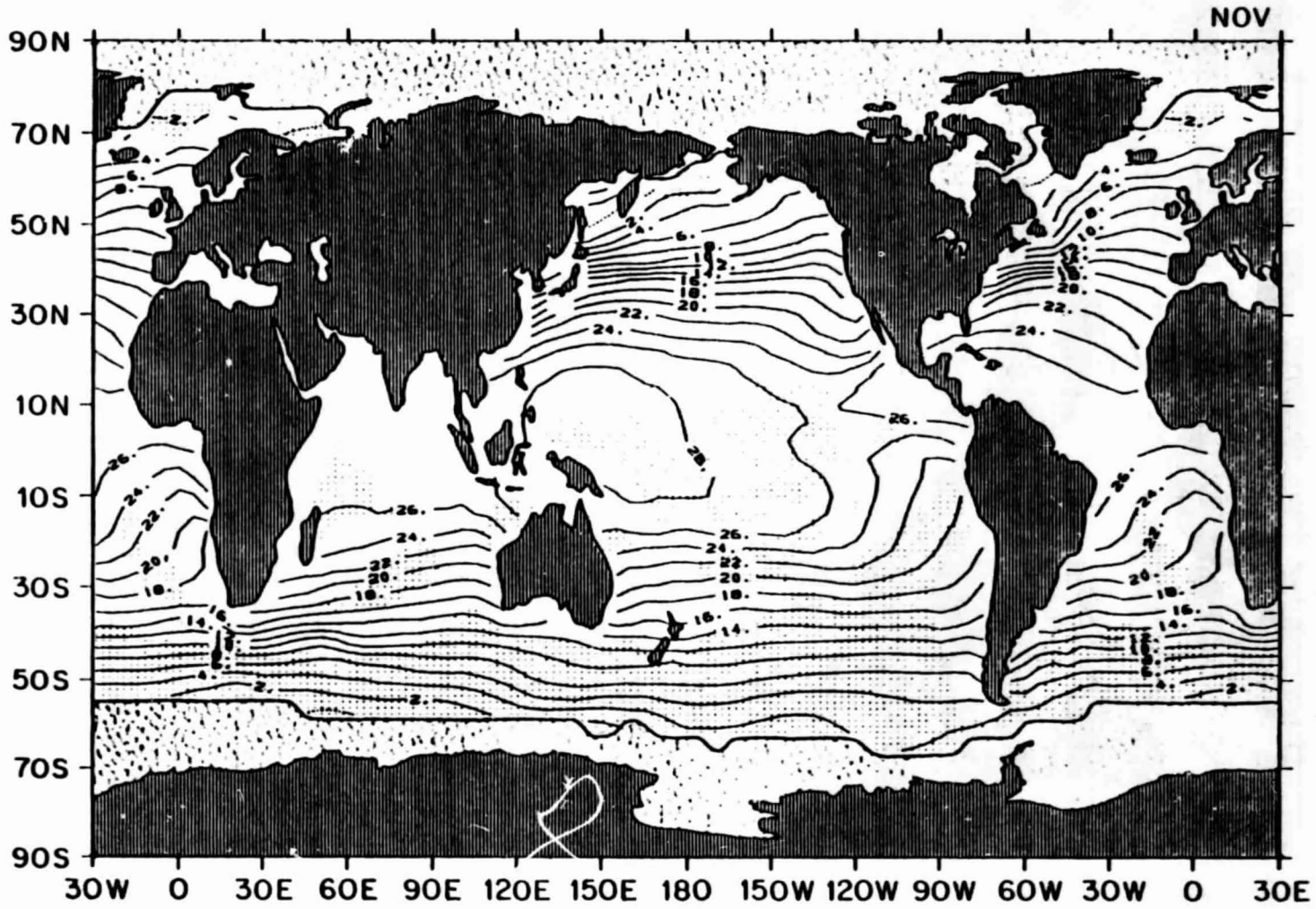

1.51 December mean air temperature (°C)

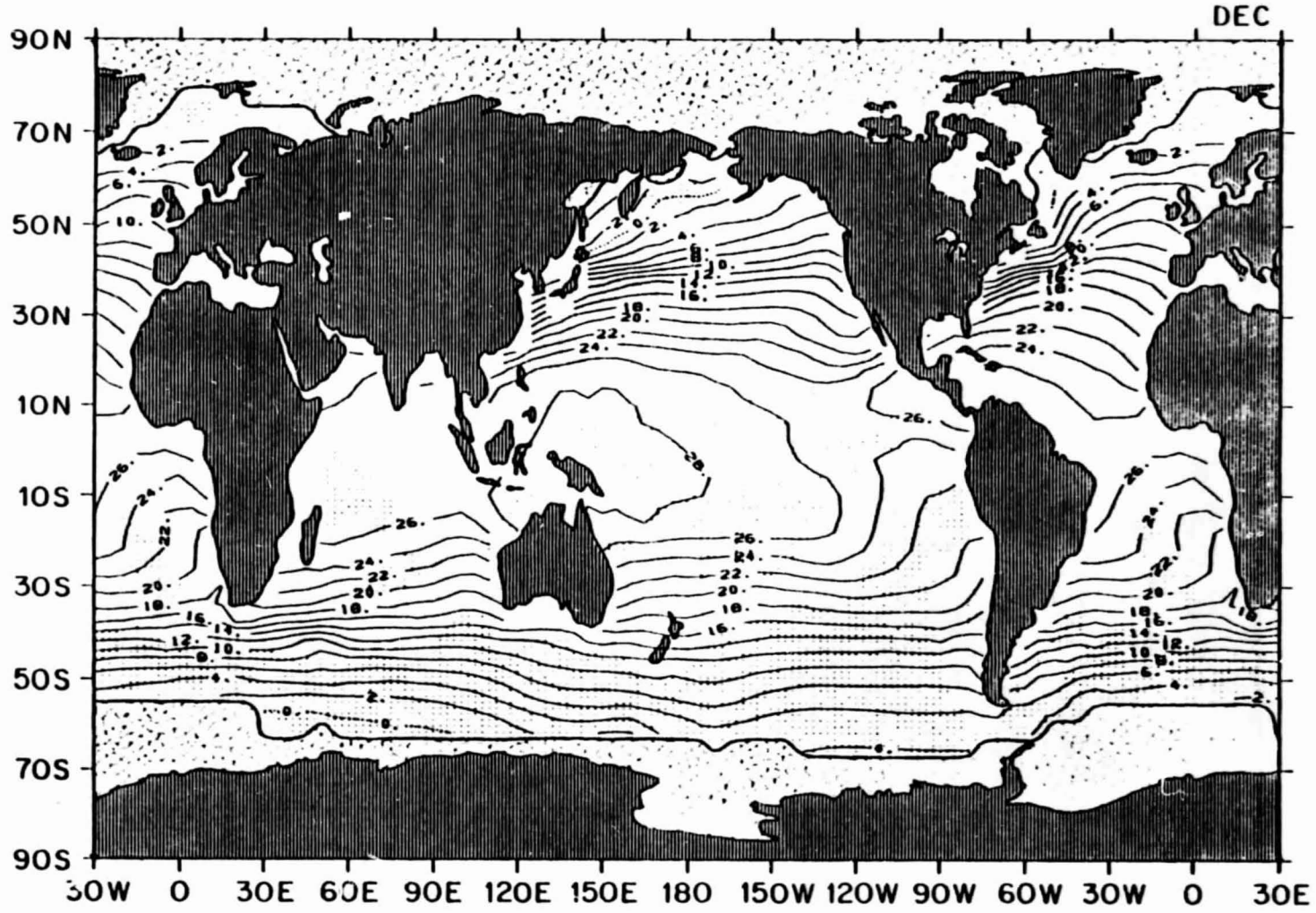

1.52 Annual mean air temperature (°C)

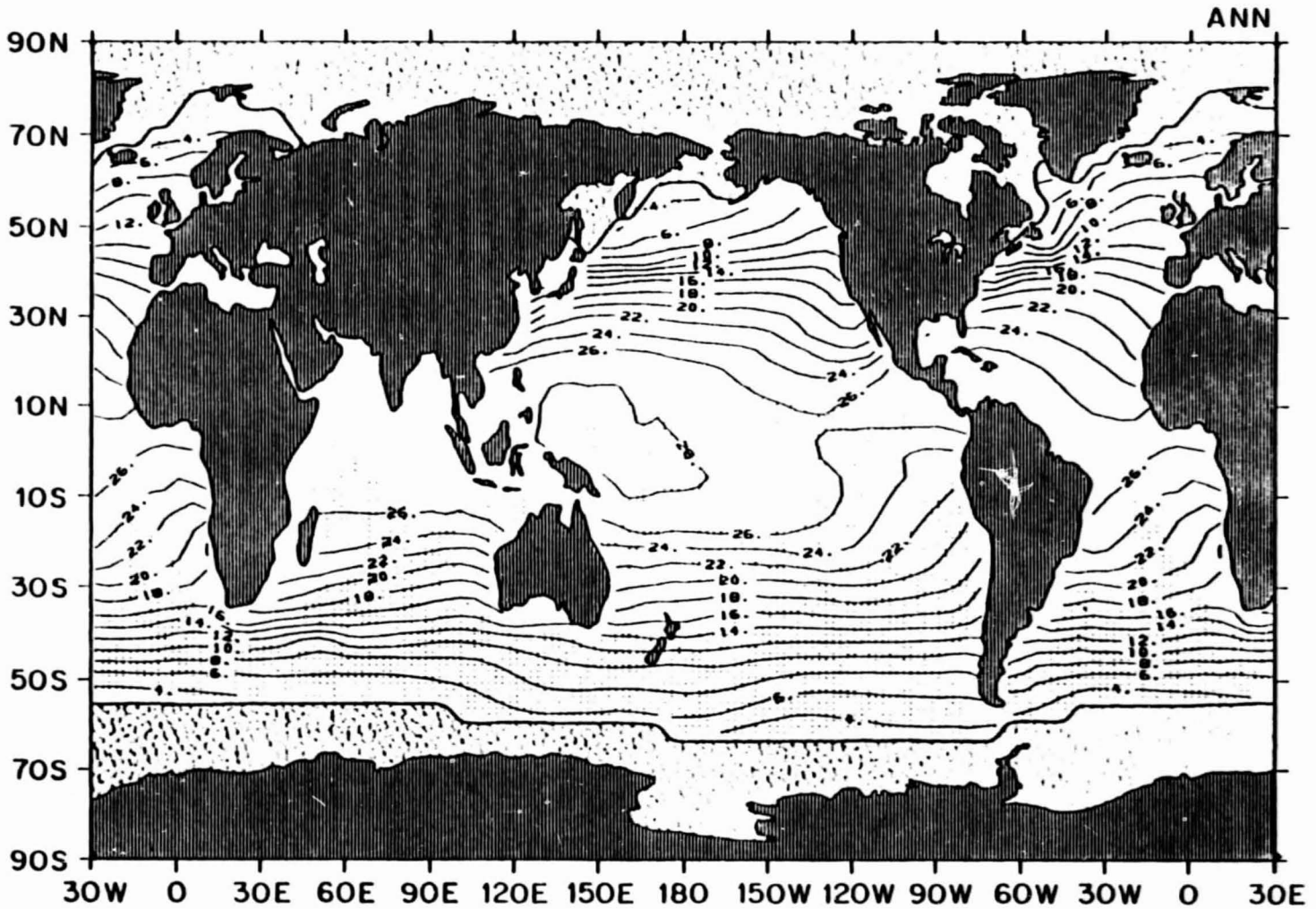

AIR SPECIFIC HUMIDITY

1.53 January mean air specific humidity (gm kg^{-1})

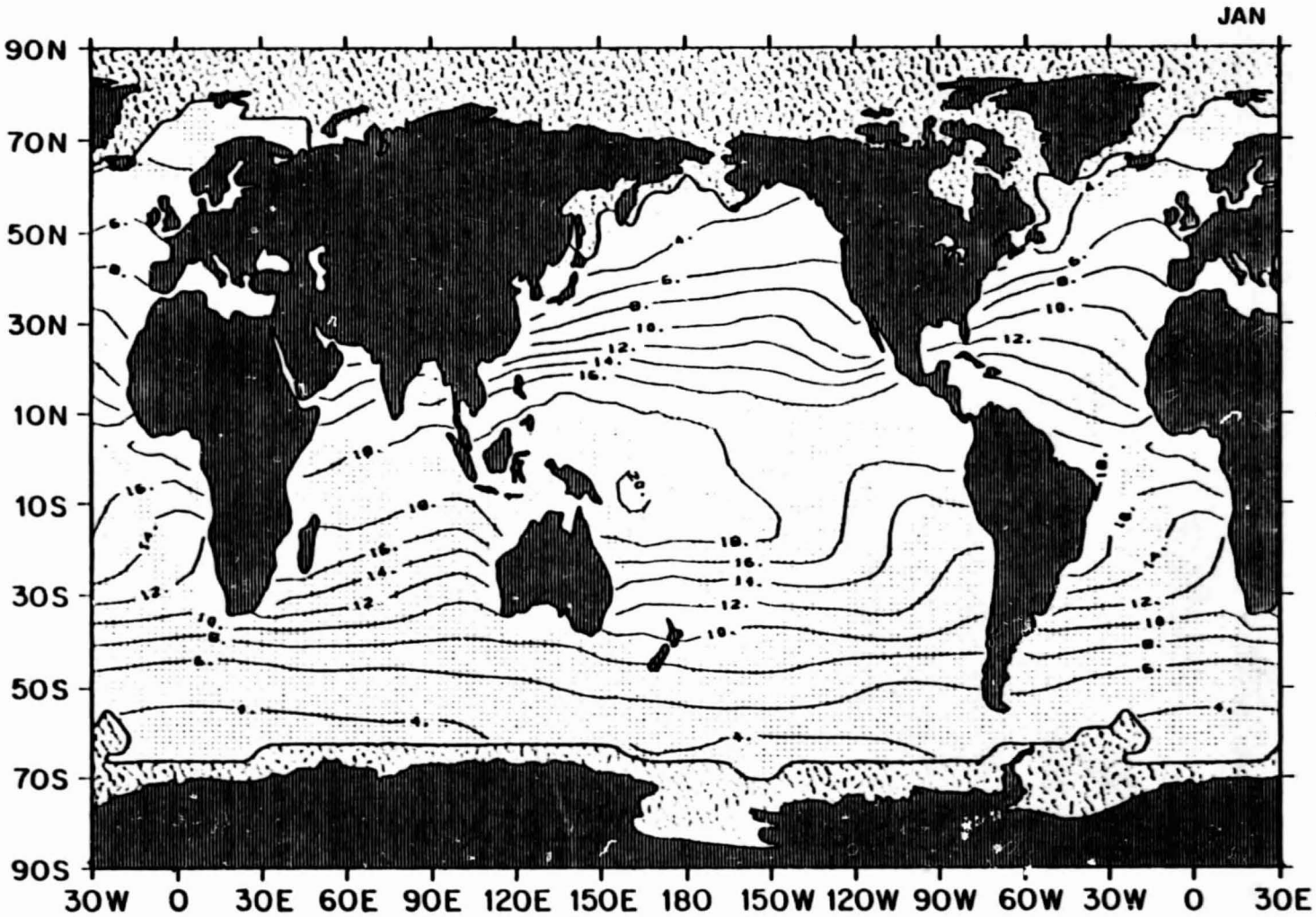

1.54 February mean air specific humidity (gm kg^{-1})

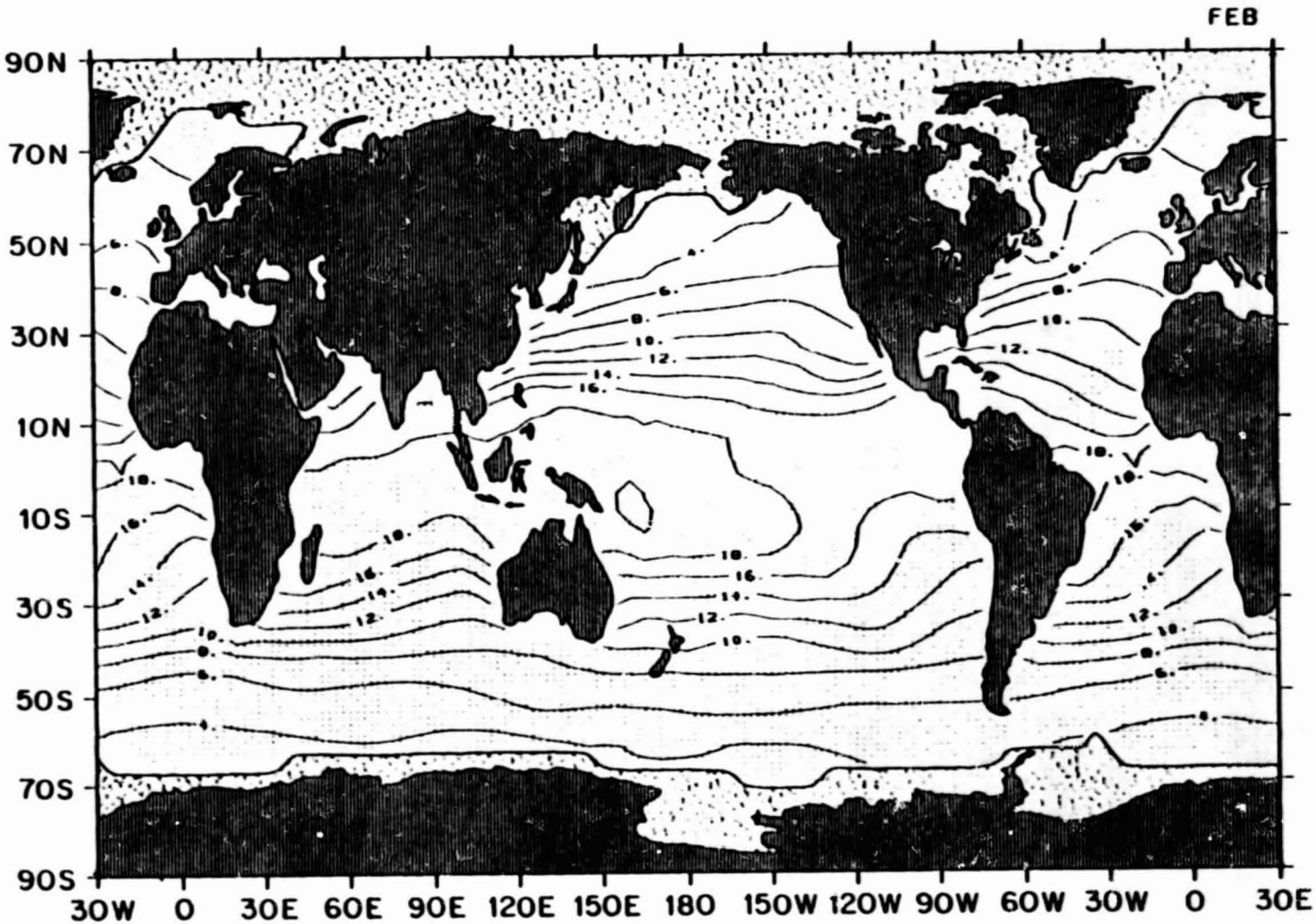

1.55 March mean air specific humidity (gm kg^{-1})

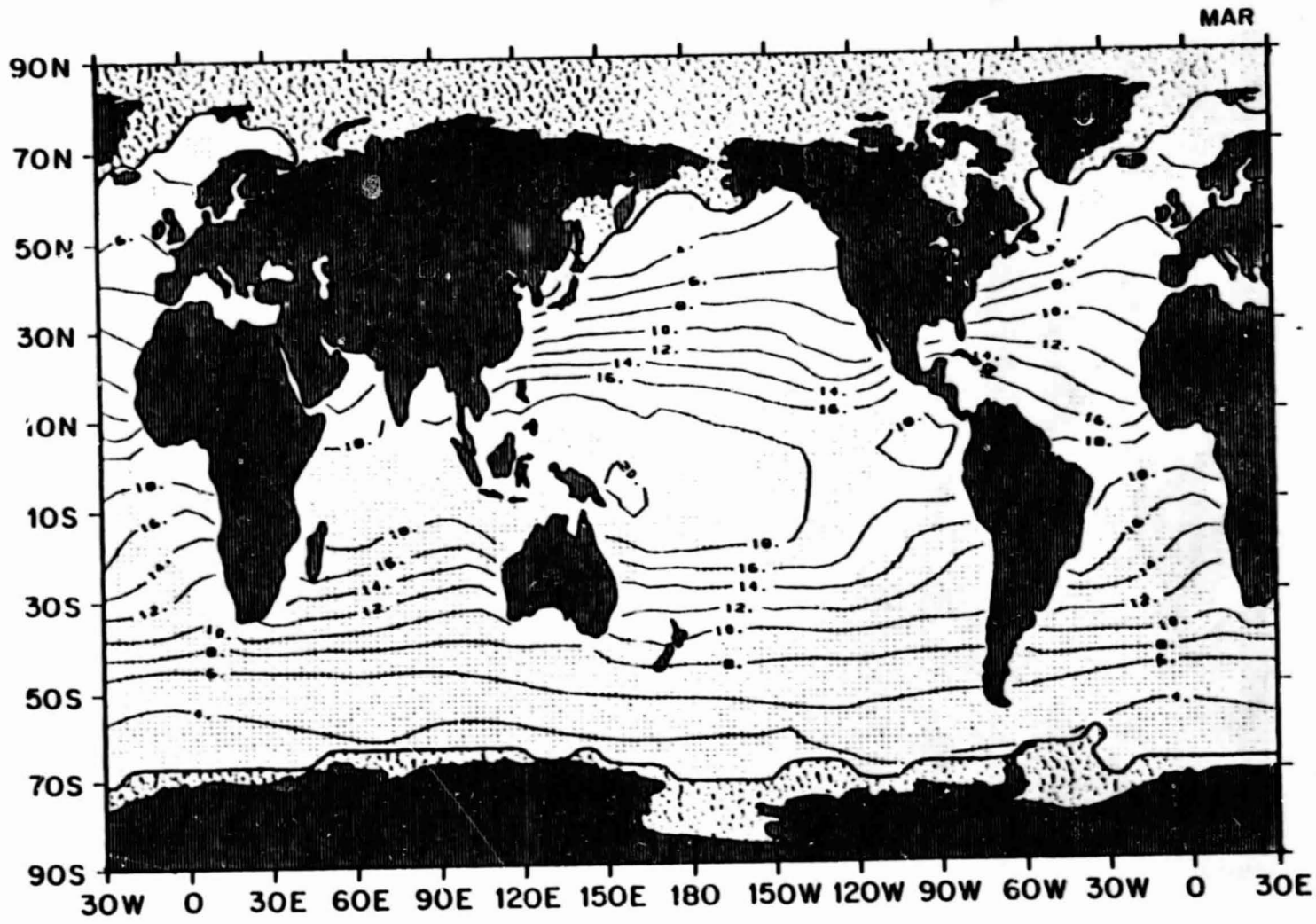

1.56 April mean air specific humidity (gm kg^{-1})

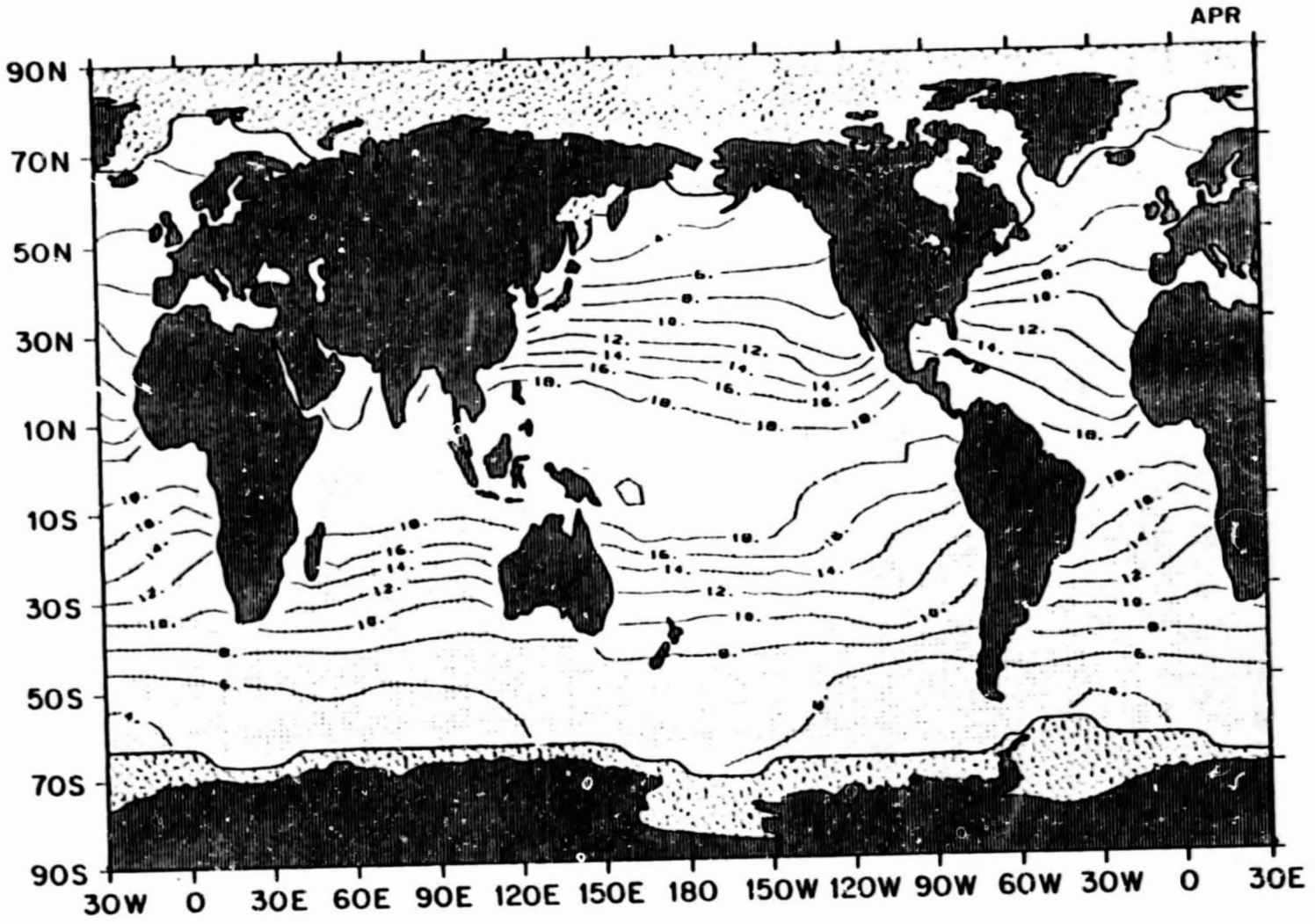

1.57 May mean air specific humidity (gm kg^{-1})

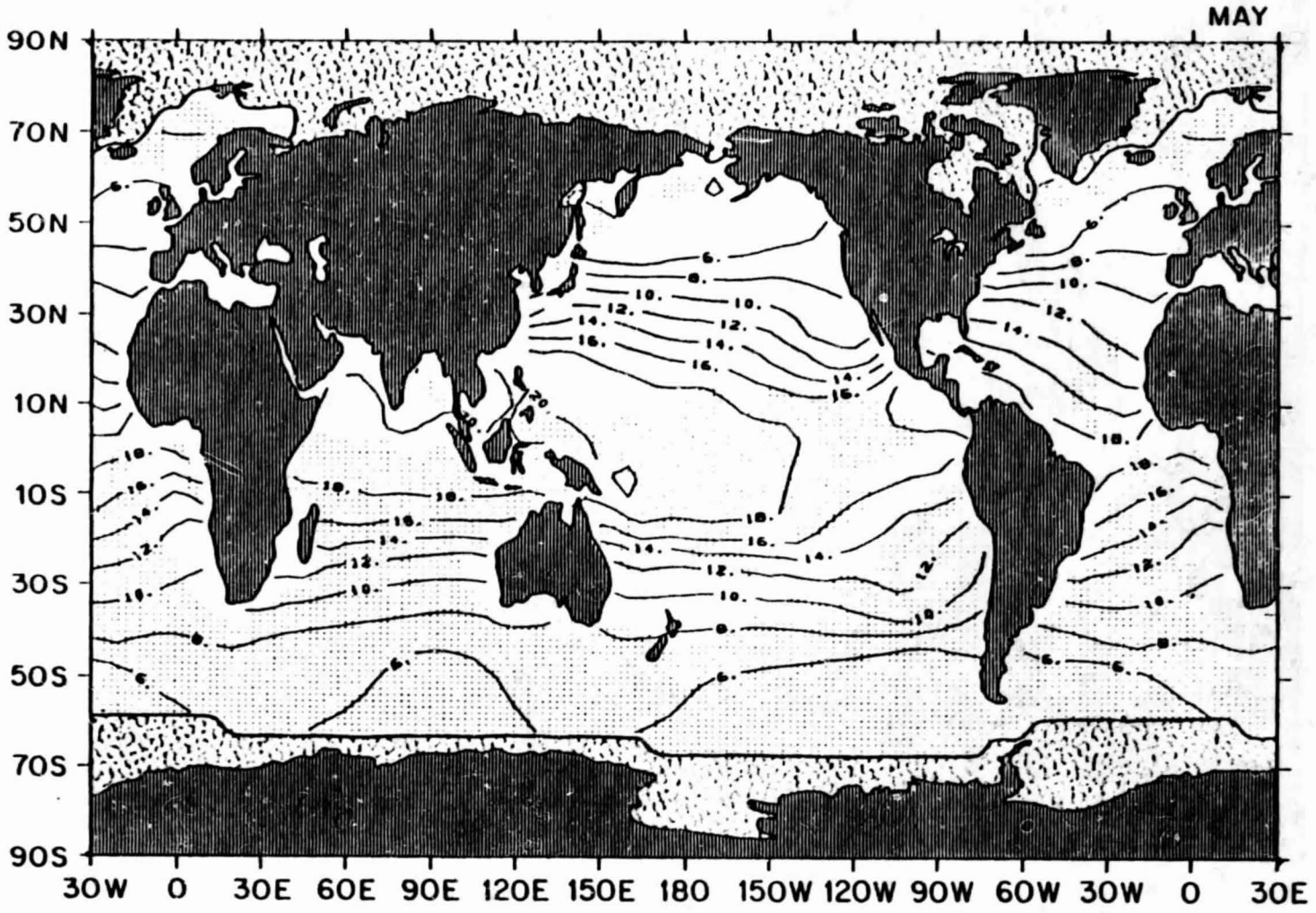

1.58 June mean air specific humidity (gm kg^{-1})

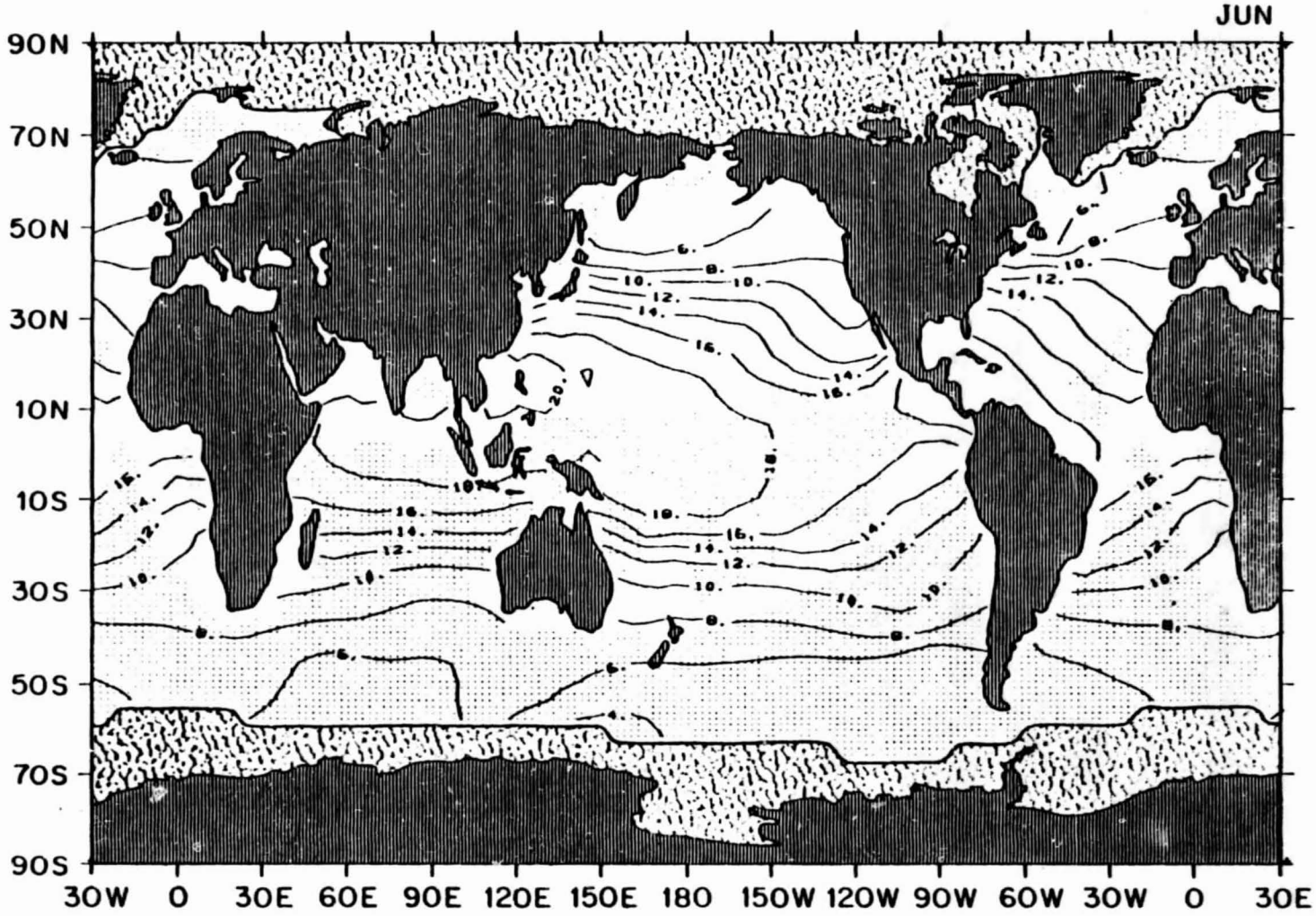

1.59 July mean air specific humidity (gm kg^{-1})

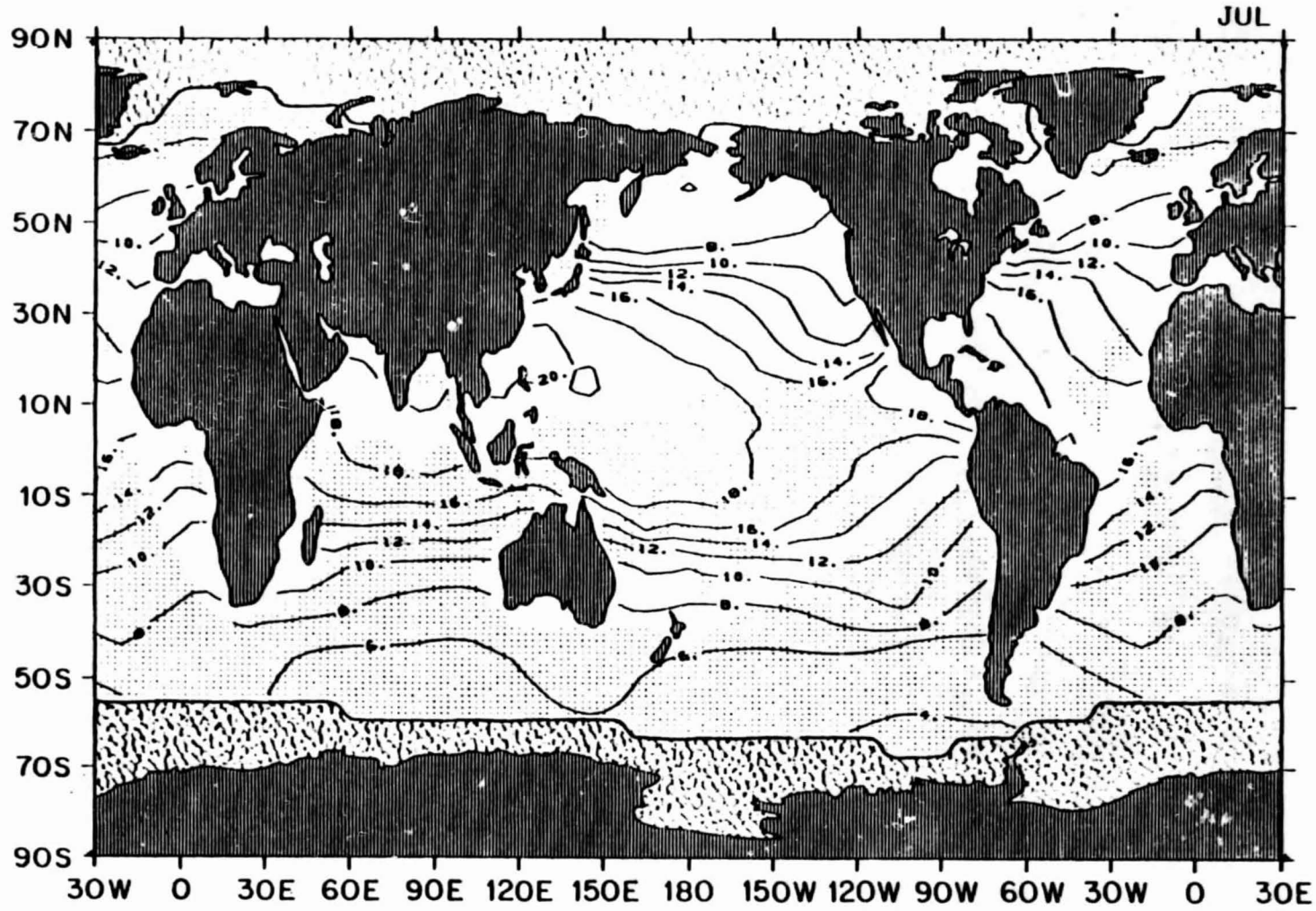

1.60 August mean air specific humidity (gm kg^{-1})

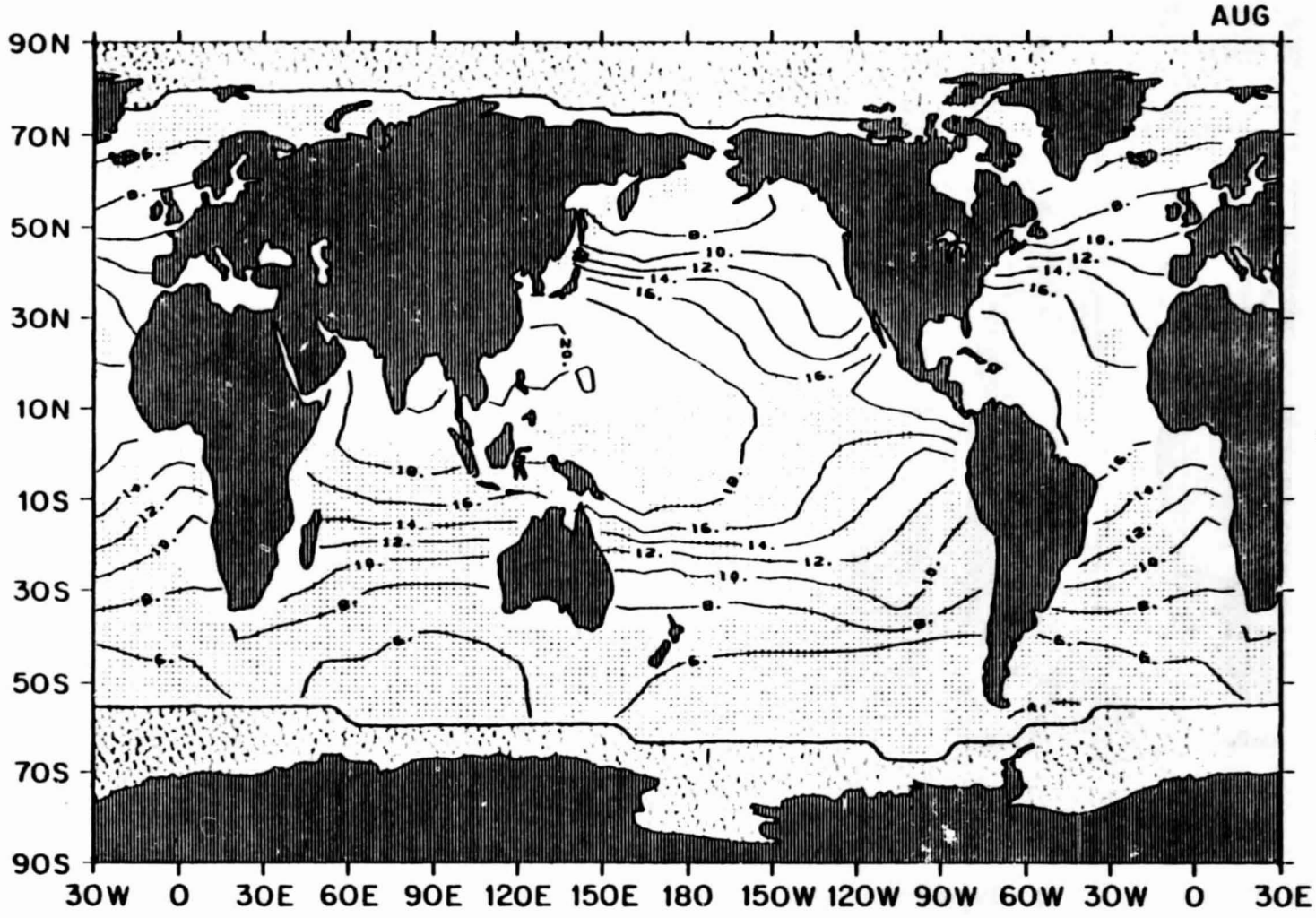

1.61 September mean air specific humidity (gm kg^{-1})

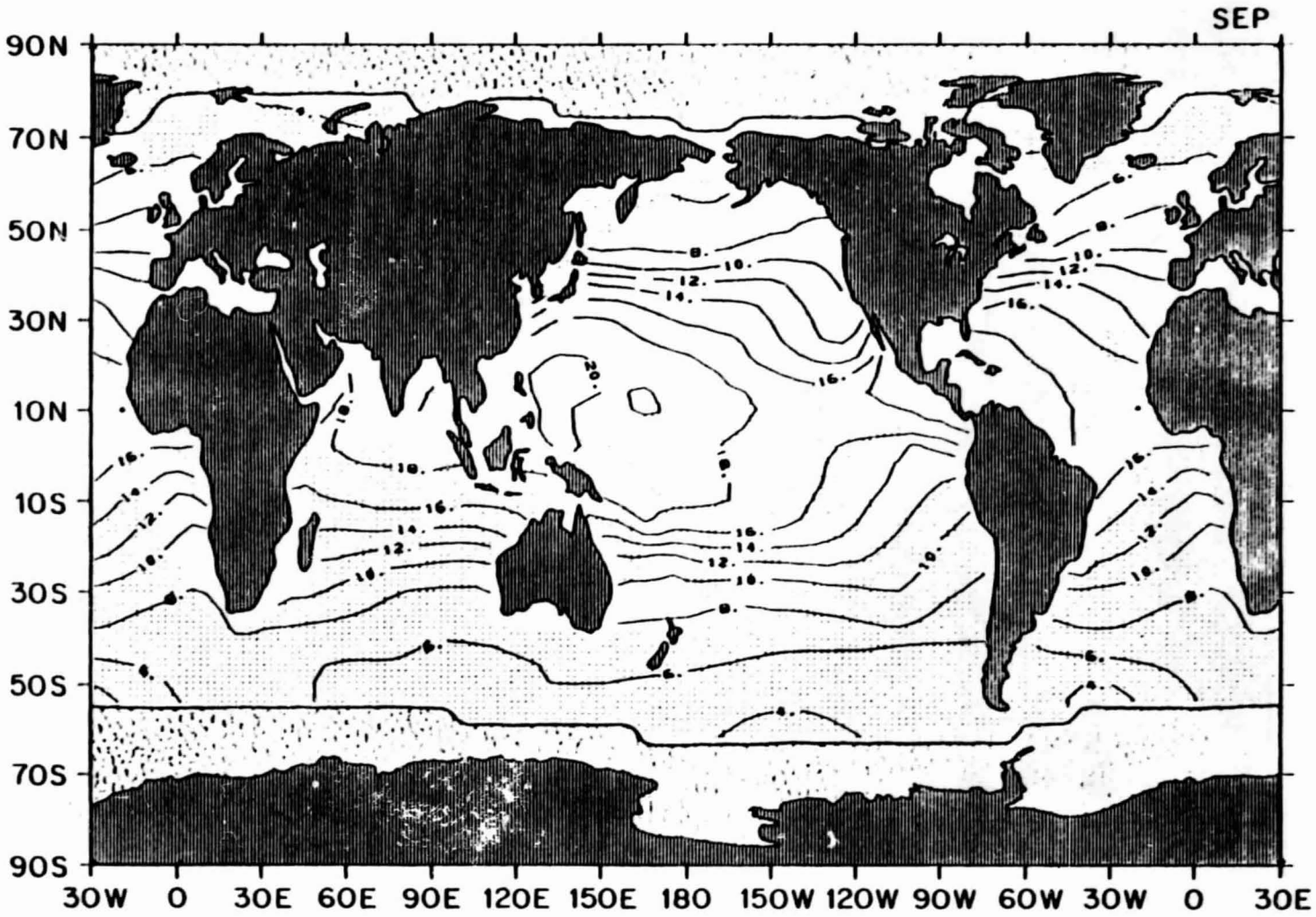

1.62 October mean air specific humidity (gm kg^{-1})

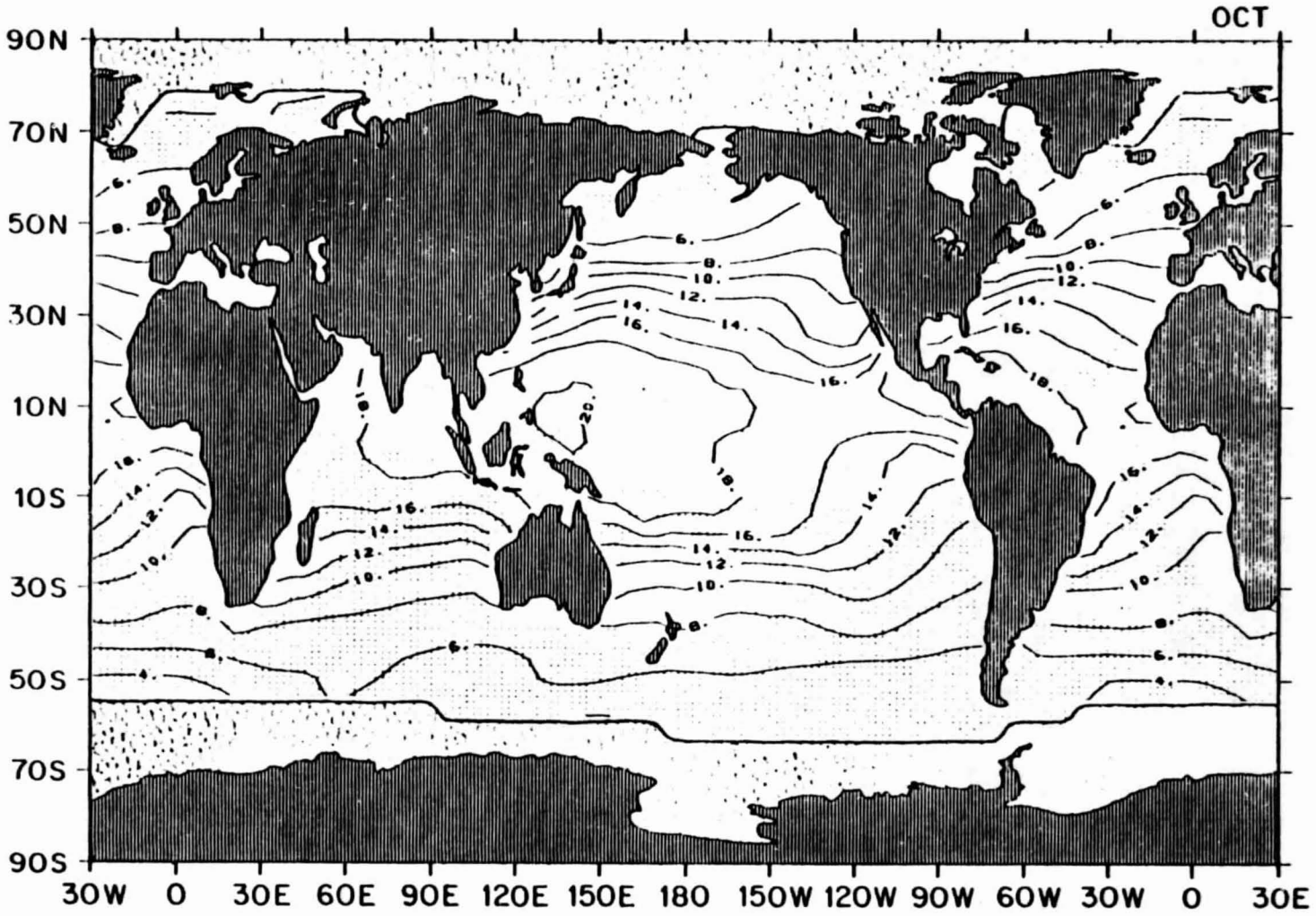

1.63 November mean air specific humidity (gm kg^{-1})

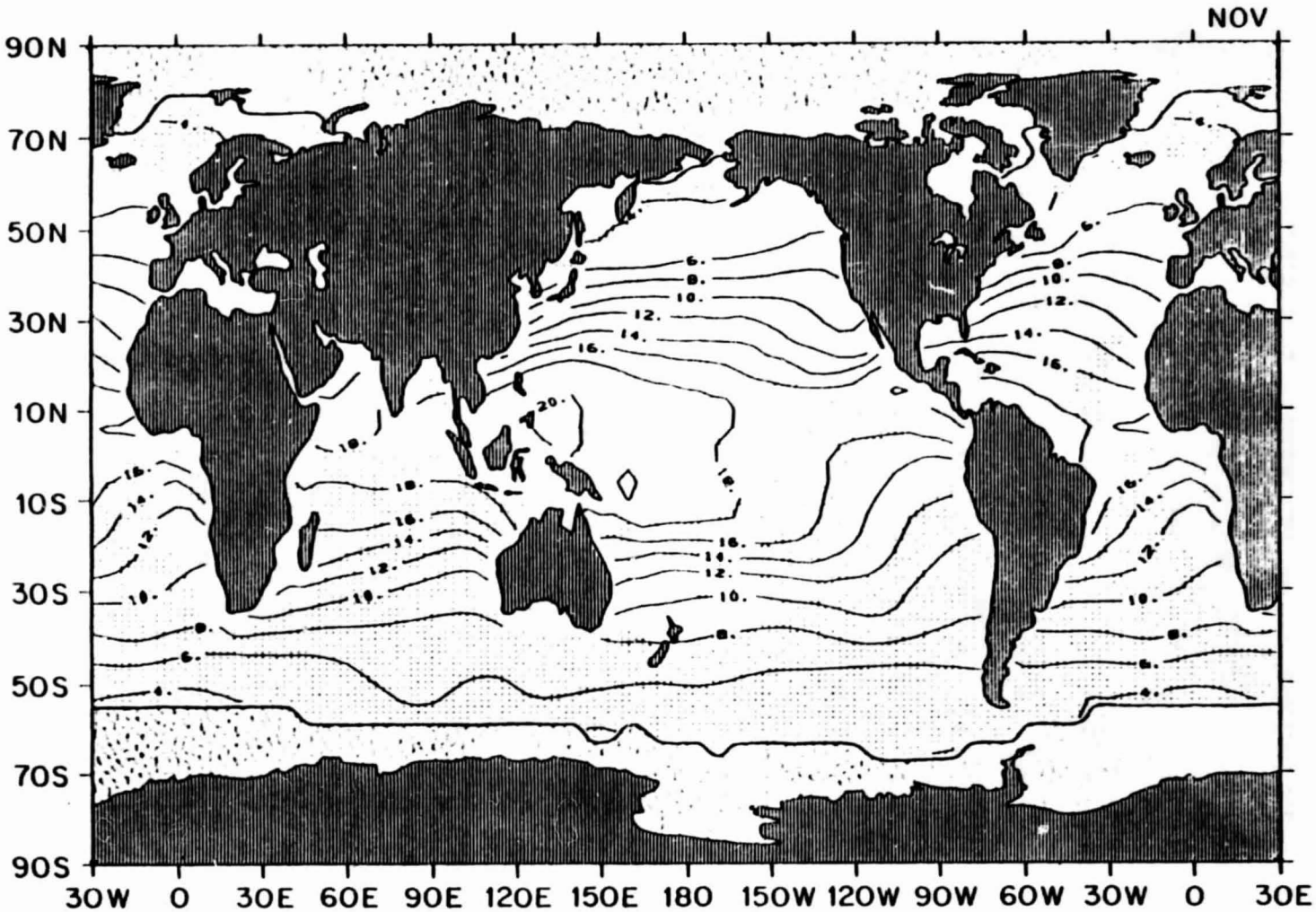

1.64 December mean air specific humidity (gm kg^{-1})

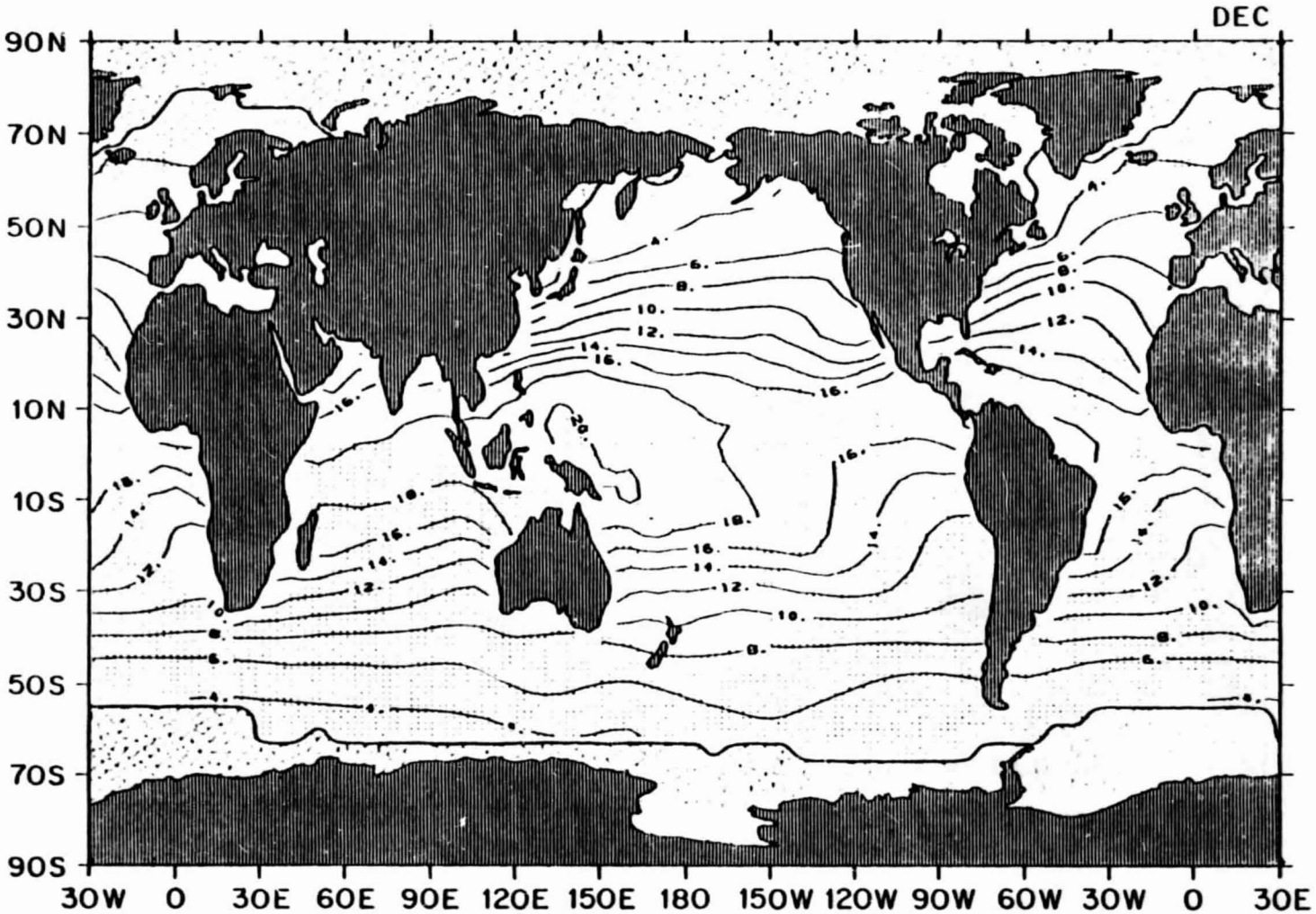

1.65 Annual mean air specific humidity (gm kg^{-1})

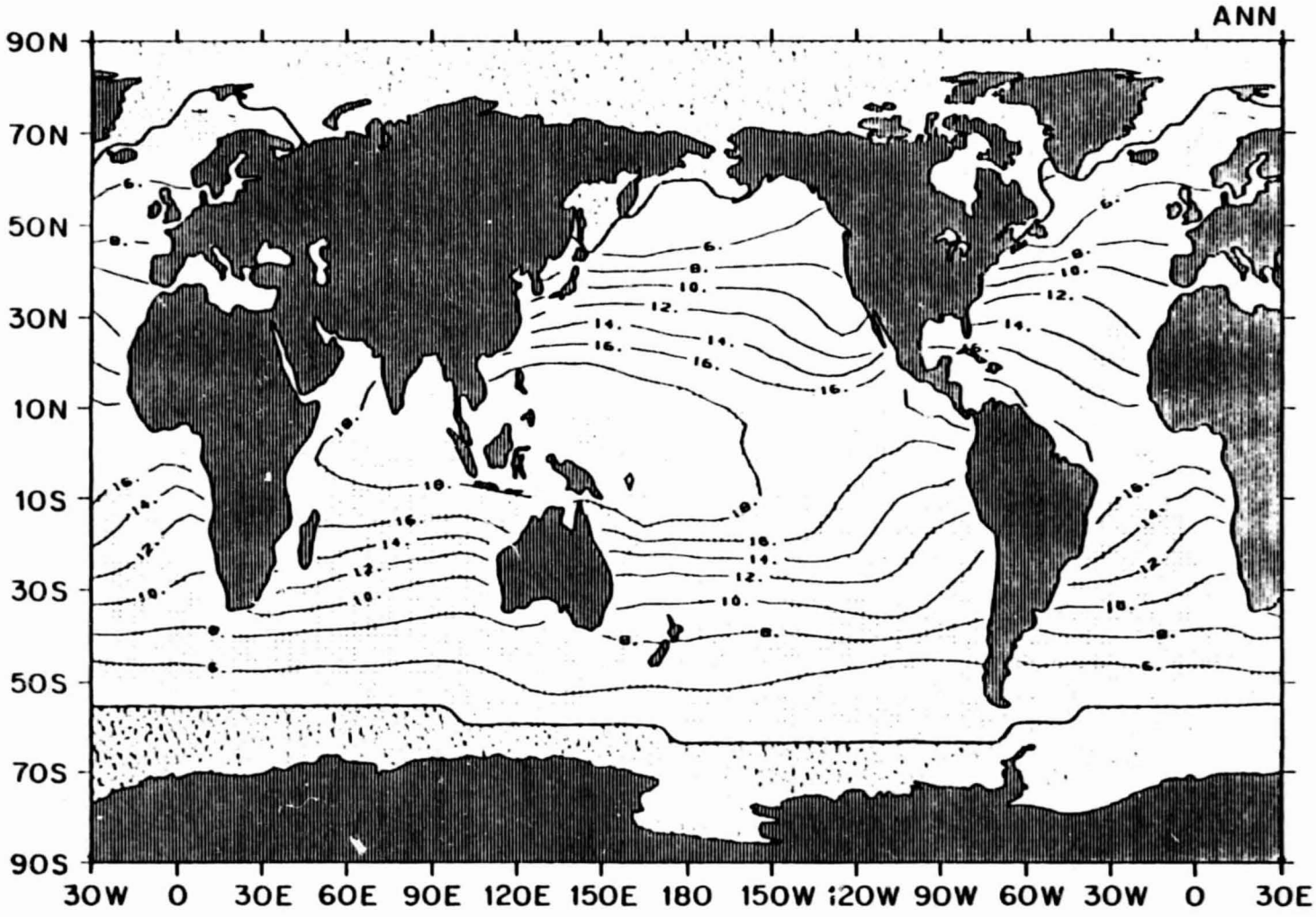

SEA - AIR SPECIFIC HUMIDITY DIFFERENCE

1.66 January mean sea - air specific humidity difference (gm kg^{-1})

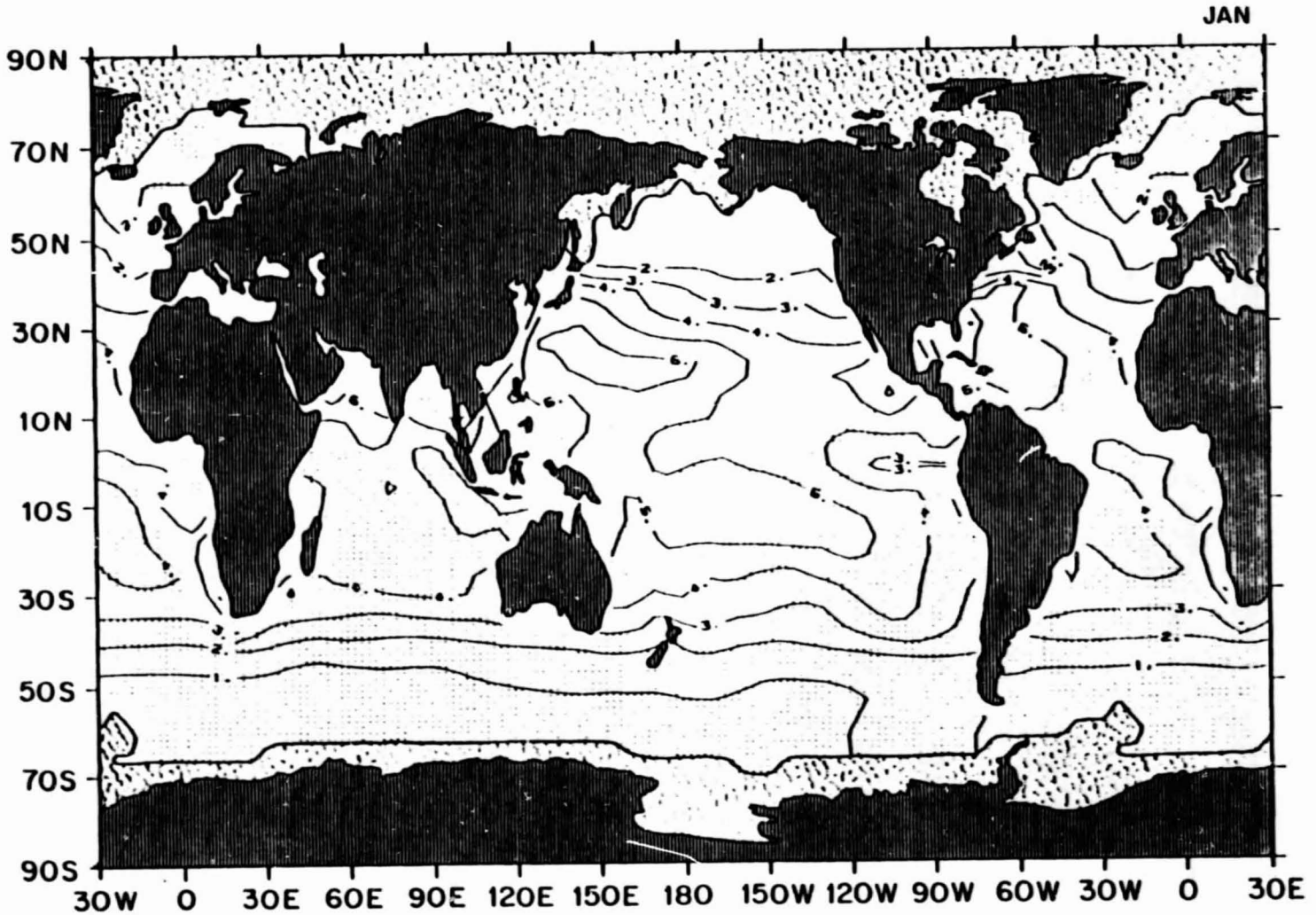

1.67 February mean sea - air specific humidity difference (gm kg^{-1})

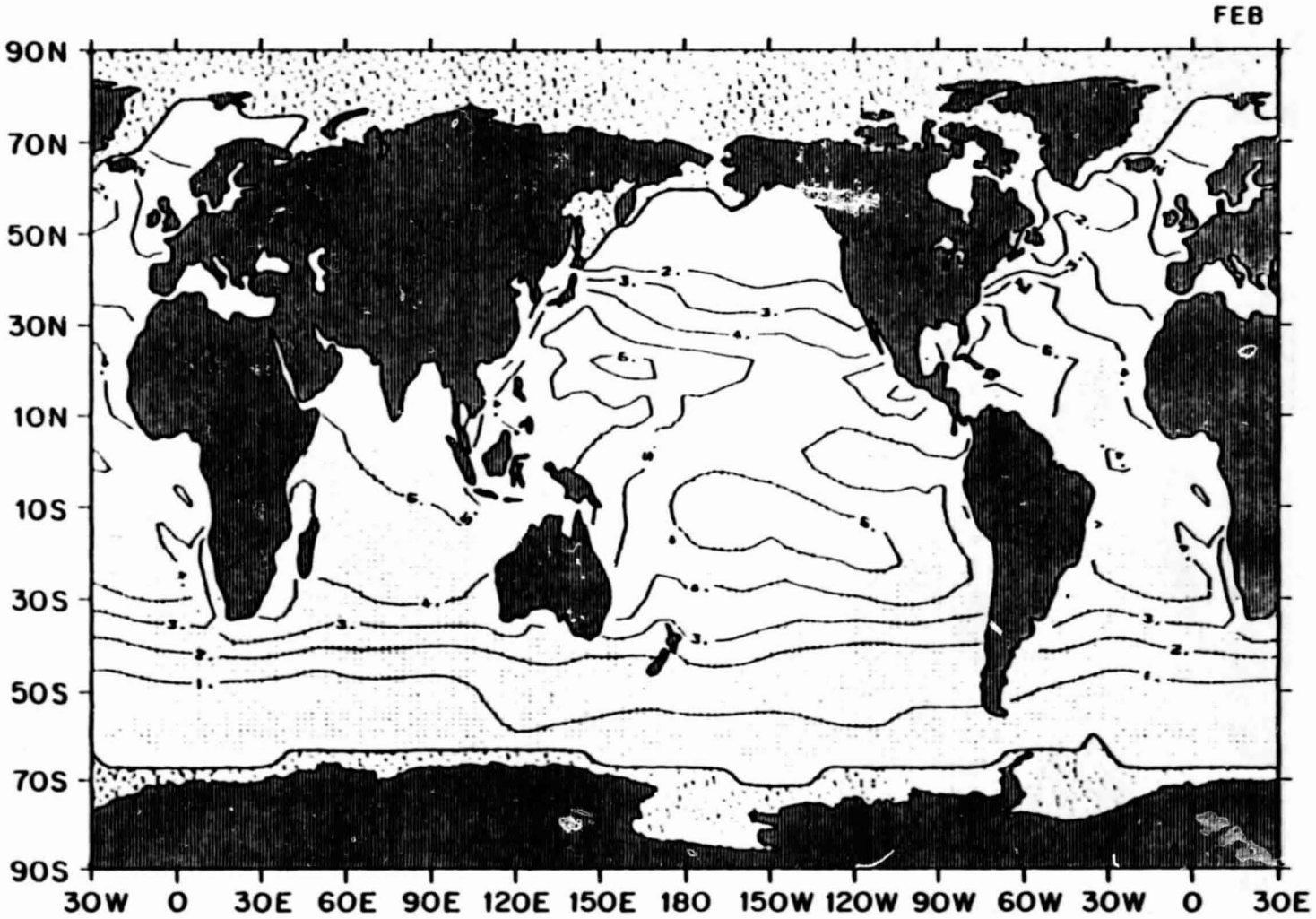

1.68 March mean sea - air specific humidity difference (gm kg^{-1})

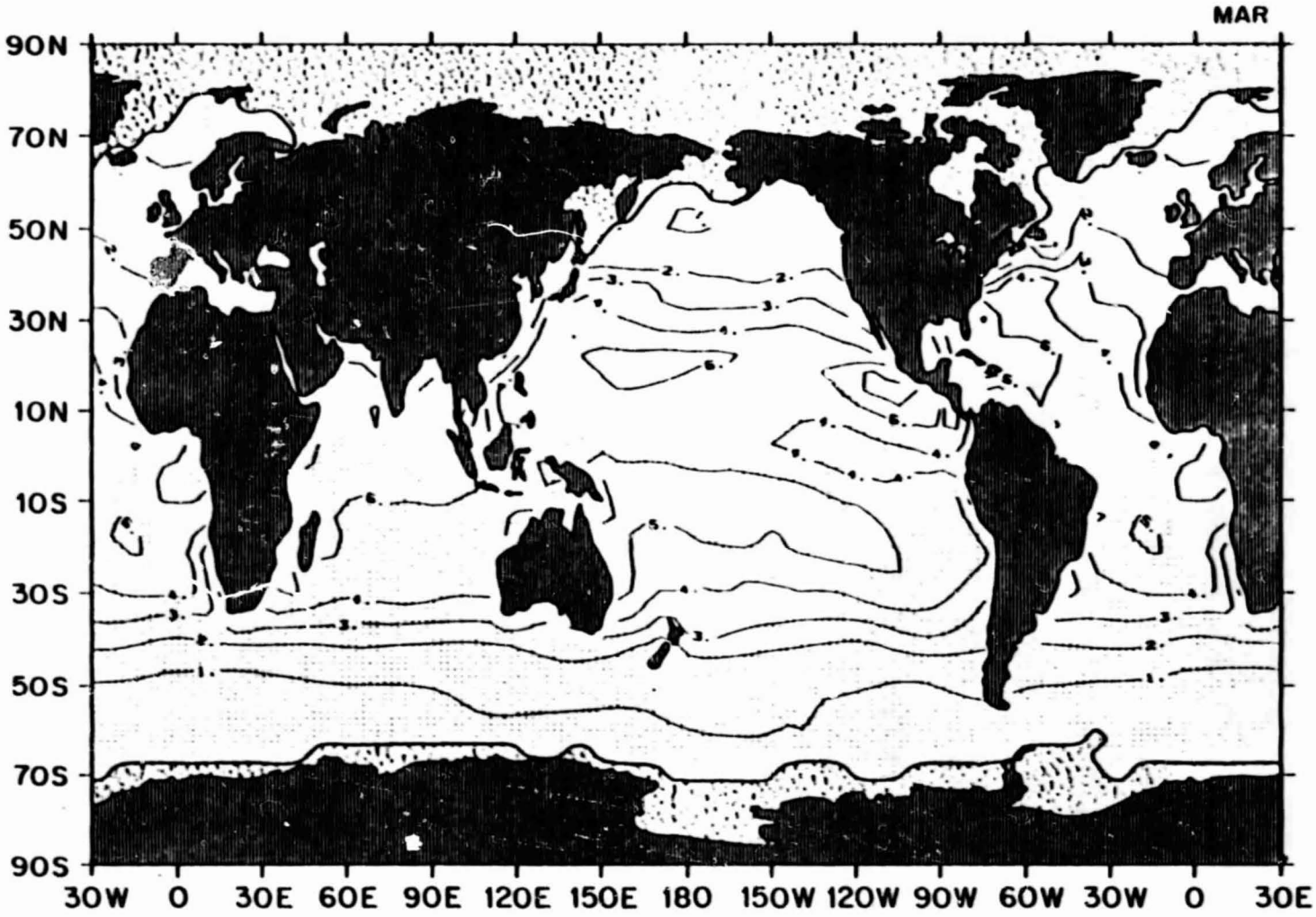

1.69 April mean sea - air specific humidity difference (gm kg^{-1})

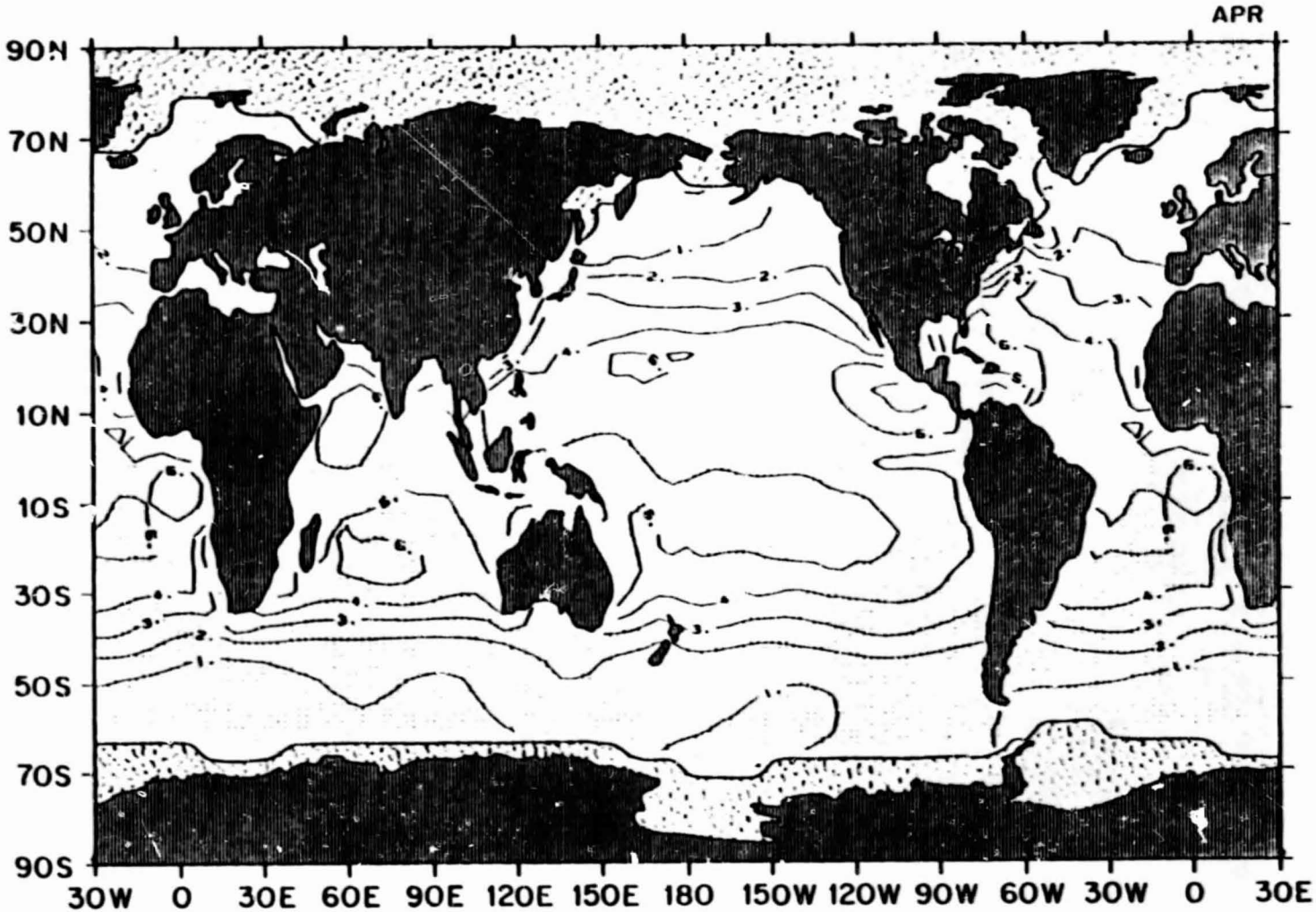

1.70 May mean sea - air specific humidity difference (gm kg^{-1})

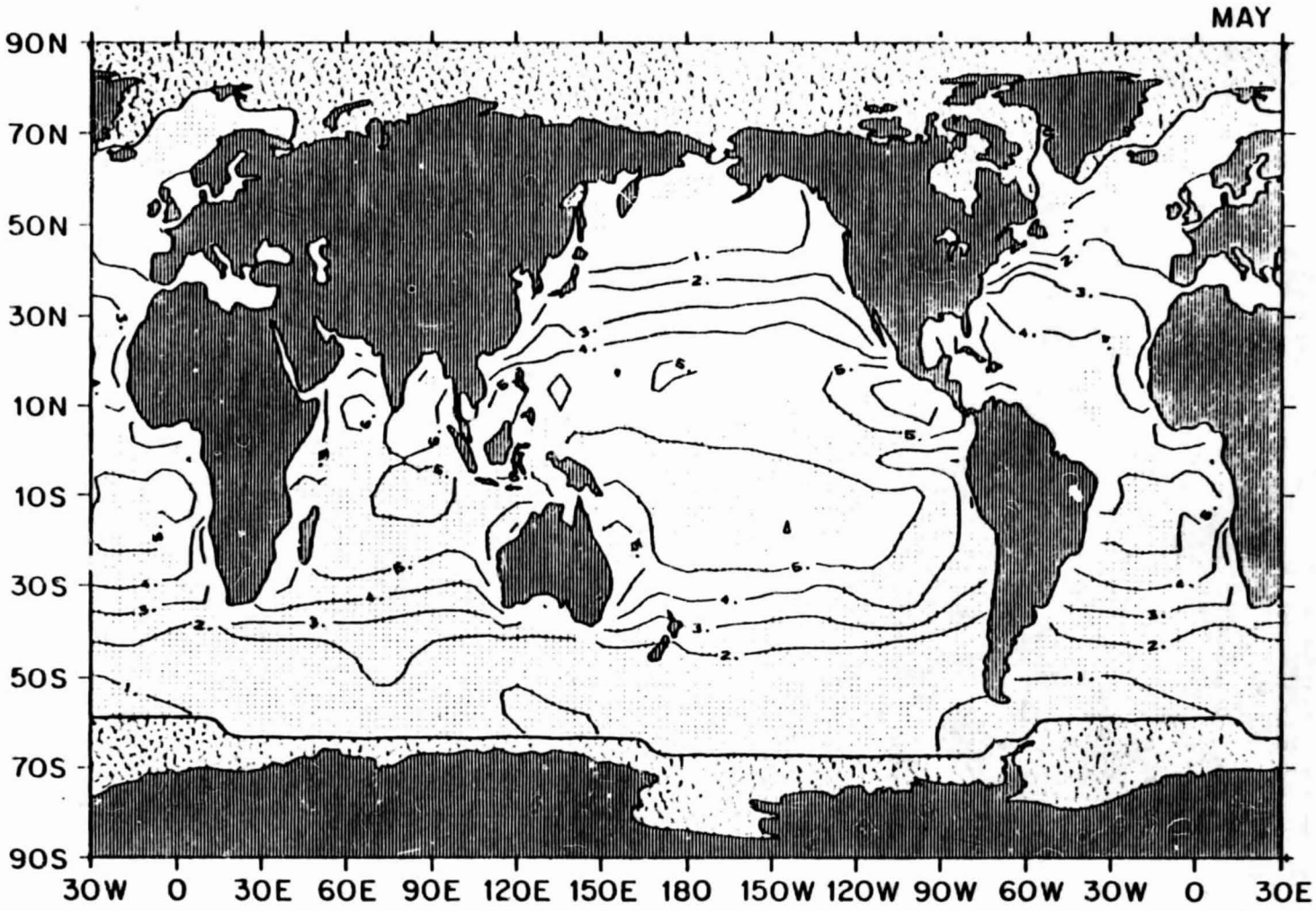

1.71 June mean sea - air specific humidity difference (gm kg^{-1})

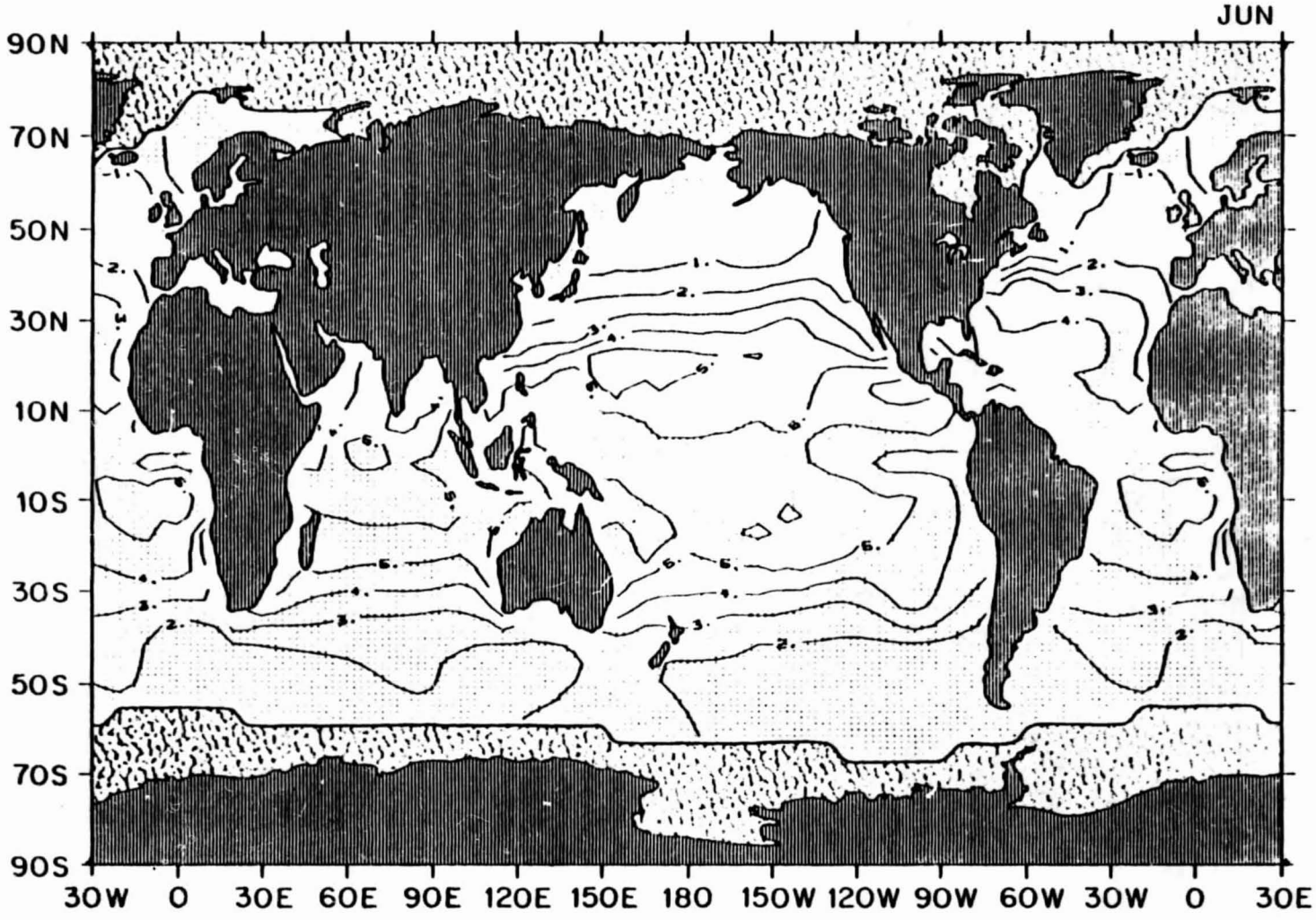

1.72 July mean sea - air specific humidity difference (gm kg^{-1})

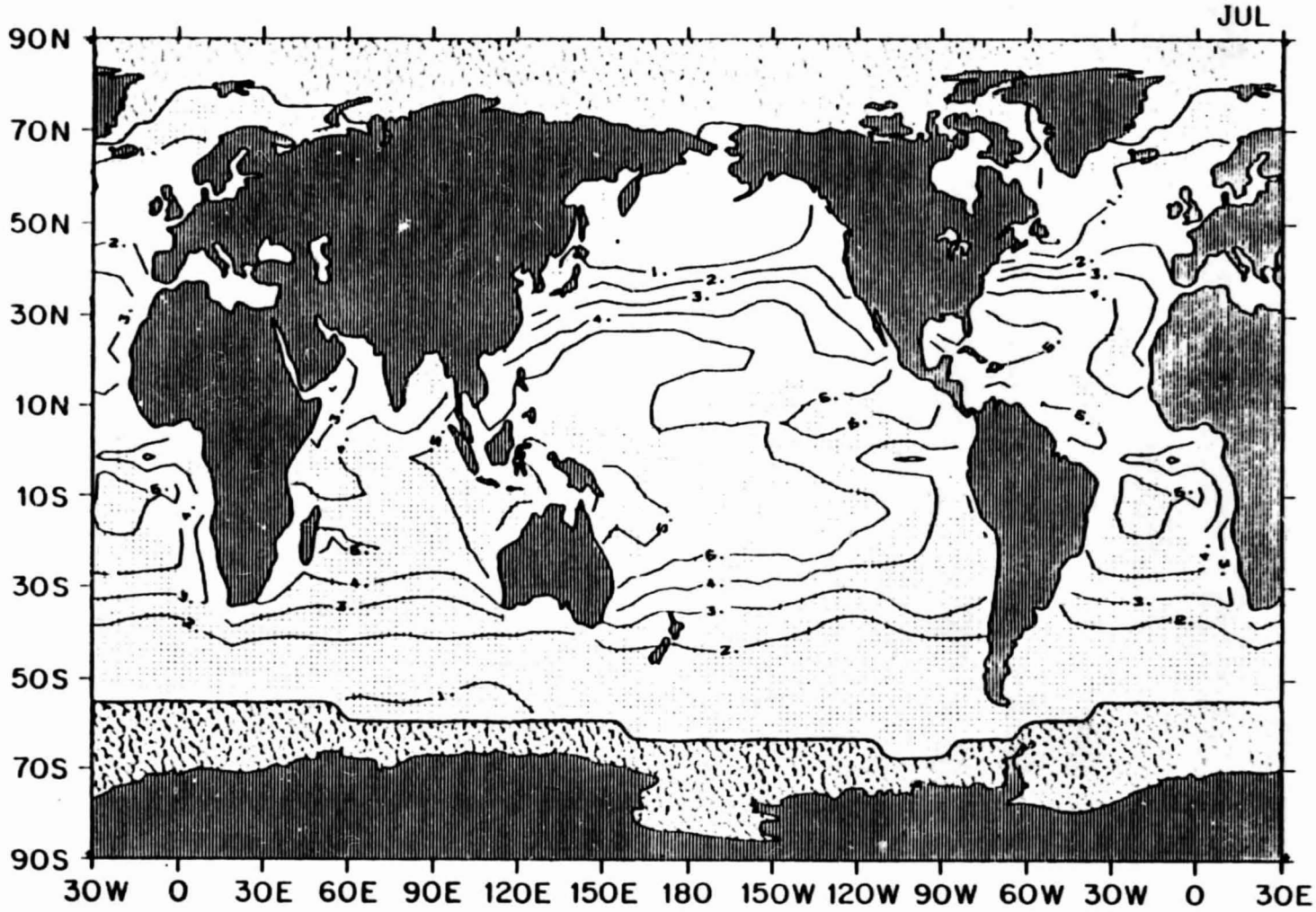

1.73 August mean sea - air specific humidity difference (gm kg^{-1})

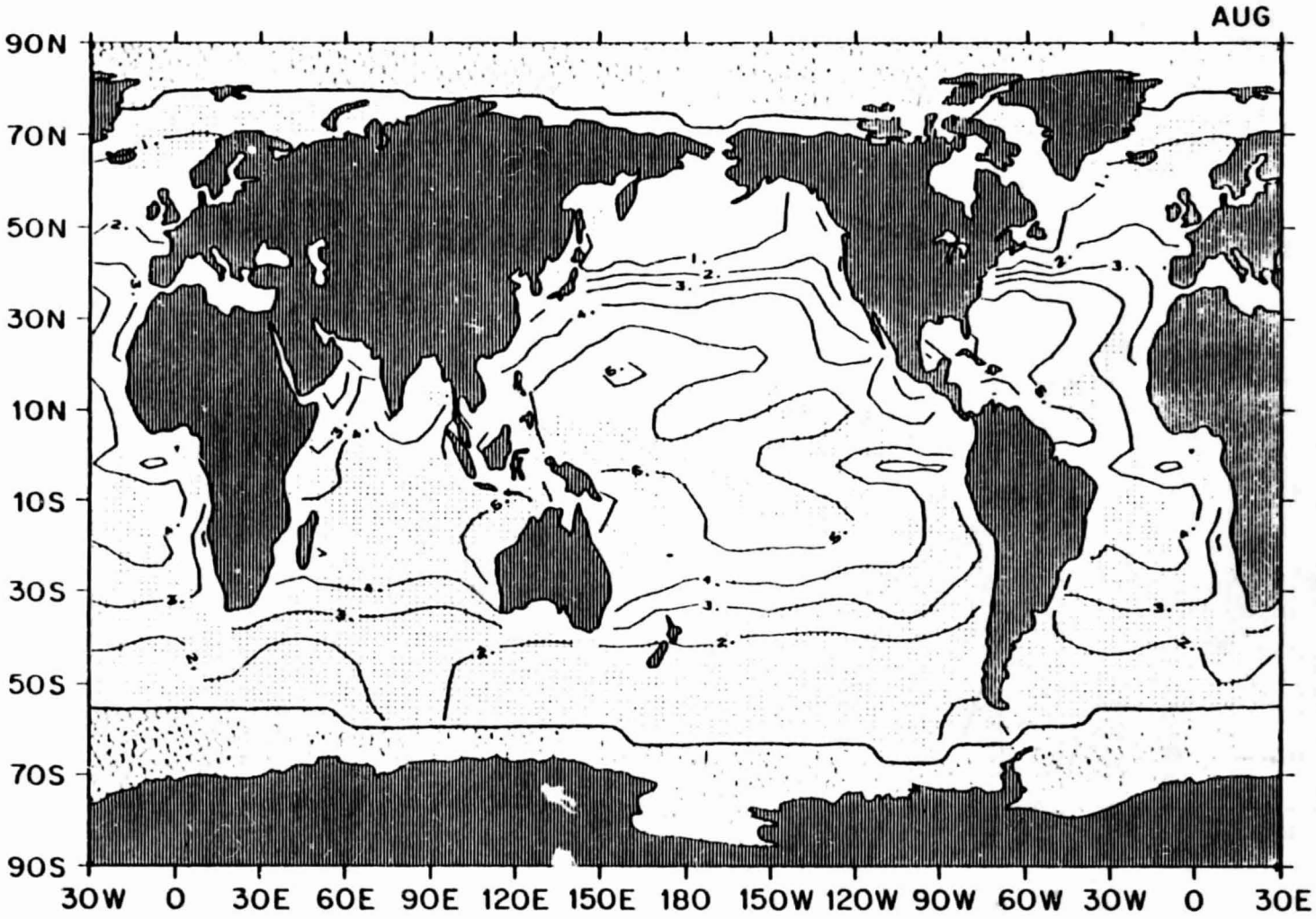

1.74 September mean sea - air specific humidity difference (gm kg^{-1})

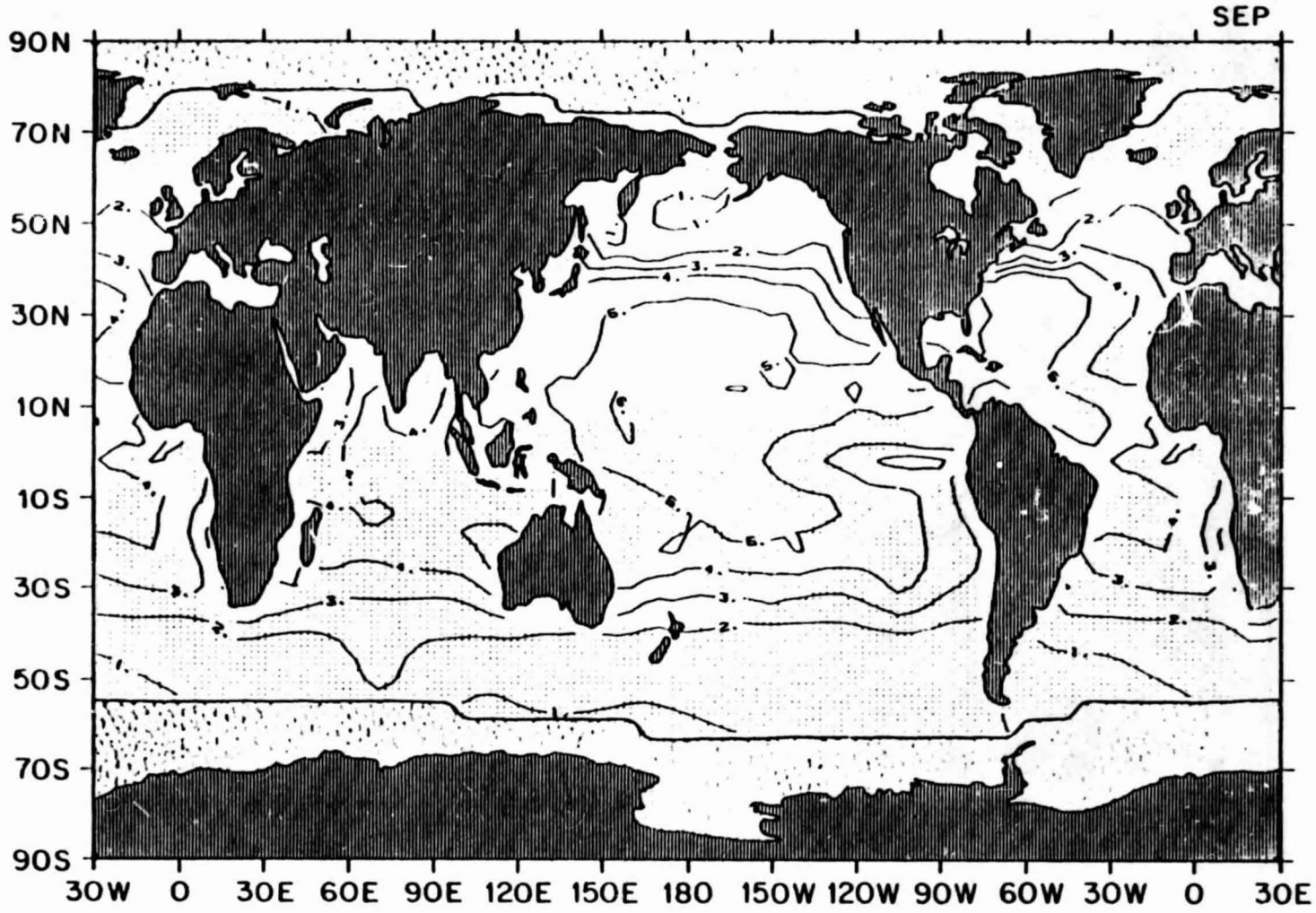

1.75 October mean sea - air specific humidity difference (gm kg^{-1})

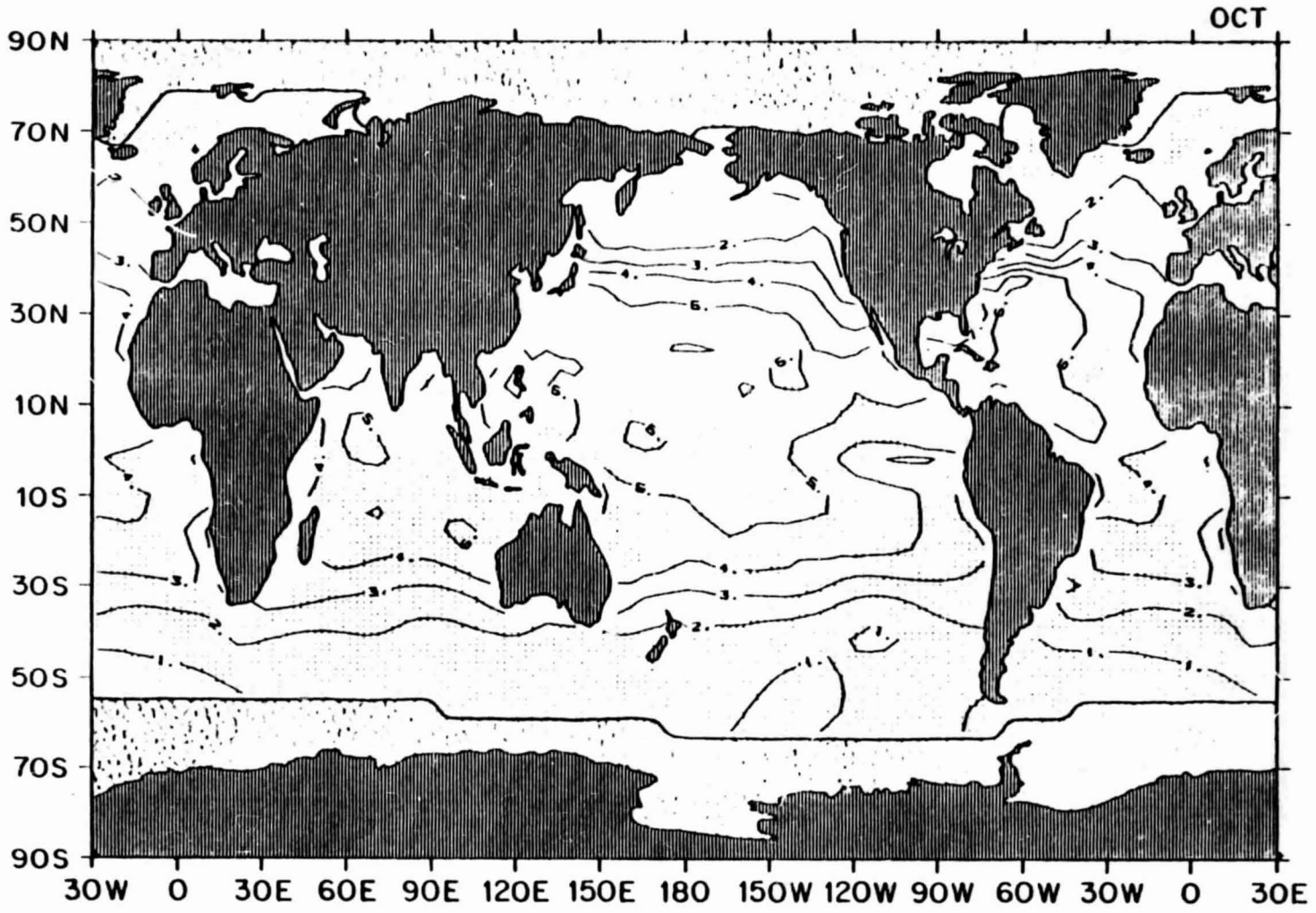

1.76 November mean sea - air specific humidity difference (gm kg^{-1})

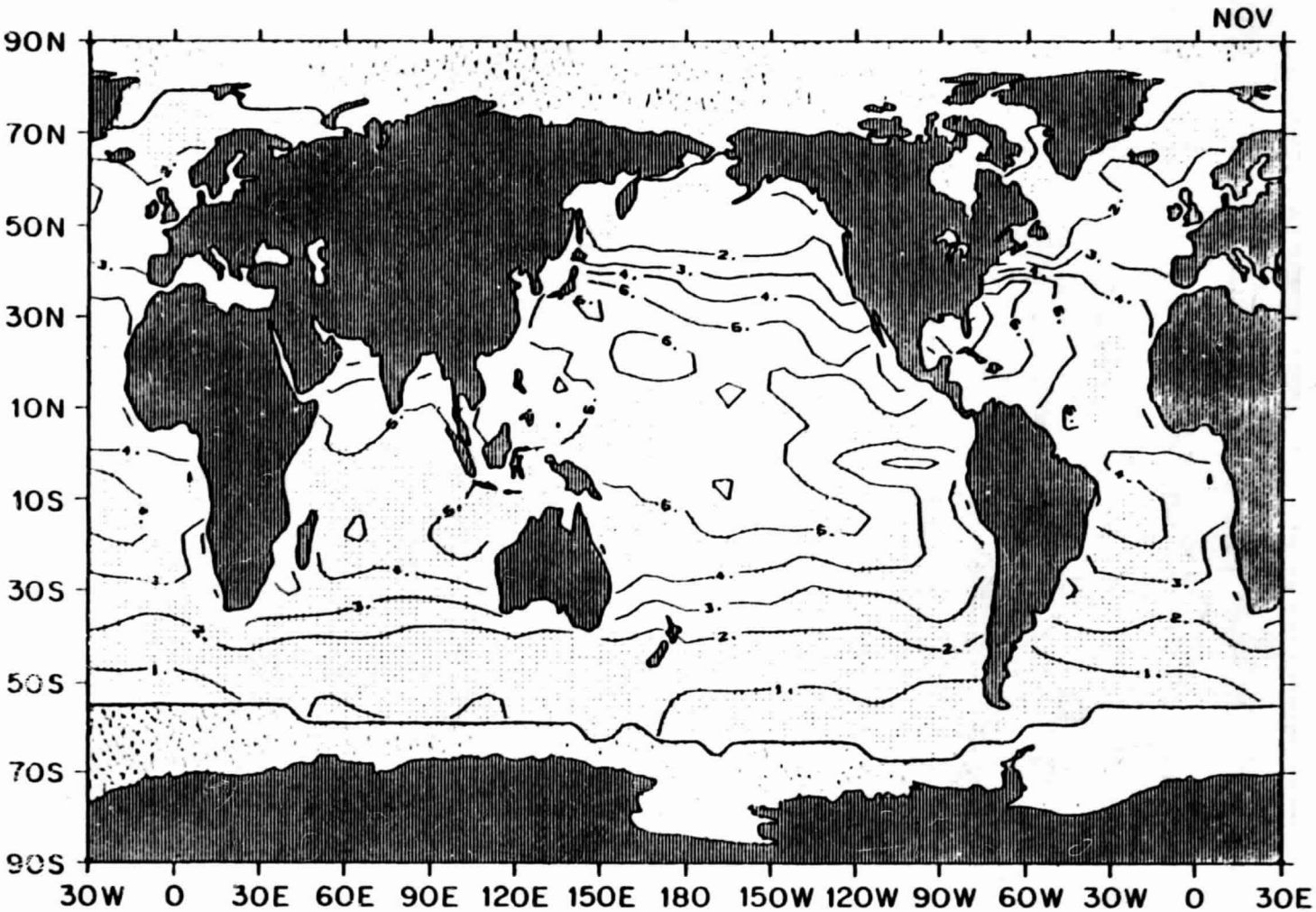

1.77 December mean sea - air specific humidity difference (gm kg^{-1})

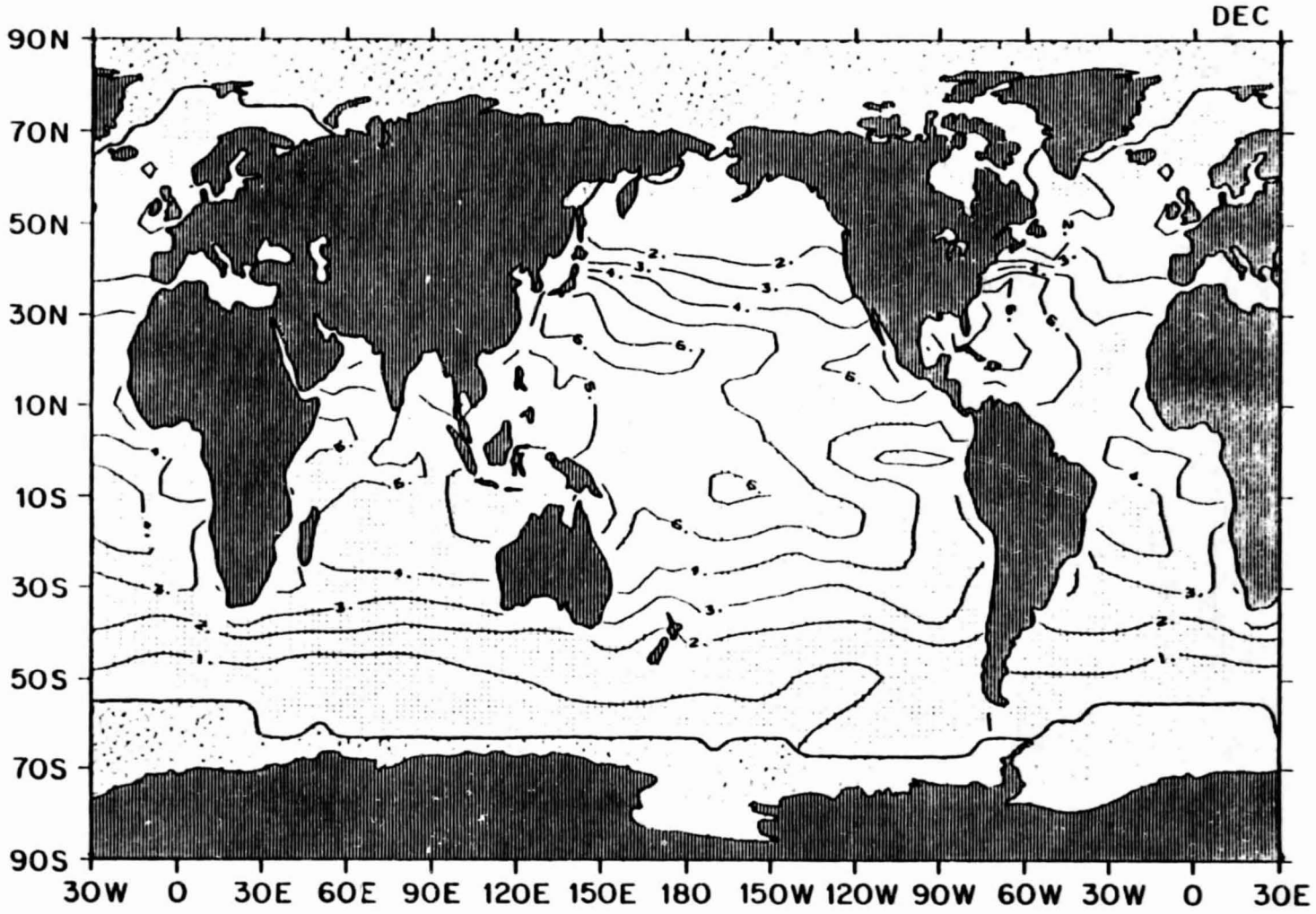

1.78 Annual mean sea - air specific humidity difference (gm kg-1)

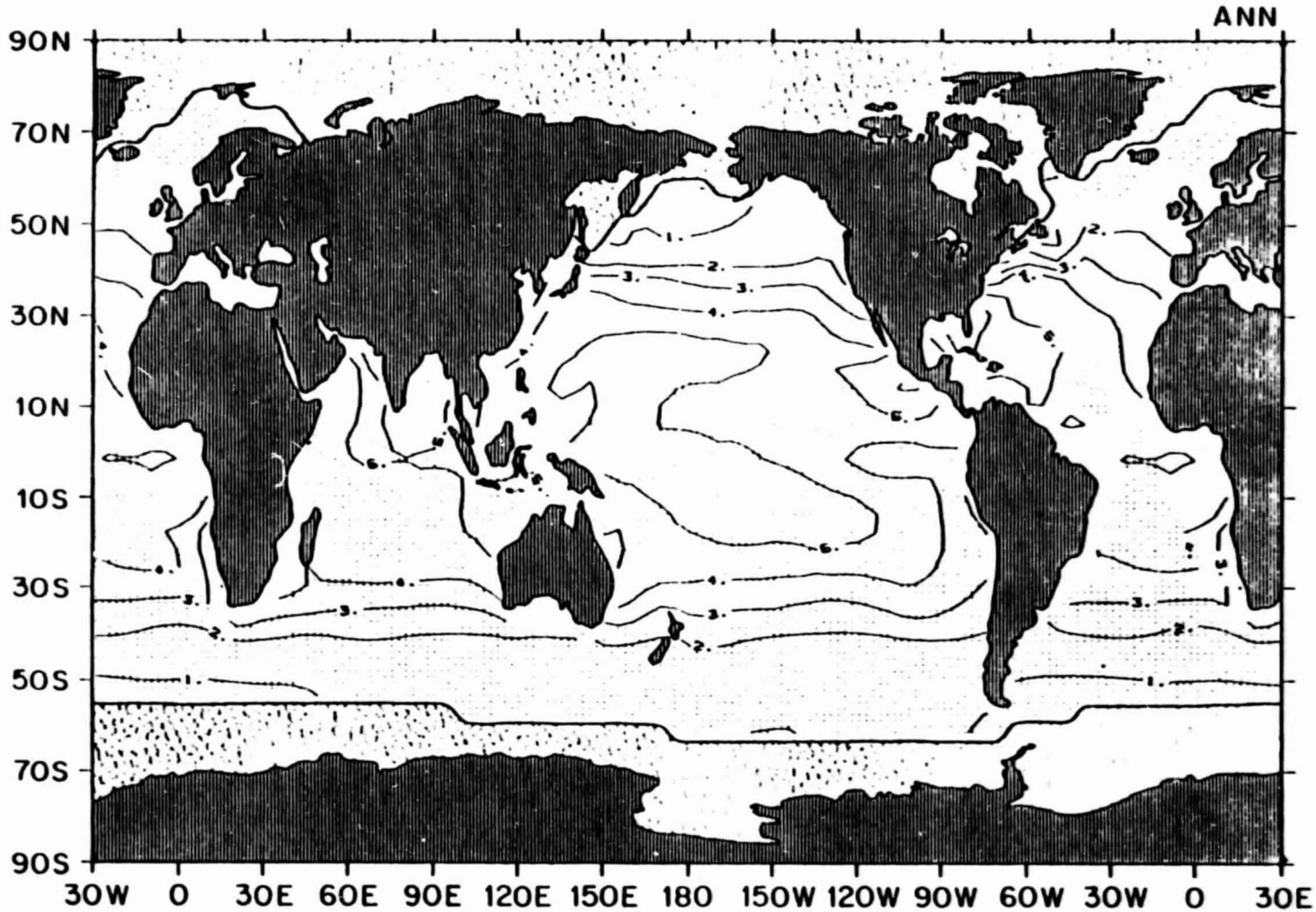

CLOUDINESS

1.79 January mean cloudiness (fractions)

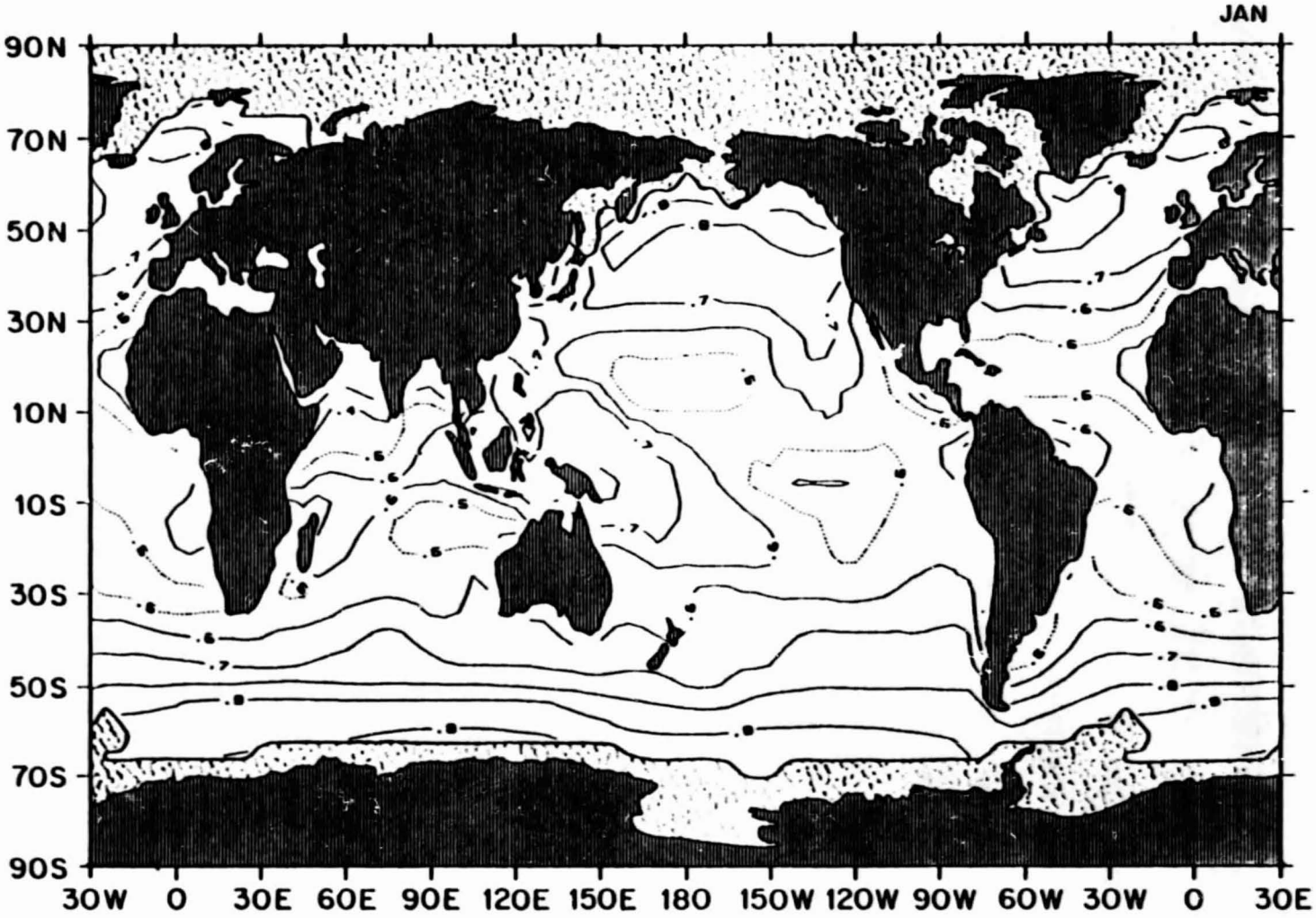

1.80 February mean cloudiness (fractions)

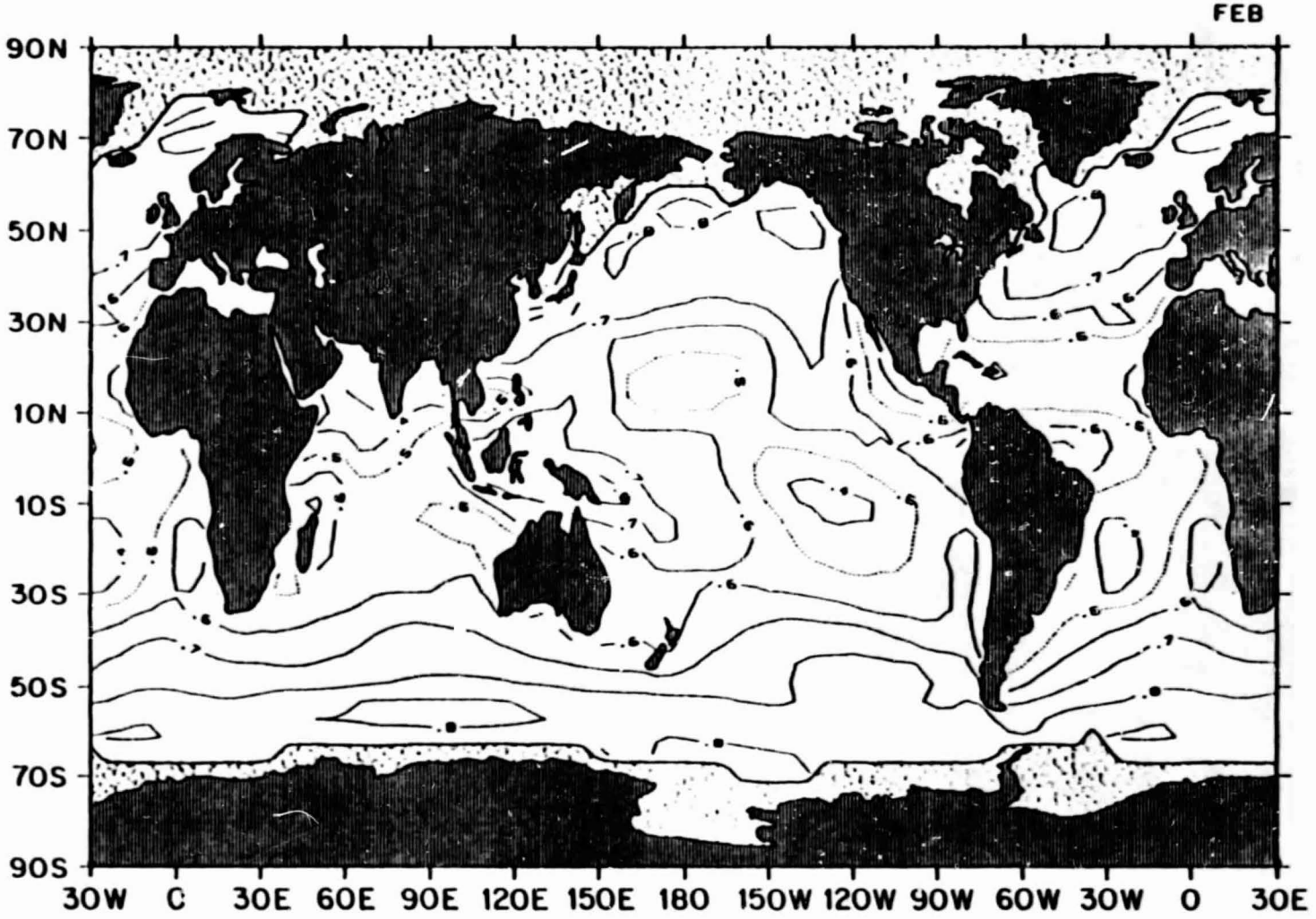

1.81 March mean cloudiness (fractions)

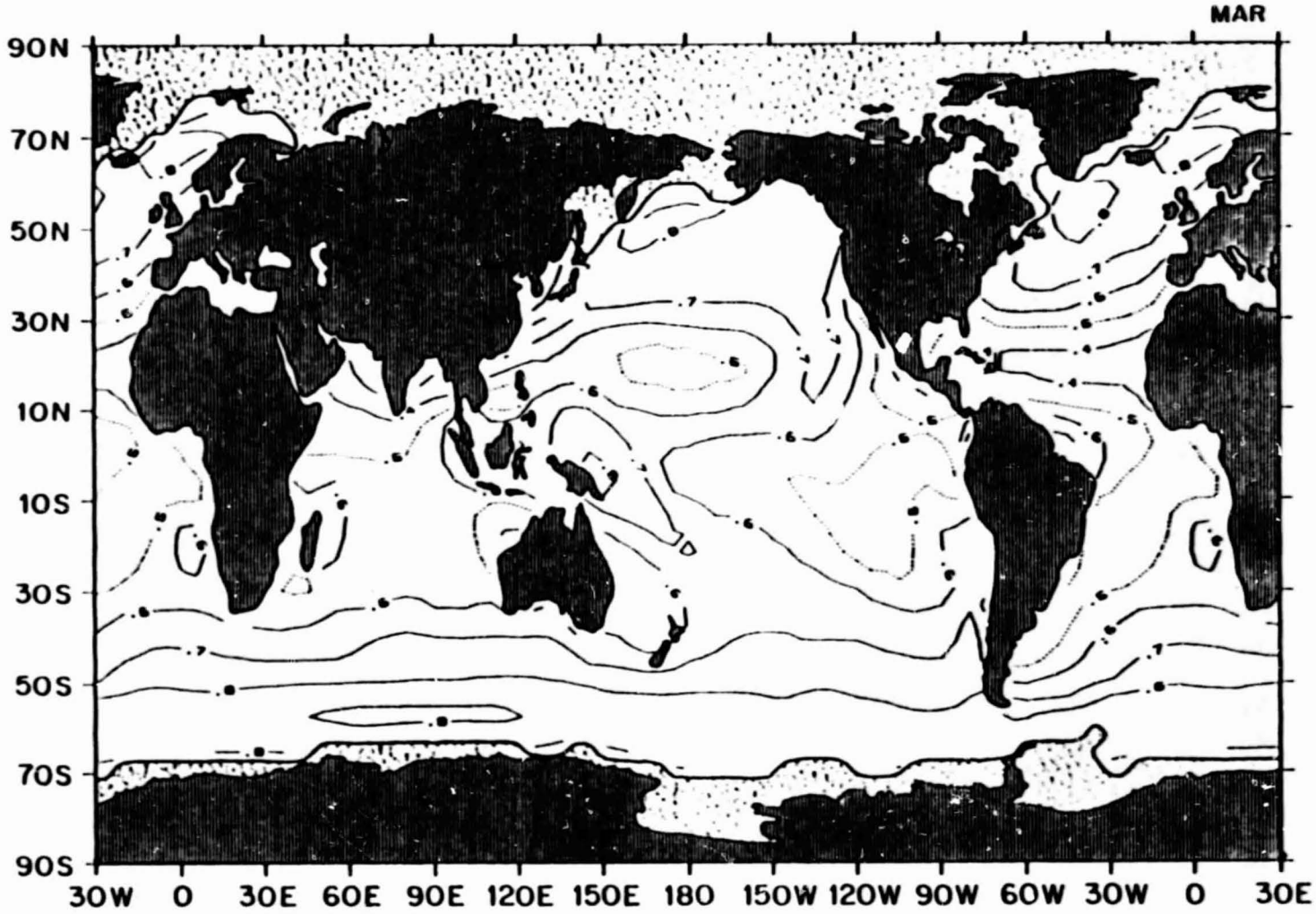

1.82 April mean cloudiness (fractions)

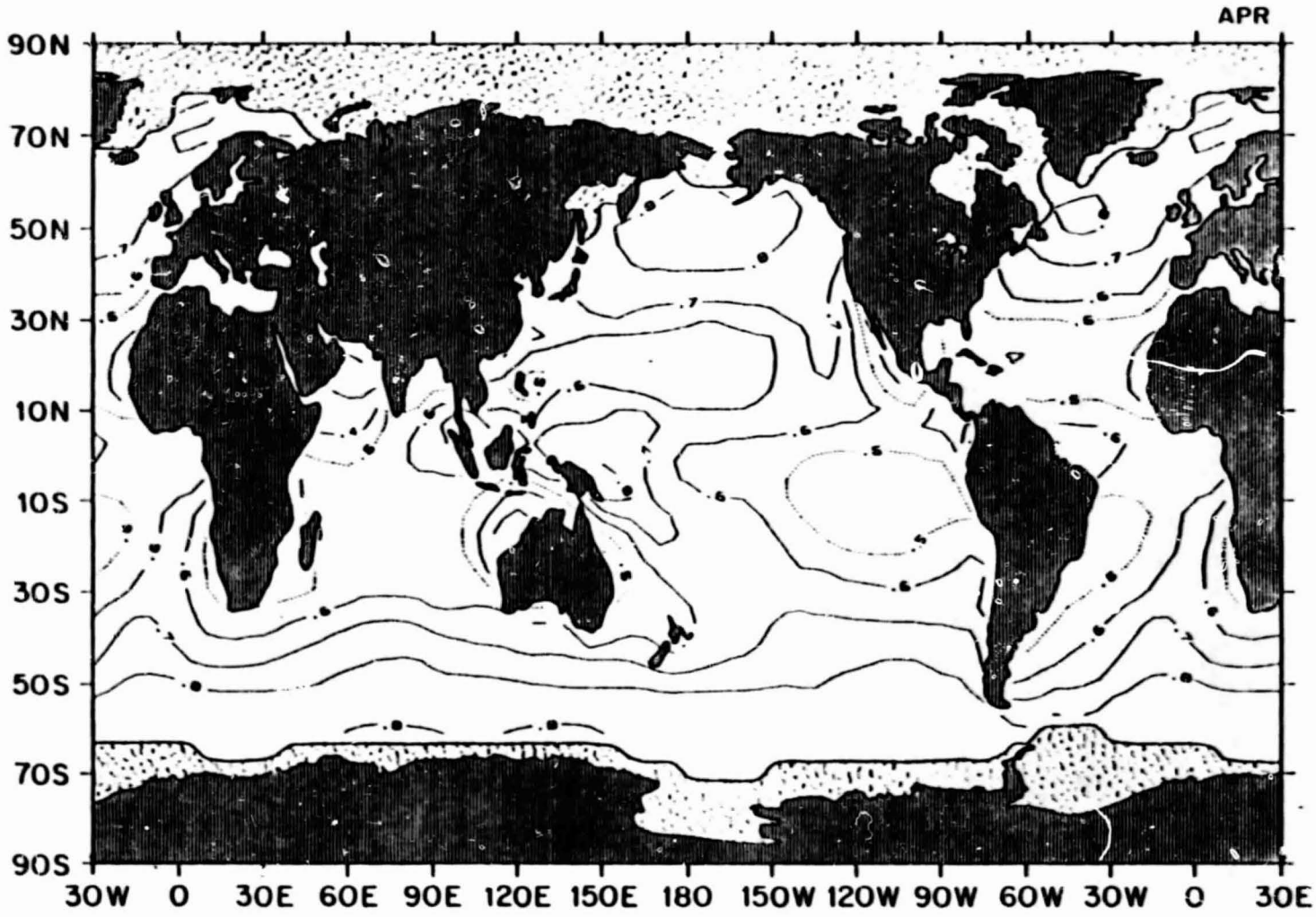

1.83 May mean cloudiness (fractions)

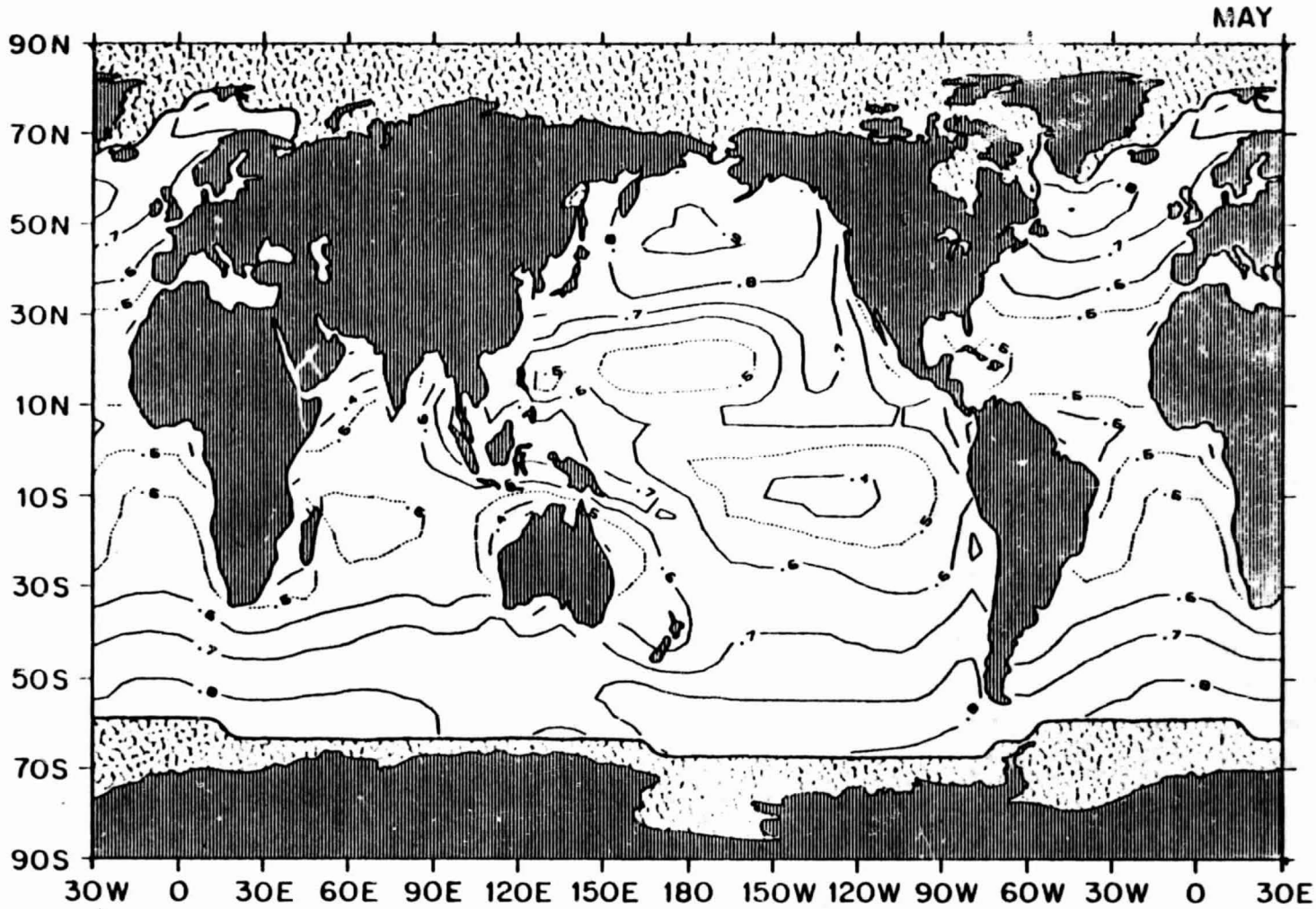

1.84 June mean cloudiness (fractions)

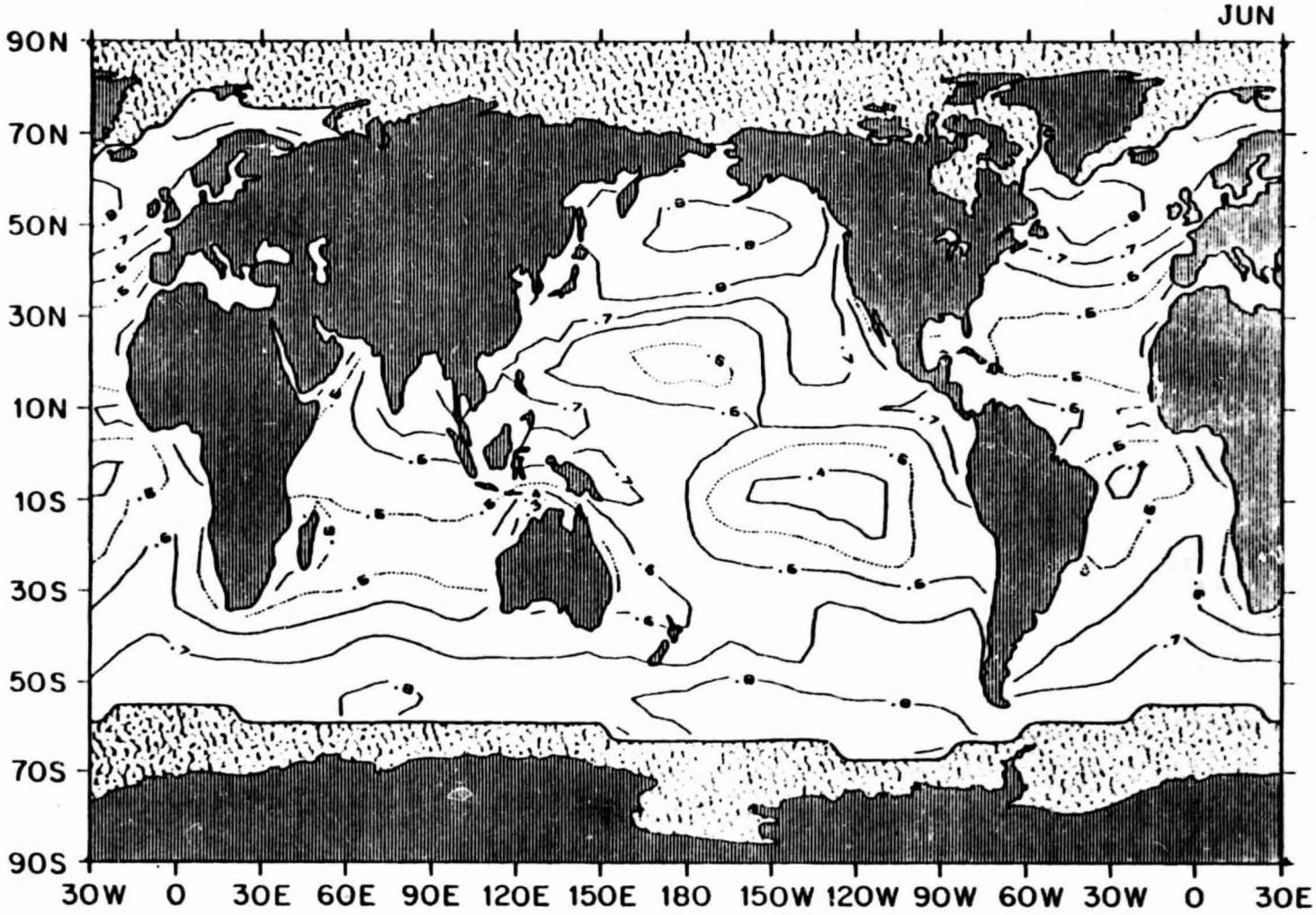

1.85 July mean cloudiness (fractions)

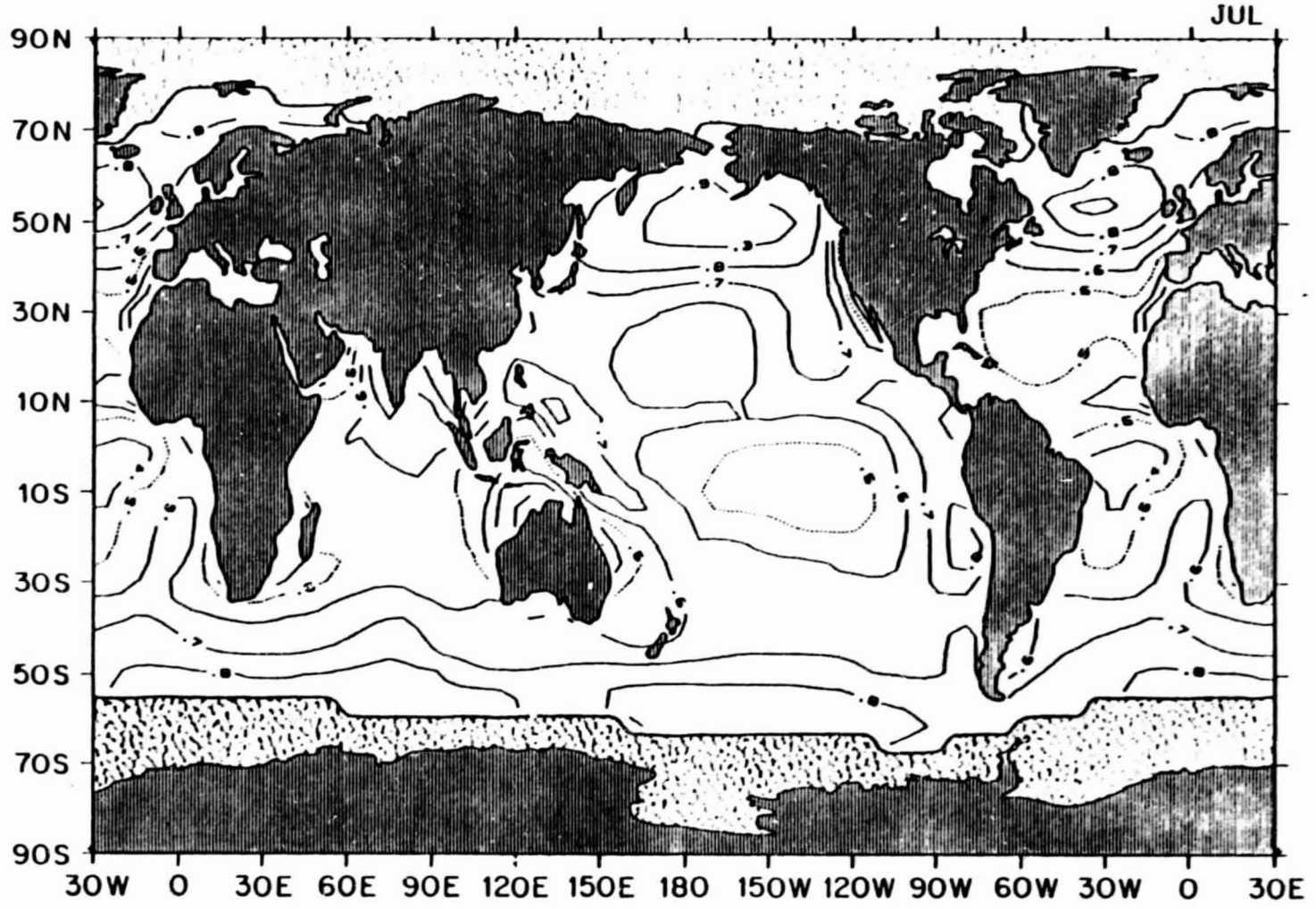

1.86 August mean cloudiness (fractions)

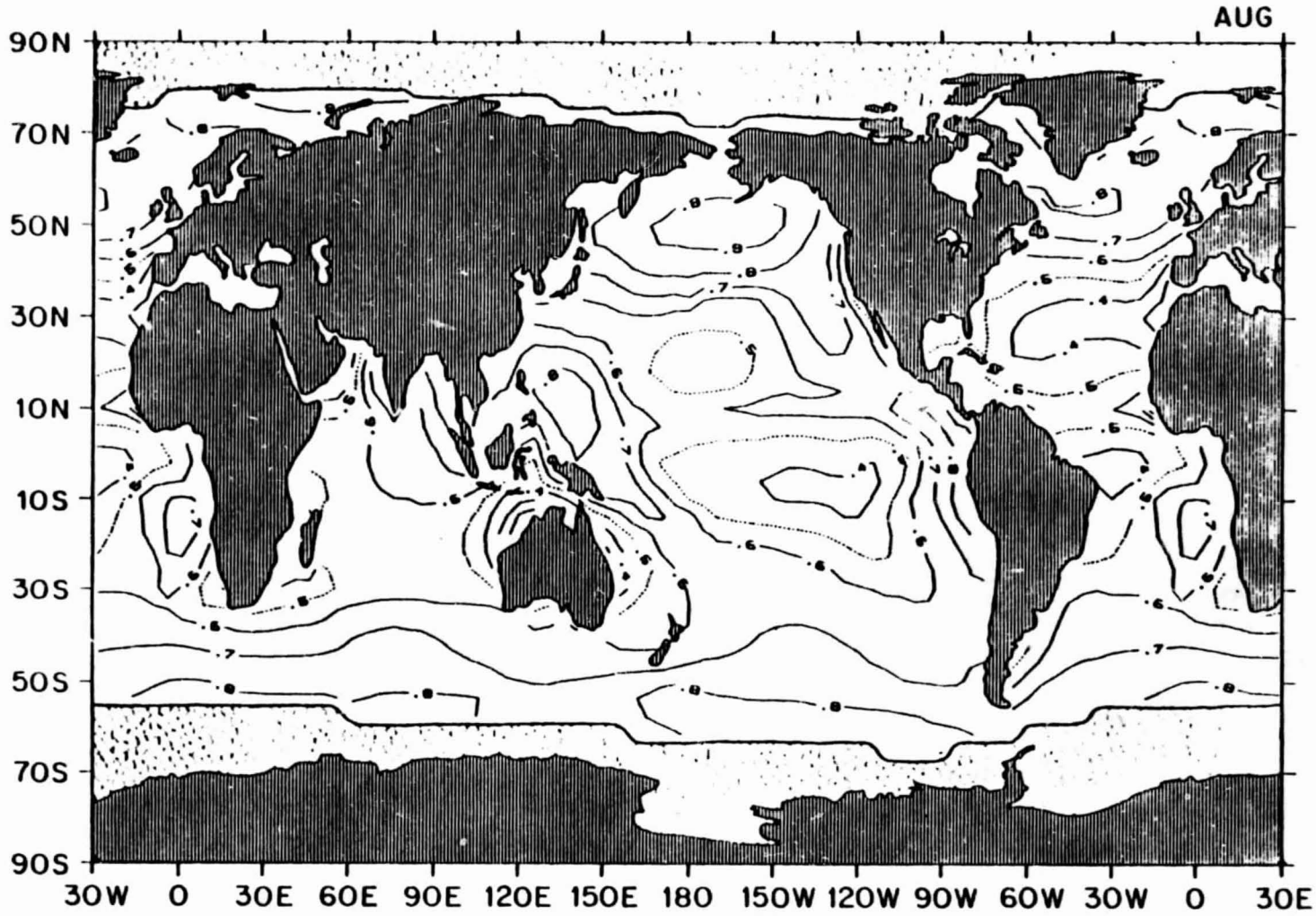

1.87 September mean cloudiness (fractions)

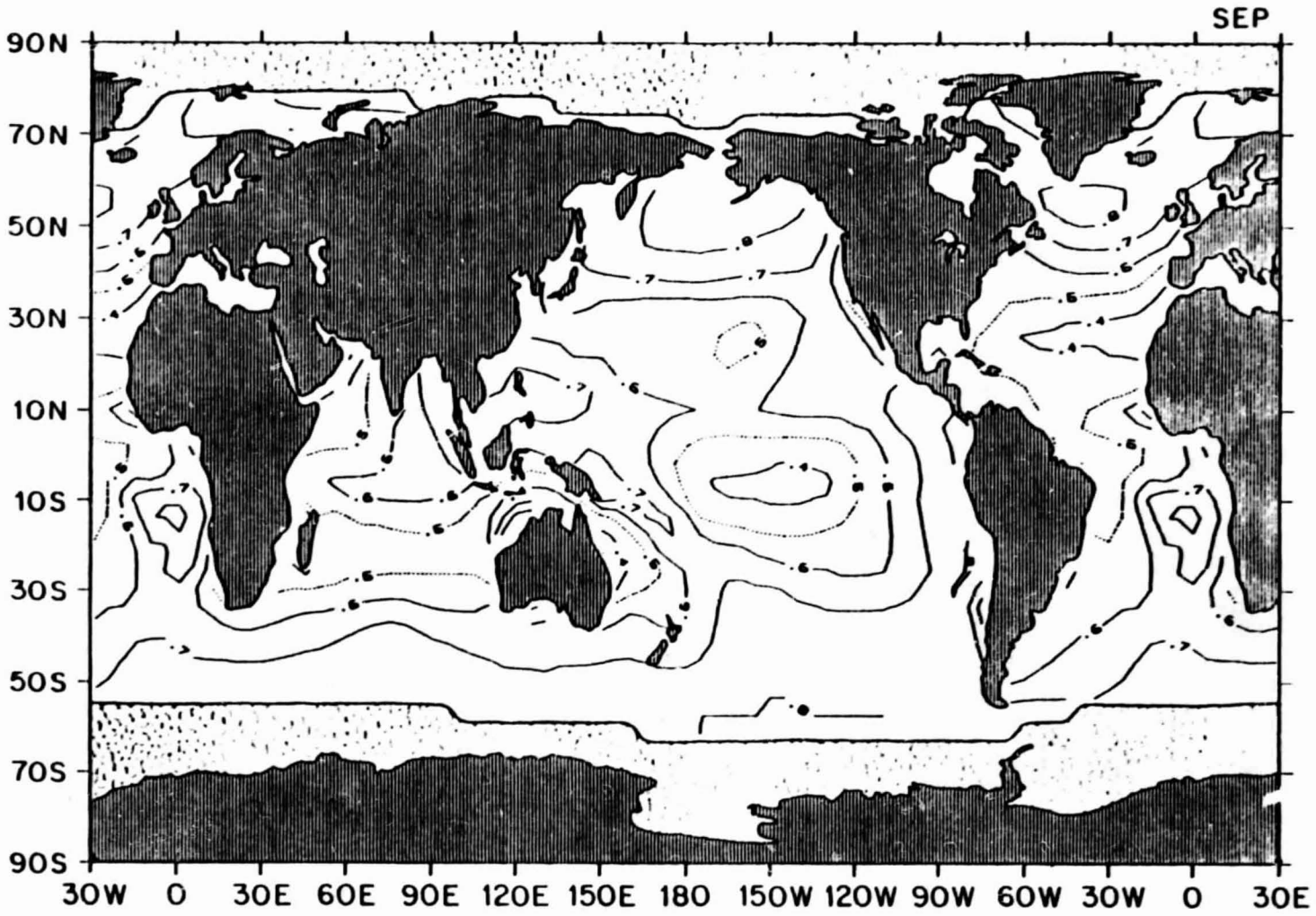

1.88 October mean cloudiness (fractions)

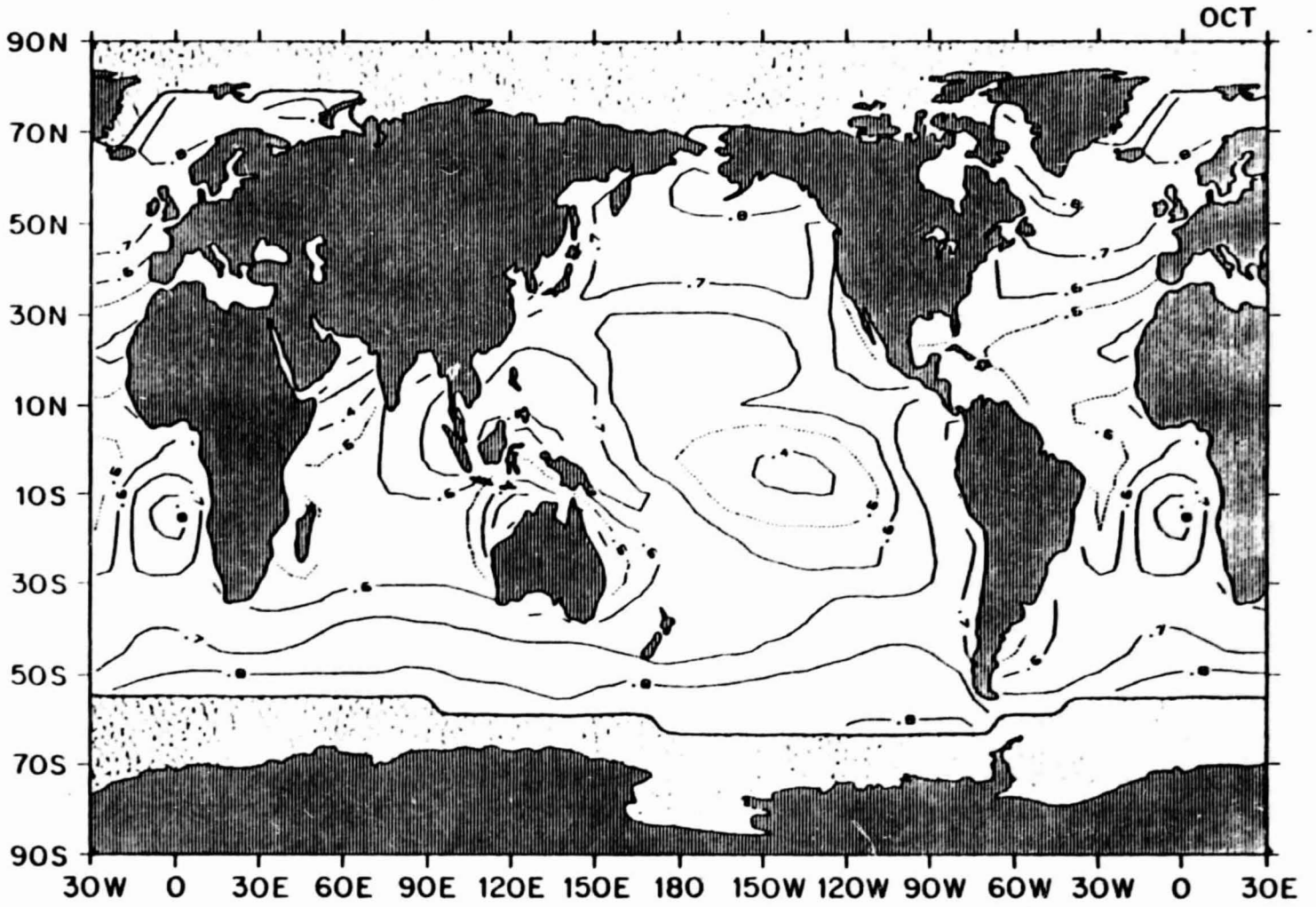

1.89 November mean cloudiness (fractions)

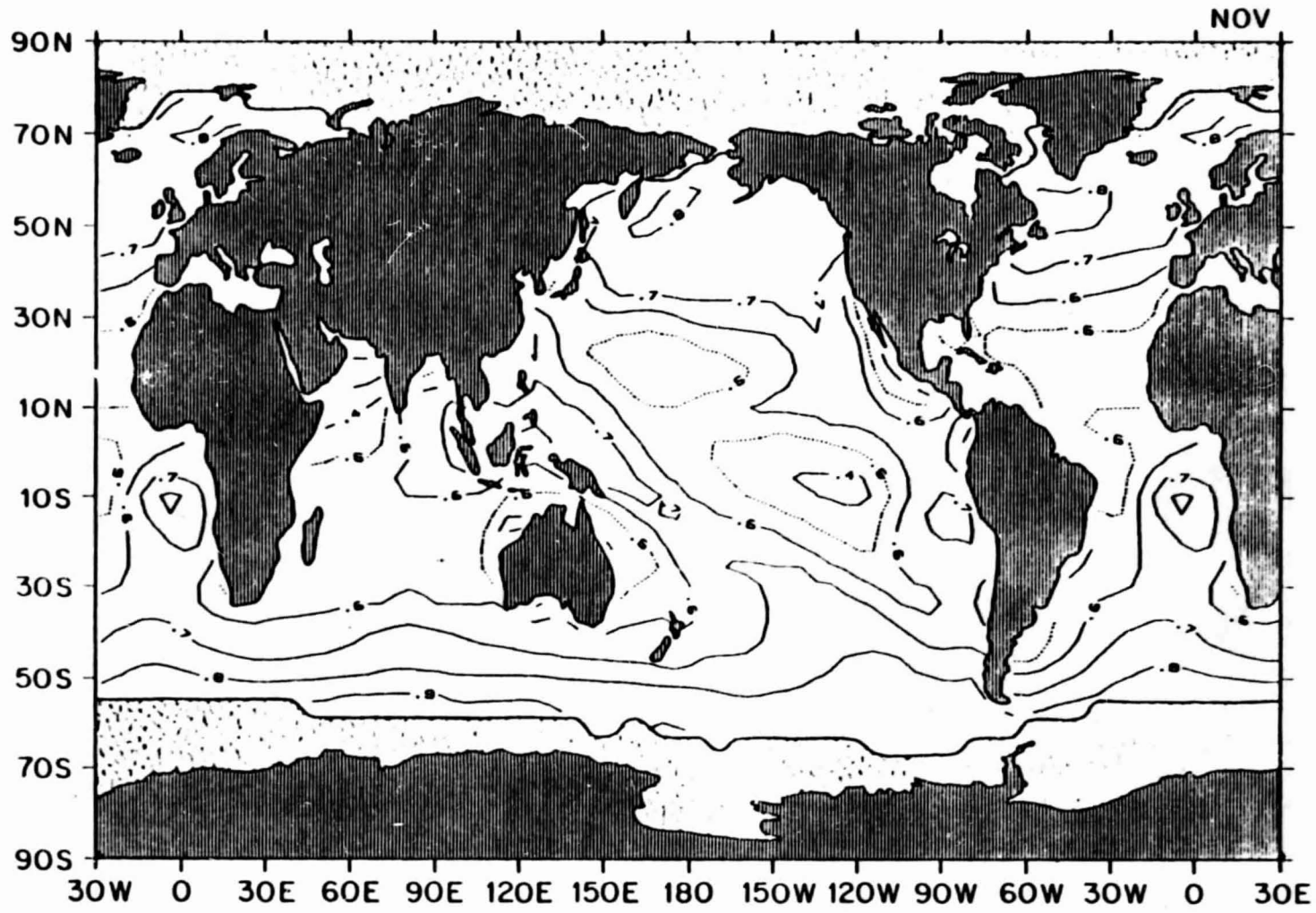

1.90 December mean cloudiness (fractions)

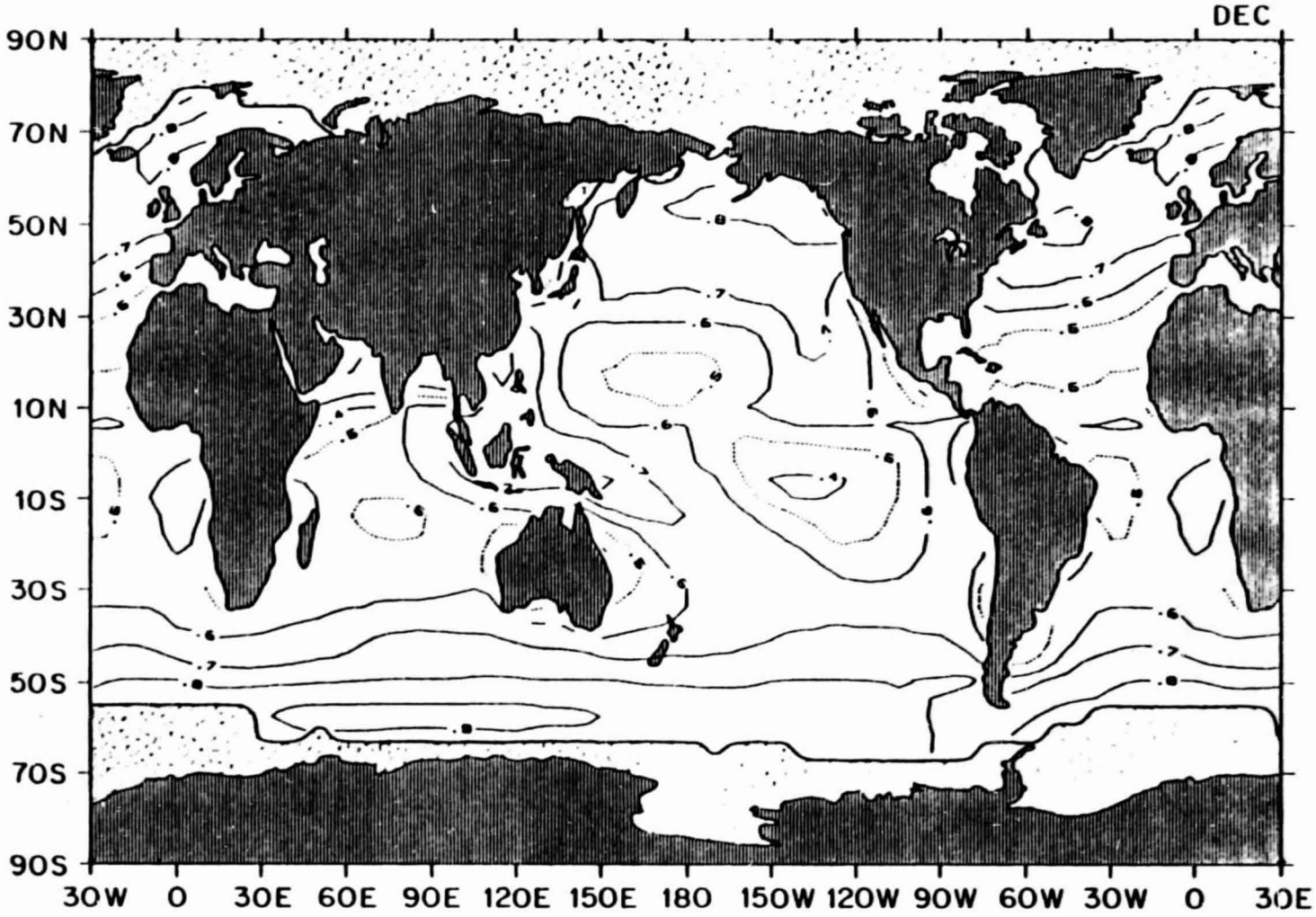

1.91 Annual mean cloudiness (fractions)

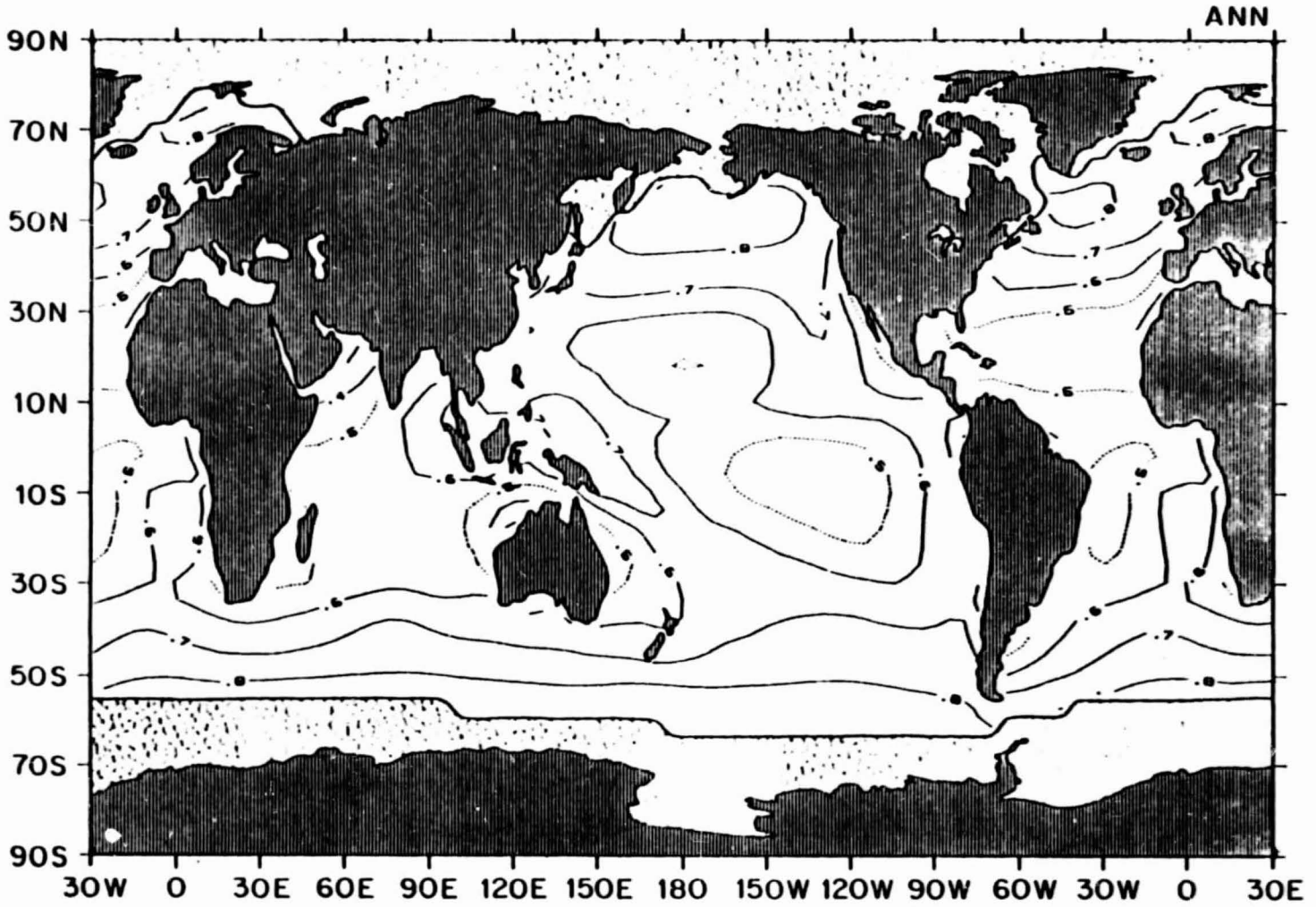

SEA LEVEL PRESSURE

1.92 January mean sea level pressure (mb)

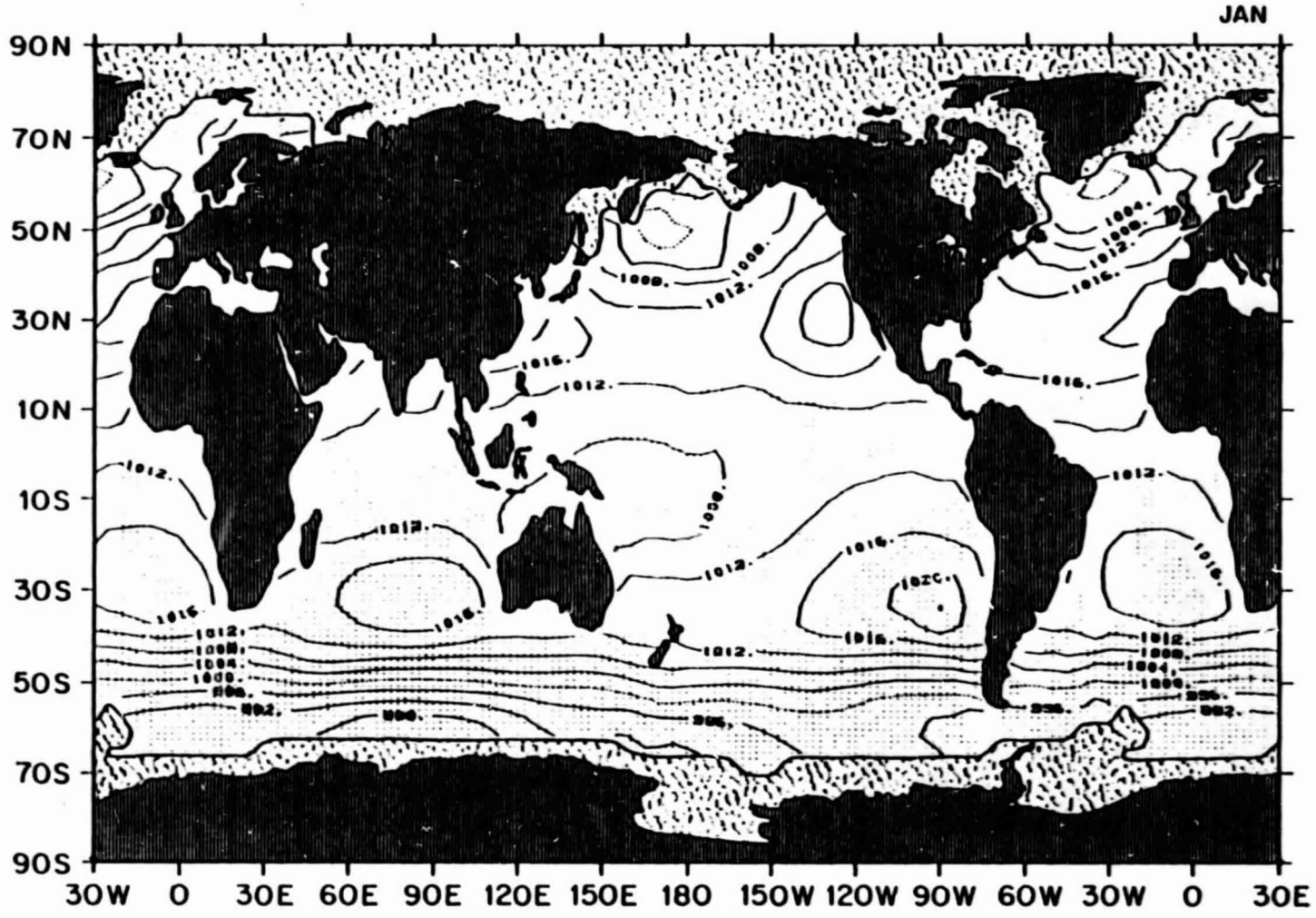

1.93 February mean sea level pressure (mb)

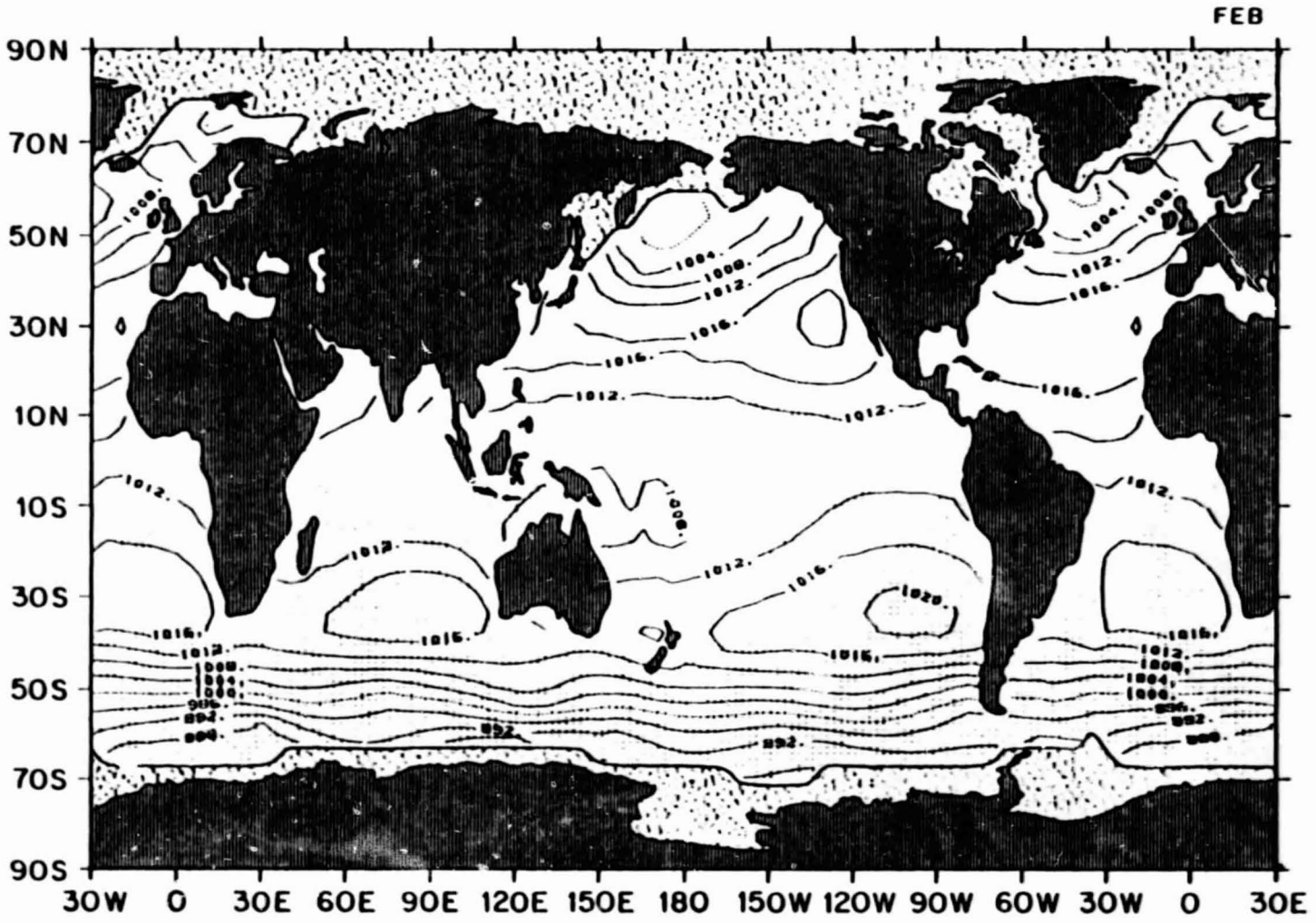

1.94 March mean sea level pressure (mb)

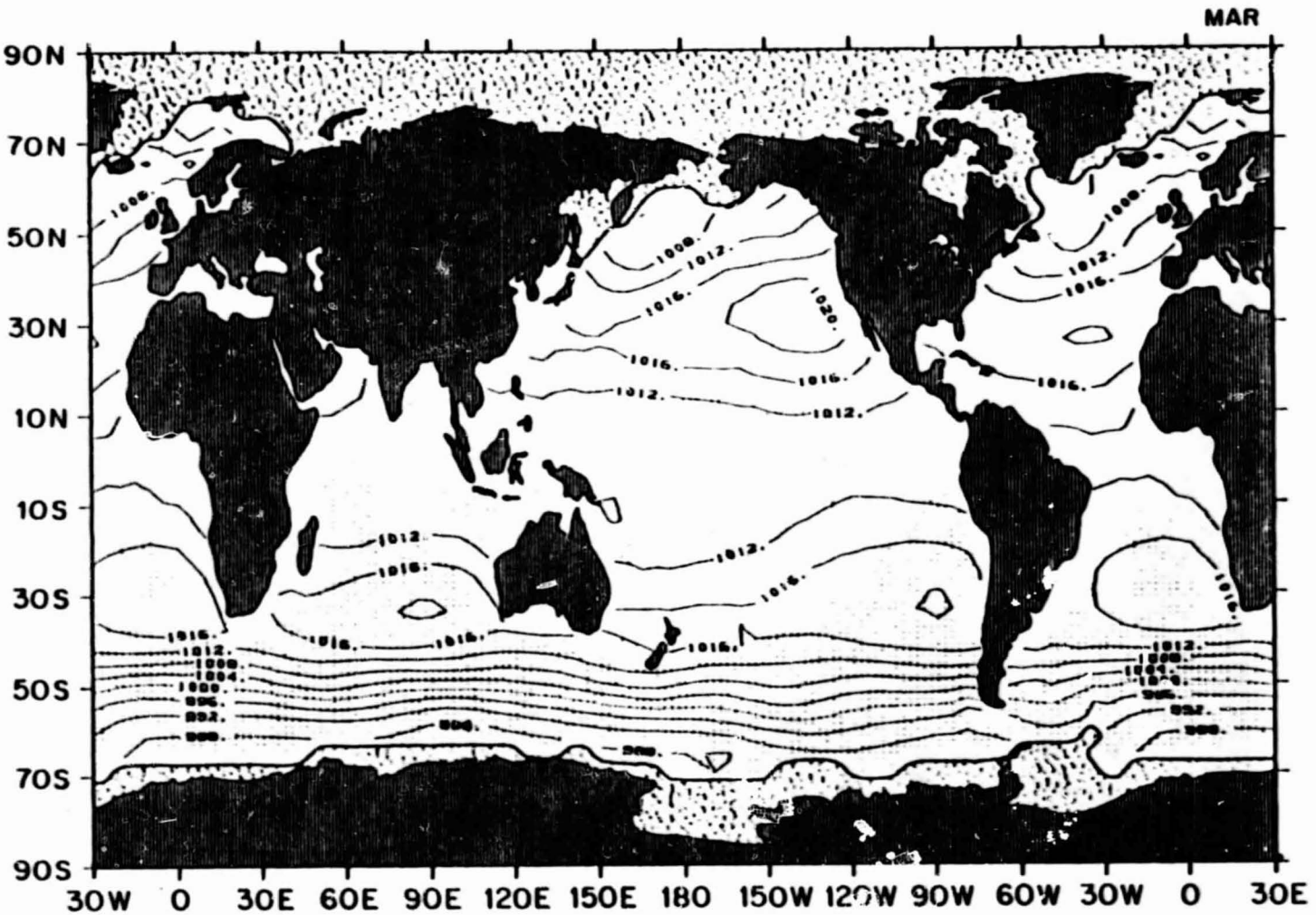

1.95 April mean sea level pressure (mb)

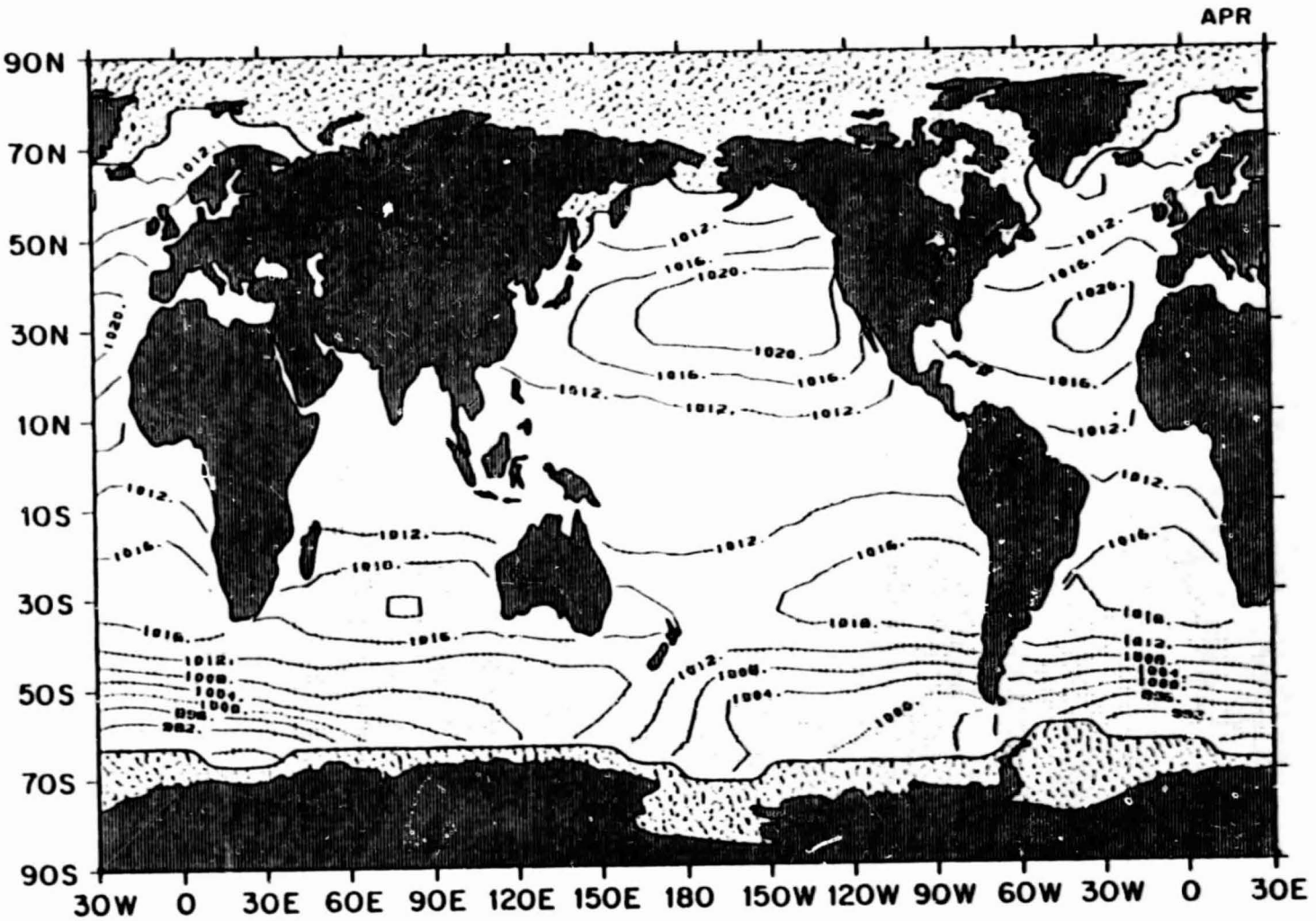

1.96 May mean sea level pressure (mb)

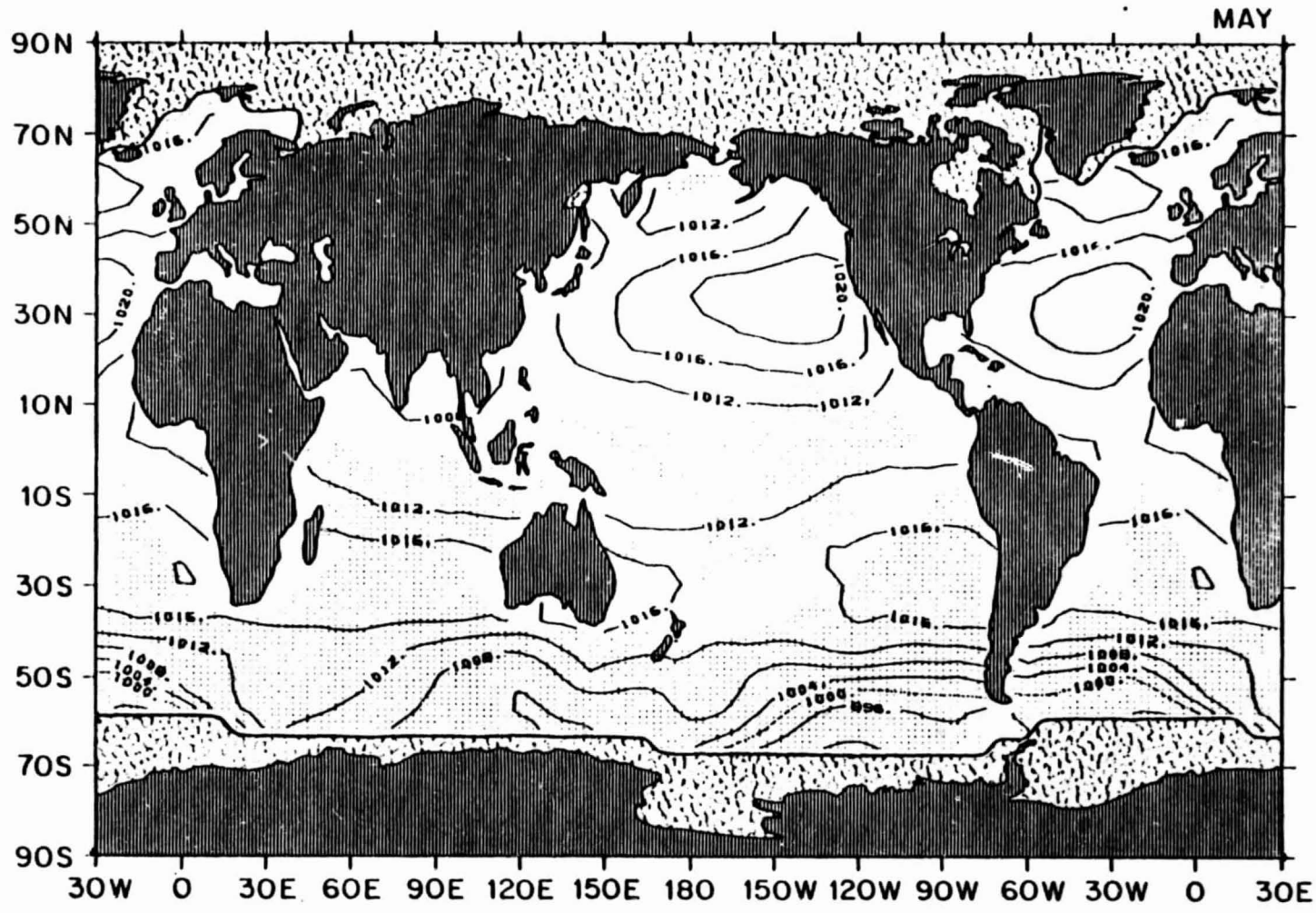

1.97 June mean sea level pressure (mb)

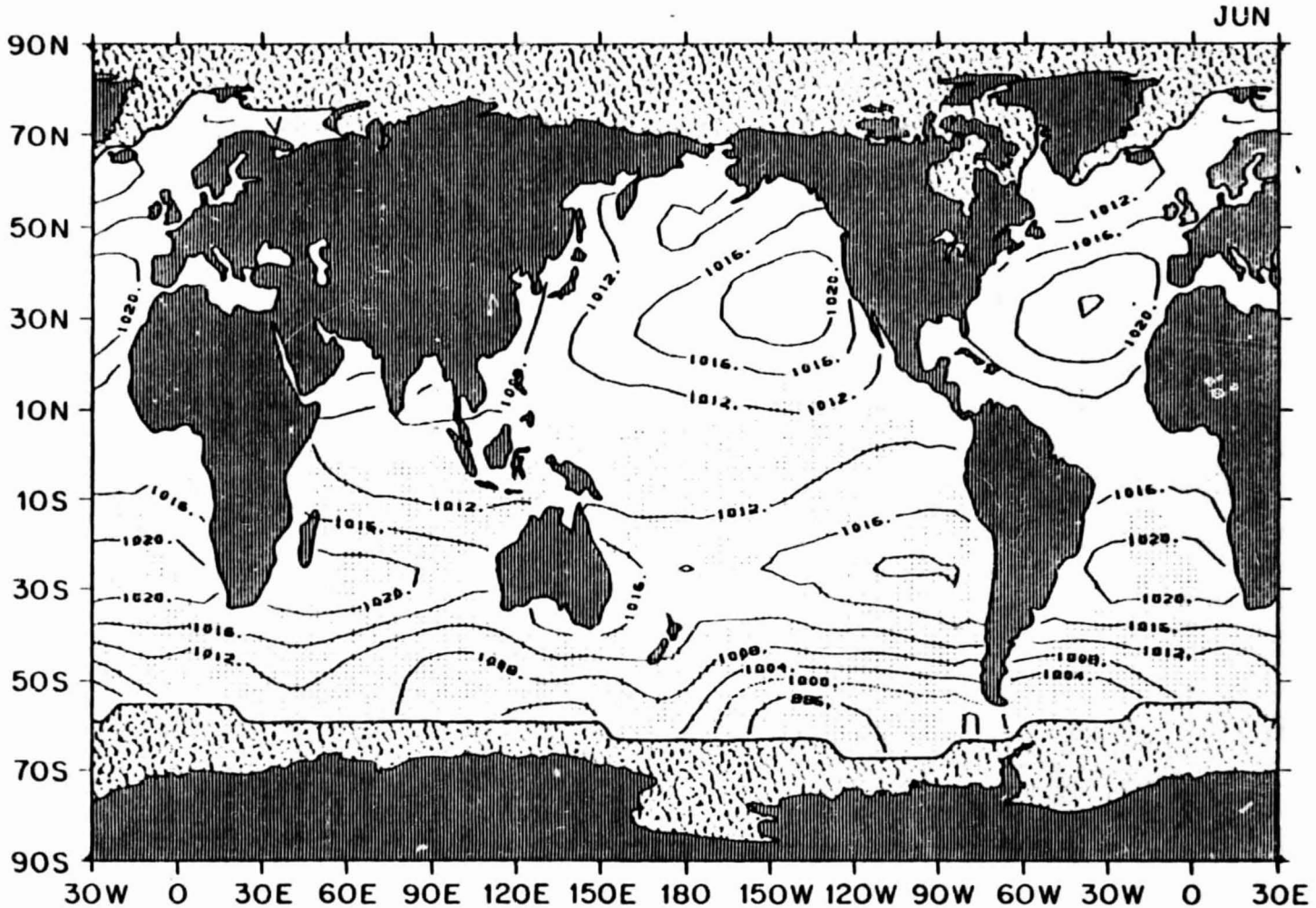

1.98 July mean sea level pressure (mb)

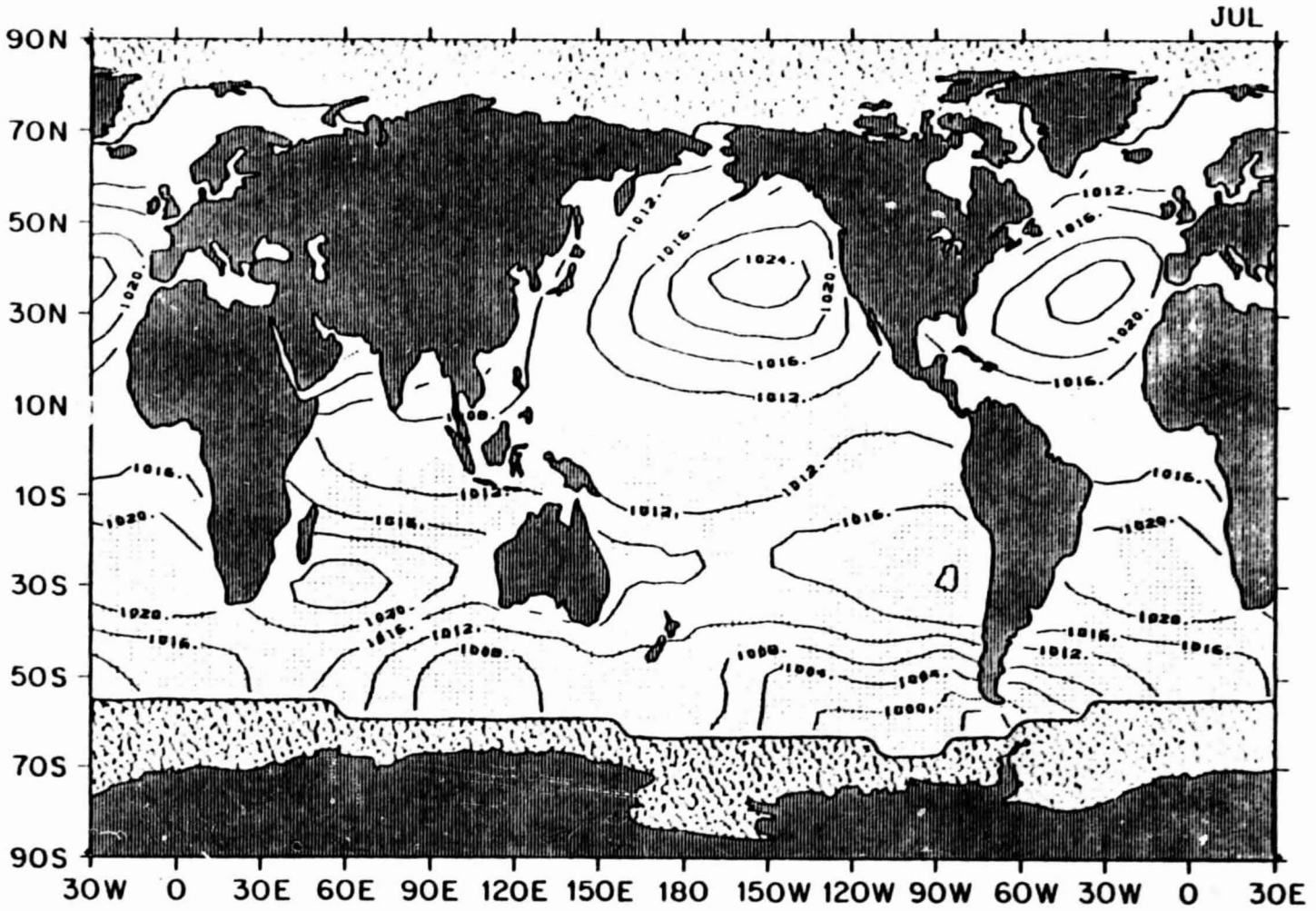

1.99 August mean sea level pressure (mb)

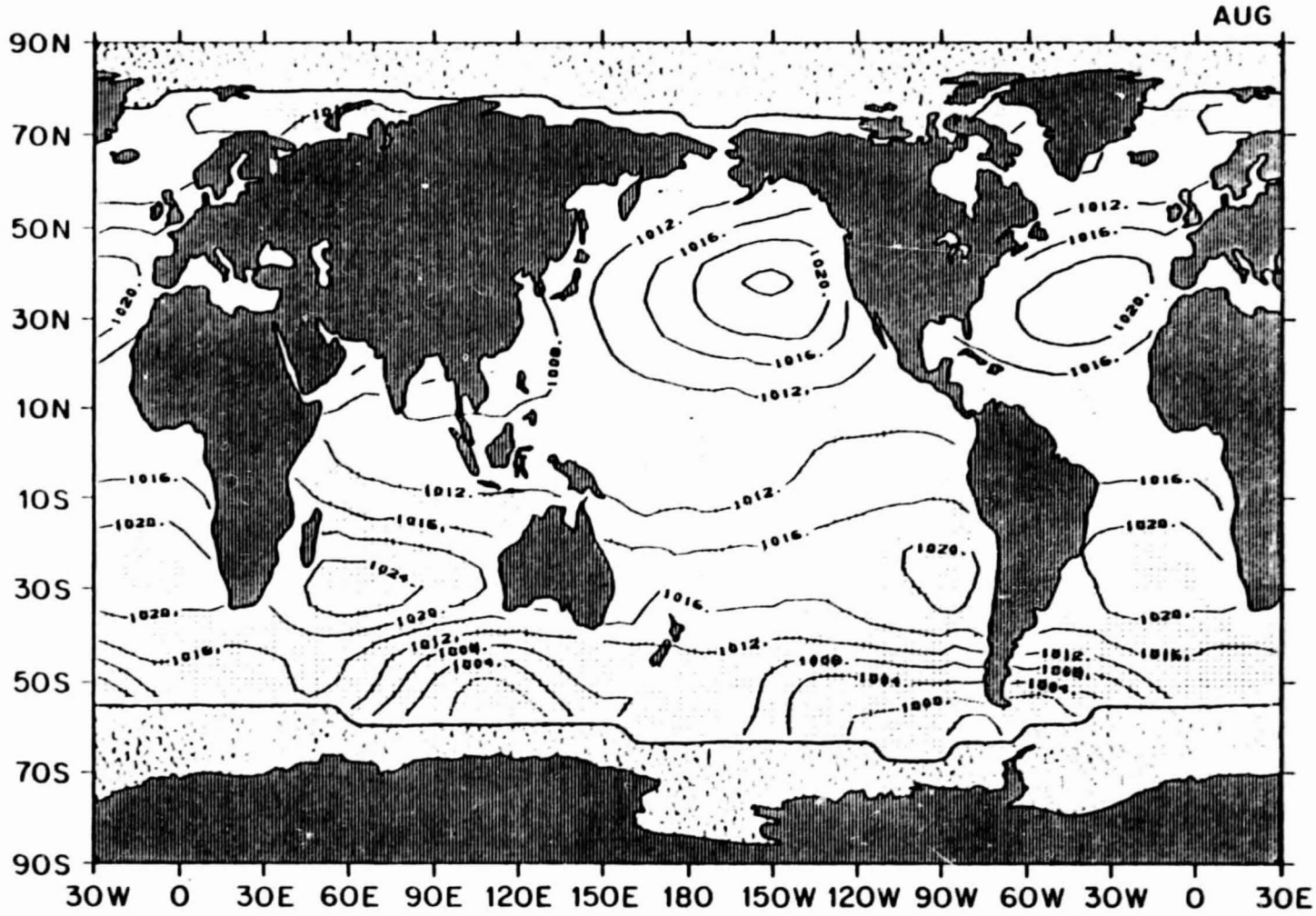

1.100 September mean sea level pressure (mb)

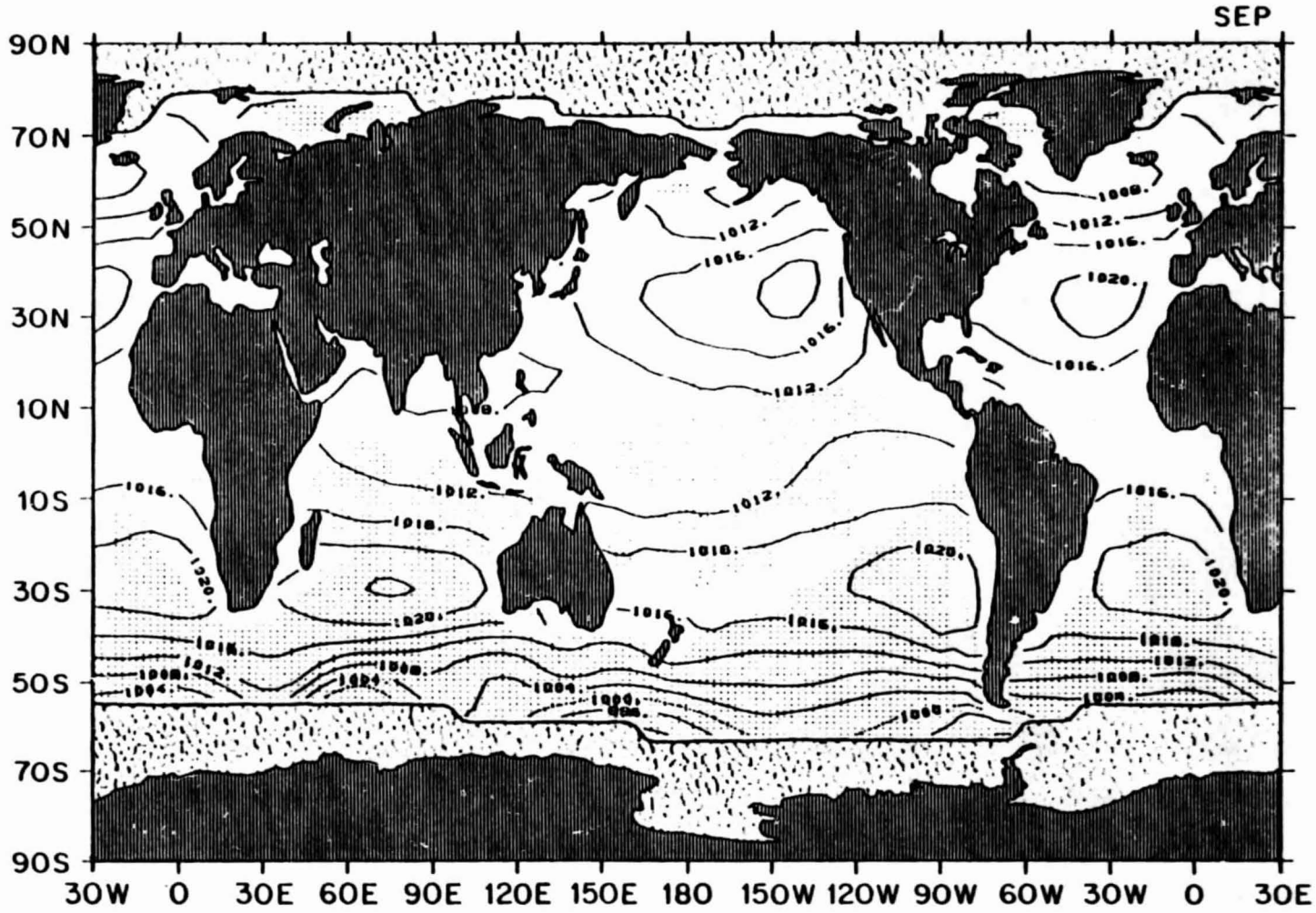

1.101 October mean sea level pressure (mb)

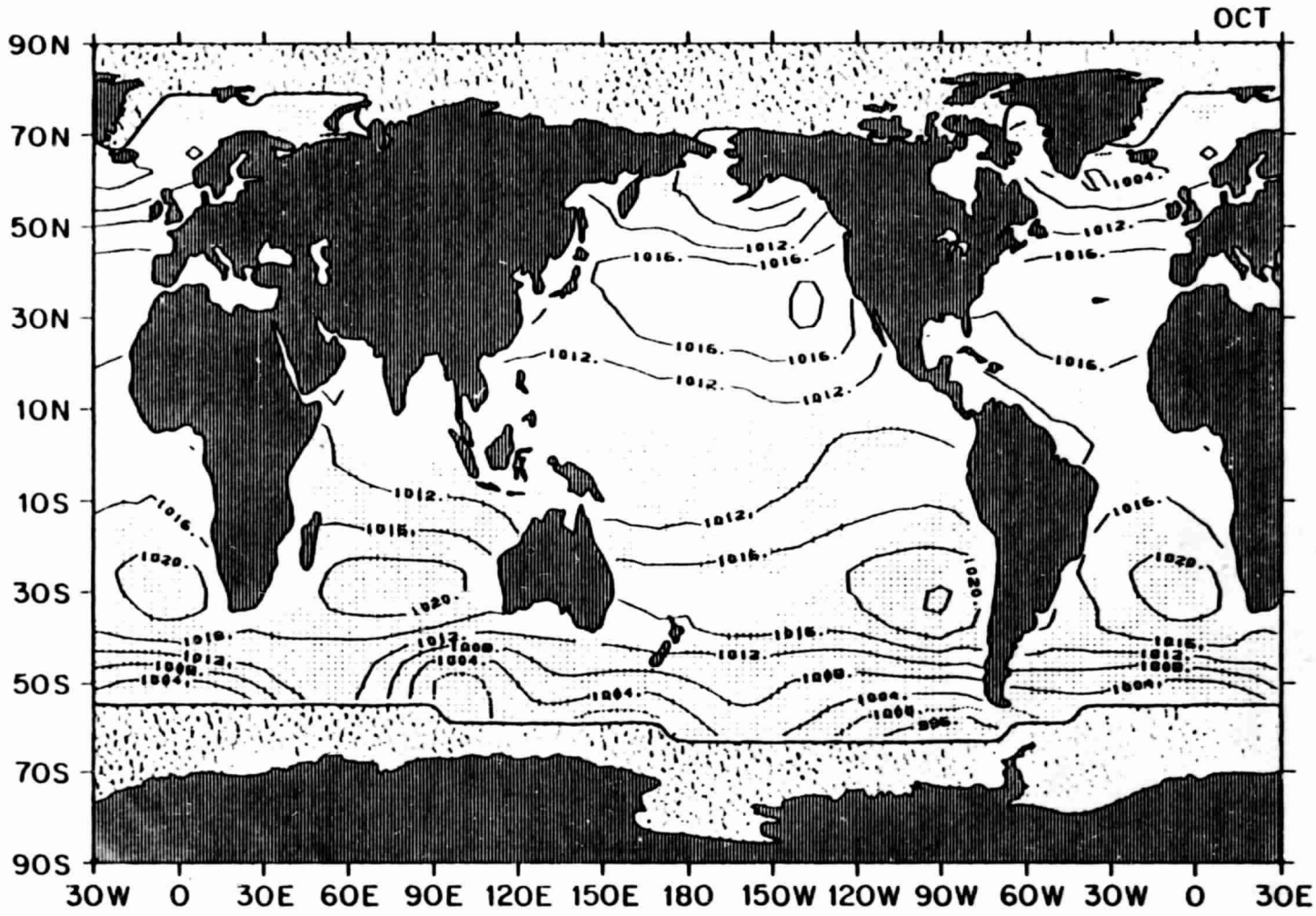

1.102 November mean sea level pressure (mb)

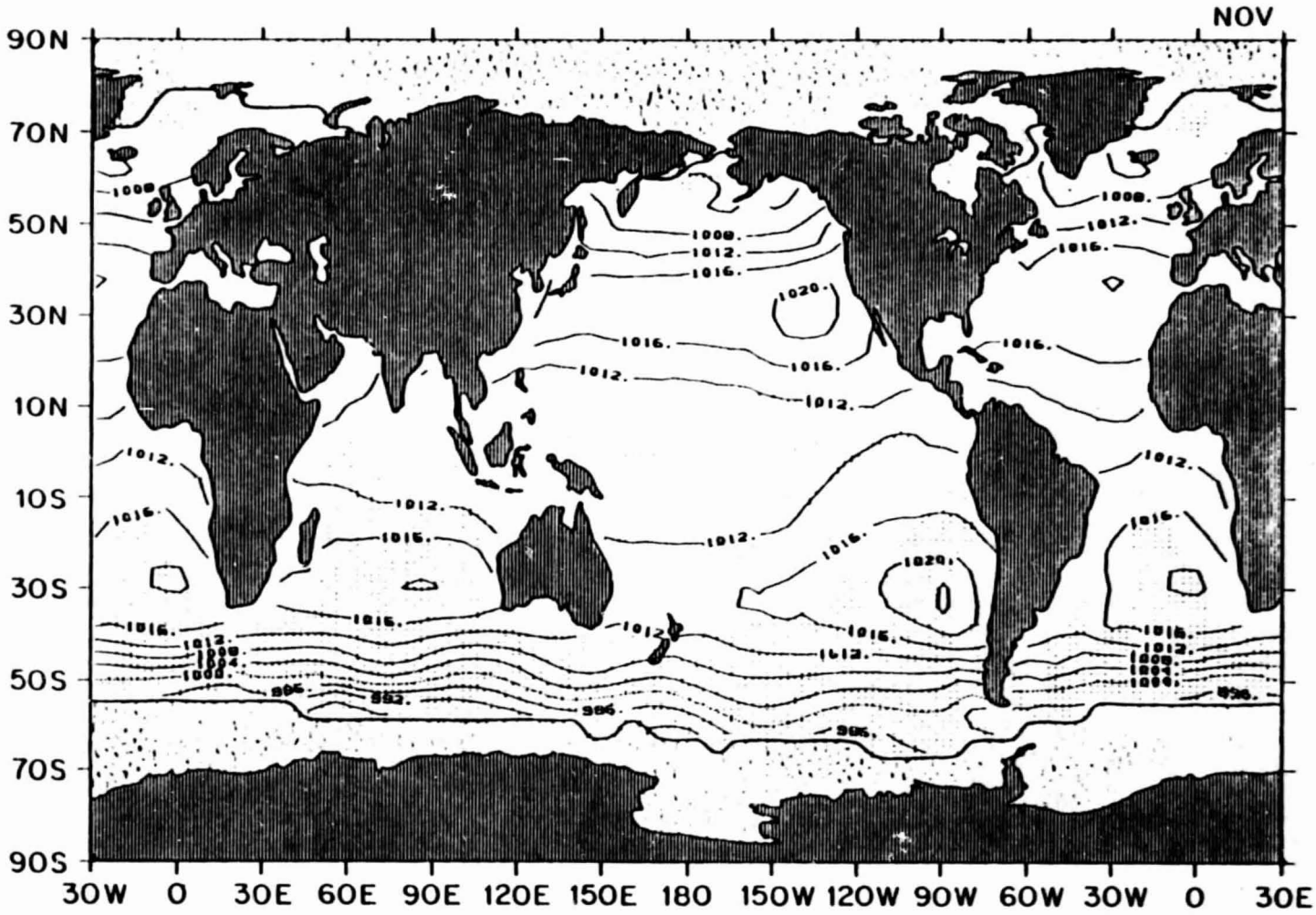

1.103 December mean sea level pressure (mb)

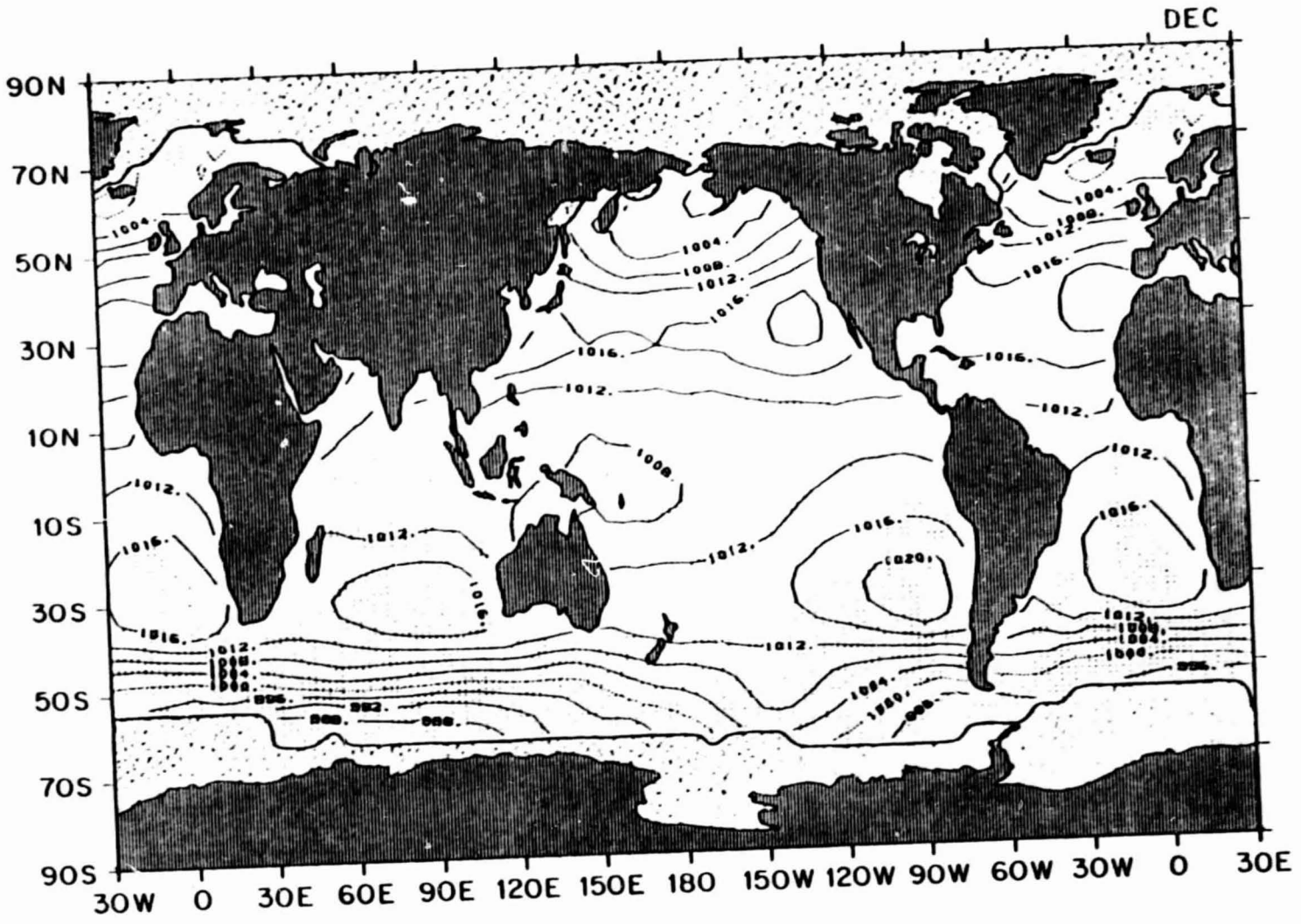

1.104 Annual mean sea level pressure (mb)

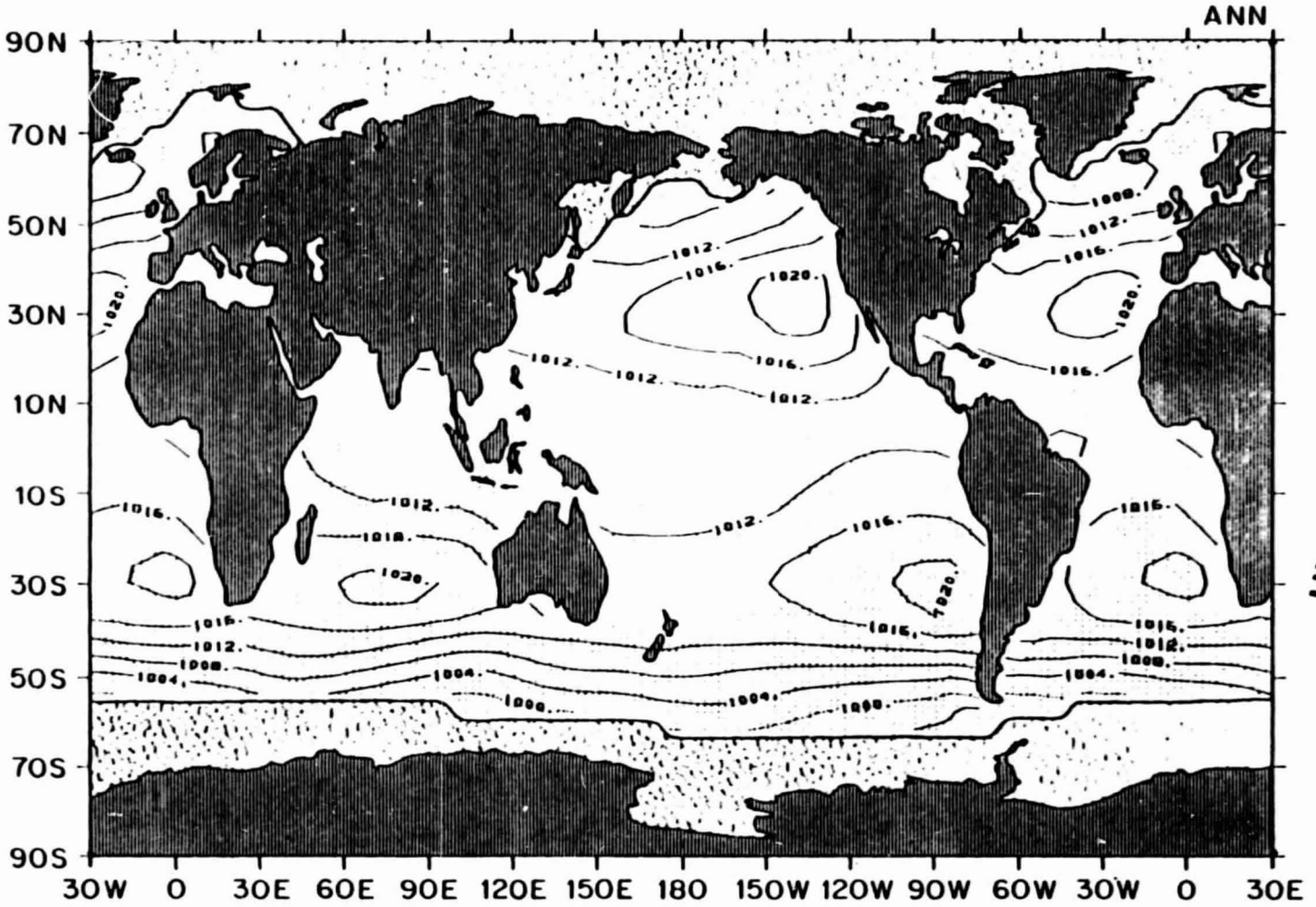

ATLAS OF THE HEAT BUDGET
OF THE ICE-FREE GLOBAL OCEAN
PART II: HEAT BUDGET COMPONENTS

THE HEAT BUDGET COMPONENTS

Spatial Patterns of the Heat Budget Components(*)

	Chart Number												
	J	F	M	A	M	J	J	A	S	O	N	D	ANN
Available Solar Heat Flux	2.1	2.2	2.3	2.4	2.5	2.6	2.7	2.8	2.9	2.10	2.11	2.12	2.13
Net Upward Long-Wave Flux	2.14	2.15	2.16	2.17	2.18	2.19	2.20	2.21	2.22	2.23	2.24	2.25	2.26
Net Downward Radiative Flux	2.27	2.28	2.29	2.30	2.31	2.32	2.33	2.34	2.35	2.36	2.37	2.38	2.39
Latent Heat Flux	2.40	2.41	2.42	2.43	2.44	2.45	2.46	2.47	2.48	2.49	2.50	2.51	2.52
Sensible Heat Flux	2.53	2.54	2.55	2.56	2.57	2.58	2.59	2.60	2.61	2.62	2.63	2.64	2.65
Net Downward Heat Flux	2.66	2.67	2.68	2.69	2.70	2.71	2.72	2.73	2.74	2.75	2.76	2.77	2.78

(*)Stippled areas are where the data density indicator is $\leq$ 2.7 (500 observations). The monthly sea-ice boundary is shown by a heavy line enclosing the shaded areas.

AVAILABLE SOLAR HEAT FLUX

2.1 January mean available solar heat flux (W m^{-2})

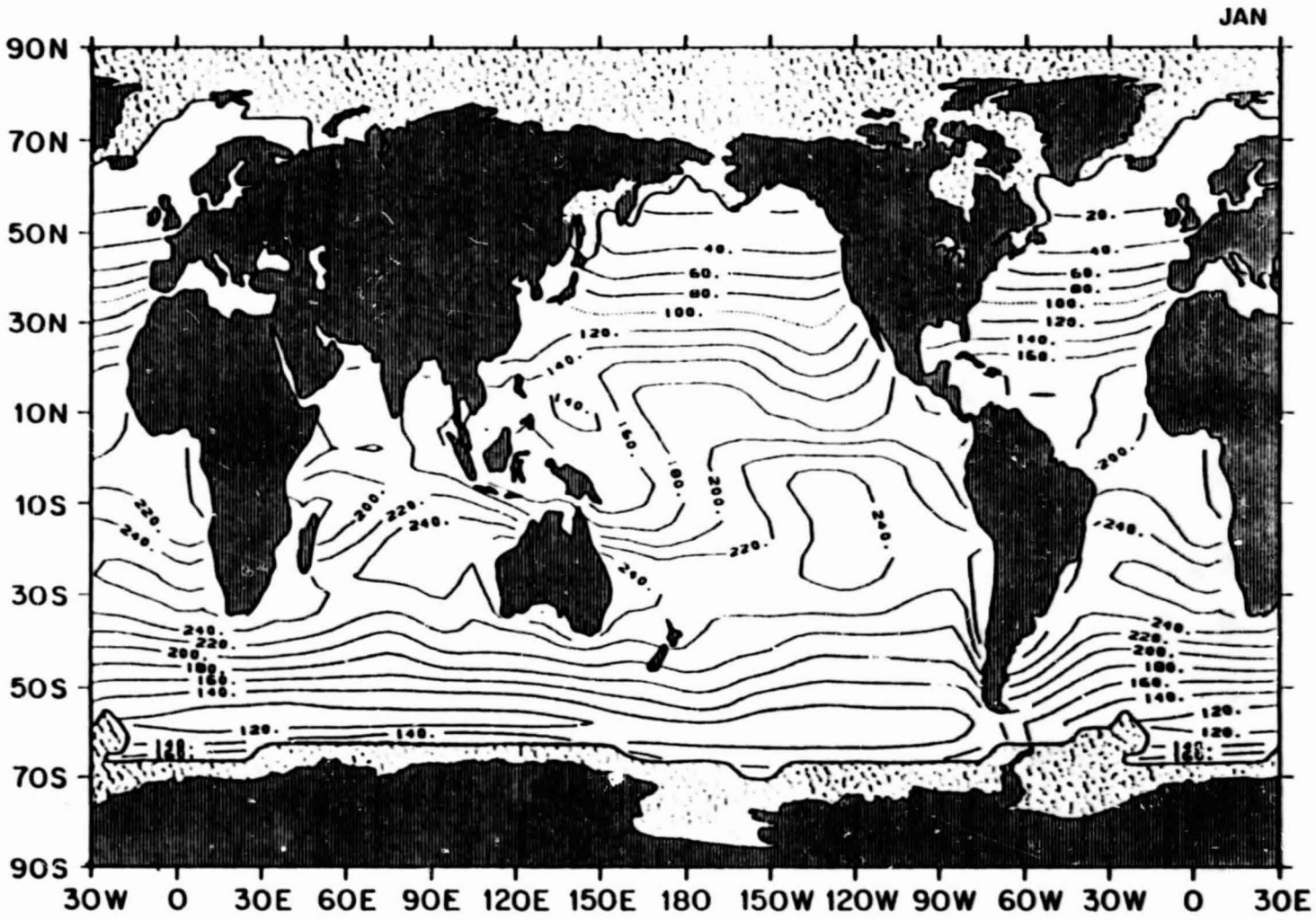

2.2 February mean available solar heat flux (W m^{-2})

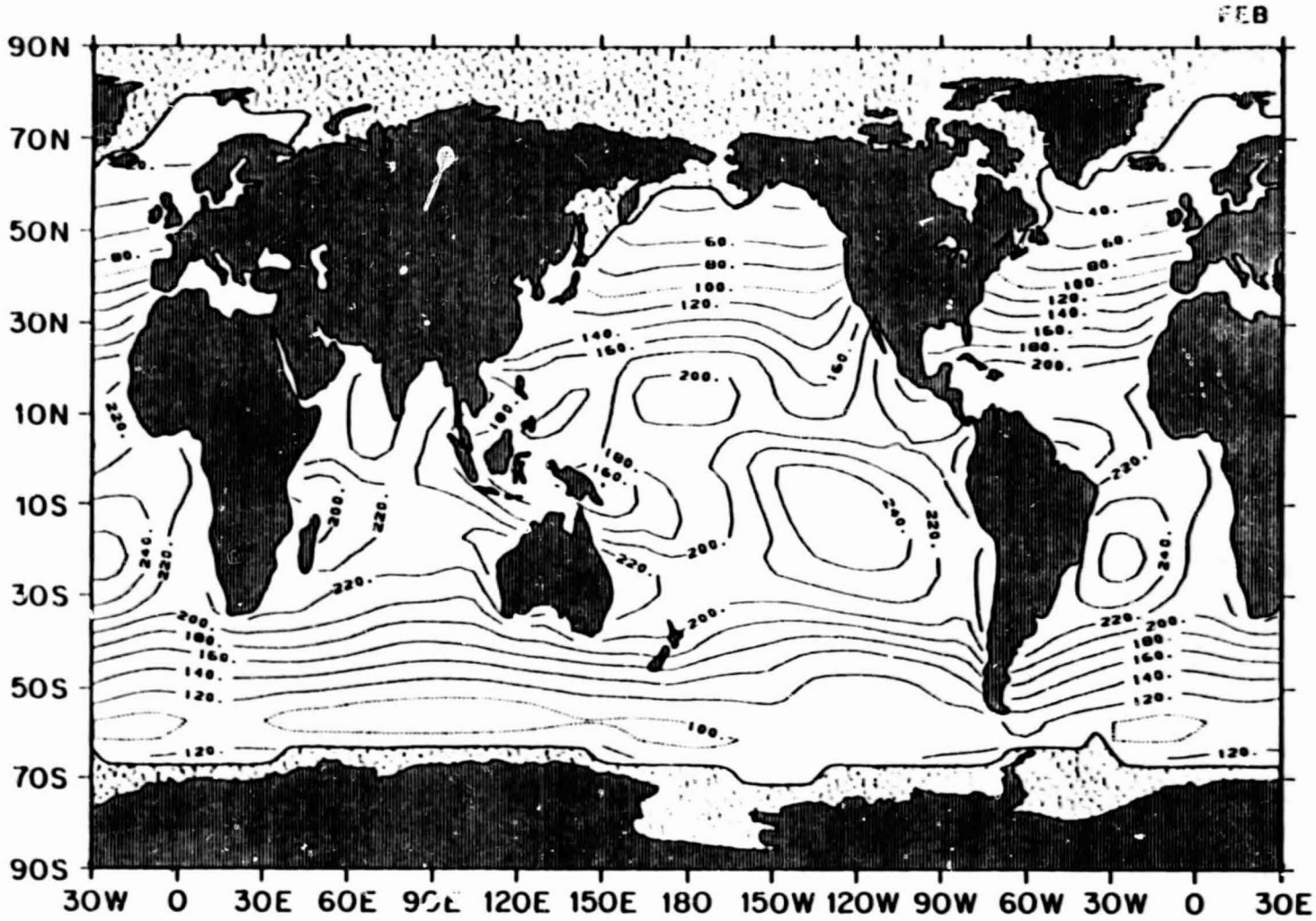

2.3 March mean available solar heat flux (W m^{-2})

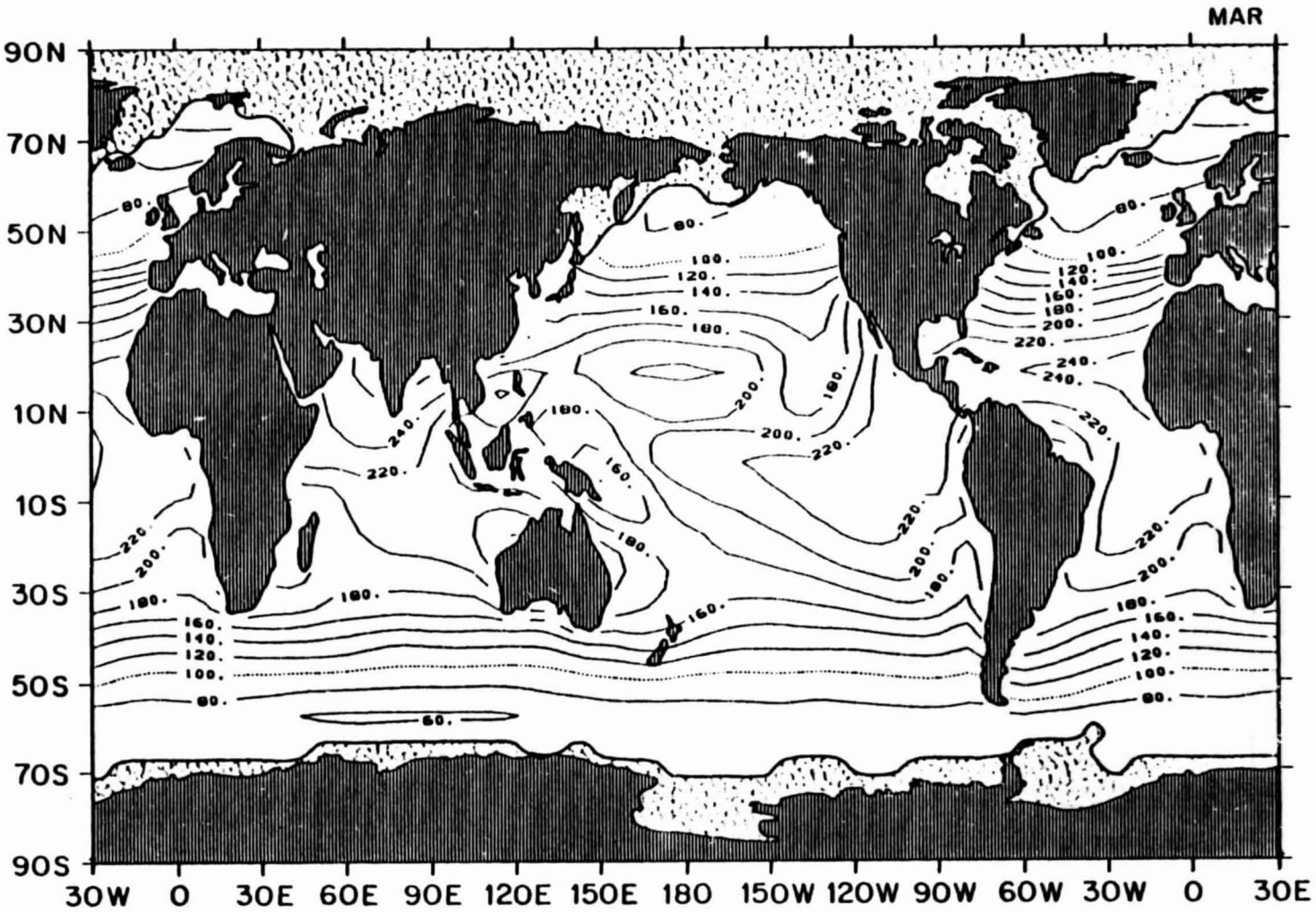

2.4 April mean available solar heat flux (W m^{-2})

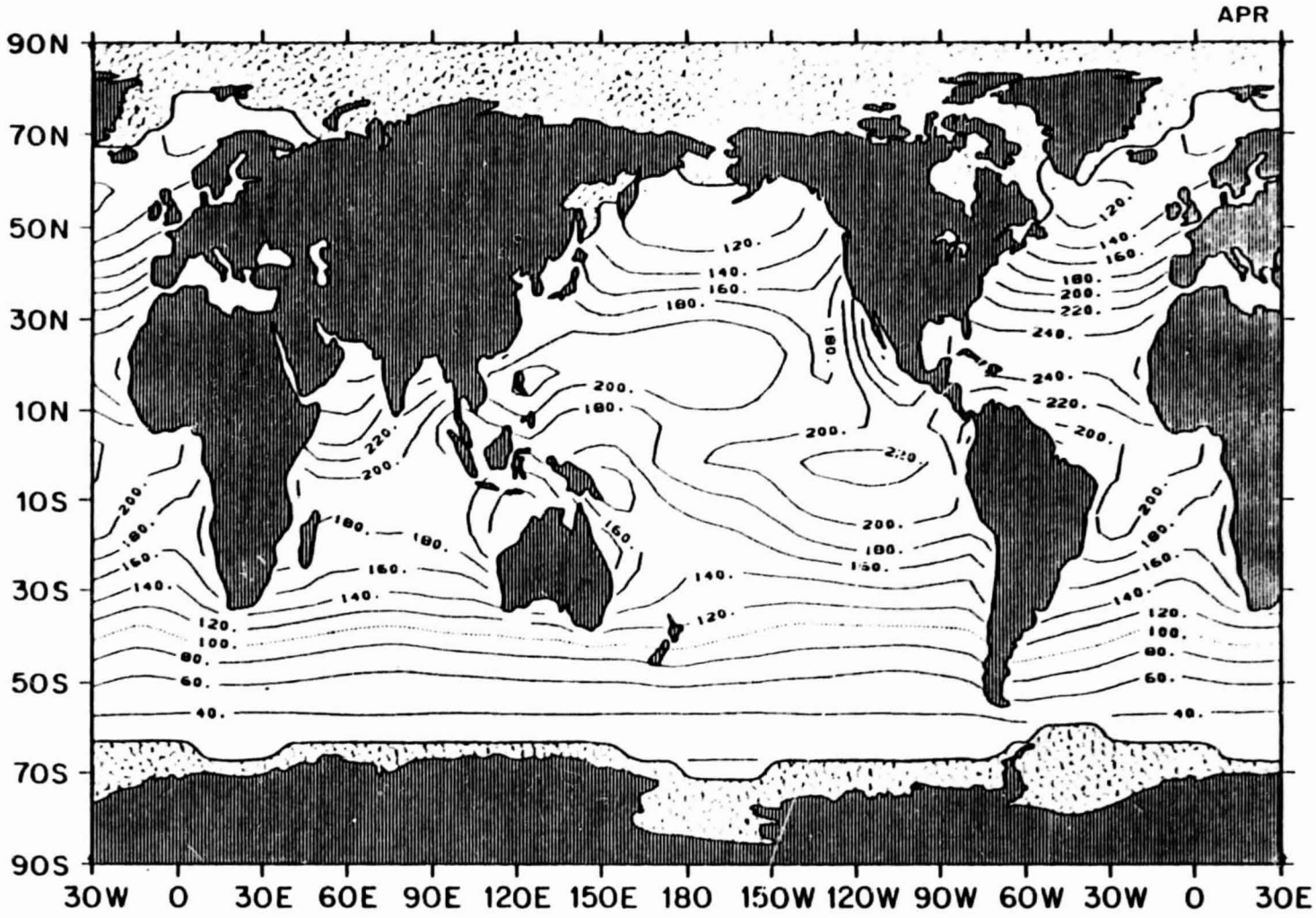

2.5 May mean available solar heat flux (W m^{-2})

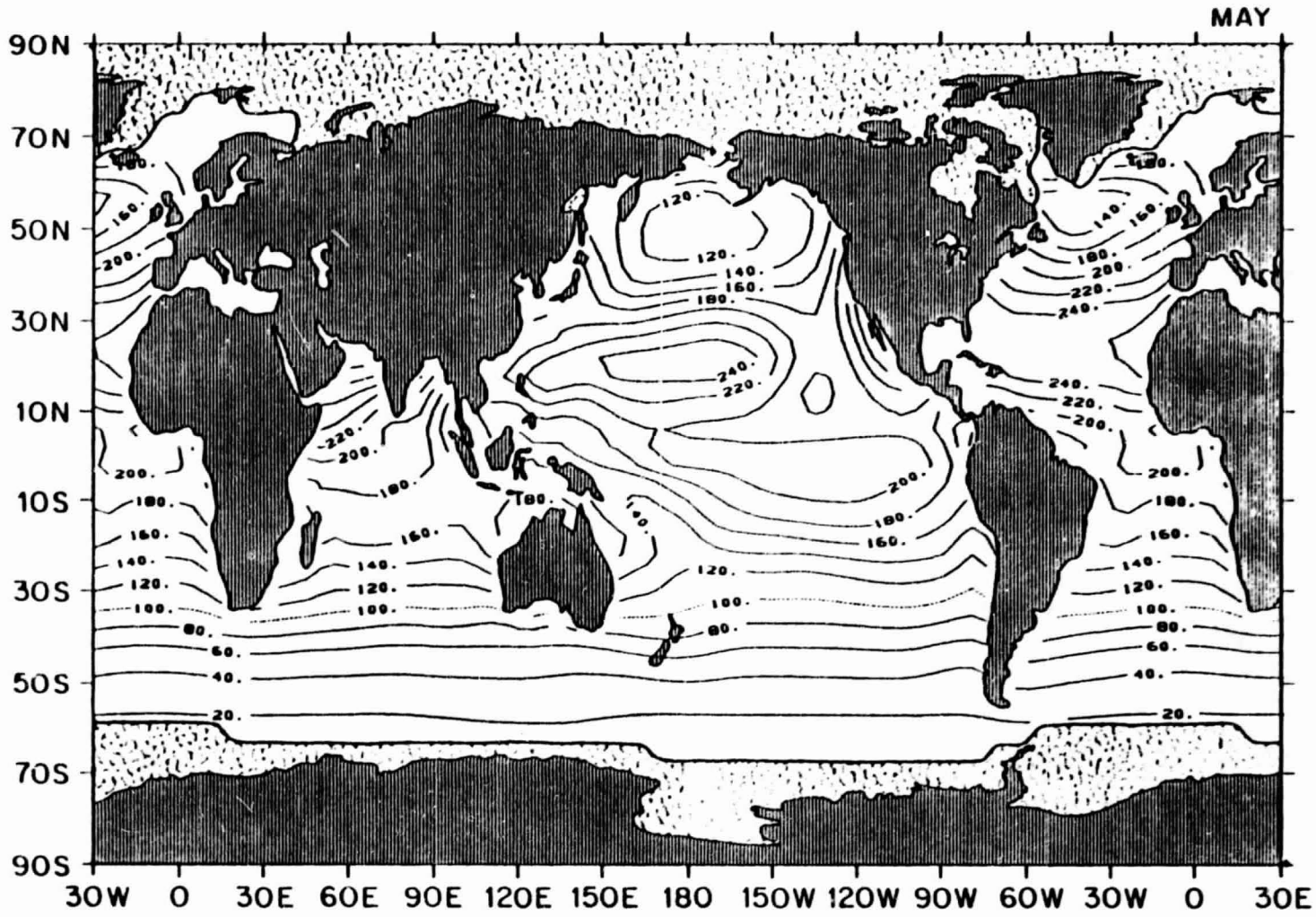

2.6 June mean available solar heat flux (W m^{-2})

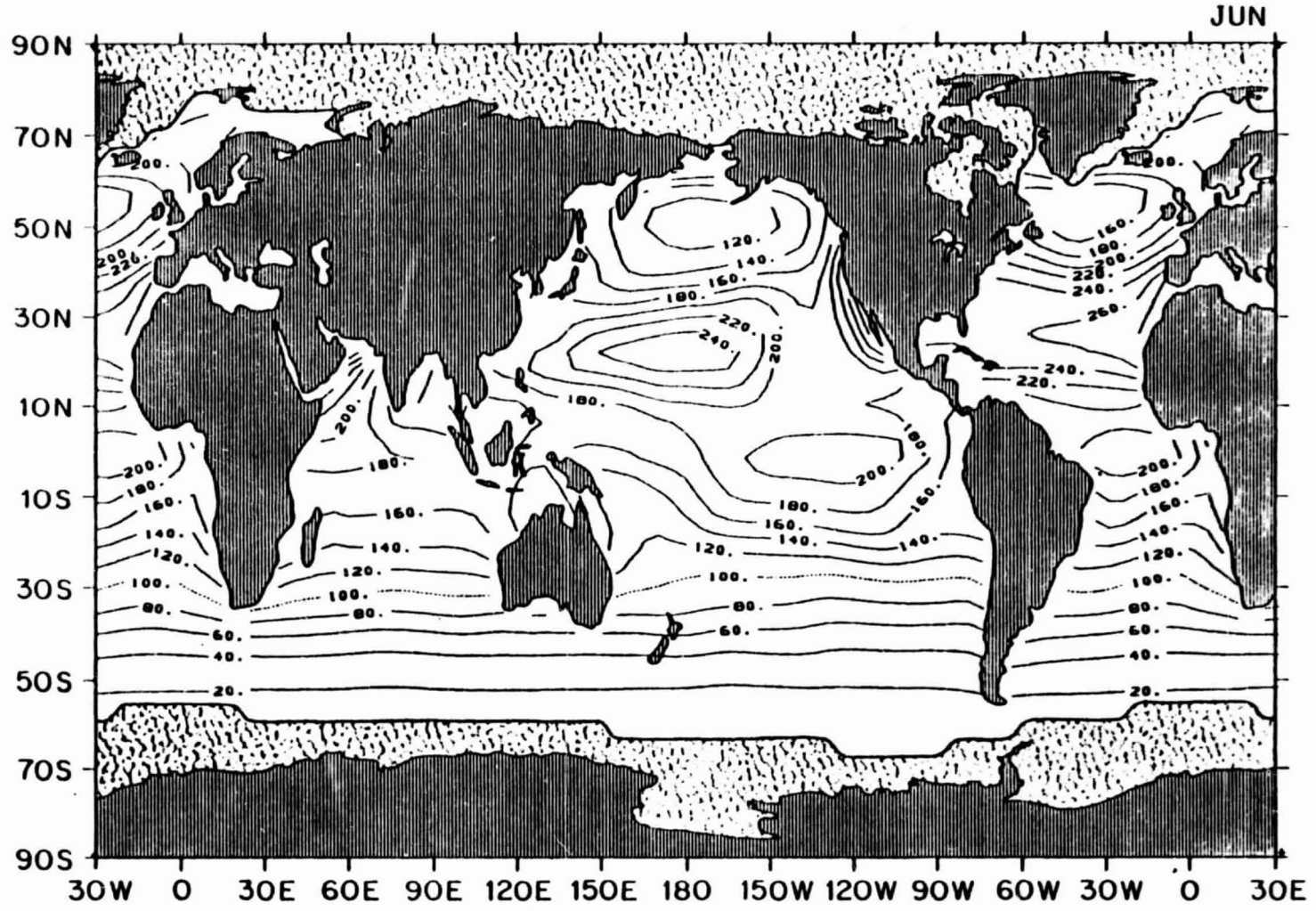

2.7 July mean available solar heat flux (W m^{-2})

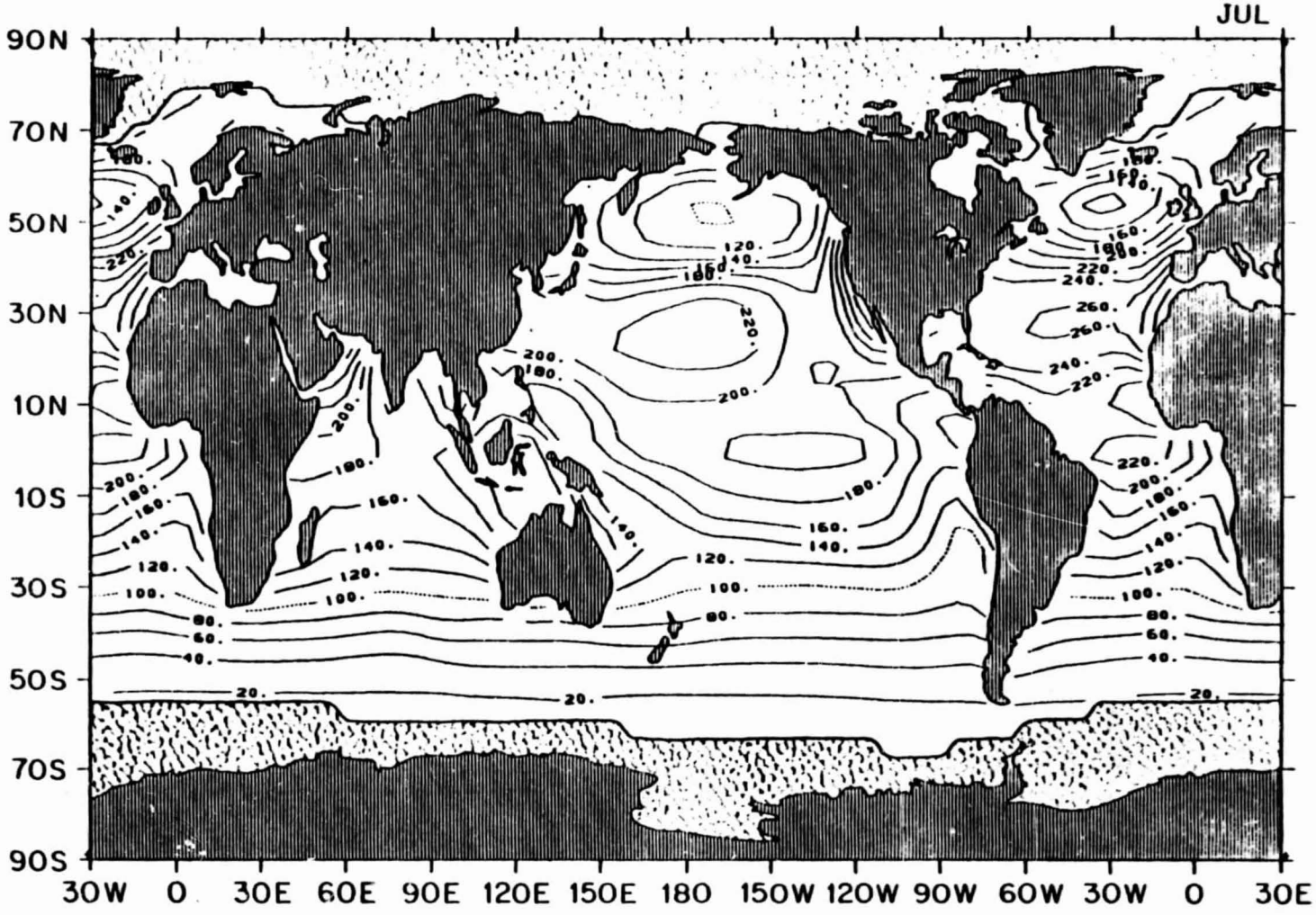

2.8 August mean available solar heat flux (W m^{-2})

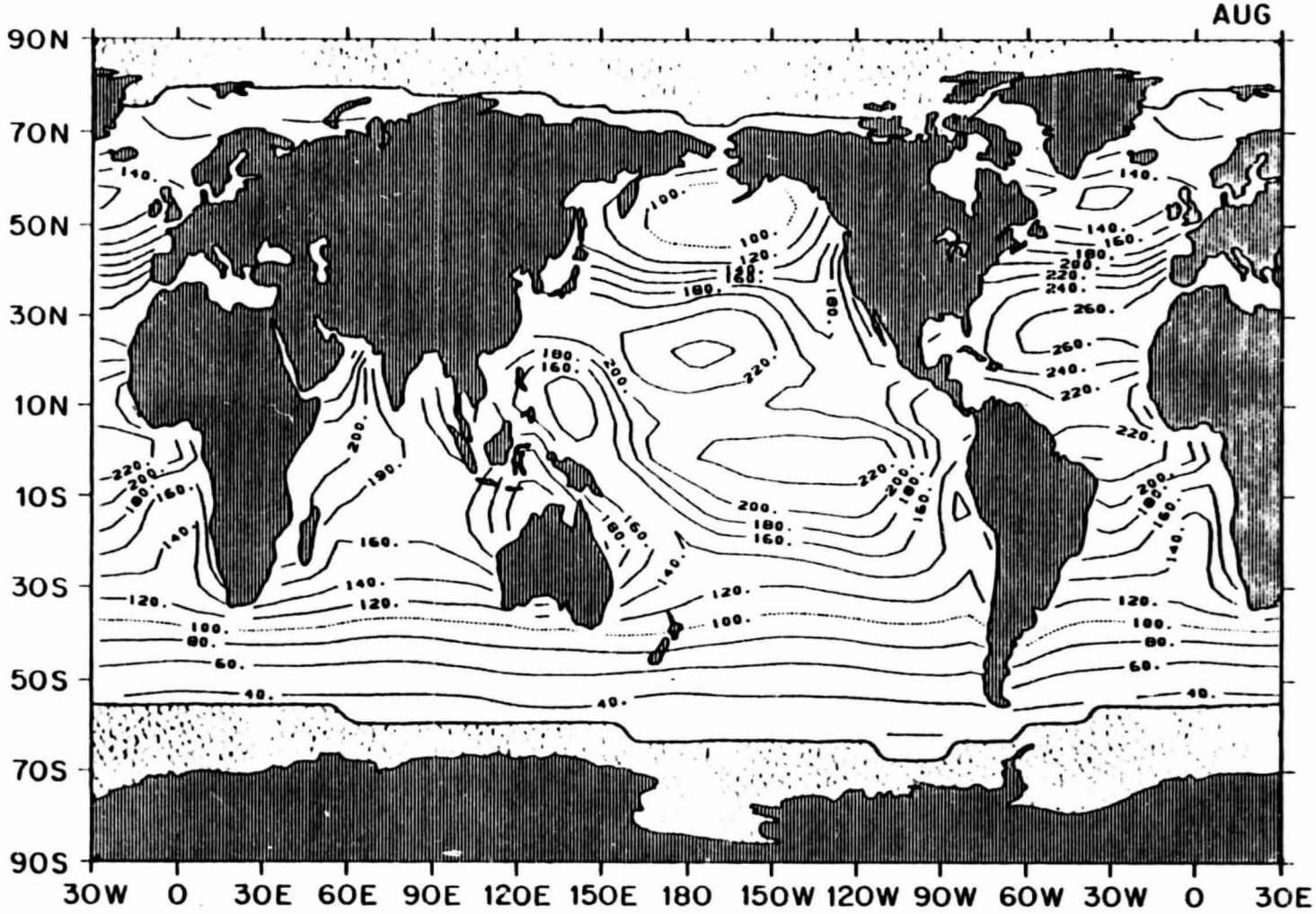

2.9 September mean available solar heat flux (W m^{-2})

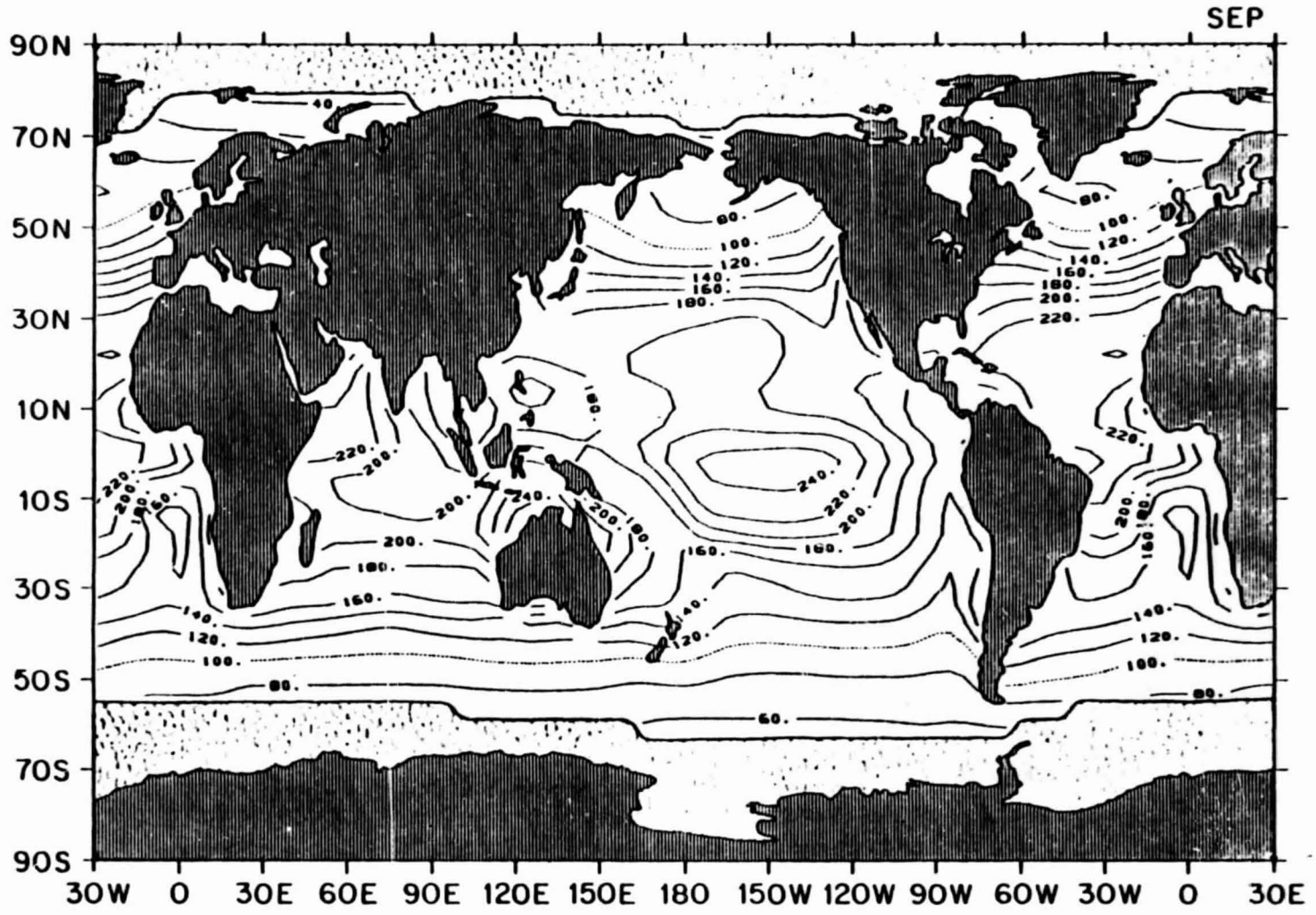

2.10 October mean available solar heat flux (W m^{-2})

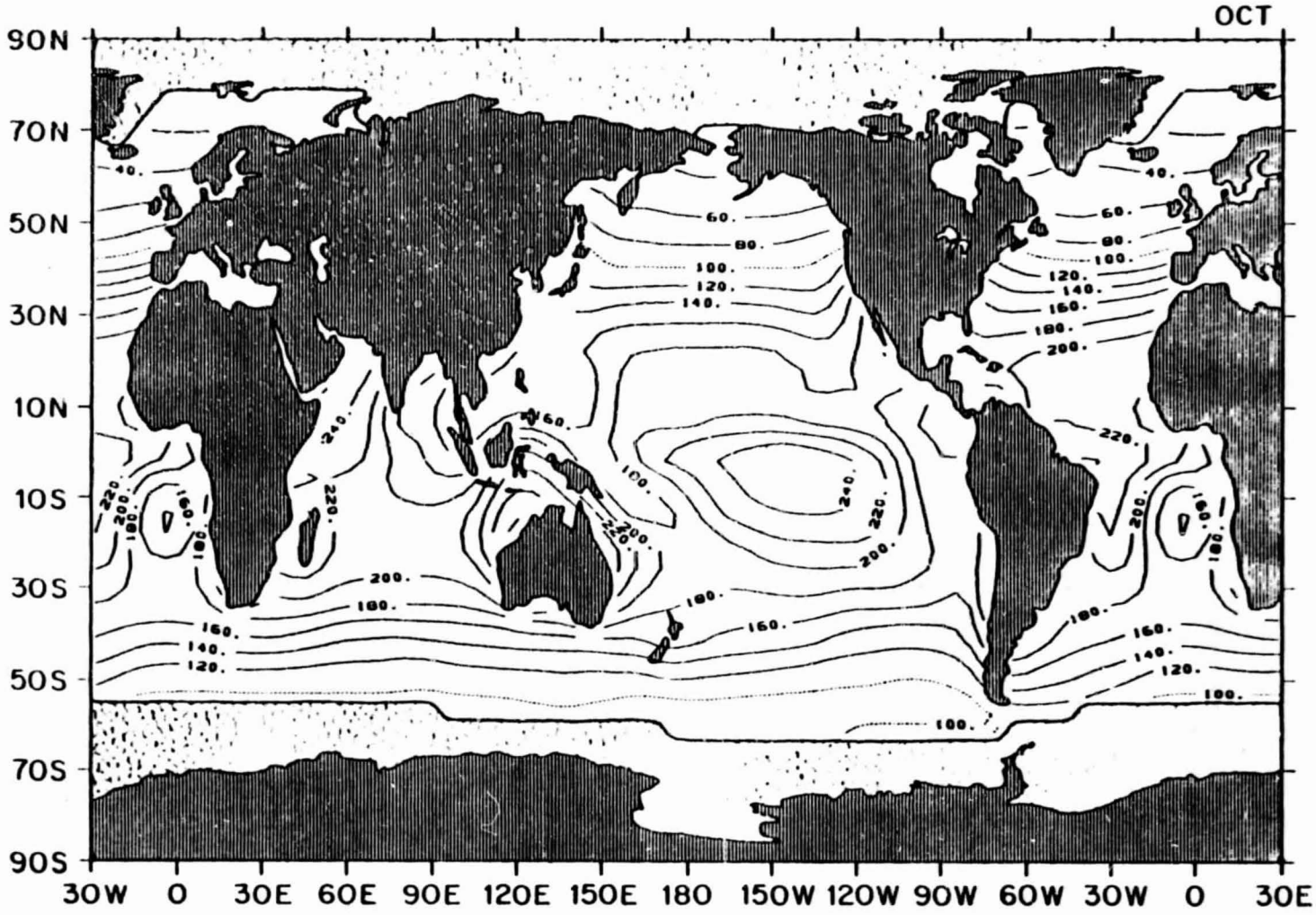

2.11 November mean available solar heat flux (W m^{-2})

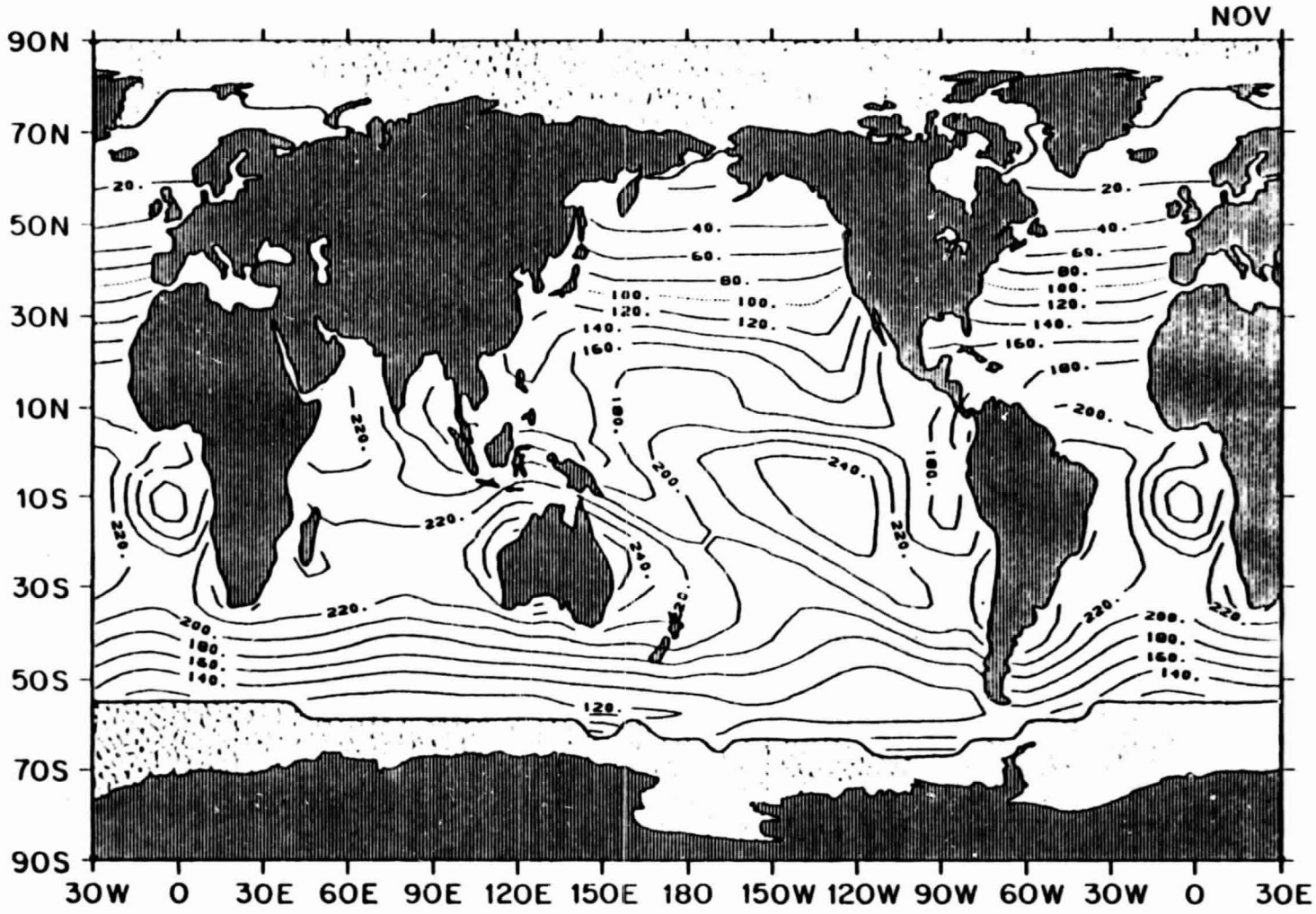

2.12 December mean available solar heat flux (W m^{-2})

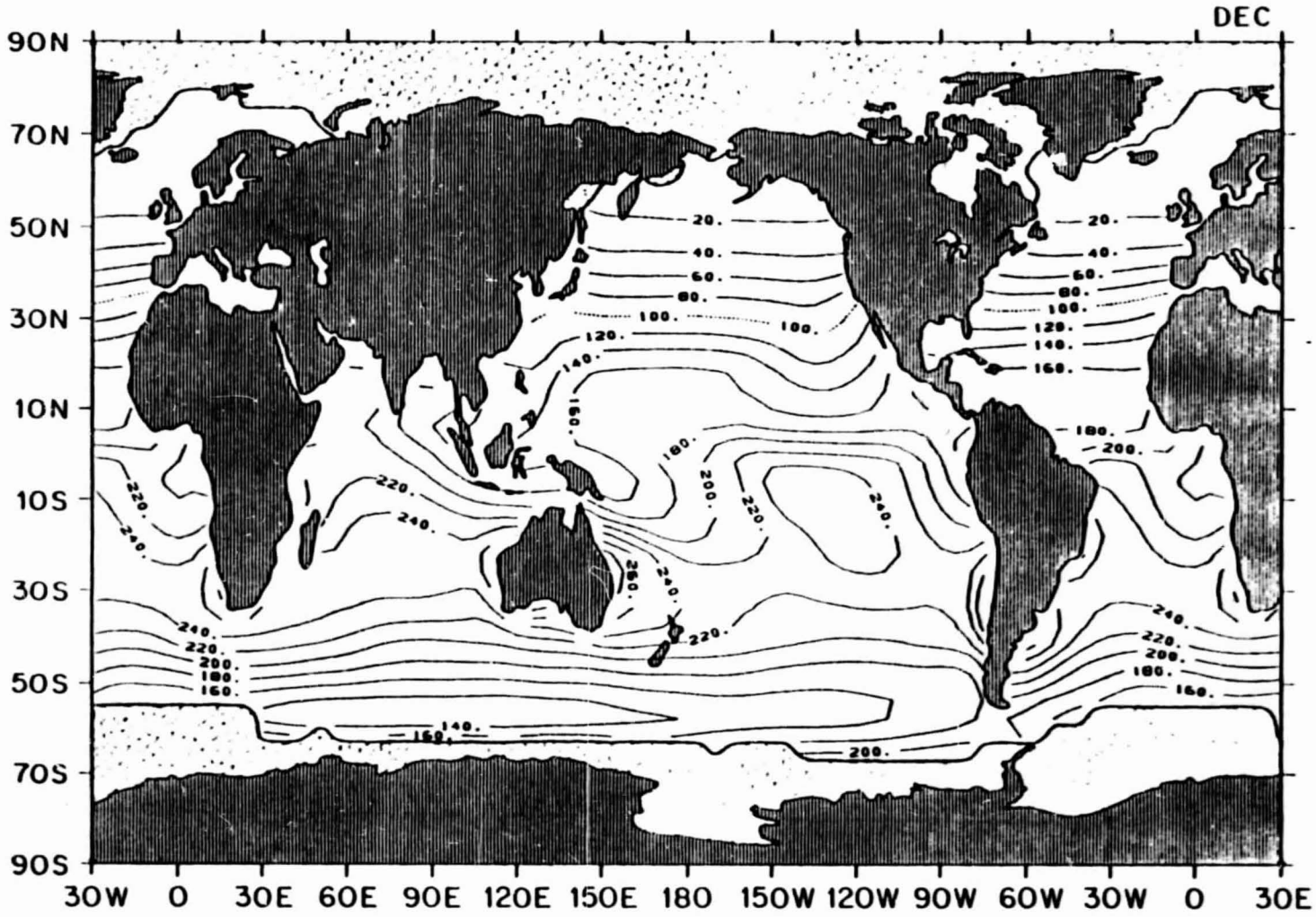

2.13 Annual mean available solar heat flux (W m-2)

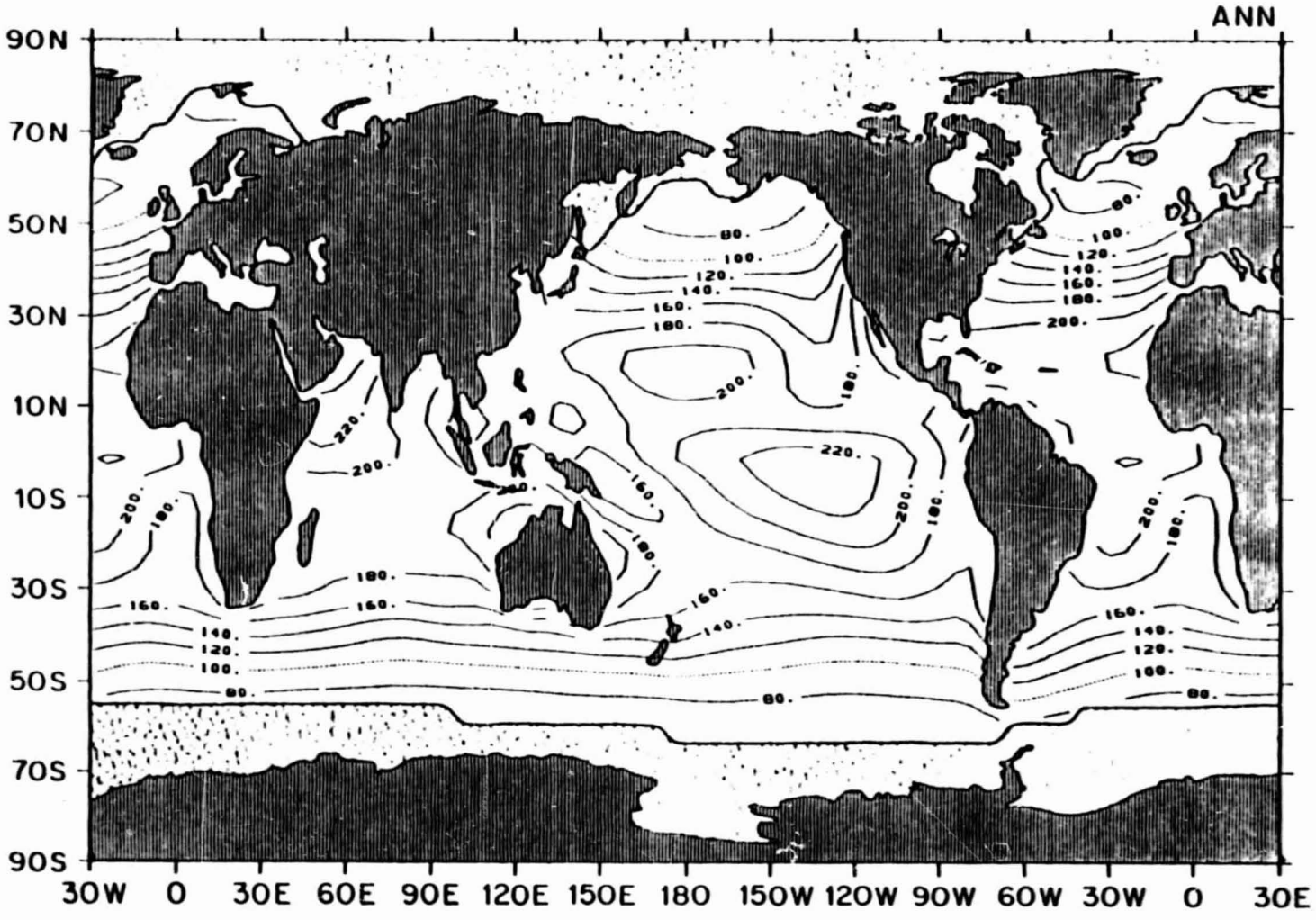

NET UPWARD LONG-WAVE FLUX

2.14 January mean net upward long-wave flux ($W\ m^{-2}$)

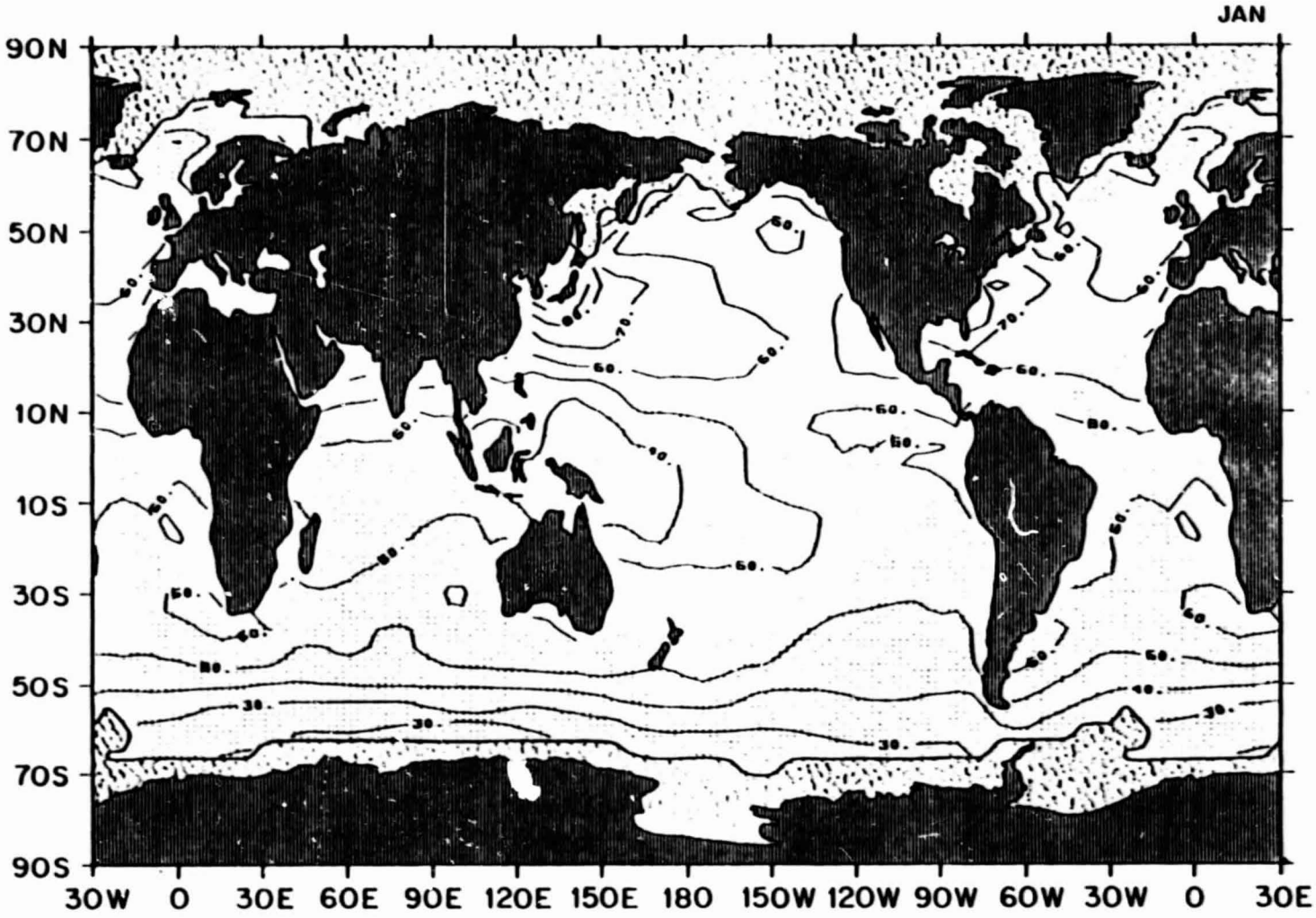

2.15 February mean net upward long-wave flux (W m^{-2})

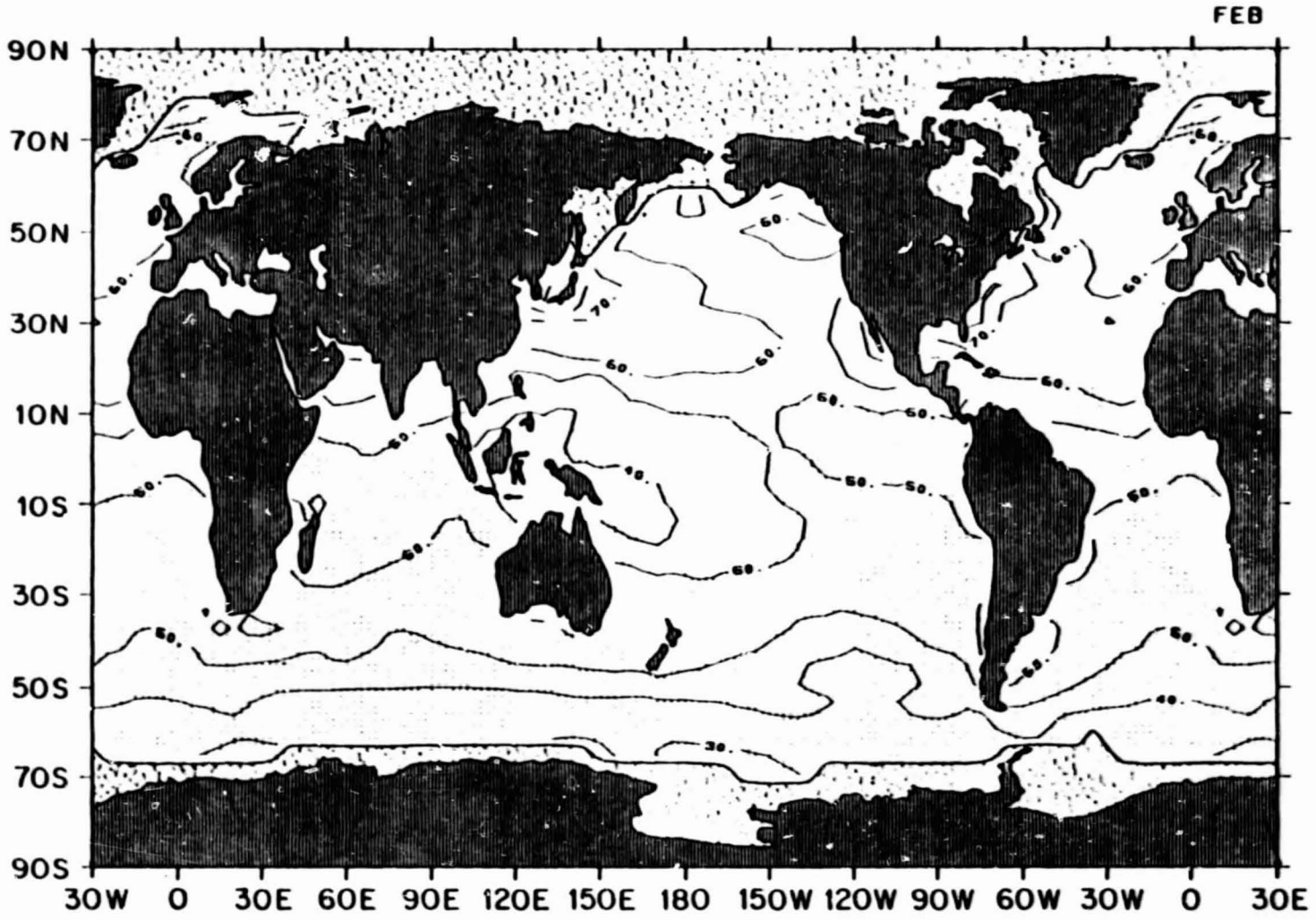

2.16 March mean net upward long-wave flux (W m^{-2})

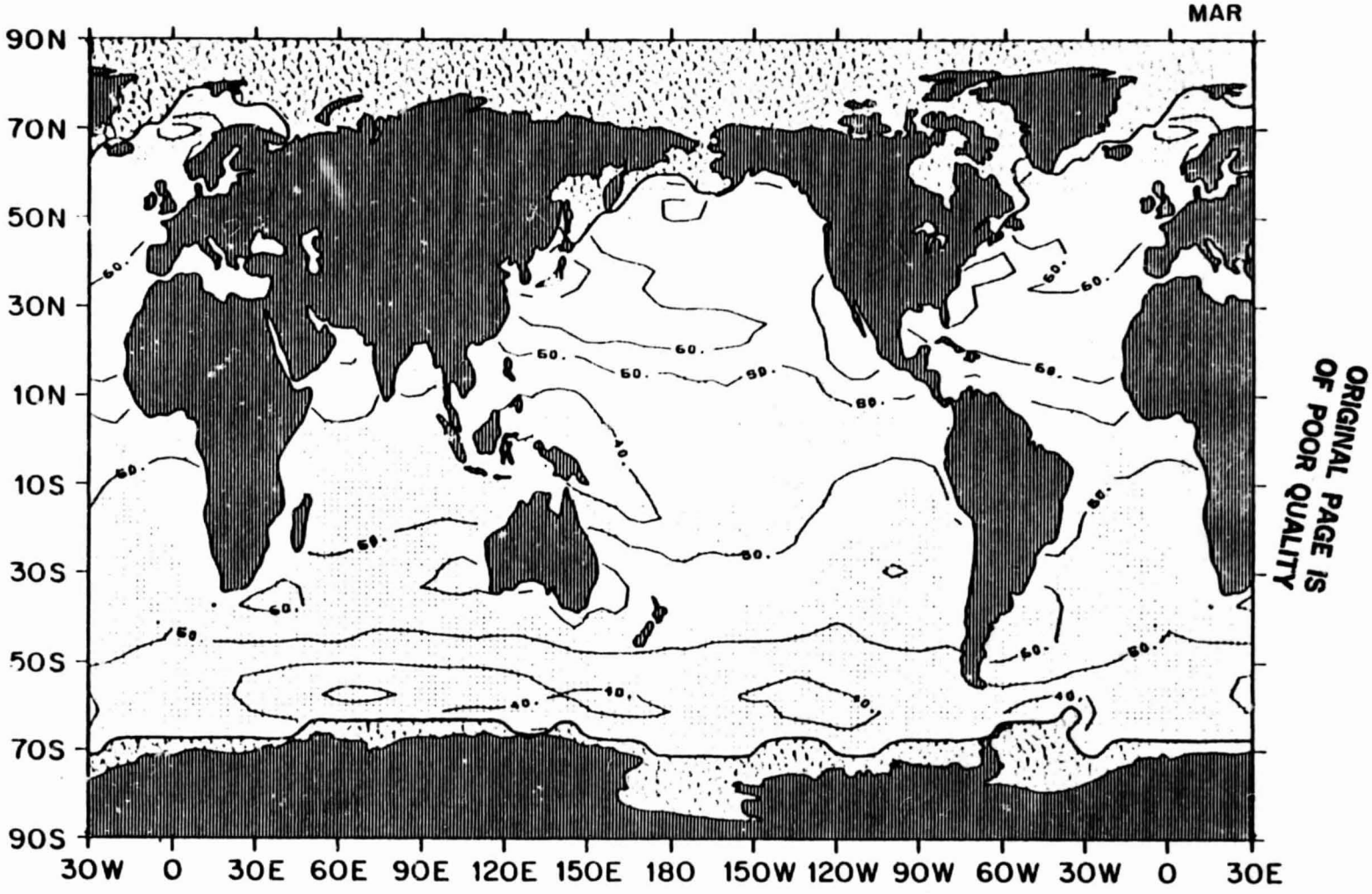

2.17 April mean net upward long-wave flux (W m^{-2})

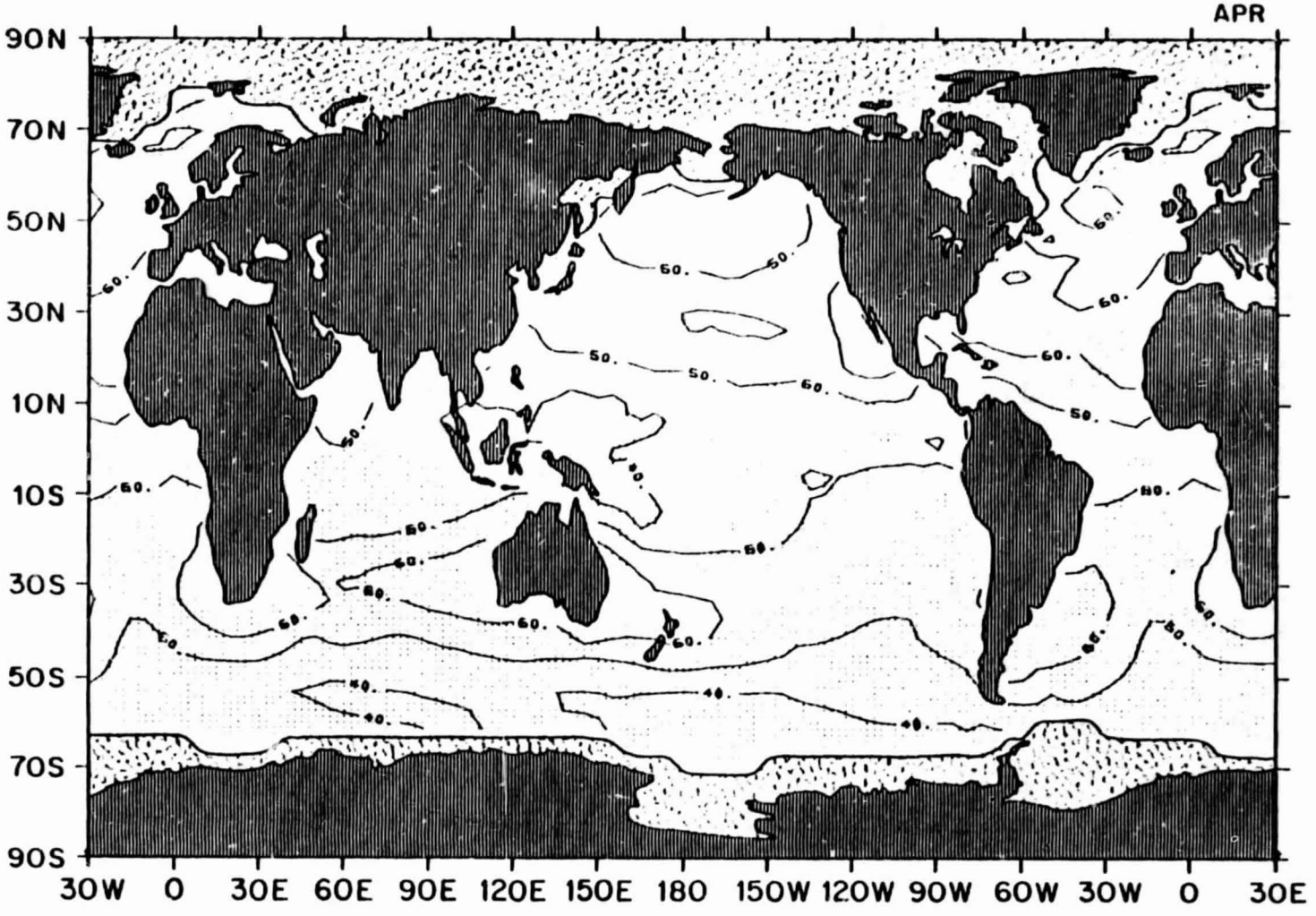

2.18 May mean net upward long-wave flux (W m^{-2})

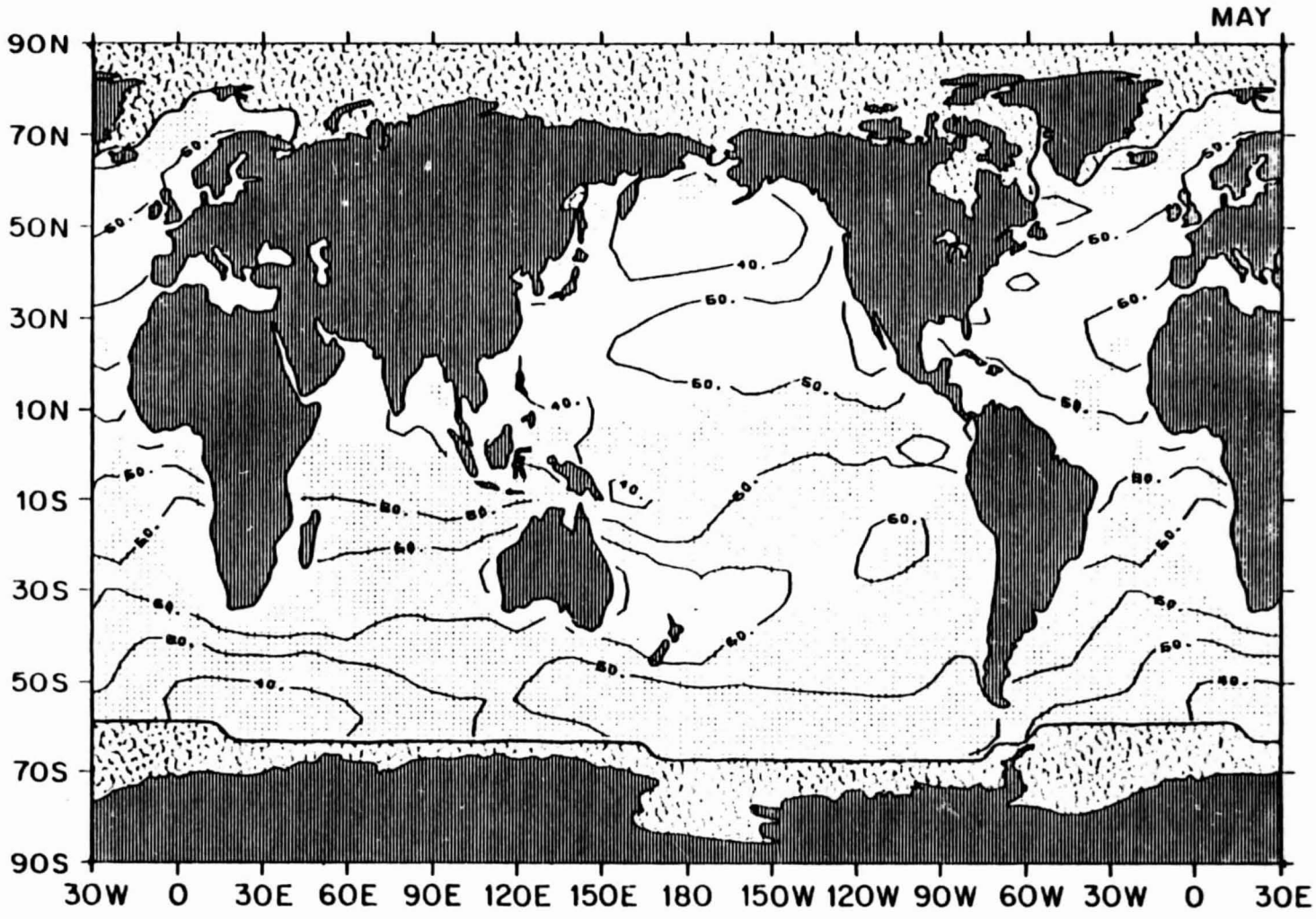

2.19 June mean net upward long-wave flux (W m^{-2})

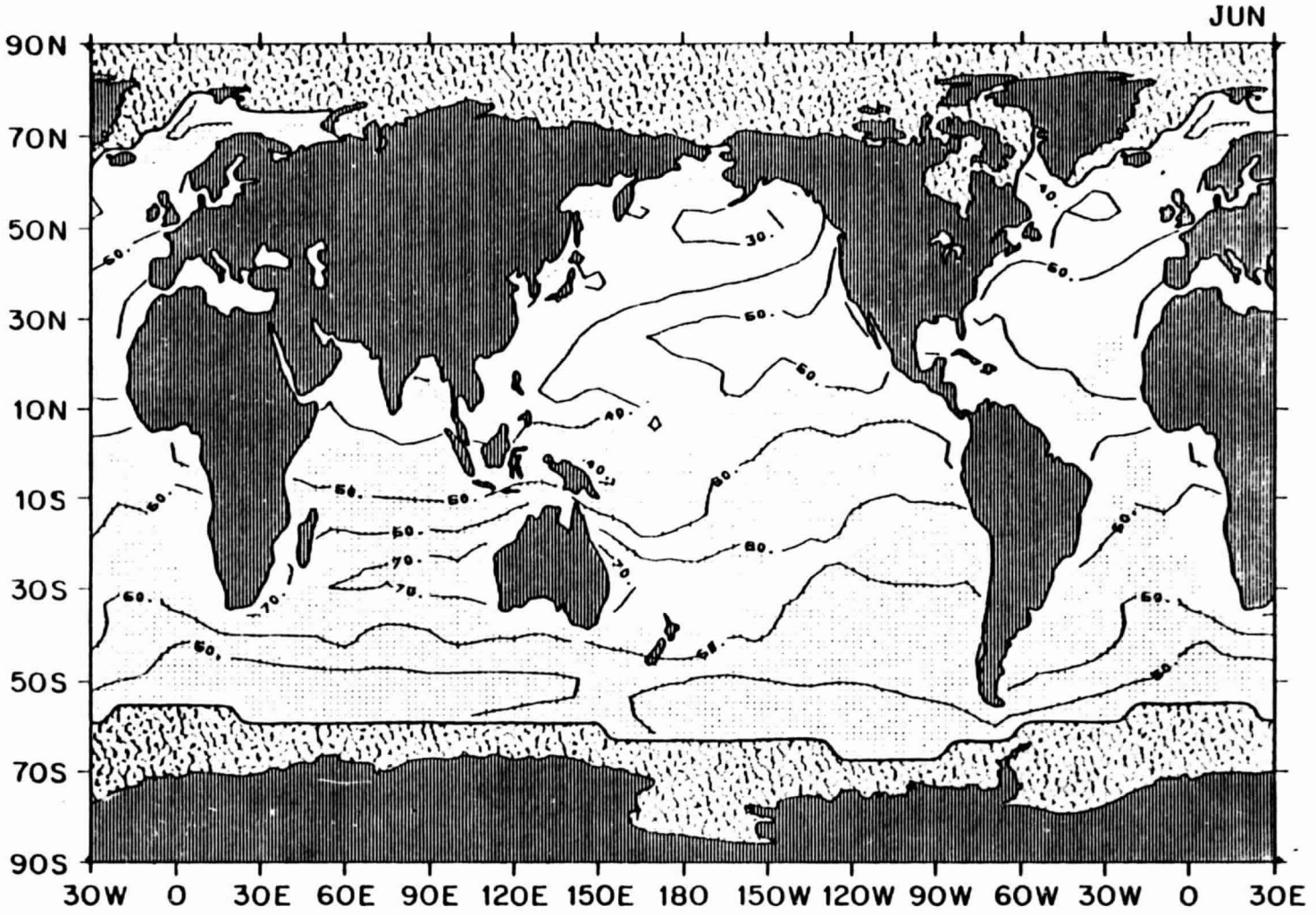

2.20 July mean net upward long-wave flux (W m^{-2})

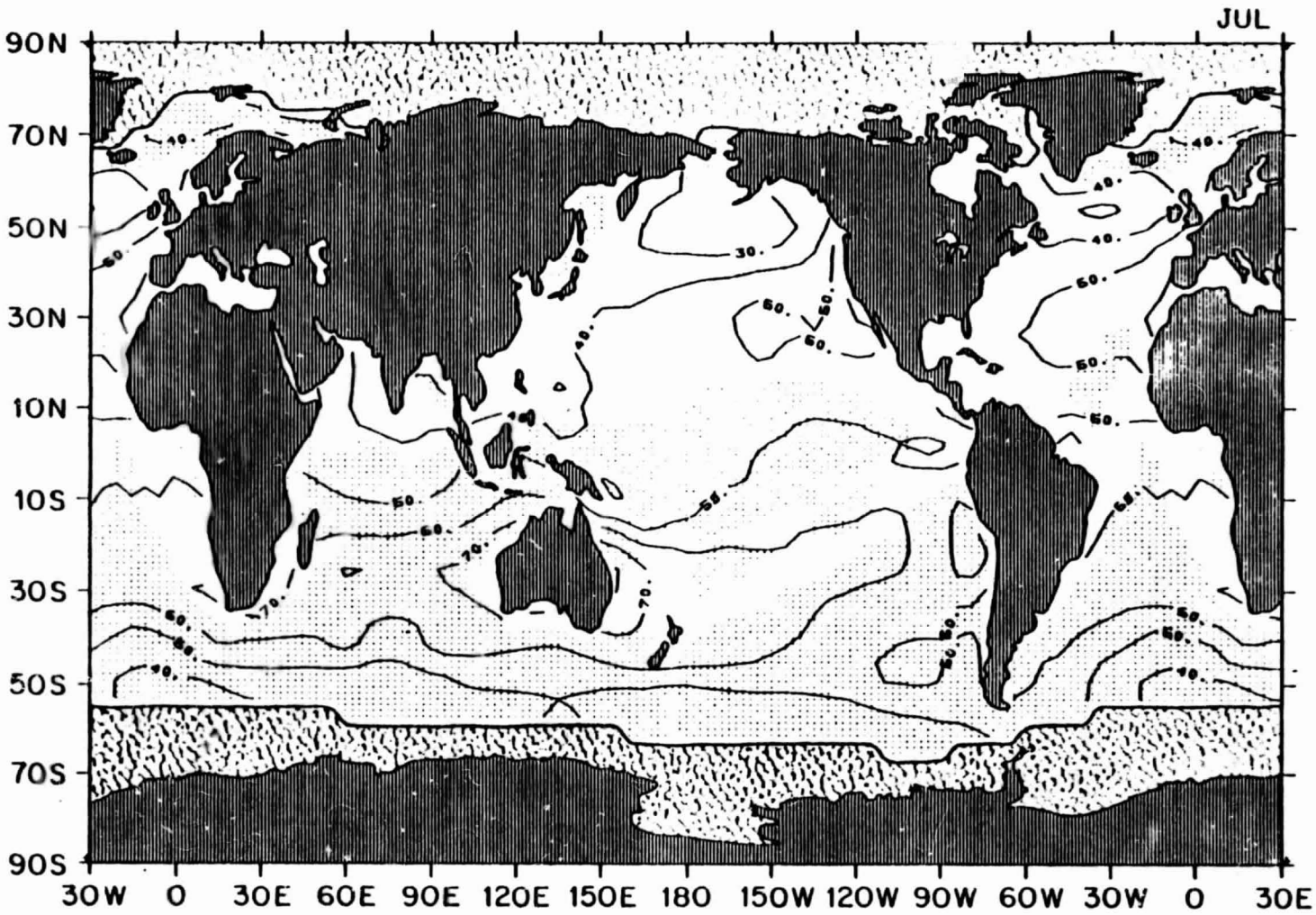

2.21 August mean net upward long-wave flux (W m^{-2})

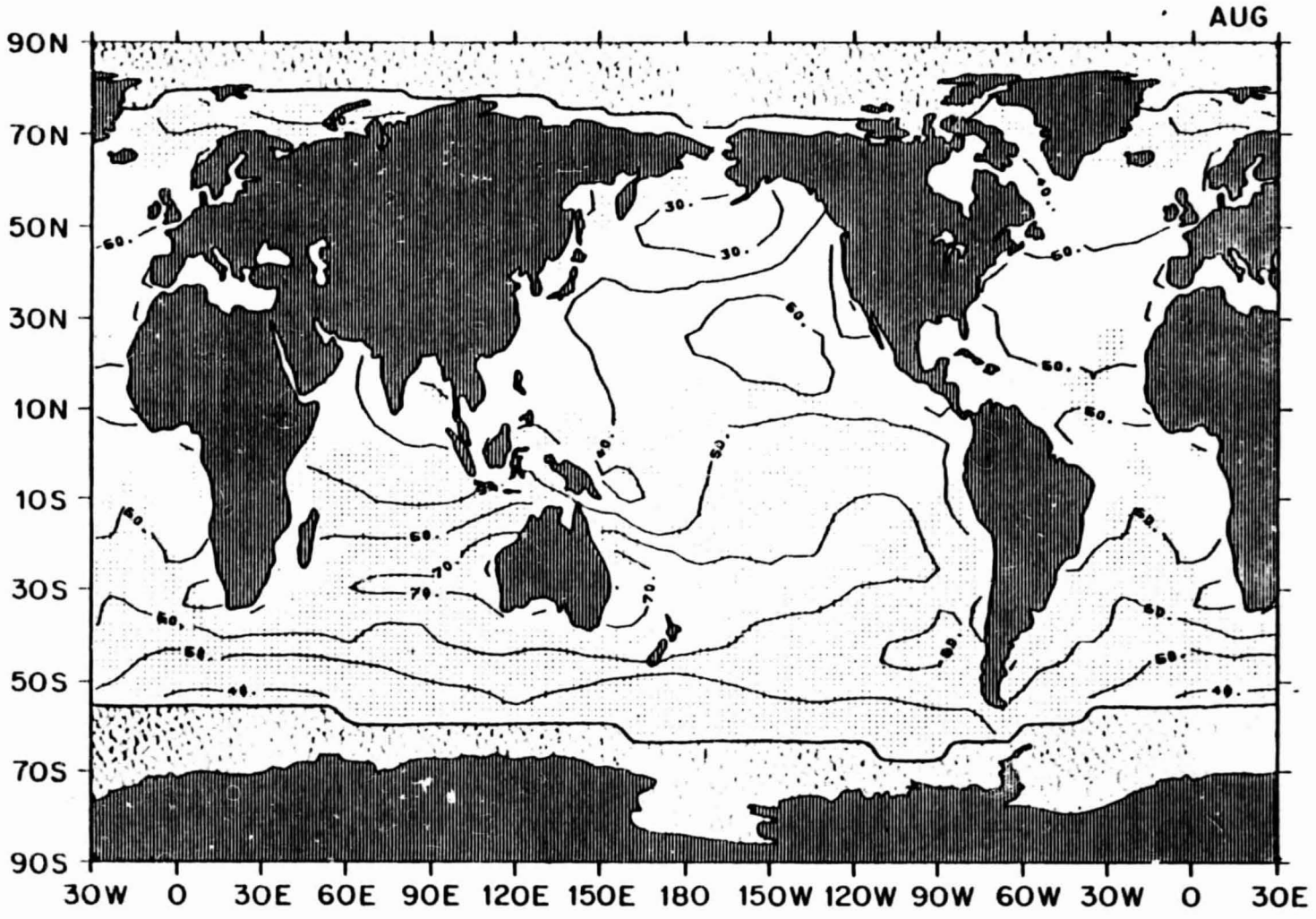

2.22 September mean net upward long-wave flux (W m^{-2})

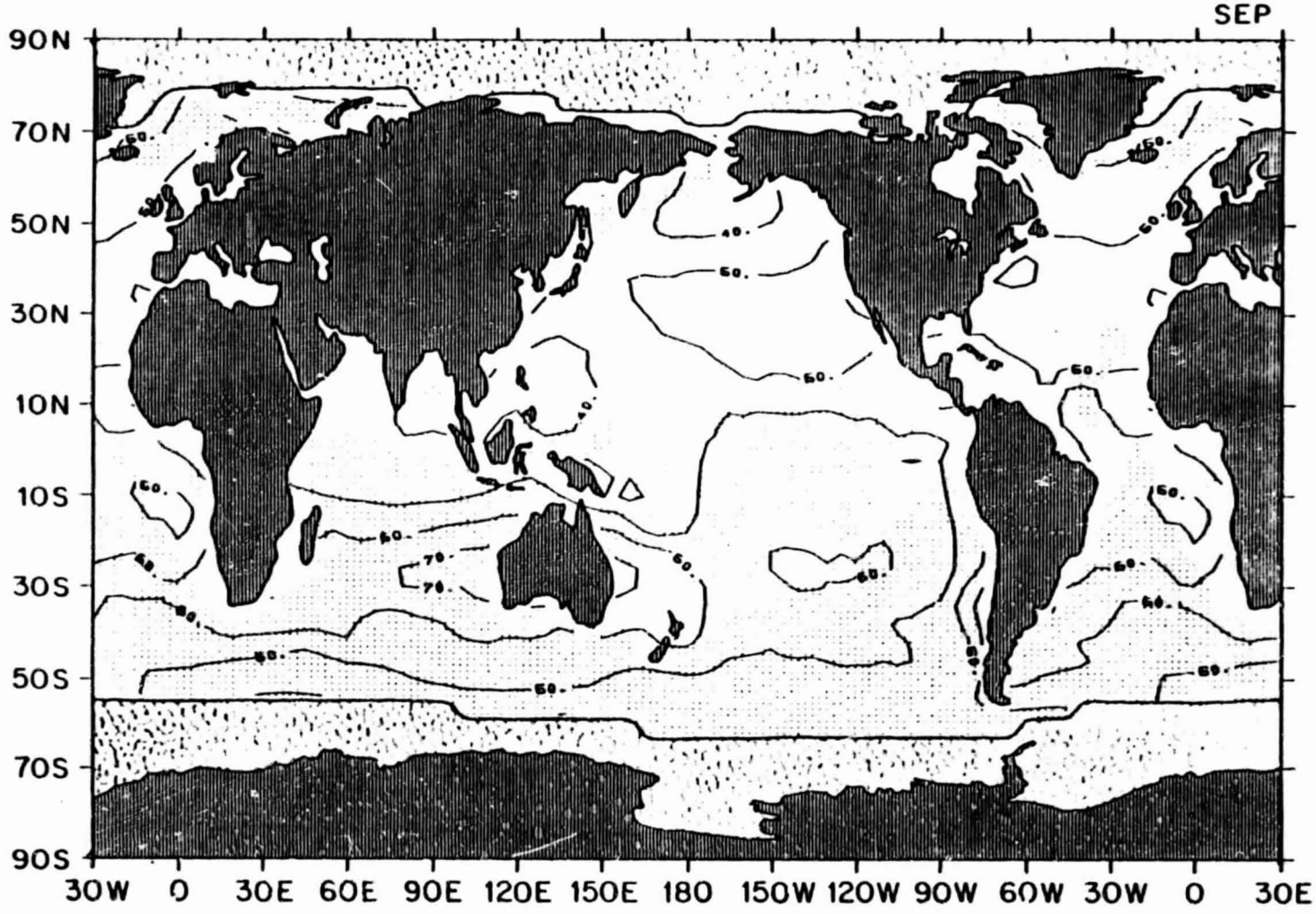

2 23 October mean net upward long-wave flux (W m^{-2})

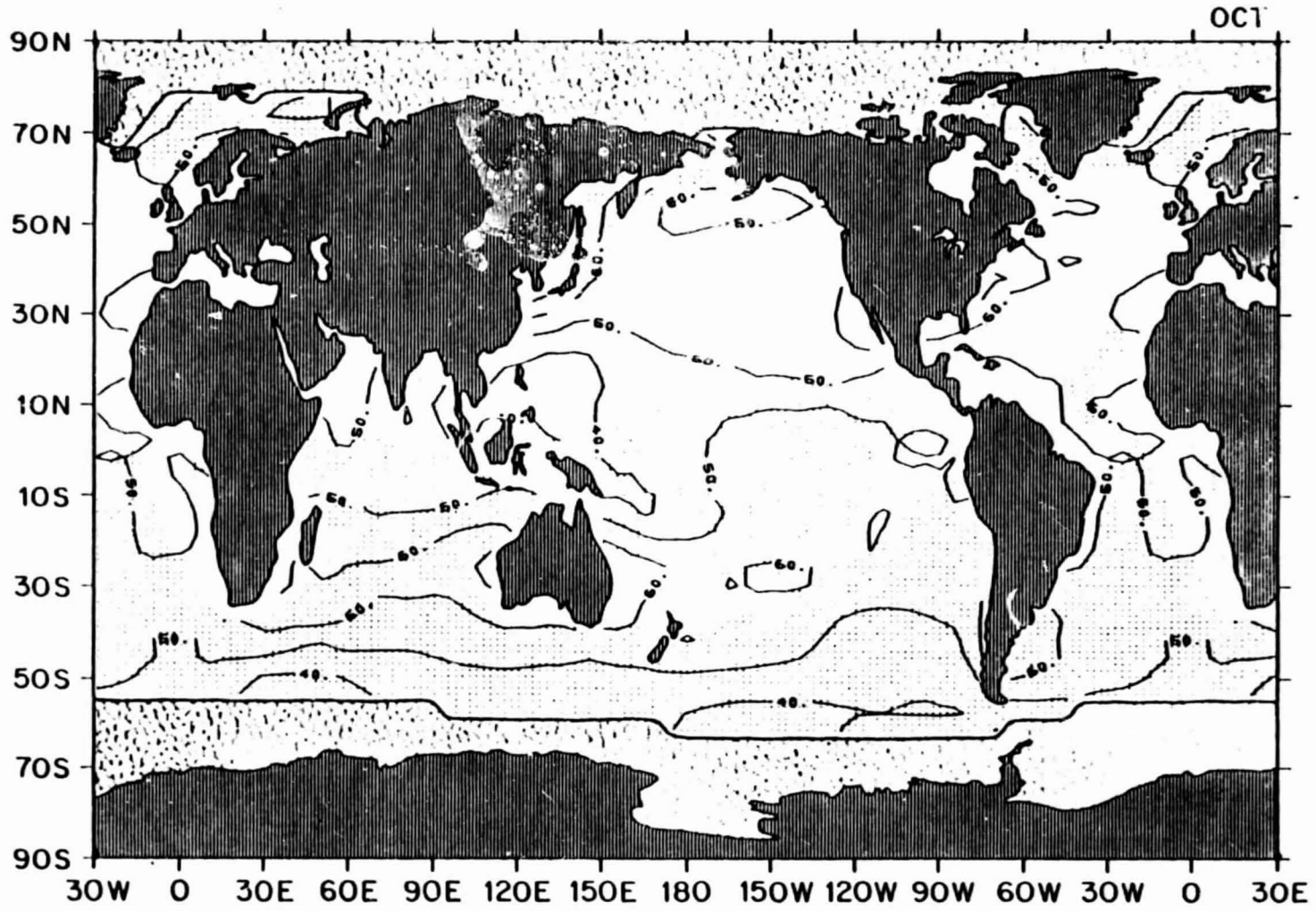

?.24 November mean net upward long-wave flux (W m^{-2})

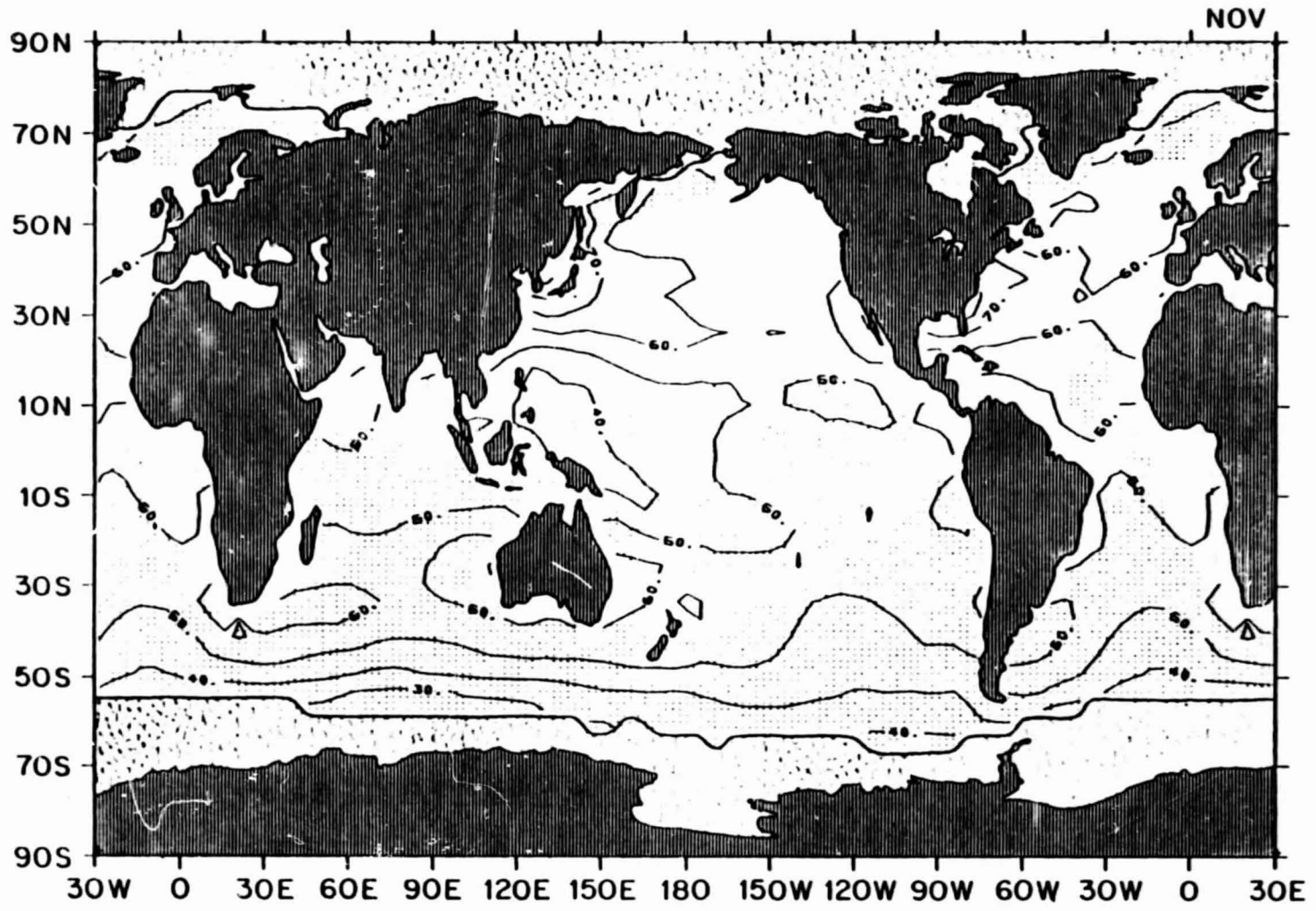

2.25 December mean net upward long-wave flux (W m^{-2})

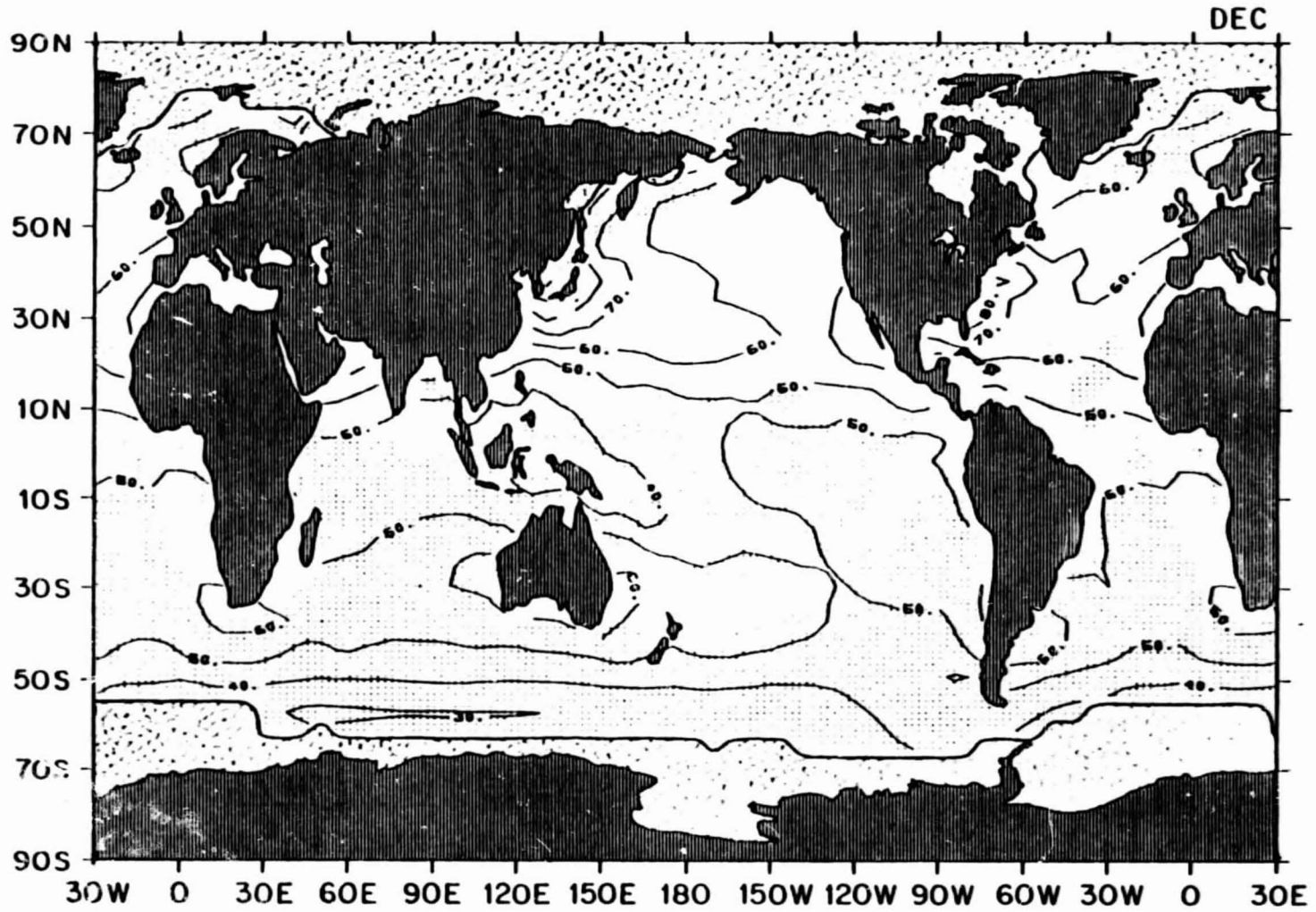

2.26 Annual mean net upward long-wave flux (W m-2)

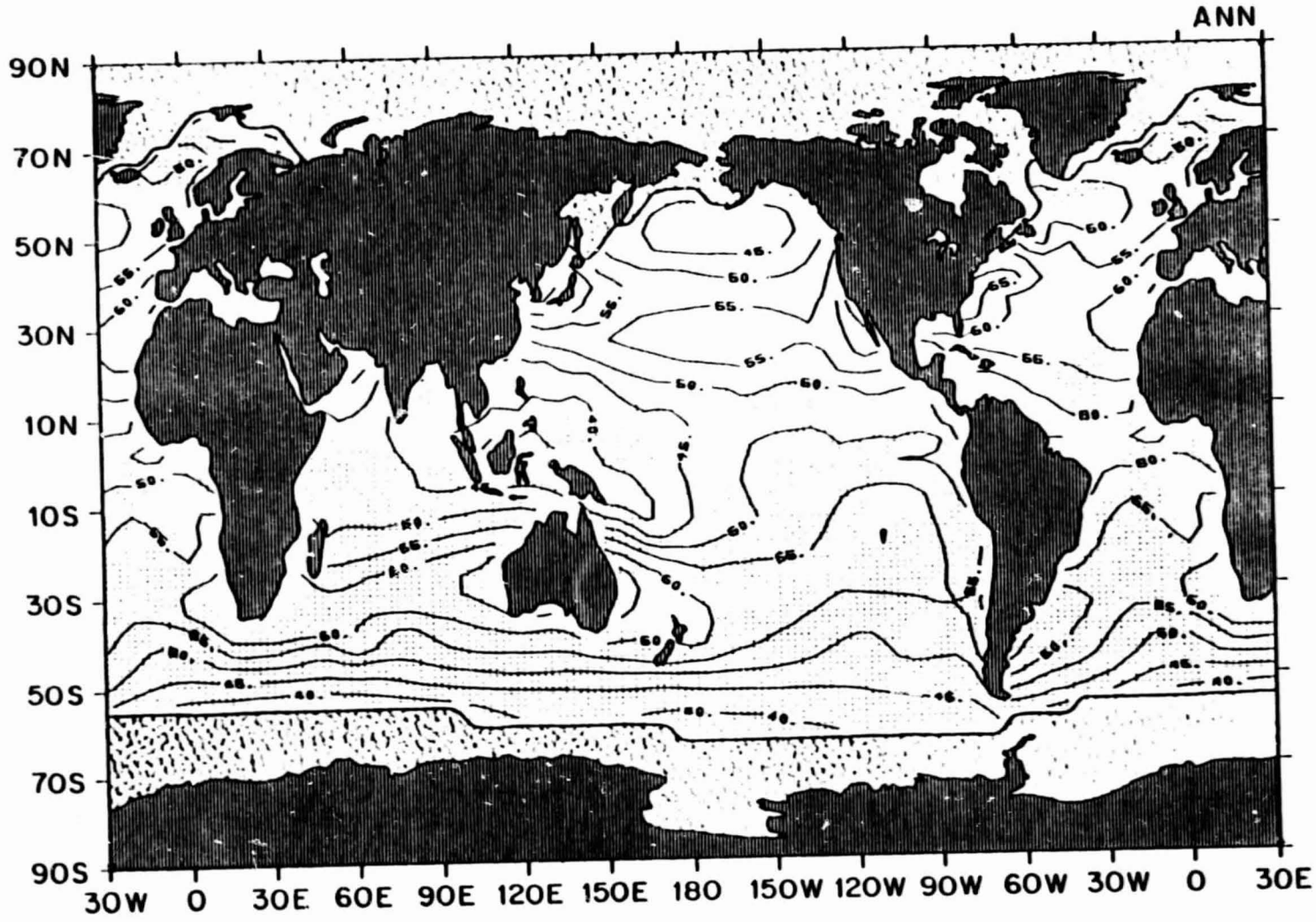

NET DOWNWARD RADIATIVE FLUX

2.27 January mean net downward radiative flux (W m^{-2})

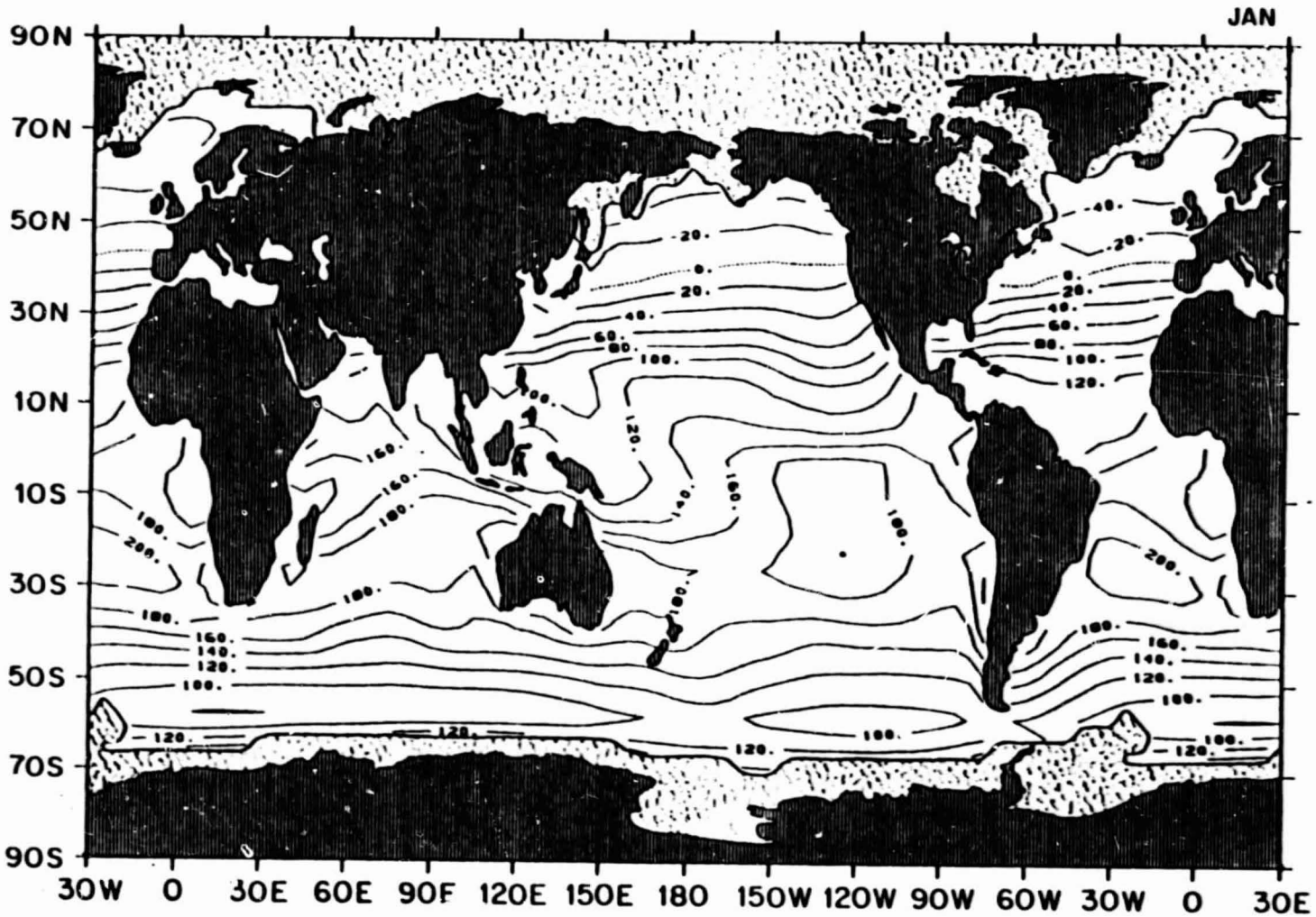

2.28 February mean net downward radiative flux (W m^{-2})

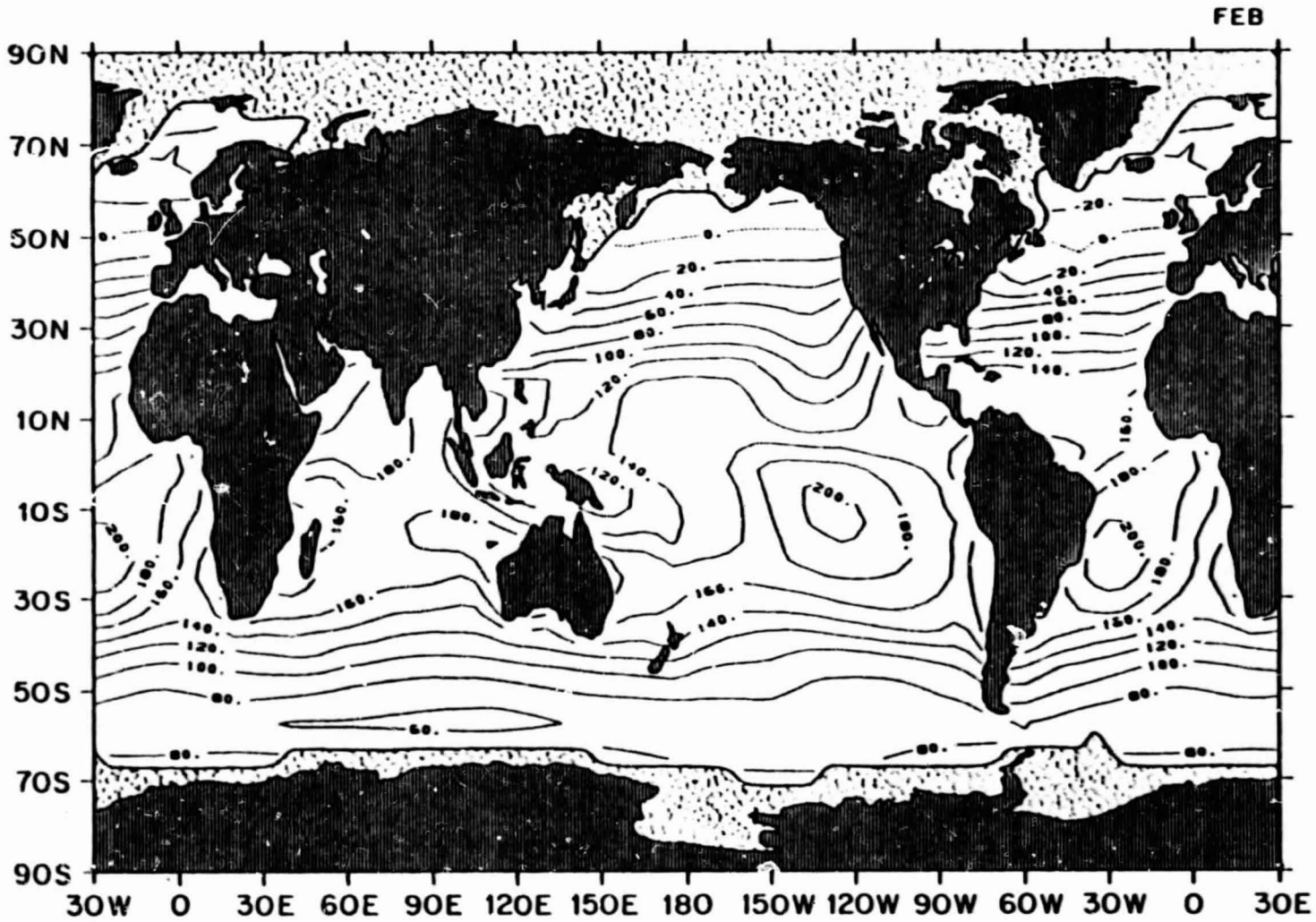

2.29 March mean net downward radiative flux (W m^{-2})

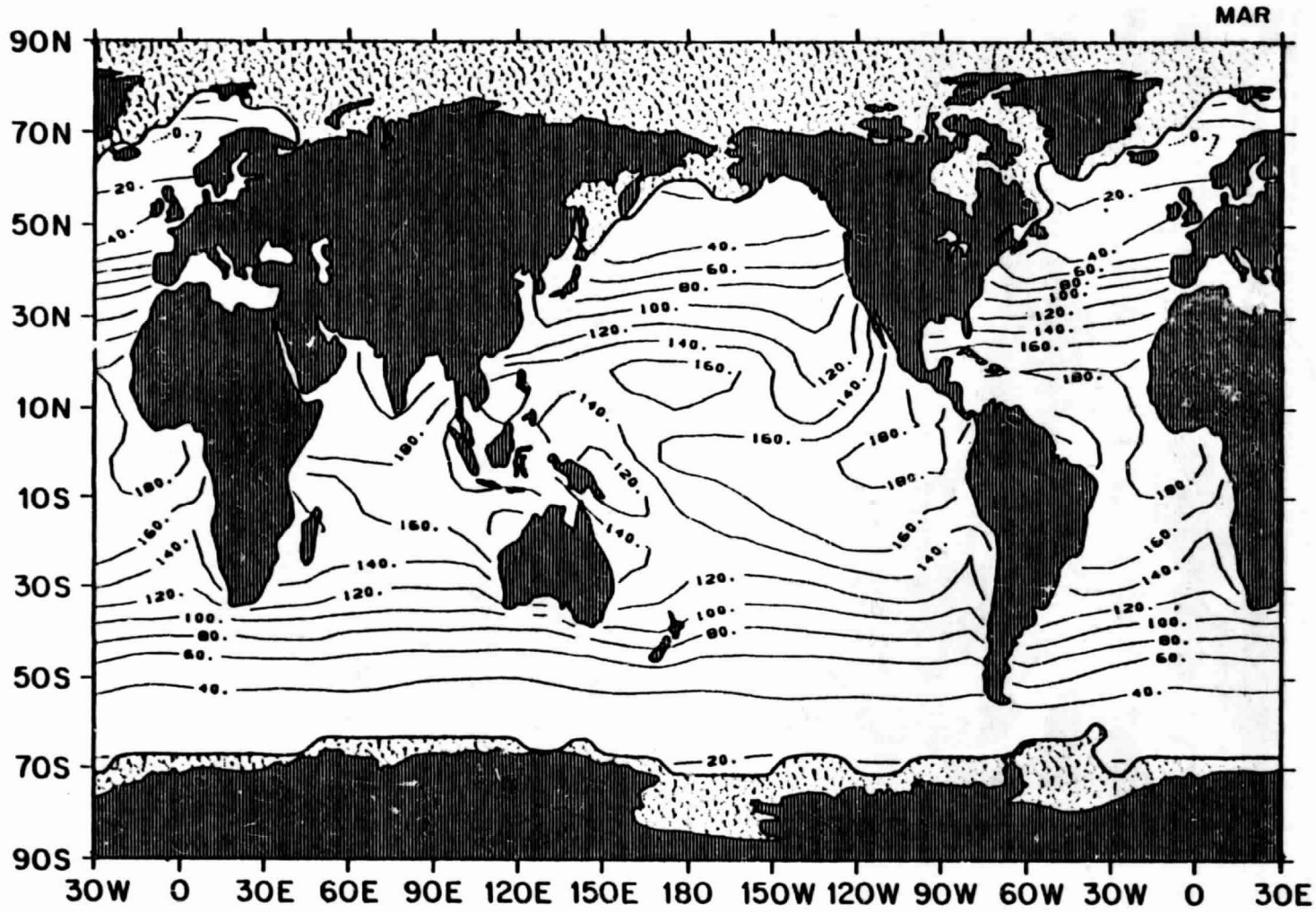

2.30 April mean net downward radiative flux (W m^{-2})

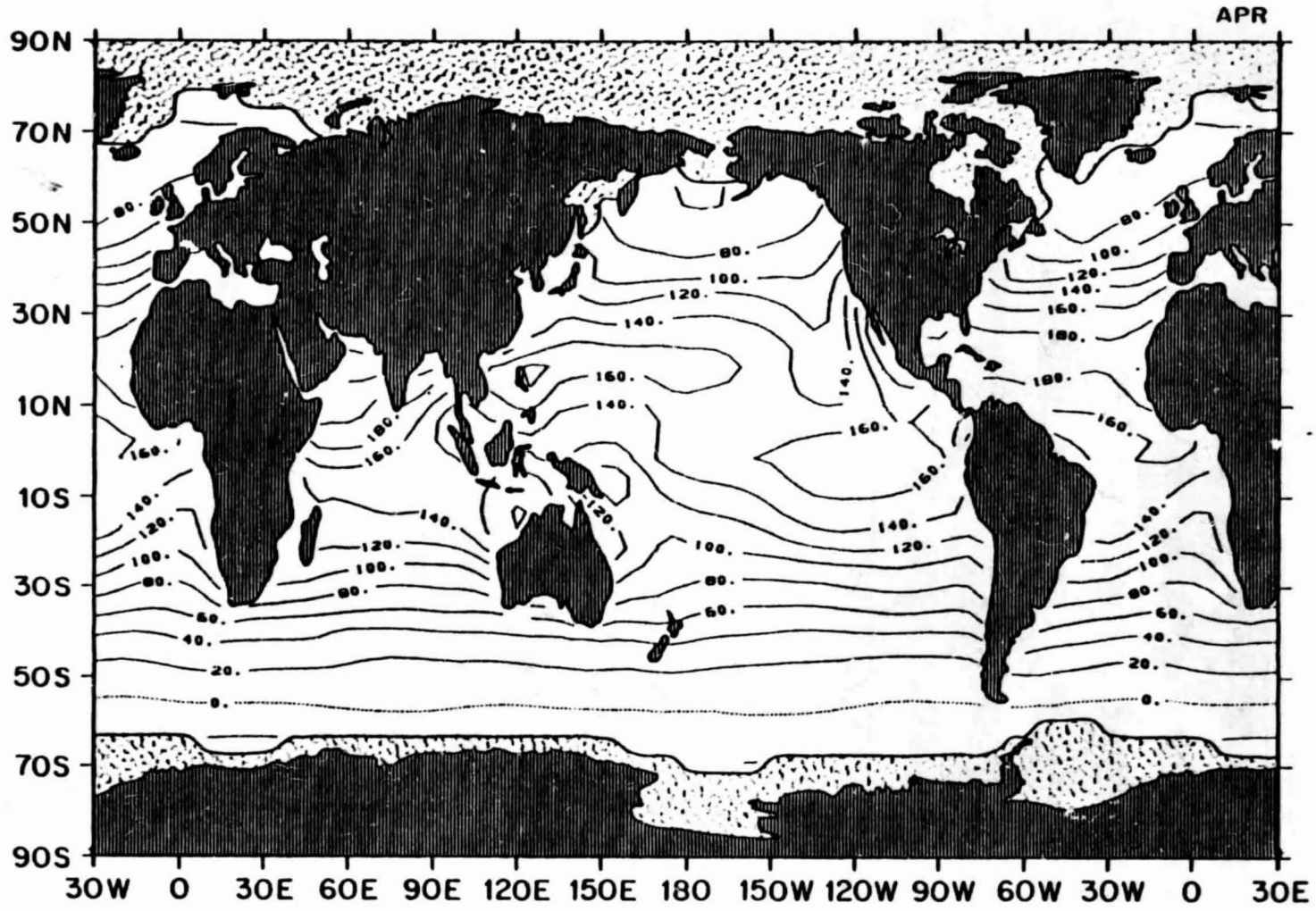

2.31 May mean net downward radiative flux (W m^{-2})

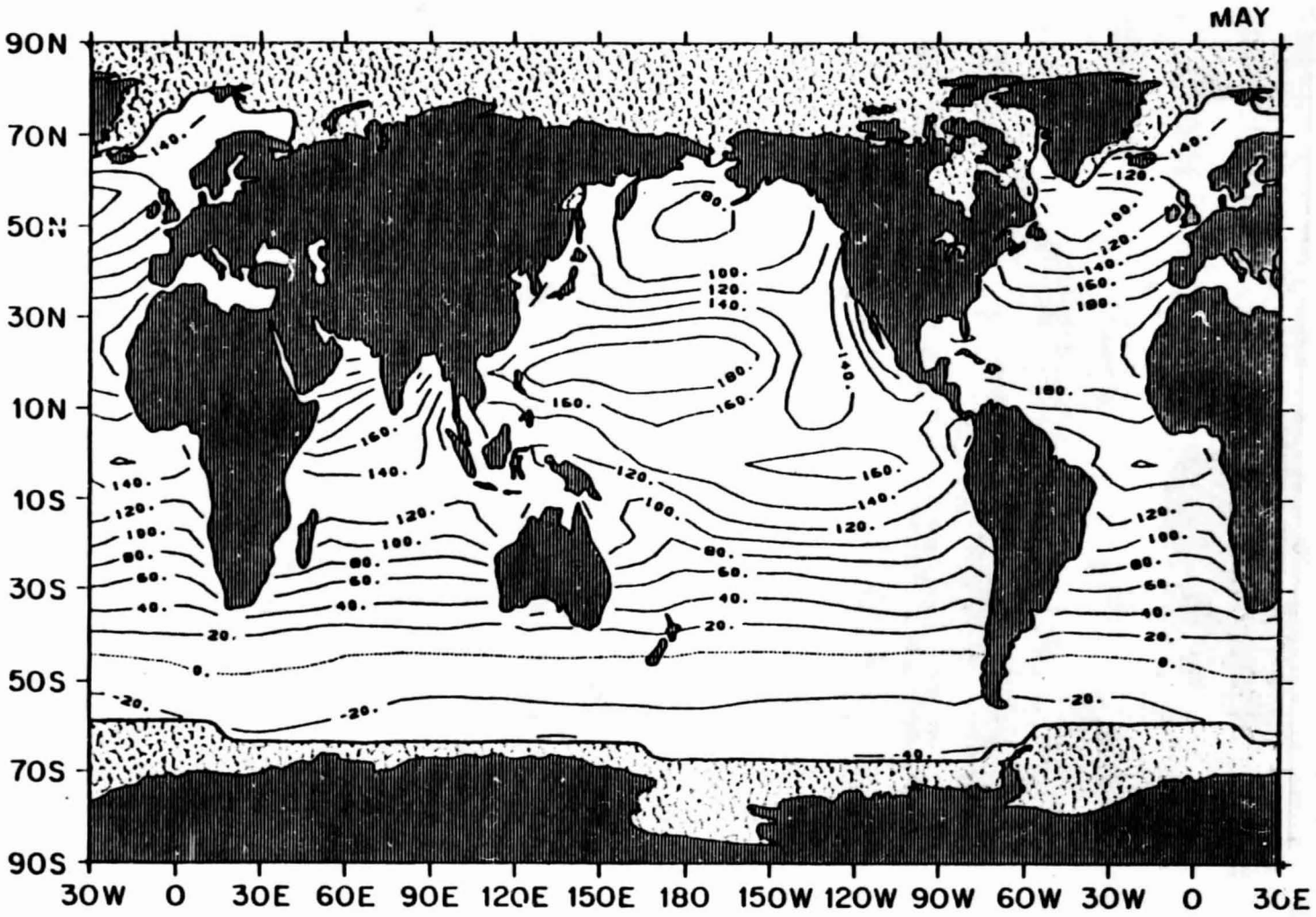

2.32 June mean net downward radiative flux (W m^{-2})

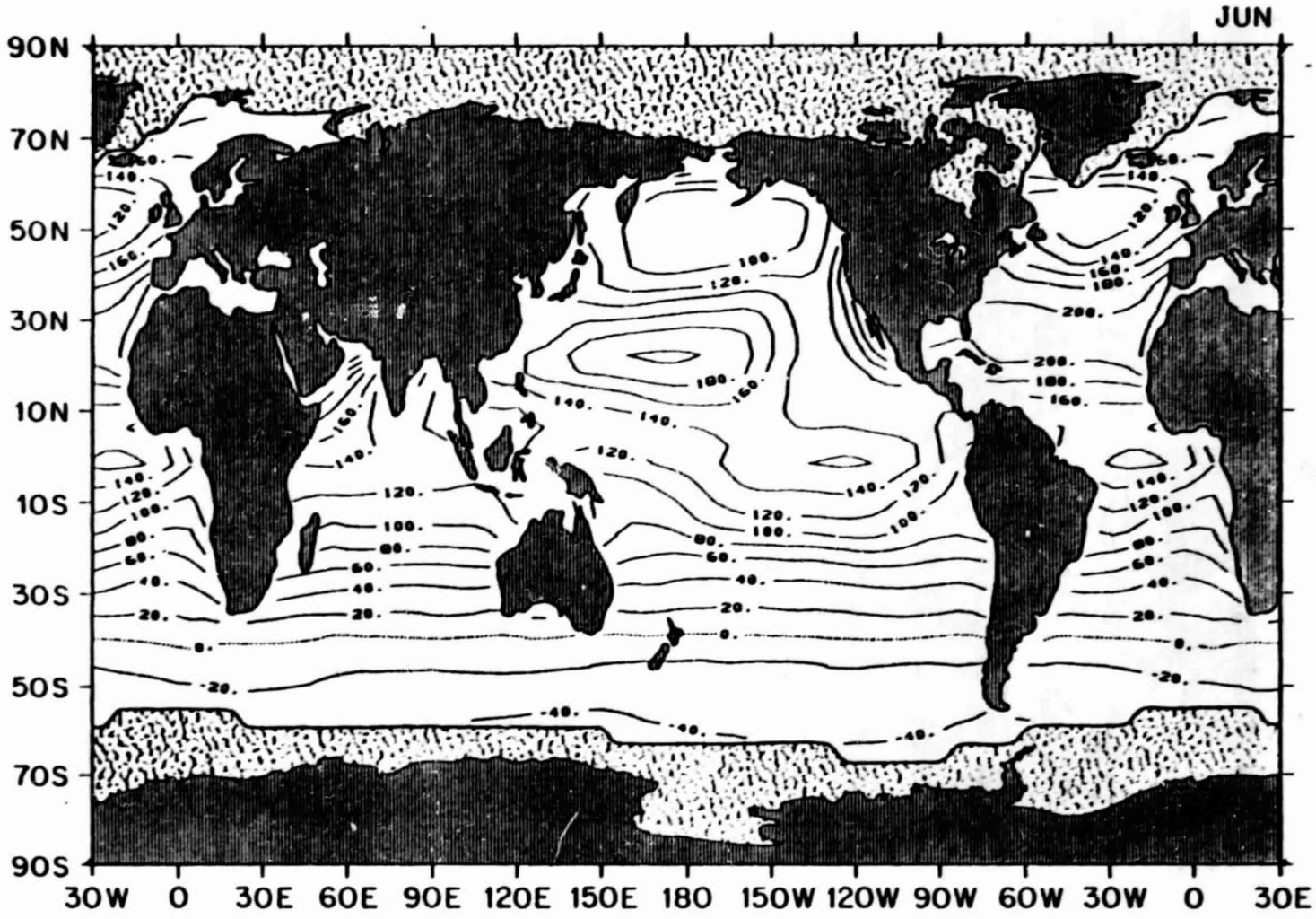

2.33 July mean net downward radiative flux (W m^{-2})

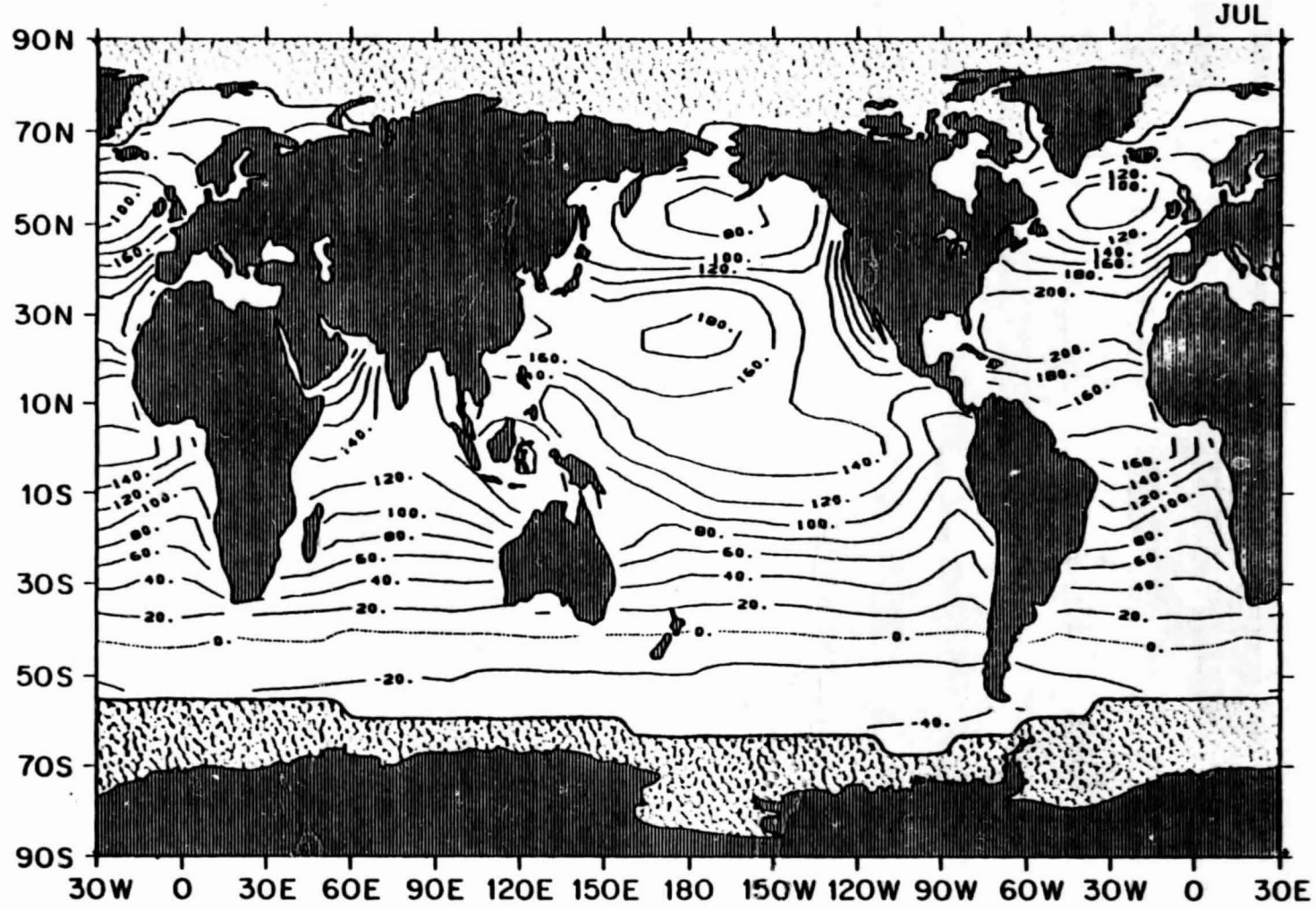

2.34 August mean net downward radiative flux (W m^{-2})

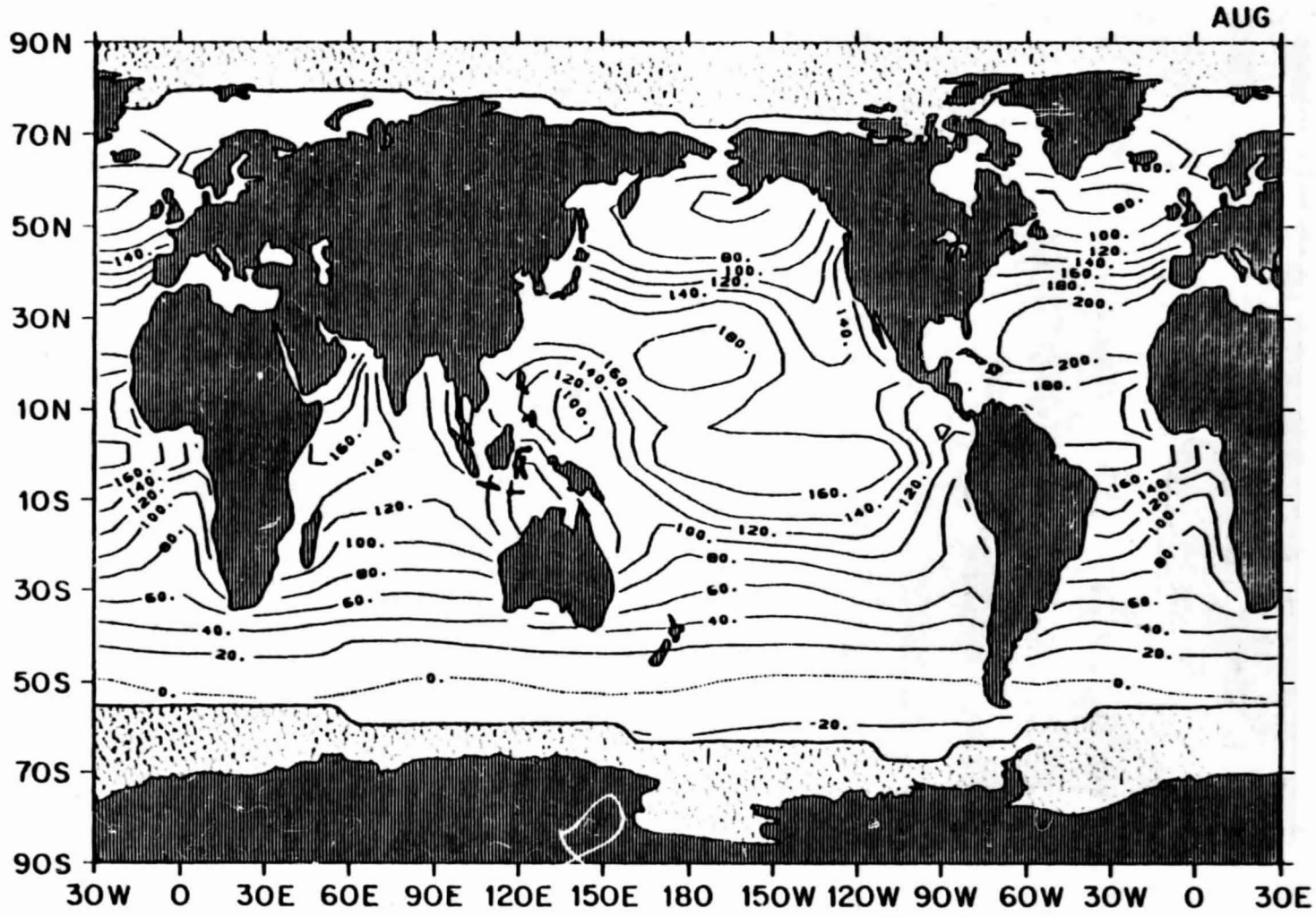

2.35 September mean net downward radiative flux (W m^{-2})

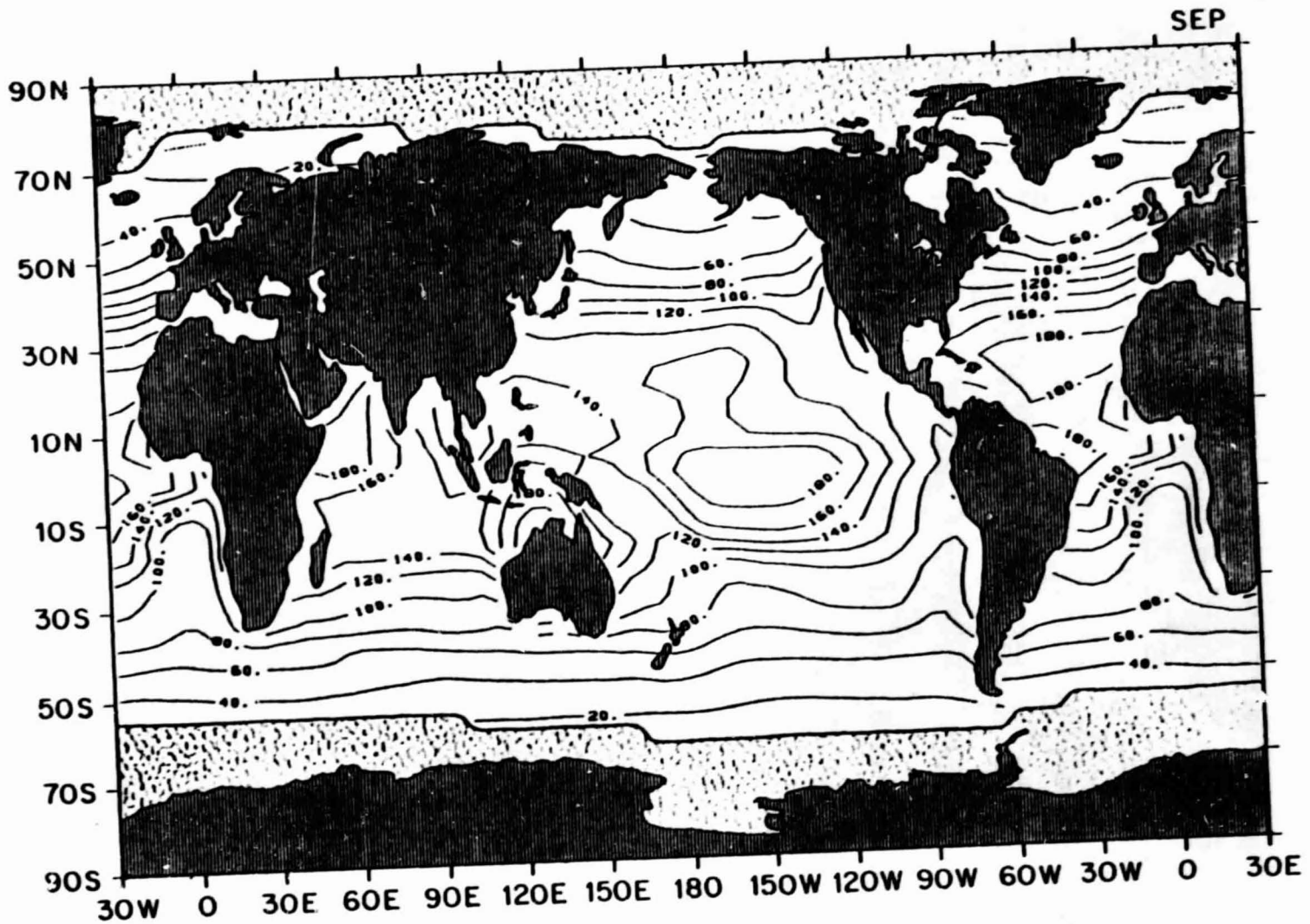

2.36 October mean net downward radiative flux (W m^{-2})

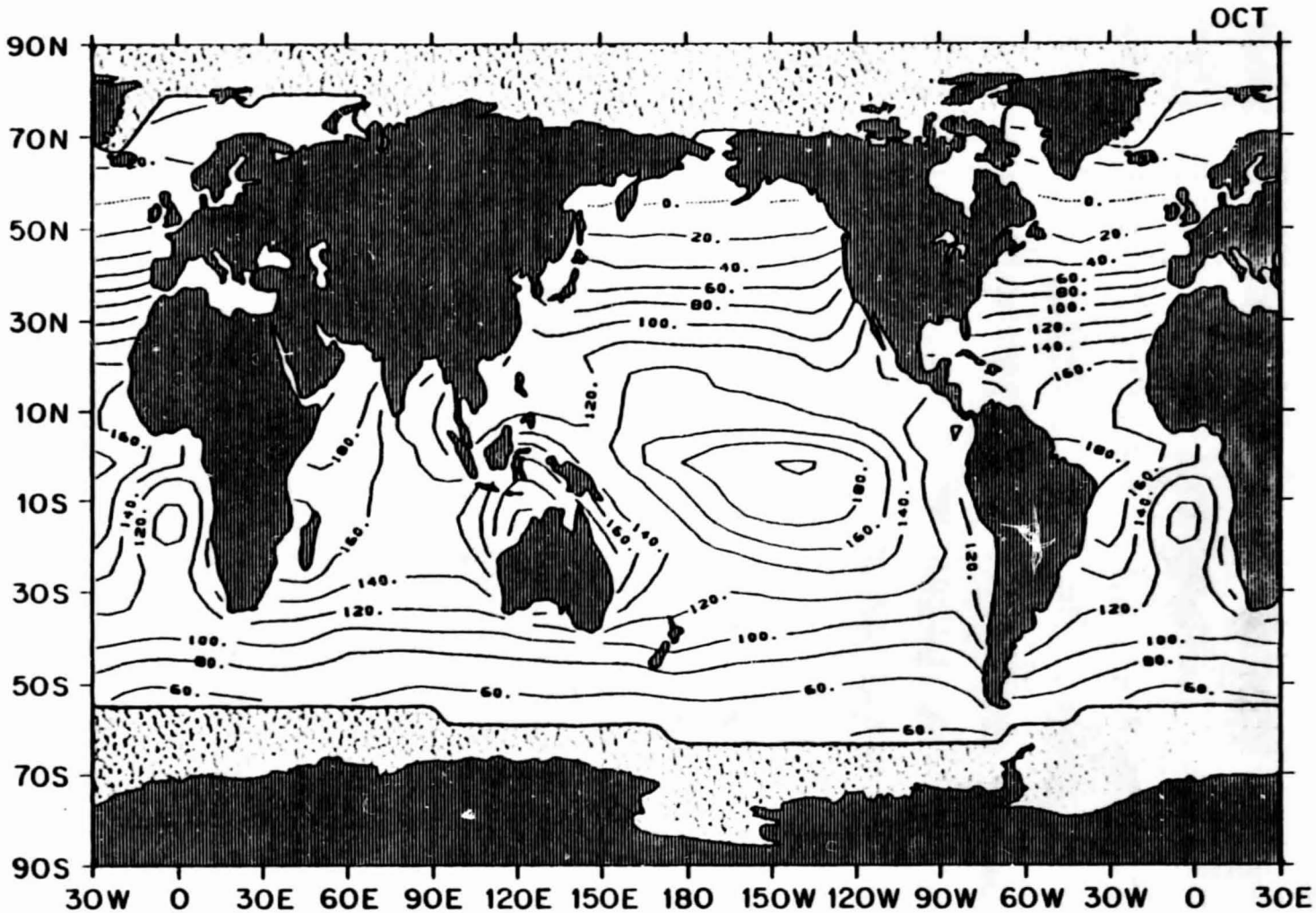

2.37 November mean net downward radiative flux (W m^{-2})

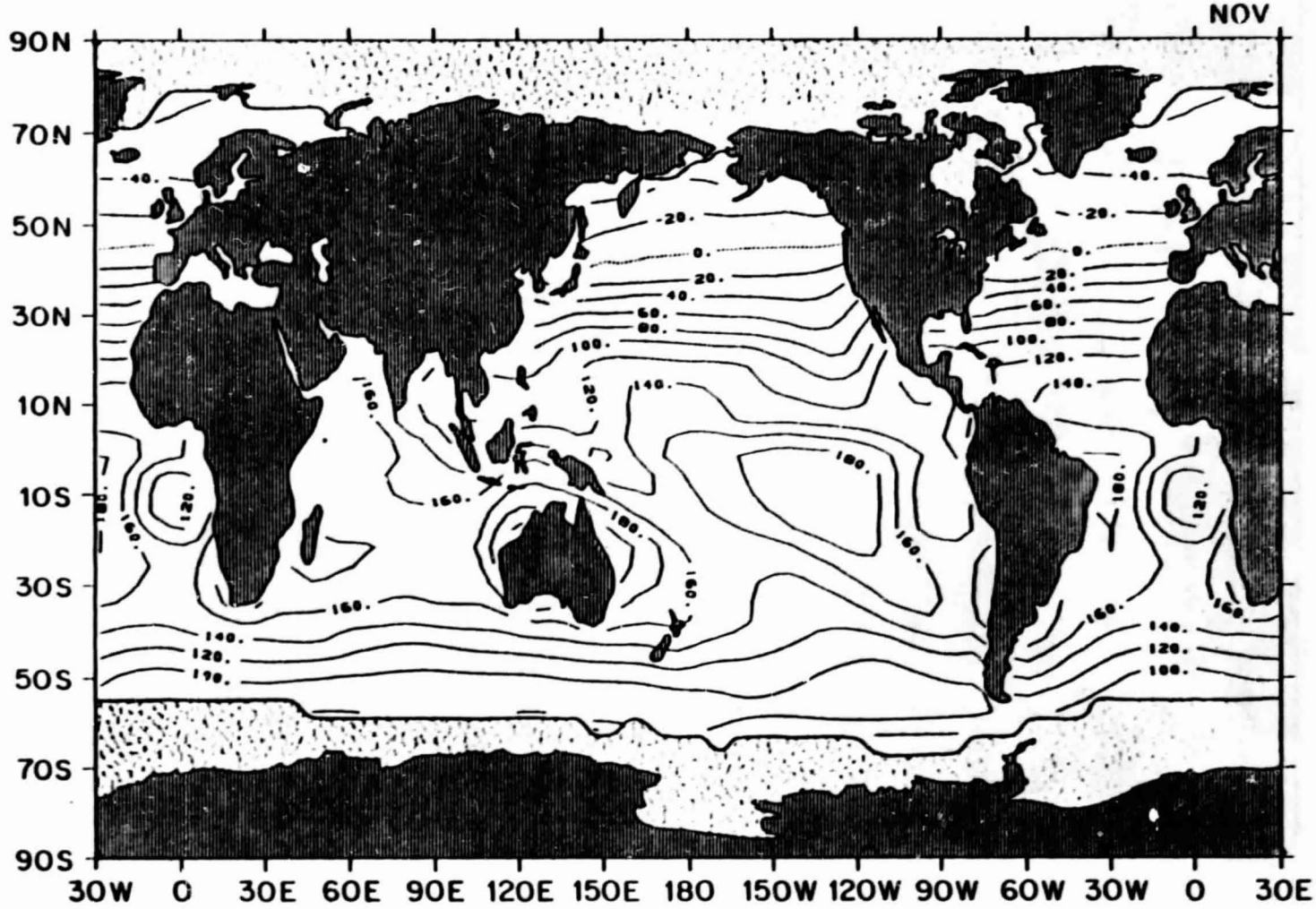

2.38 December mean net downward radiative flux (W m^{-2})

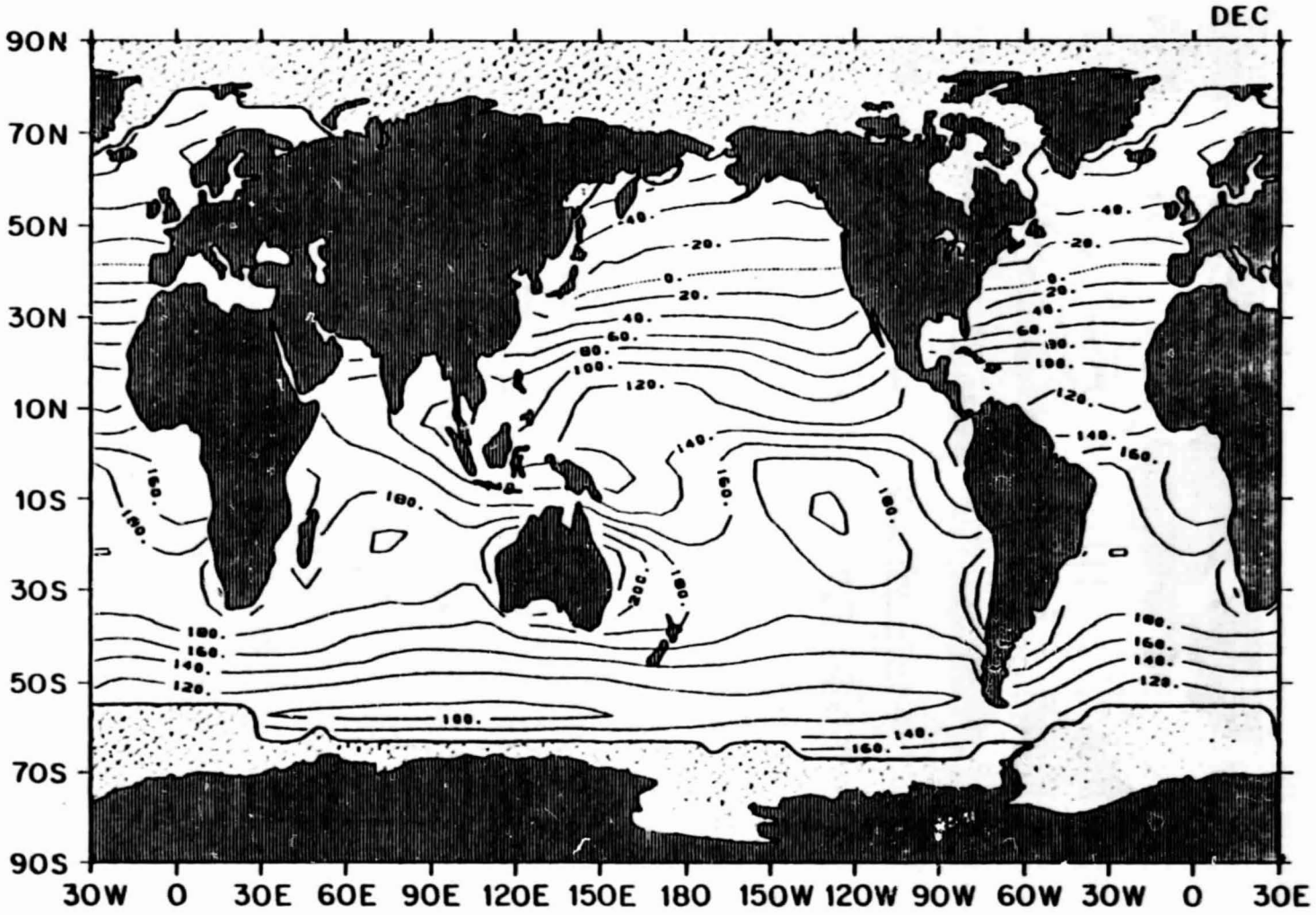

2.39 Annual mean net downward radiative flux (W m^{-2})

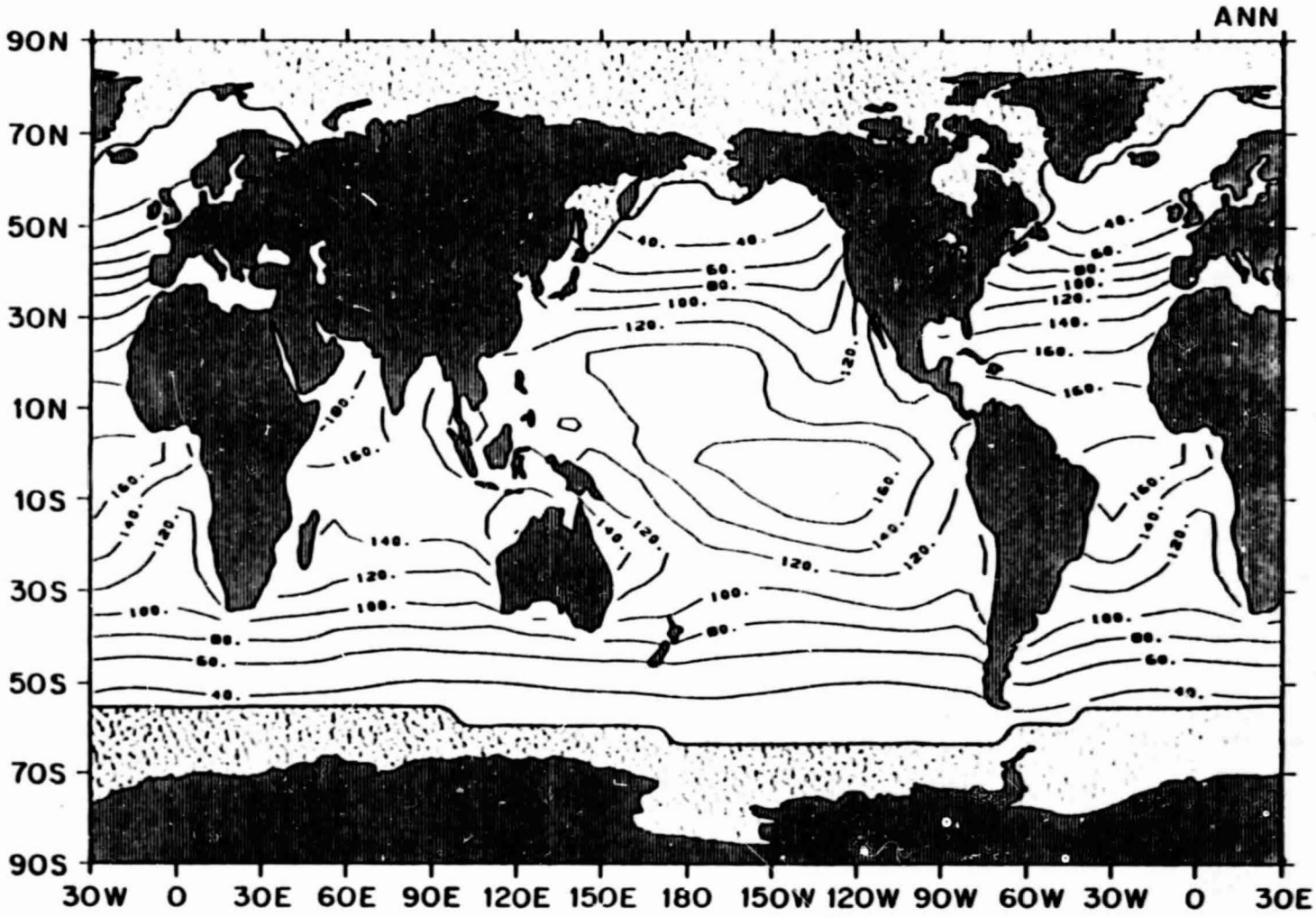

LATENT HEAT FLUX

2.40 January mean latent heat flux (W m^{-2})

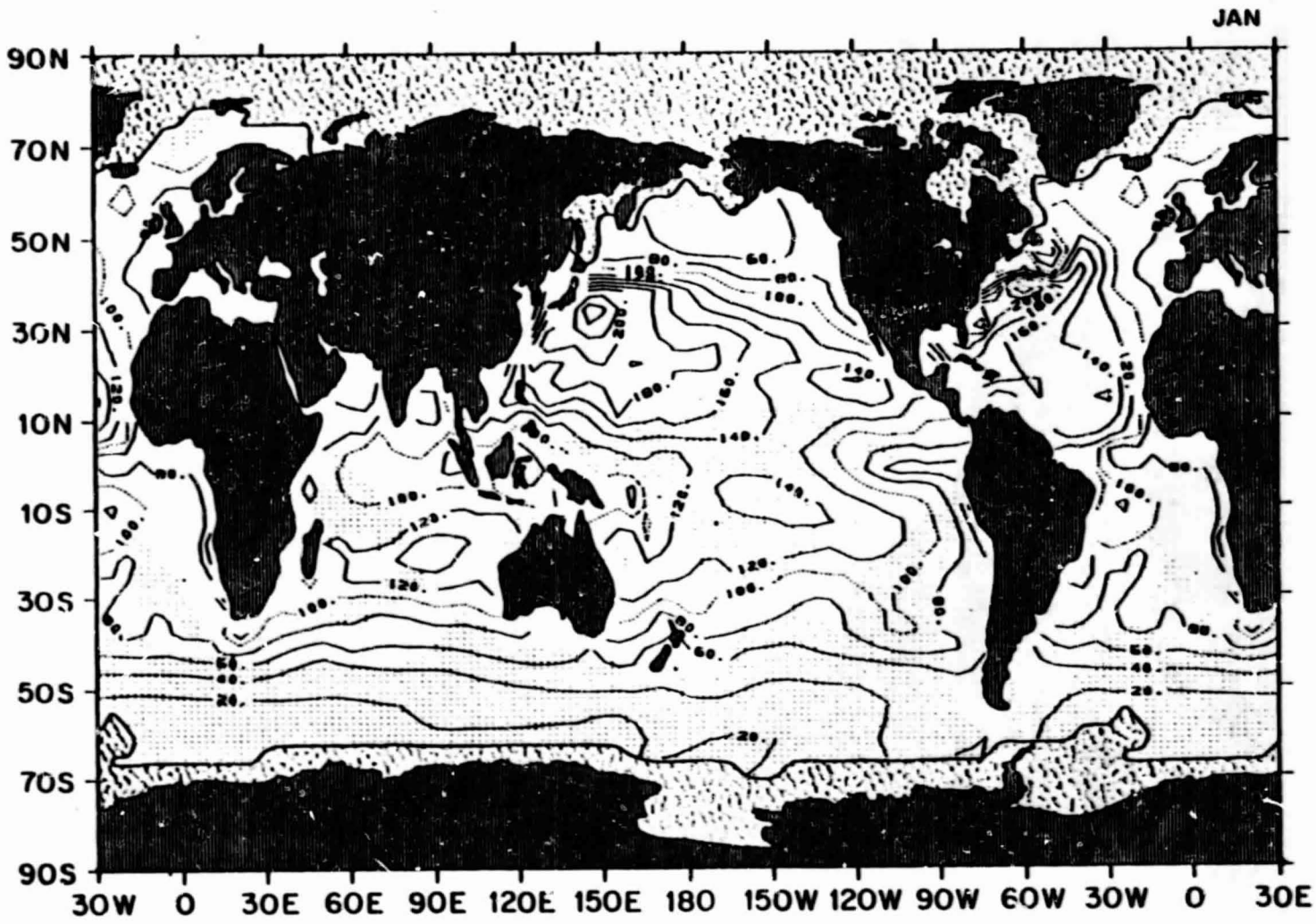

2.41 February mean latent heat flux (W m^{-2})

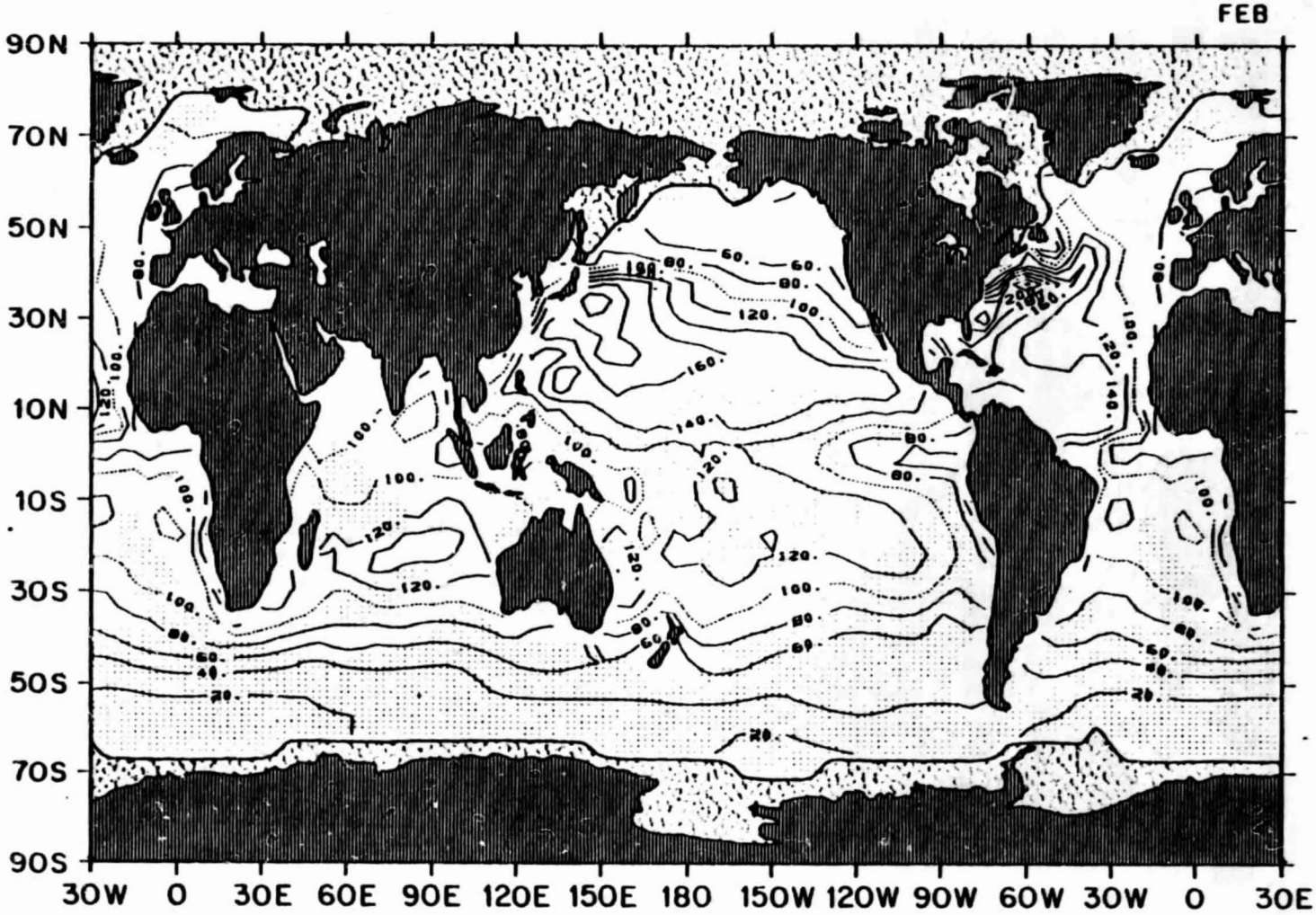

2.42 March mean latent heat flux (W m^{-2})

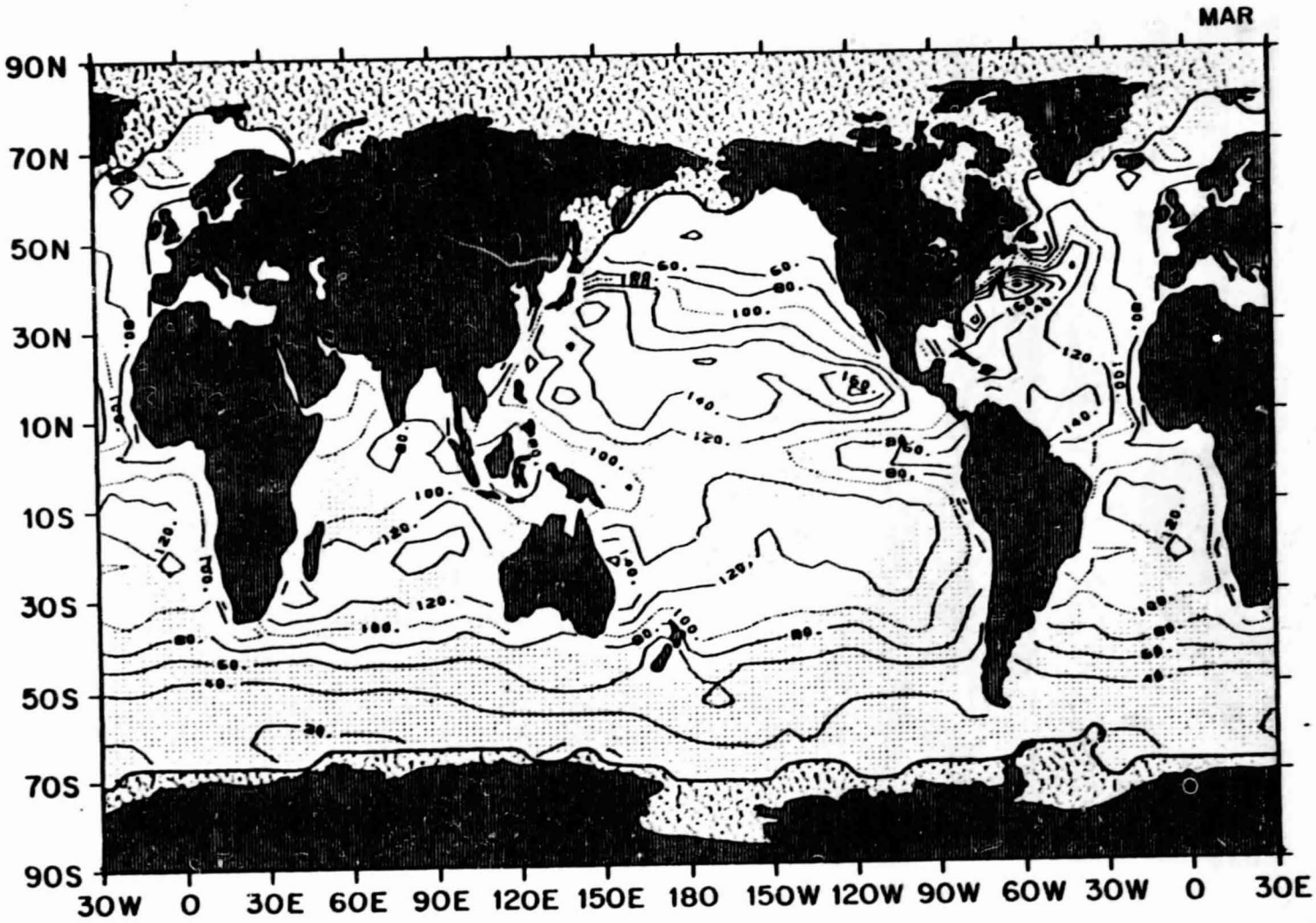

2.43 April mean latent heat flux (W m^{-2})

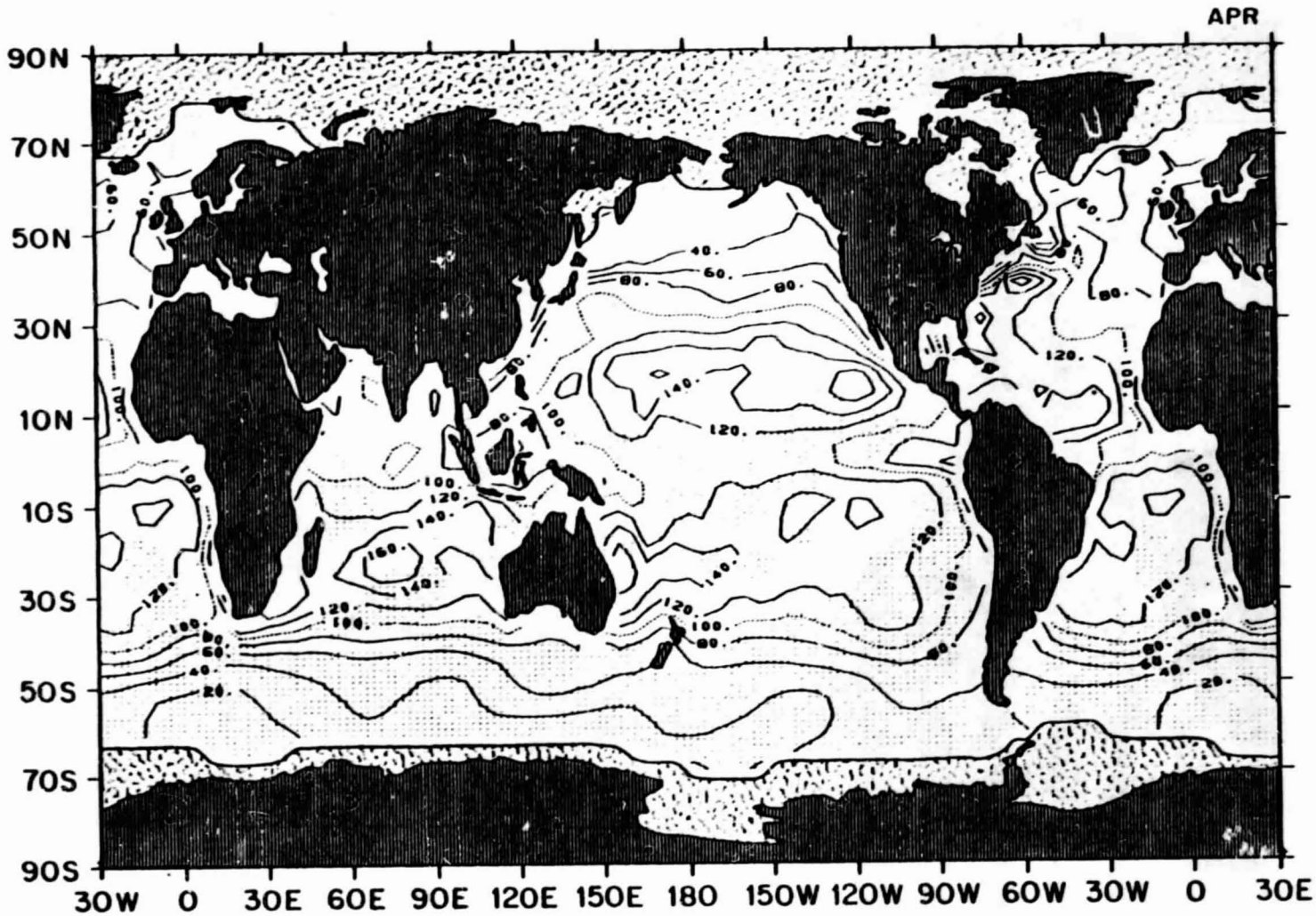

2.44 May mean latent heat flux (W m^{-2})

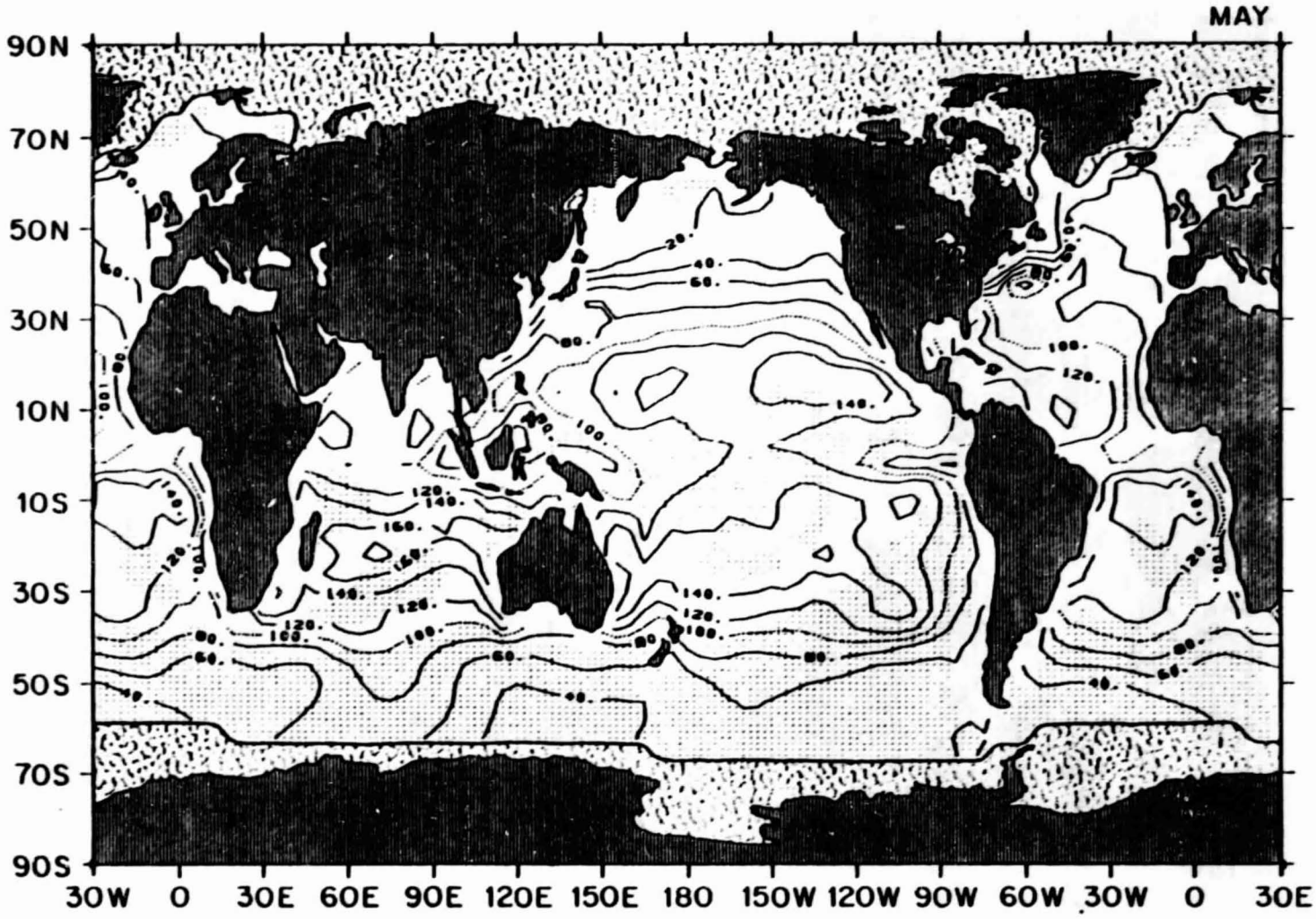

2.45 June mean latent heat flux (W m^{-2})

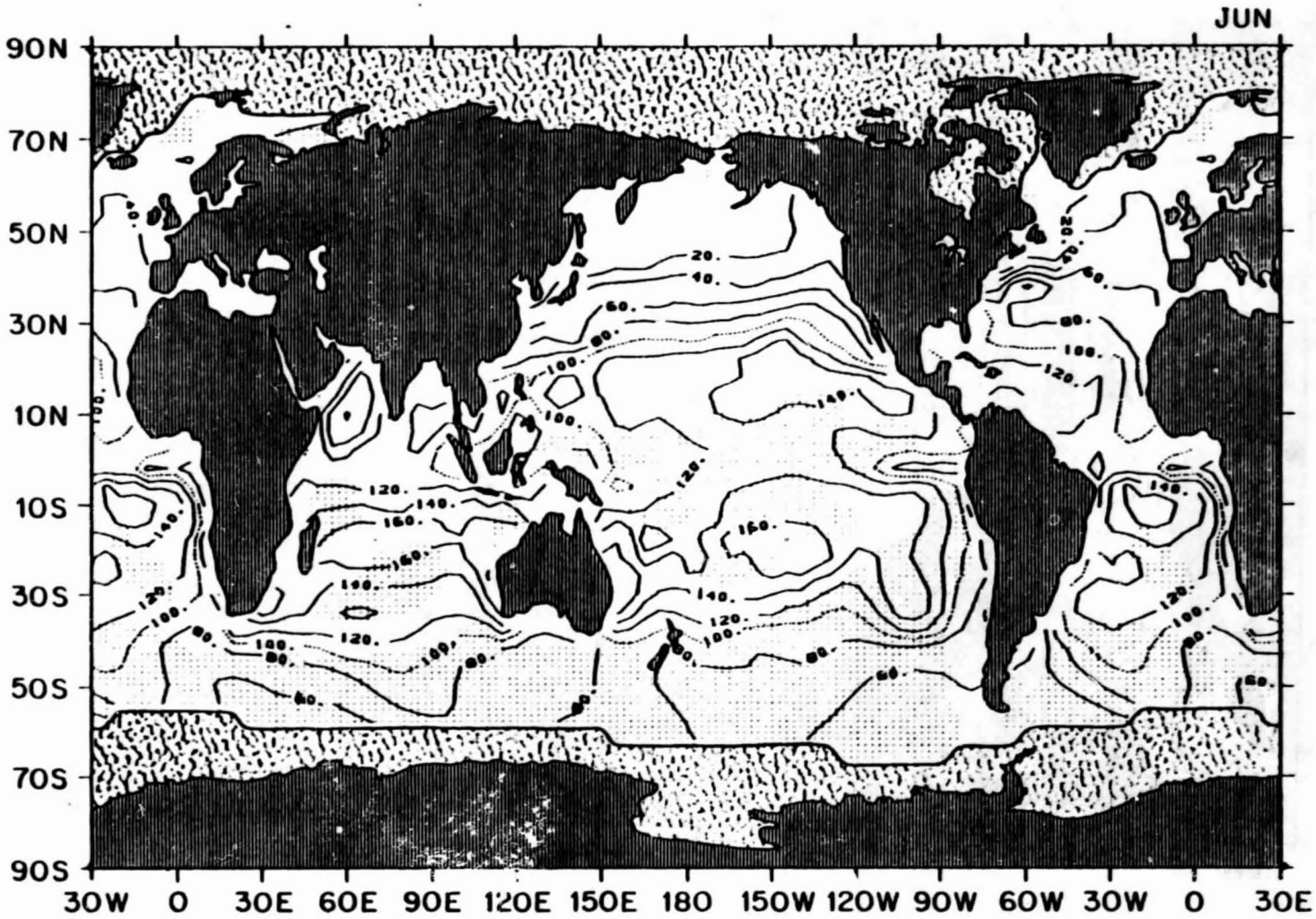

2.46 July mean latent heat flux (W m^{-2})

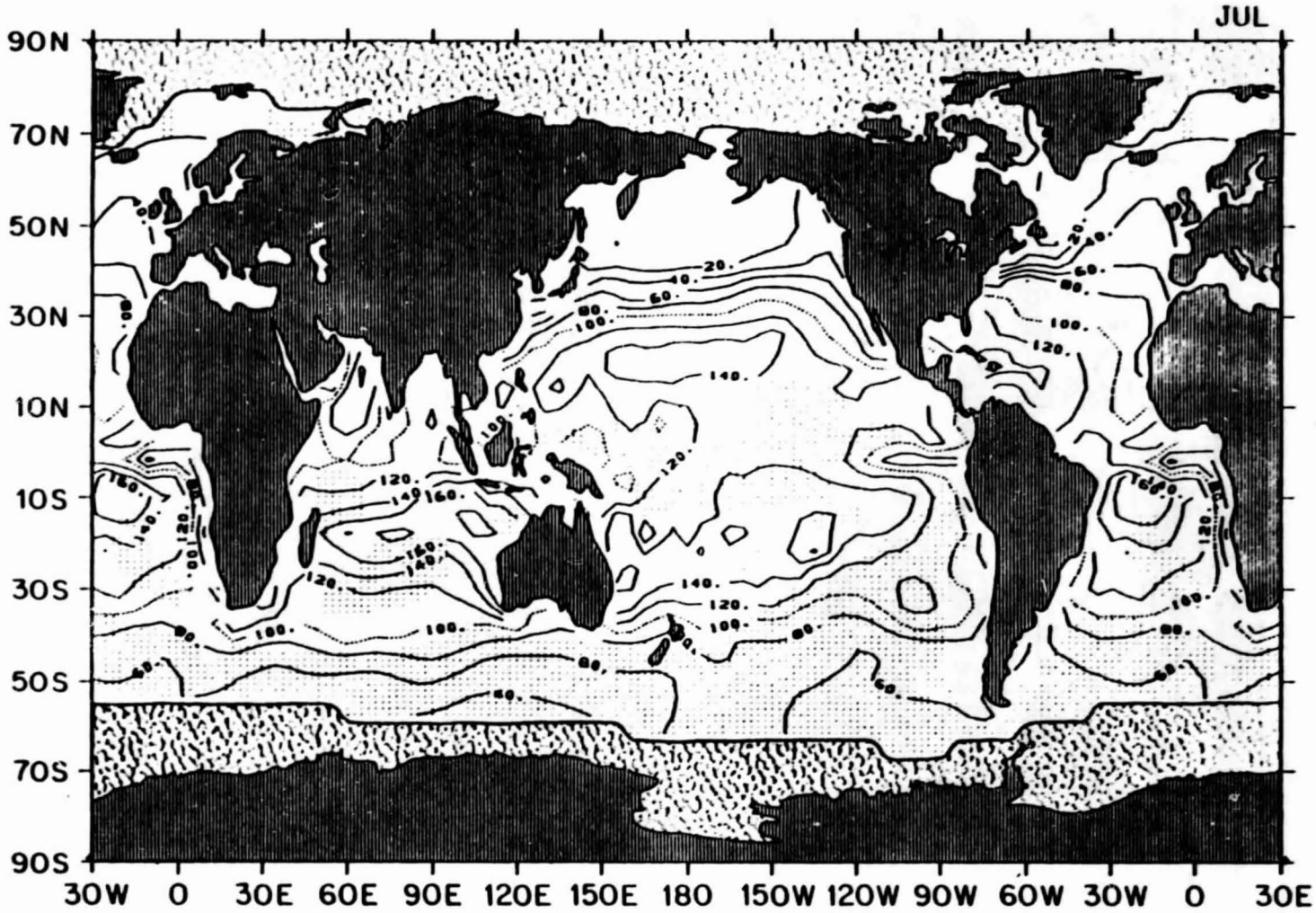

2.47 August mean latent heat flux (W m^{-2})

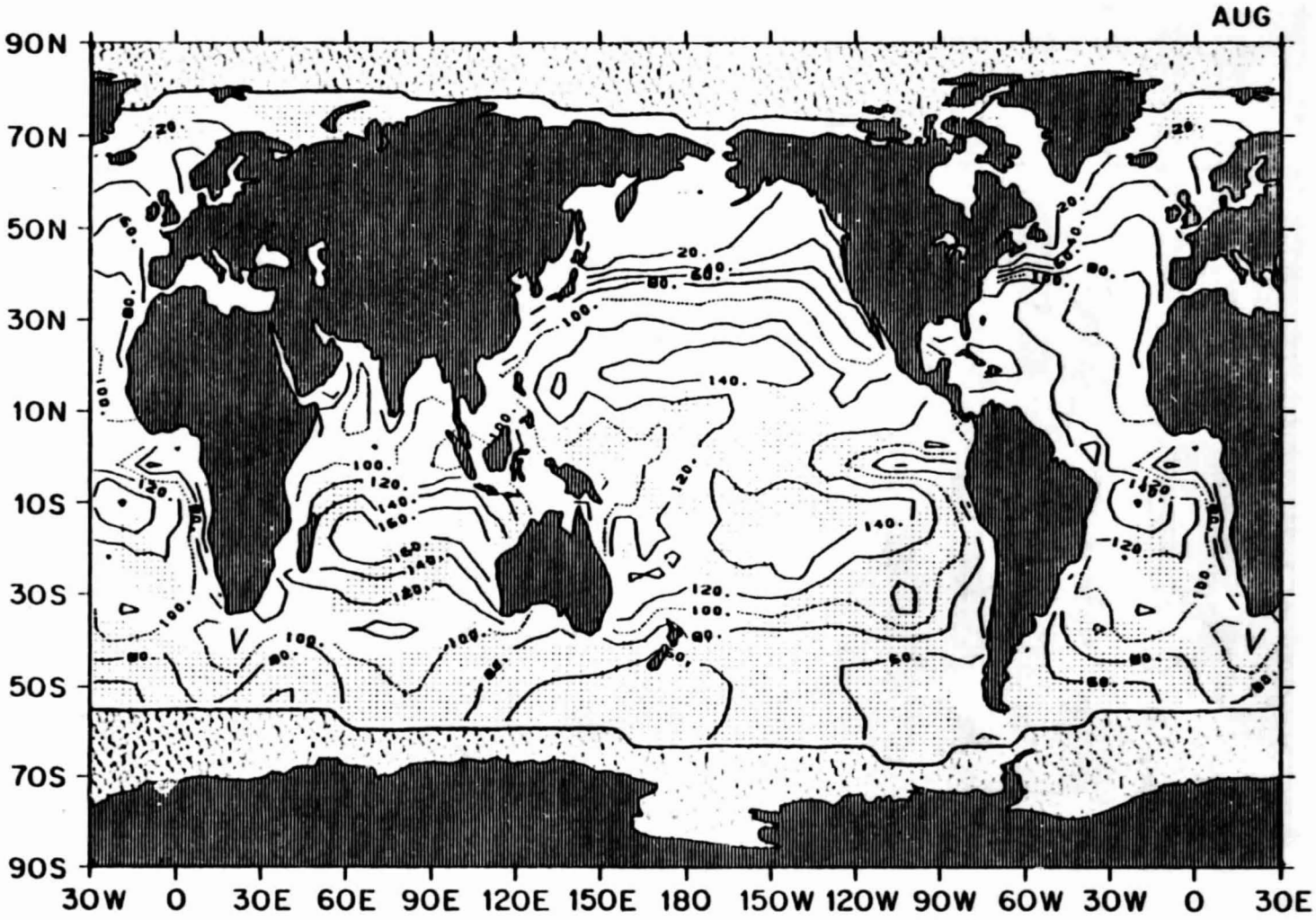

2.48 September mean latent heat flux (W m^{-2})

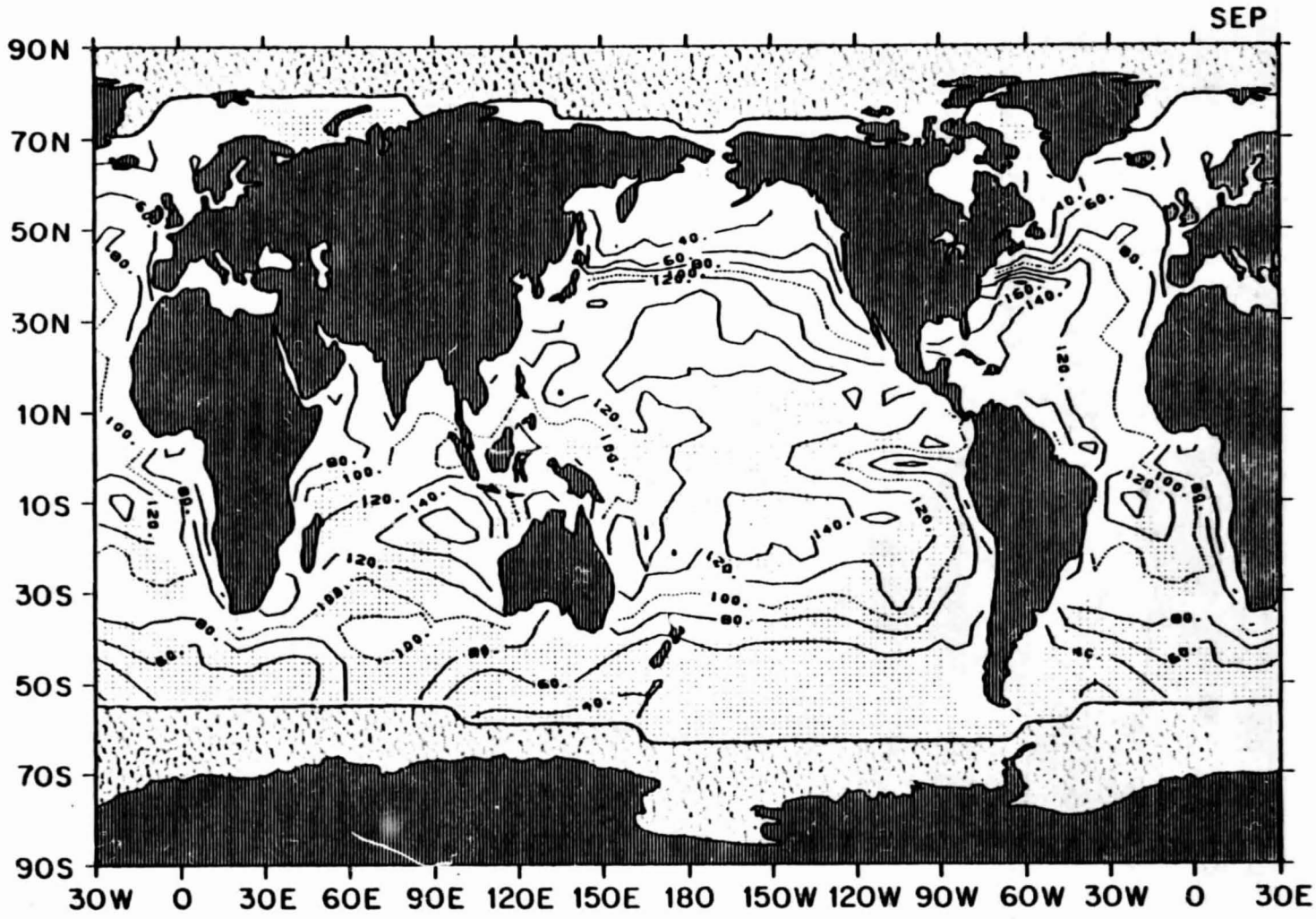

2.49 October mean latent heat flux (W m^{-2})

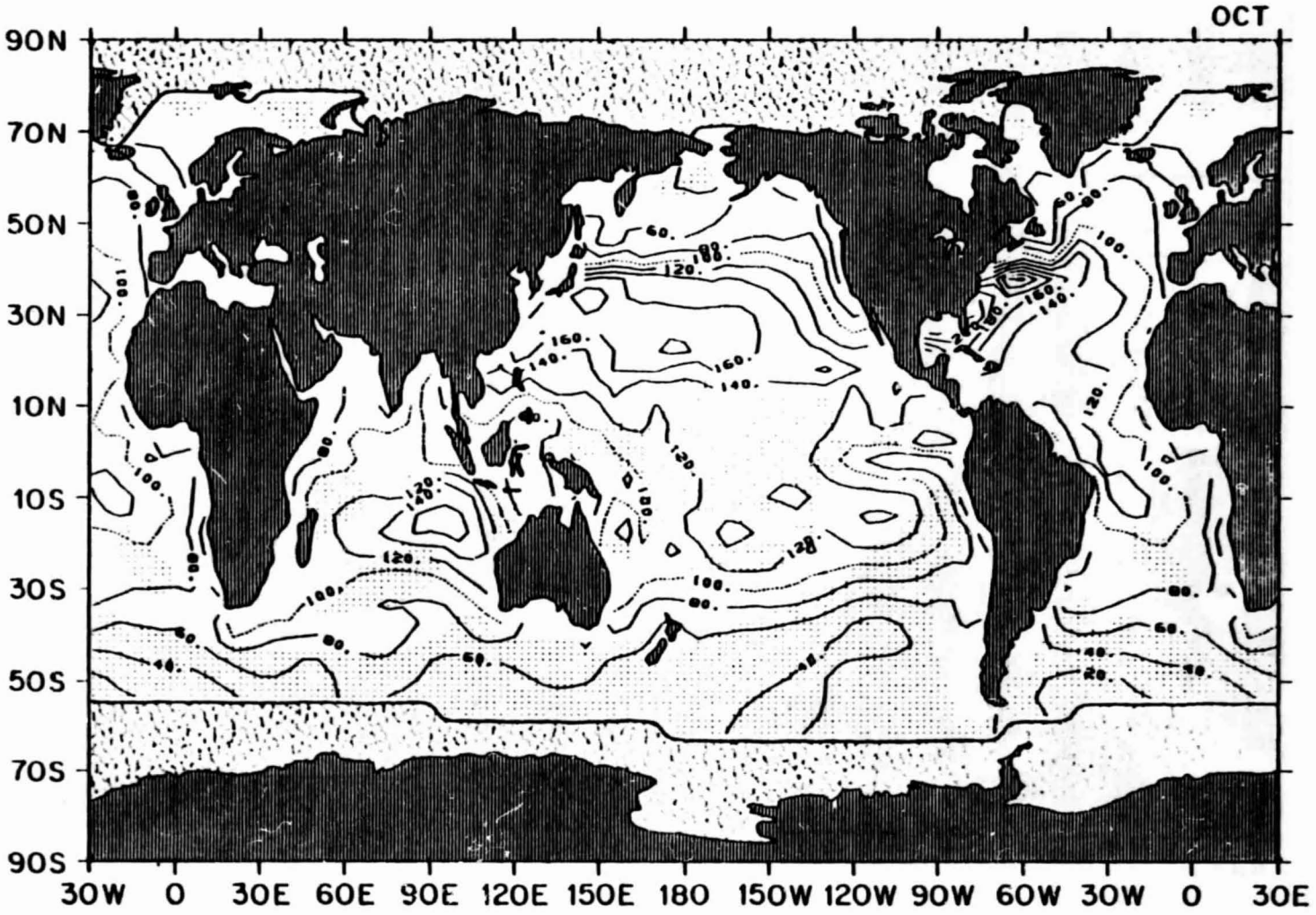

2.50 November mean latent heat flux (W m^{-2})

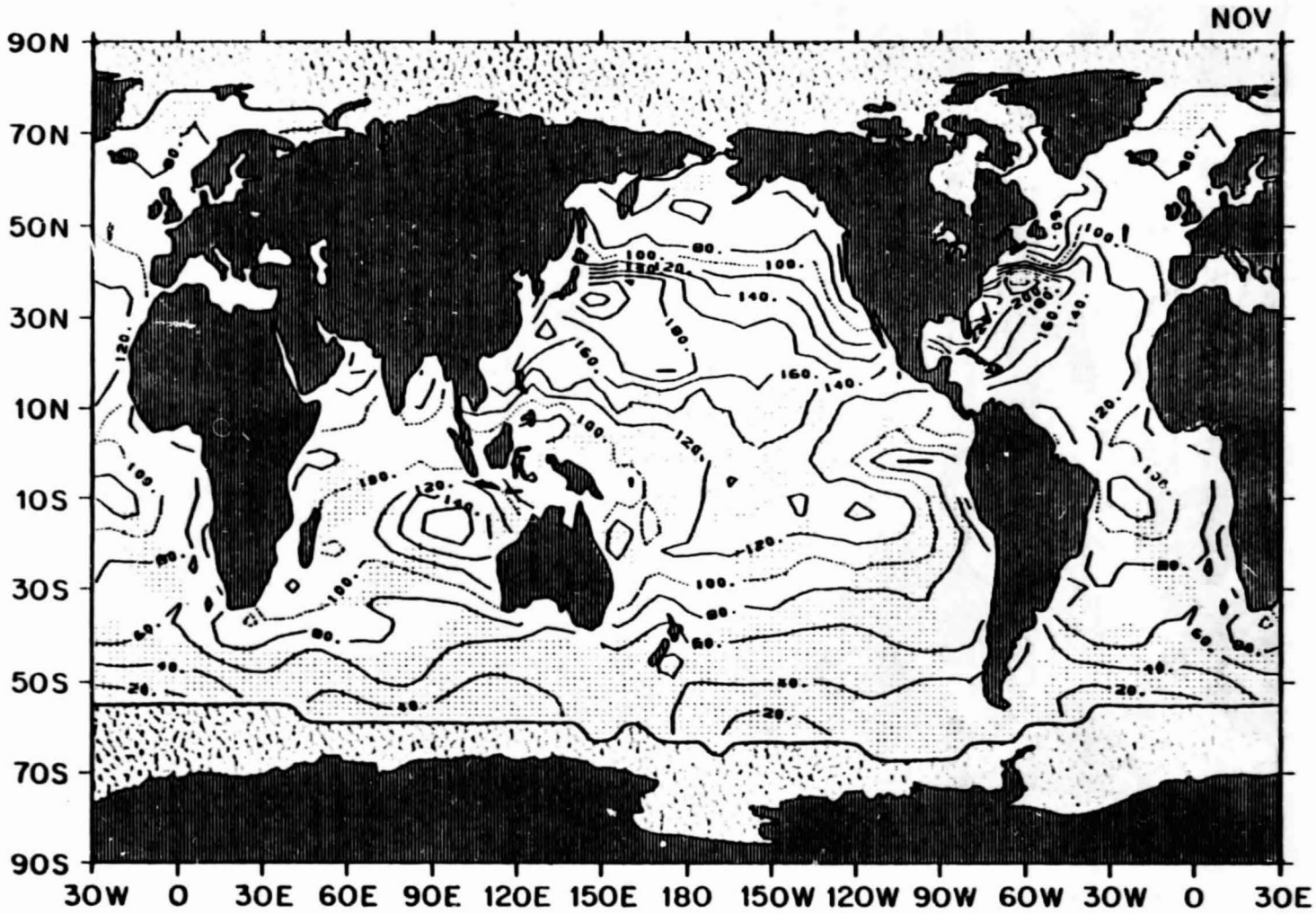

2.51 December mean latent heat flux (W m^{-2})

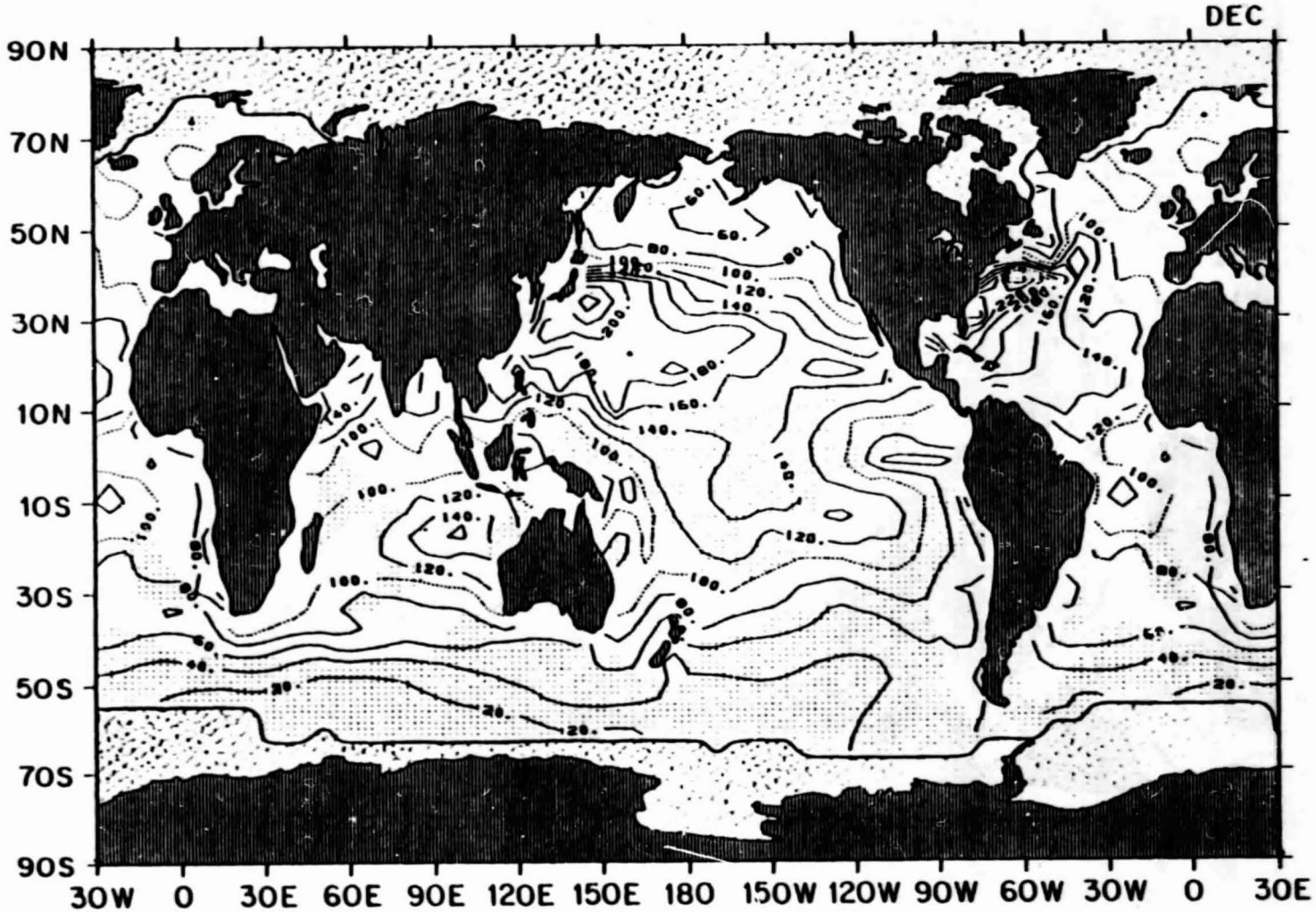

2.52 Annual mean latent heat flux (W m-2)

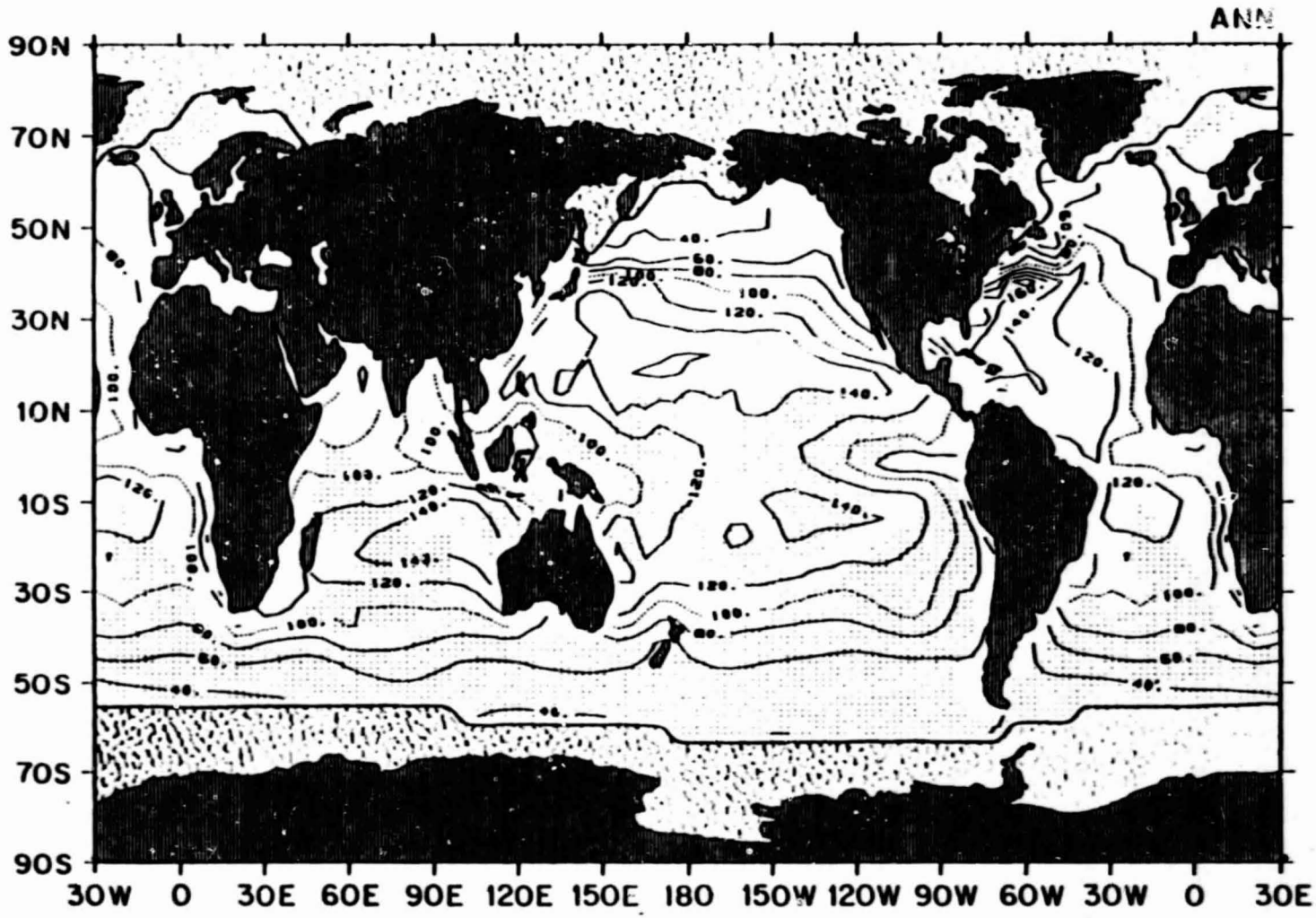

SENSIBLE HEAT FLUX

2.53 January mean sensible heat flux (W m^{-2})

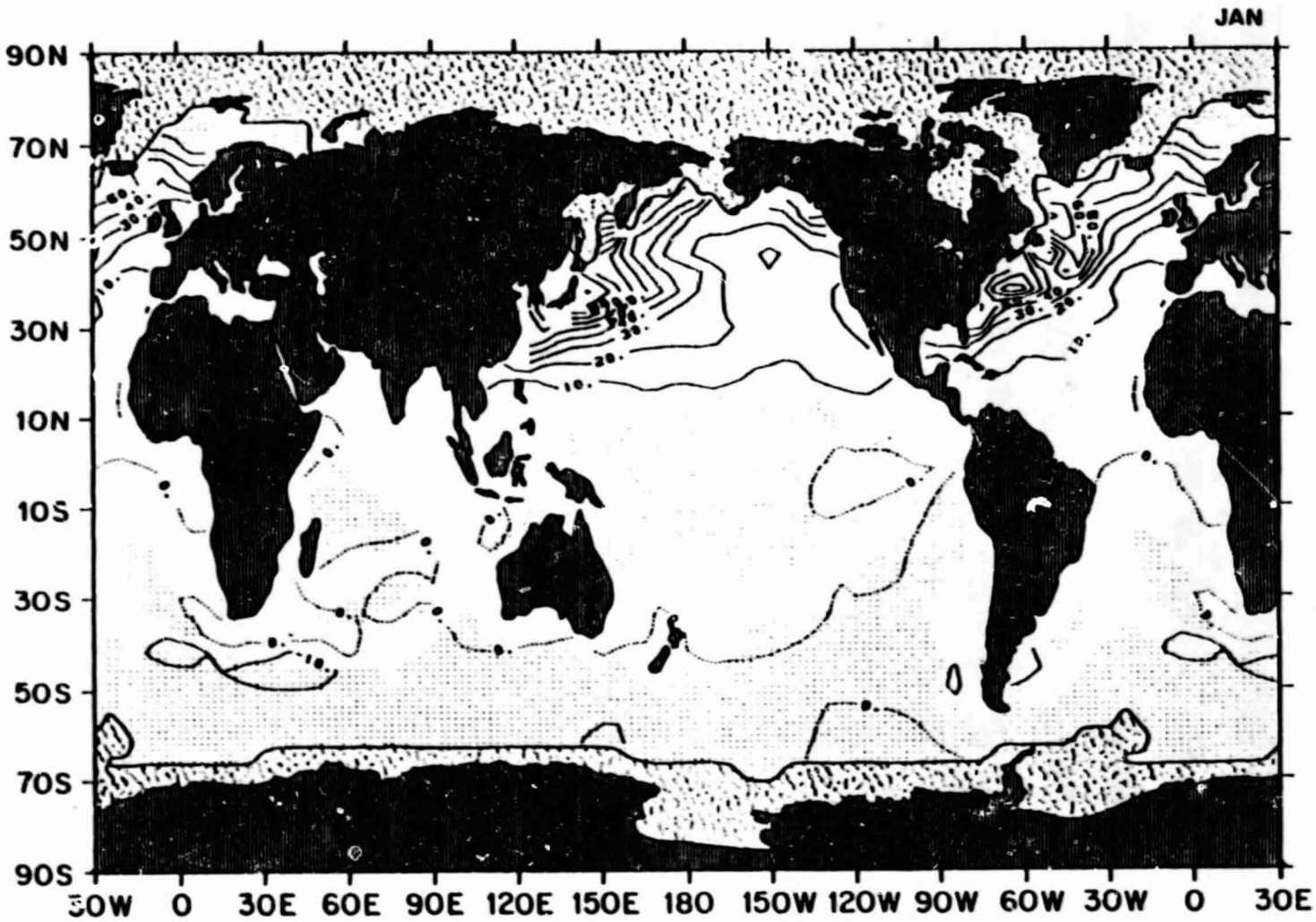

2.54 February mean sensible heat flux (W m^{-2})

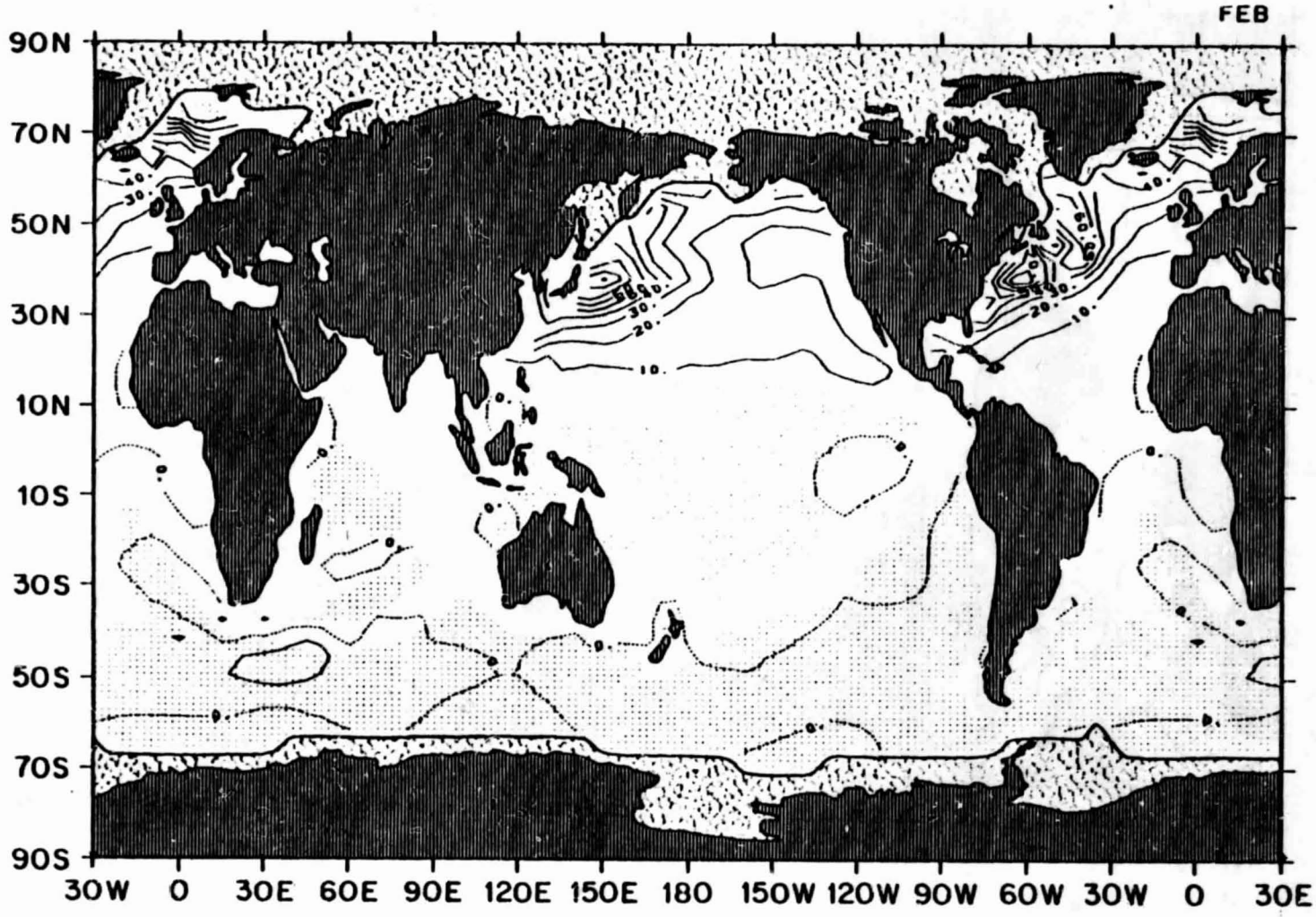

2.55 March mean sensible heat flux (W m^{-2})

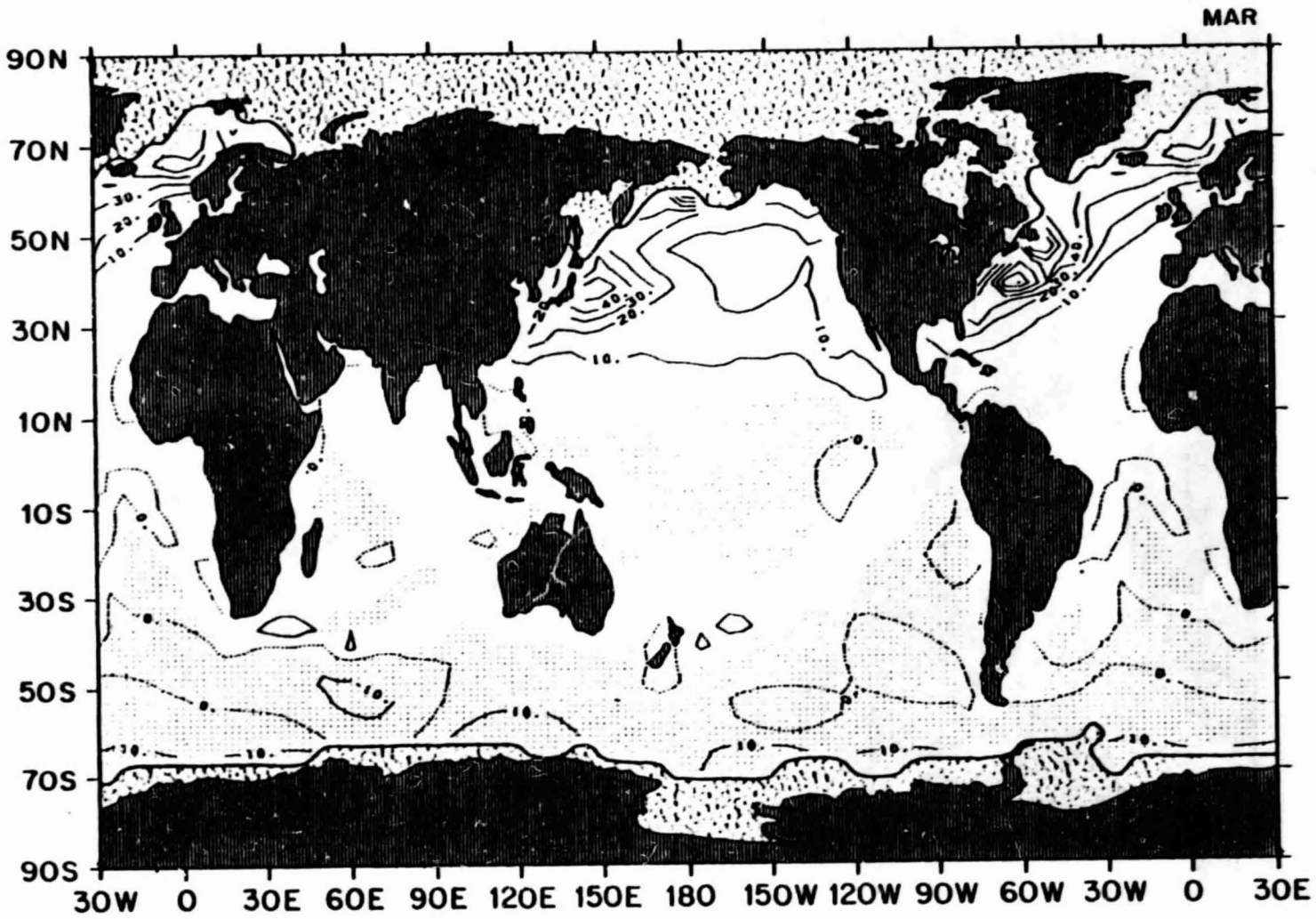

2.56 April mean sensible heat flux (W m^{-2})

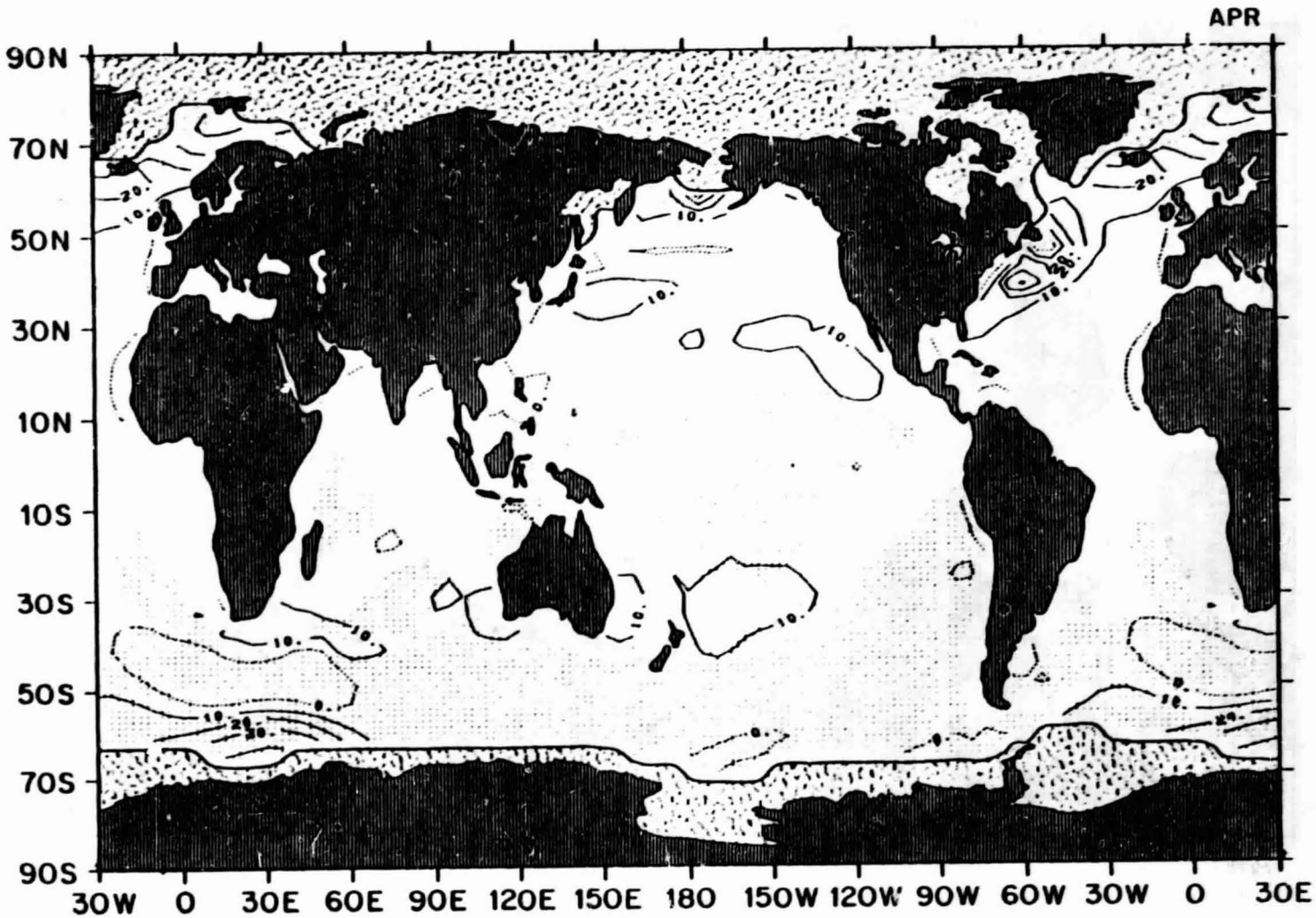

2.57 May mean sensible heat flux (W m^{-2})

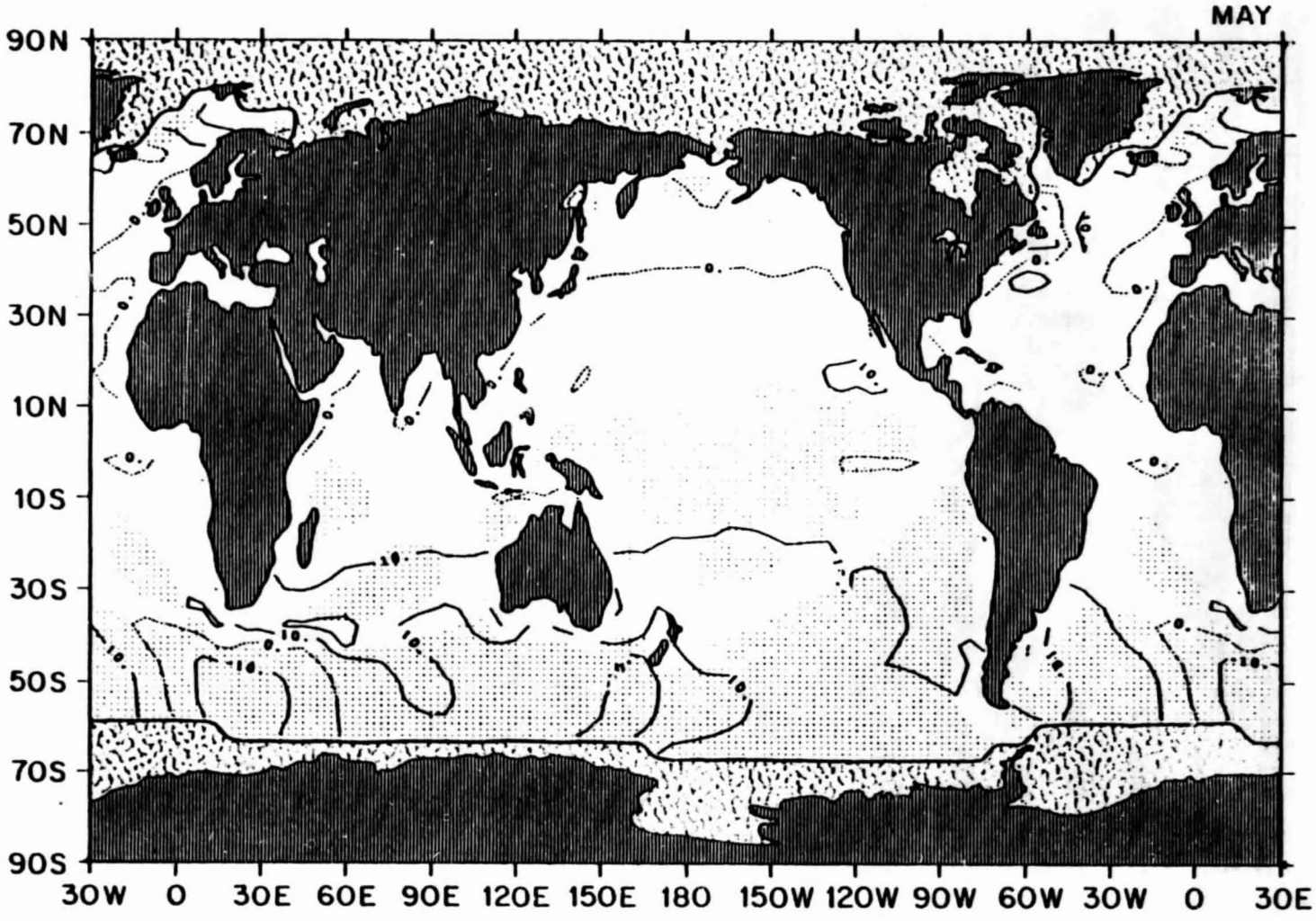

2.58 June mean sensible heat flux (W m^{-2})

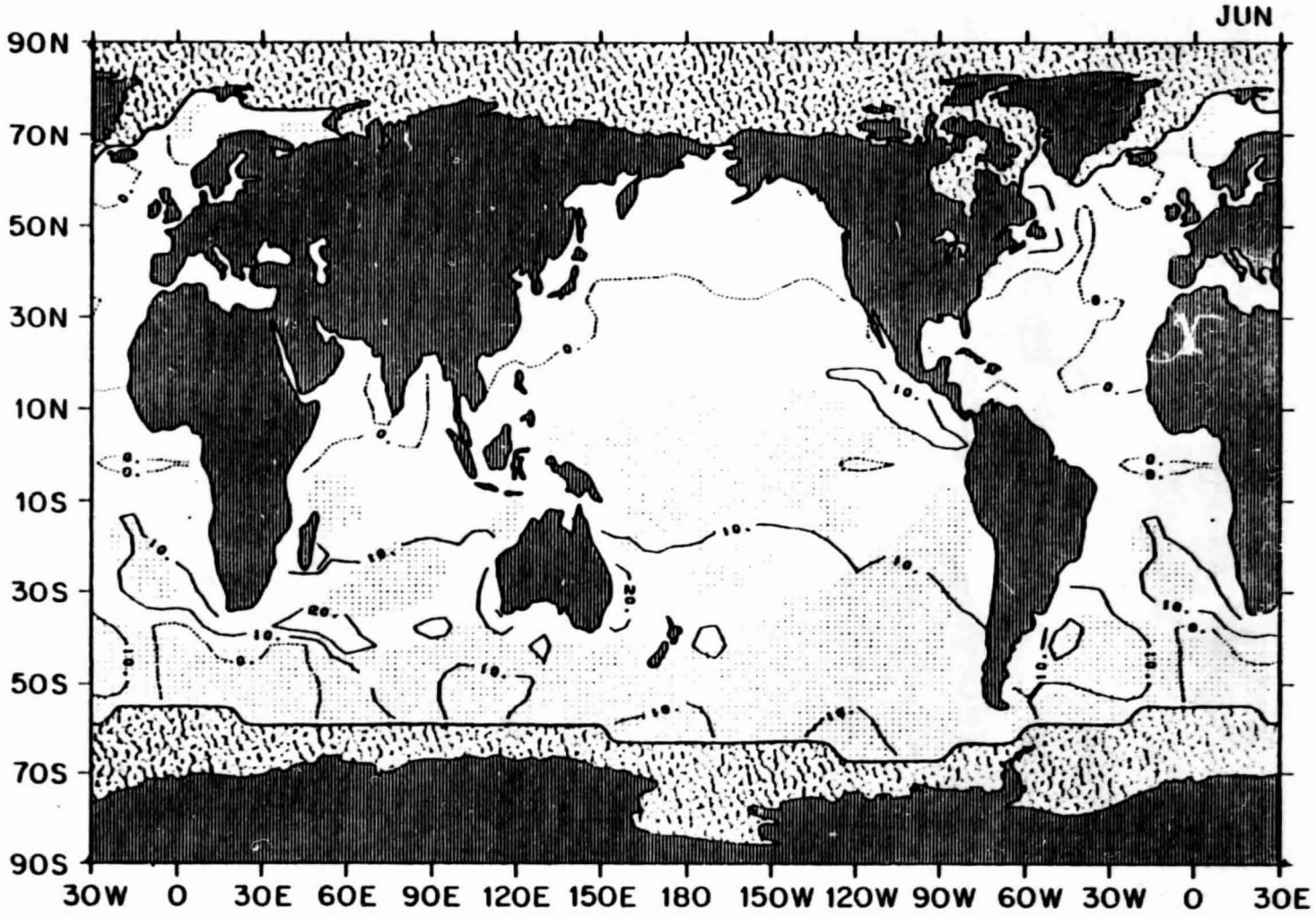

2.59 July mean sensible heat flux (W m^{-2})

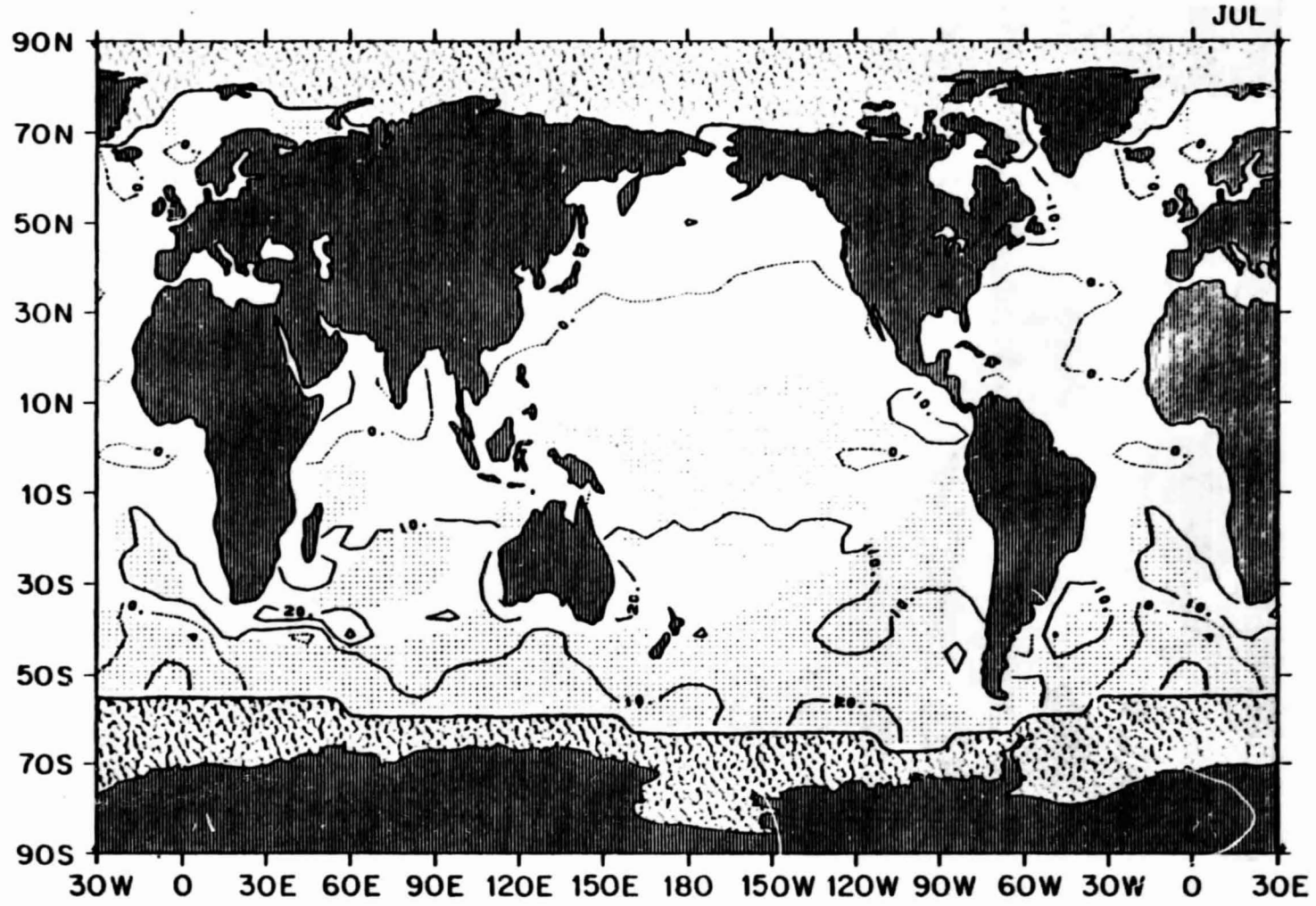

2.60 August mean sensible heat flux (W m^{-2})

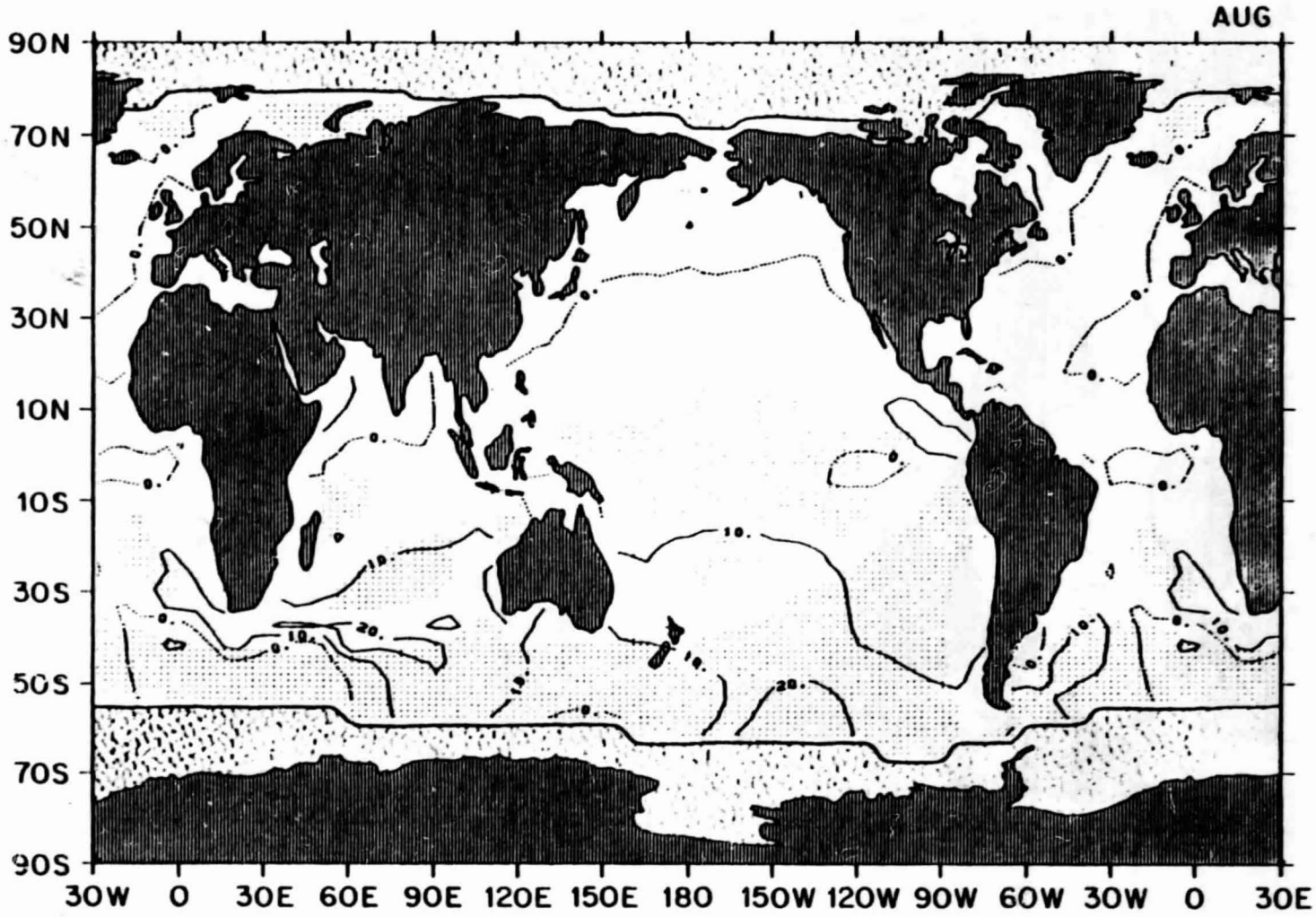

2.61 September mean sensible heat flux (W m^{-2})

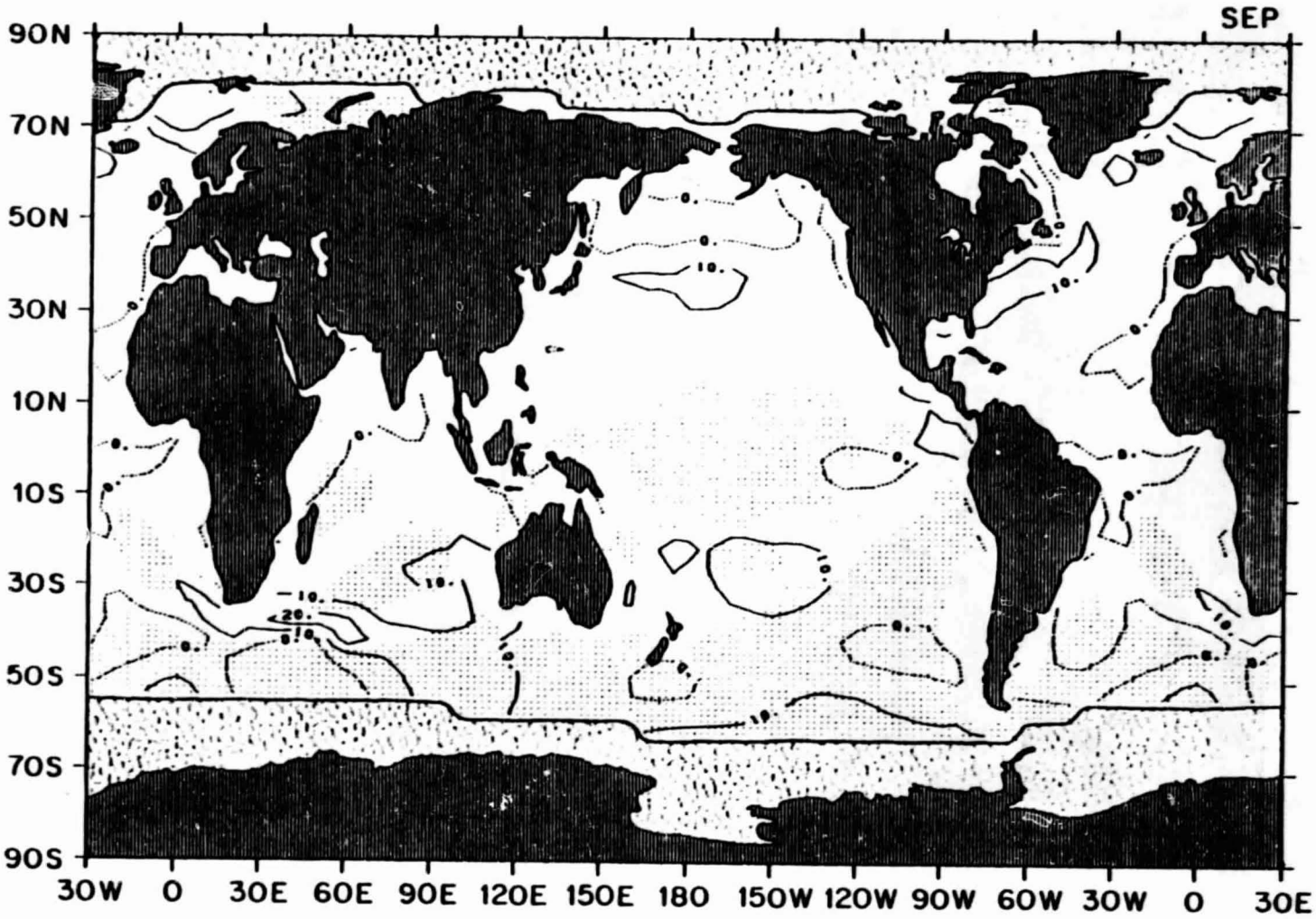

2.62 October mean sensible heat flux (W m^{-2})

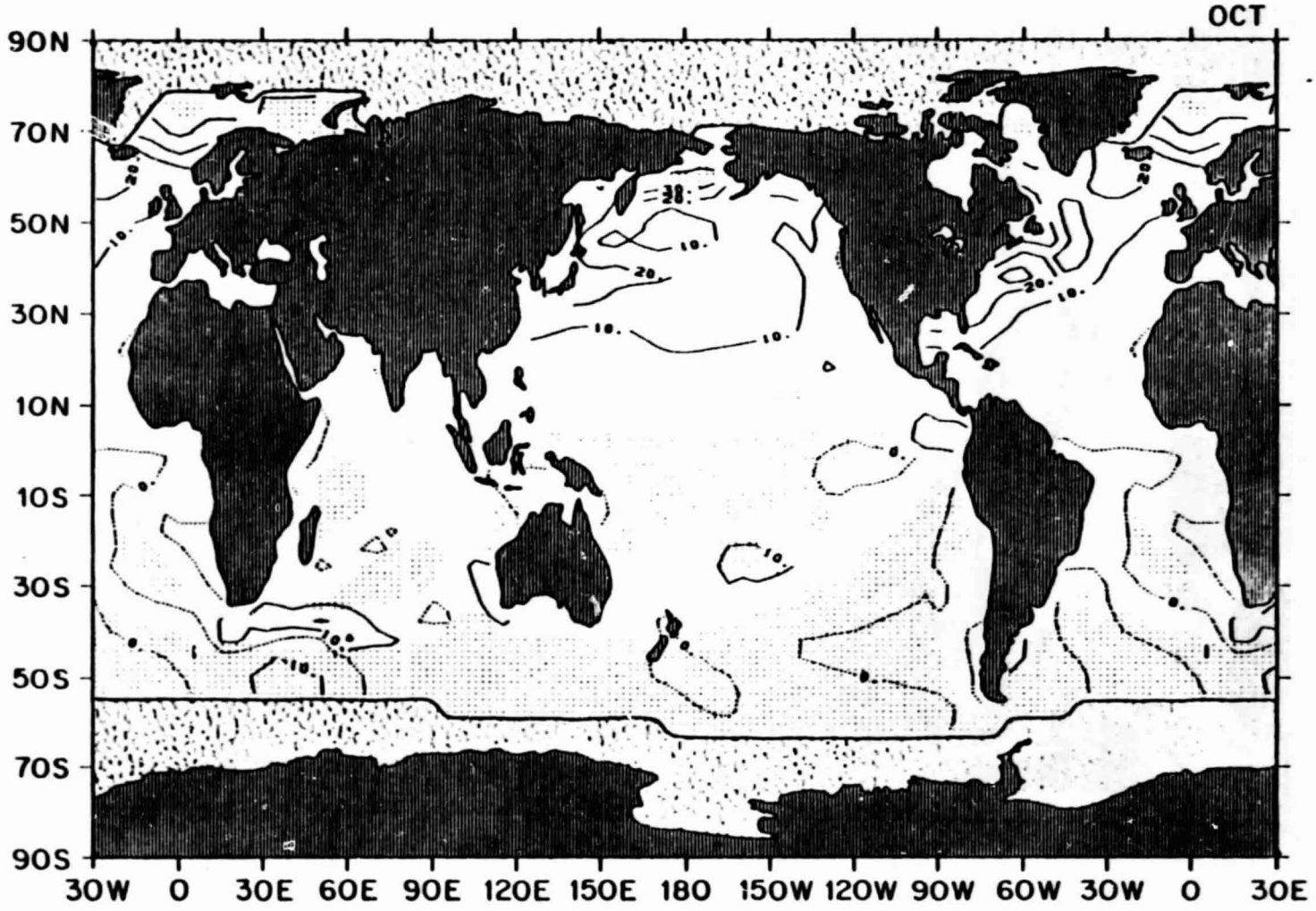

2.63 November mean sensible heat flux (W m^{-2})

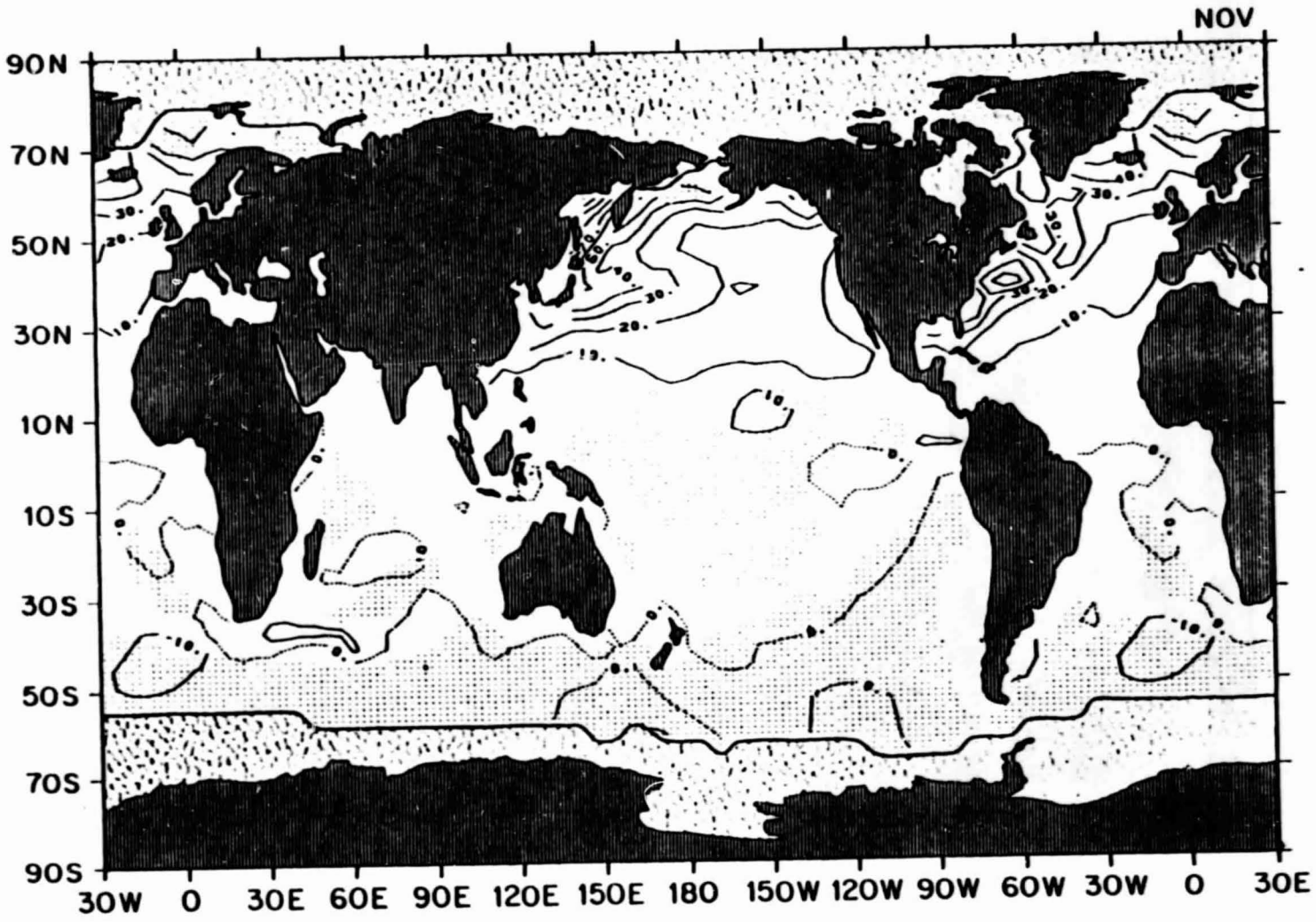

2.64 December mean sensible heat flux (W m^{-2})

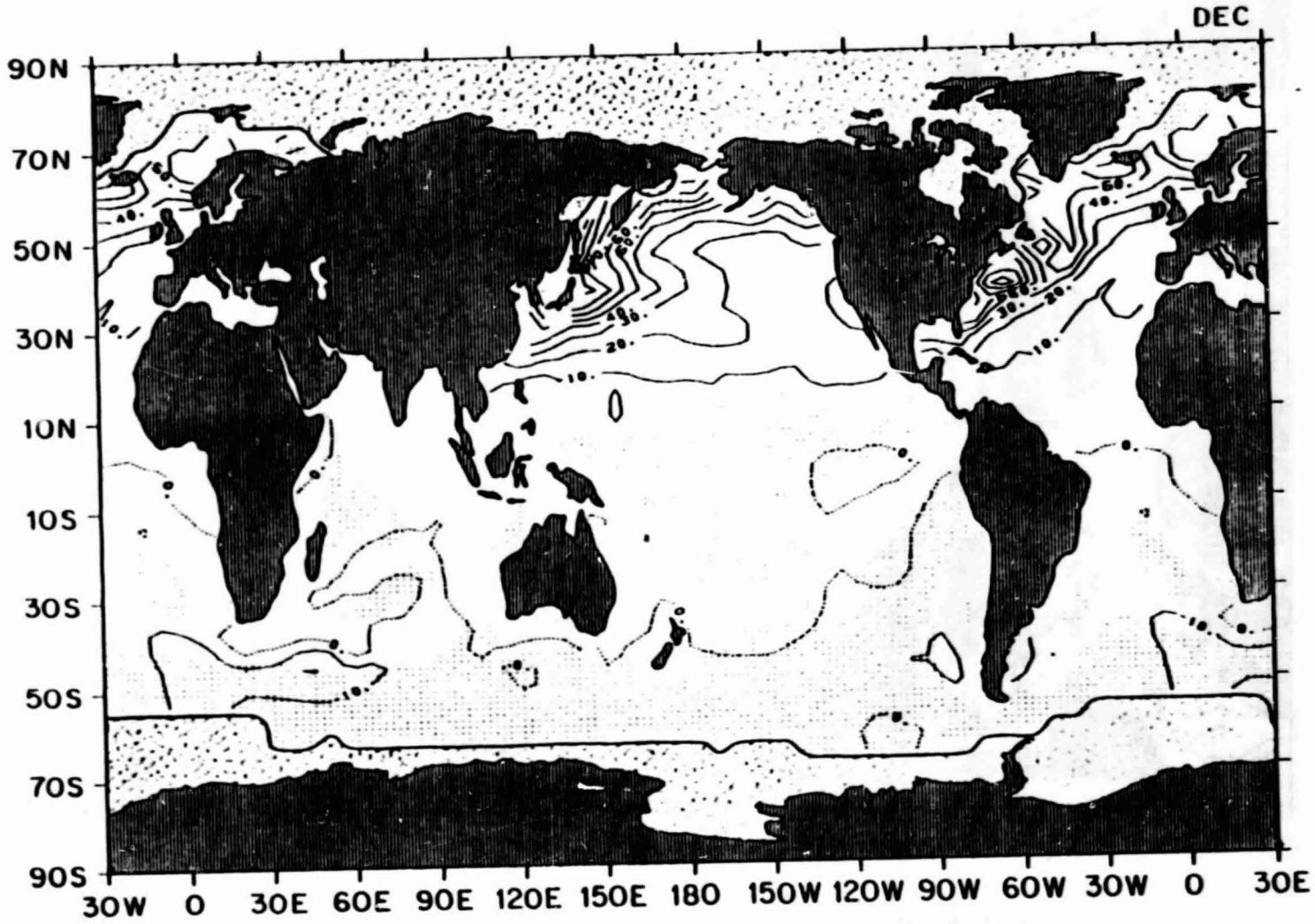

2.65 Annual mean sensible heat flux (W m-2)

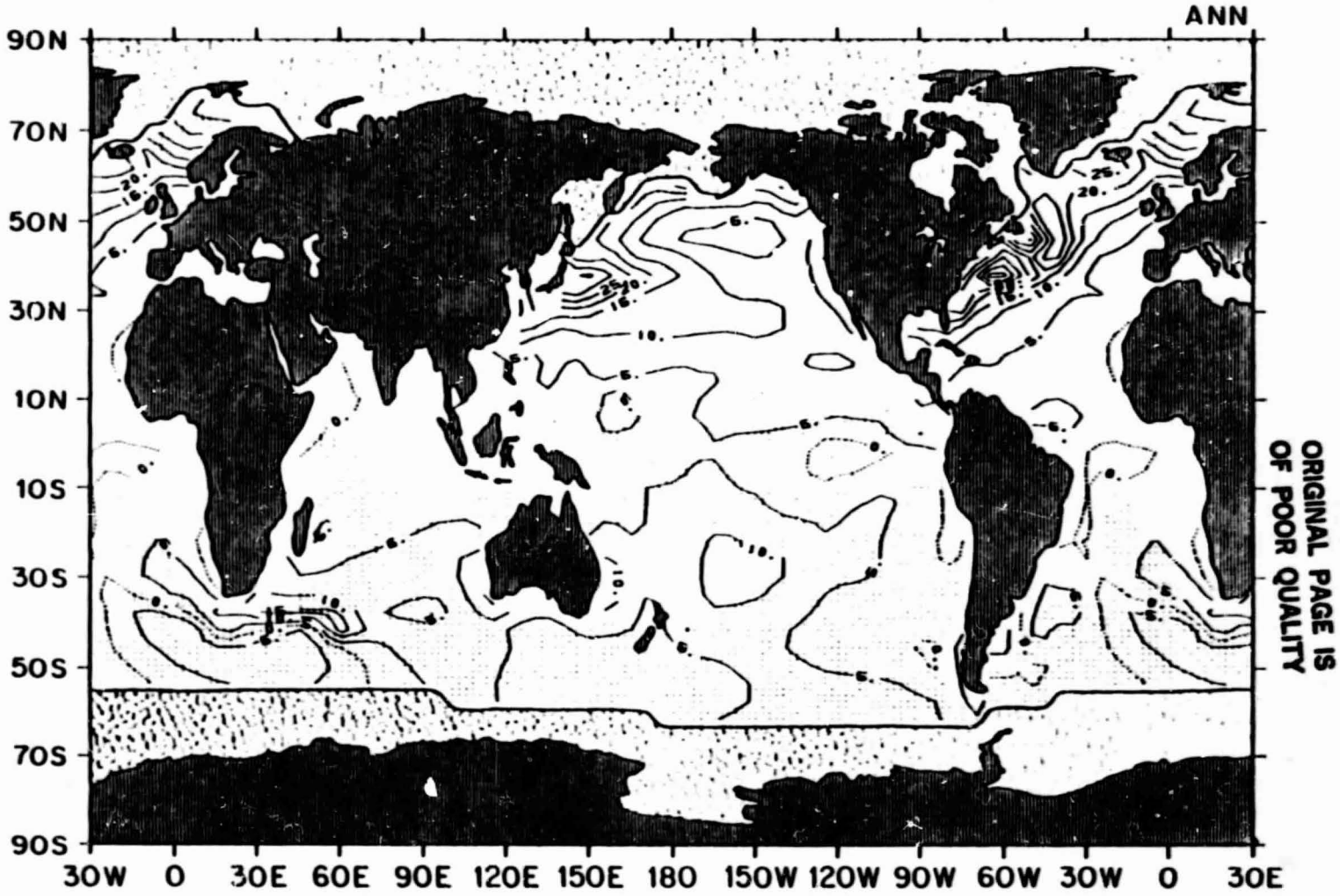

NET DOWNWARD HEAT FLUX

2.66 January mean net downward heat flux (W m^{-2})

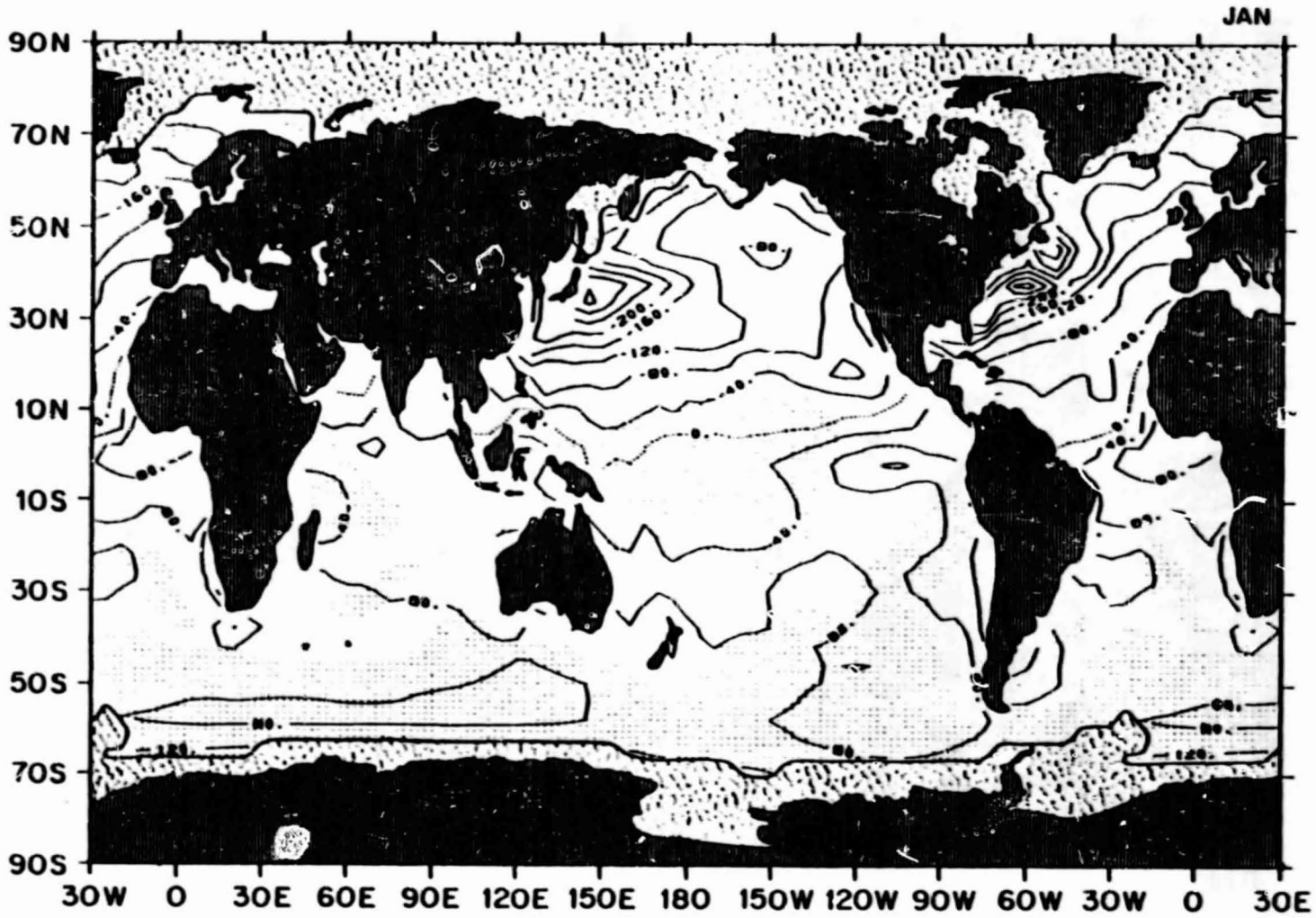

2.67 February mean net downward heat flux (W m^{-2})

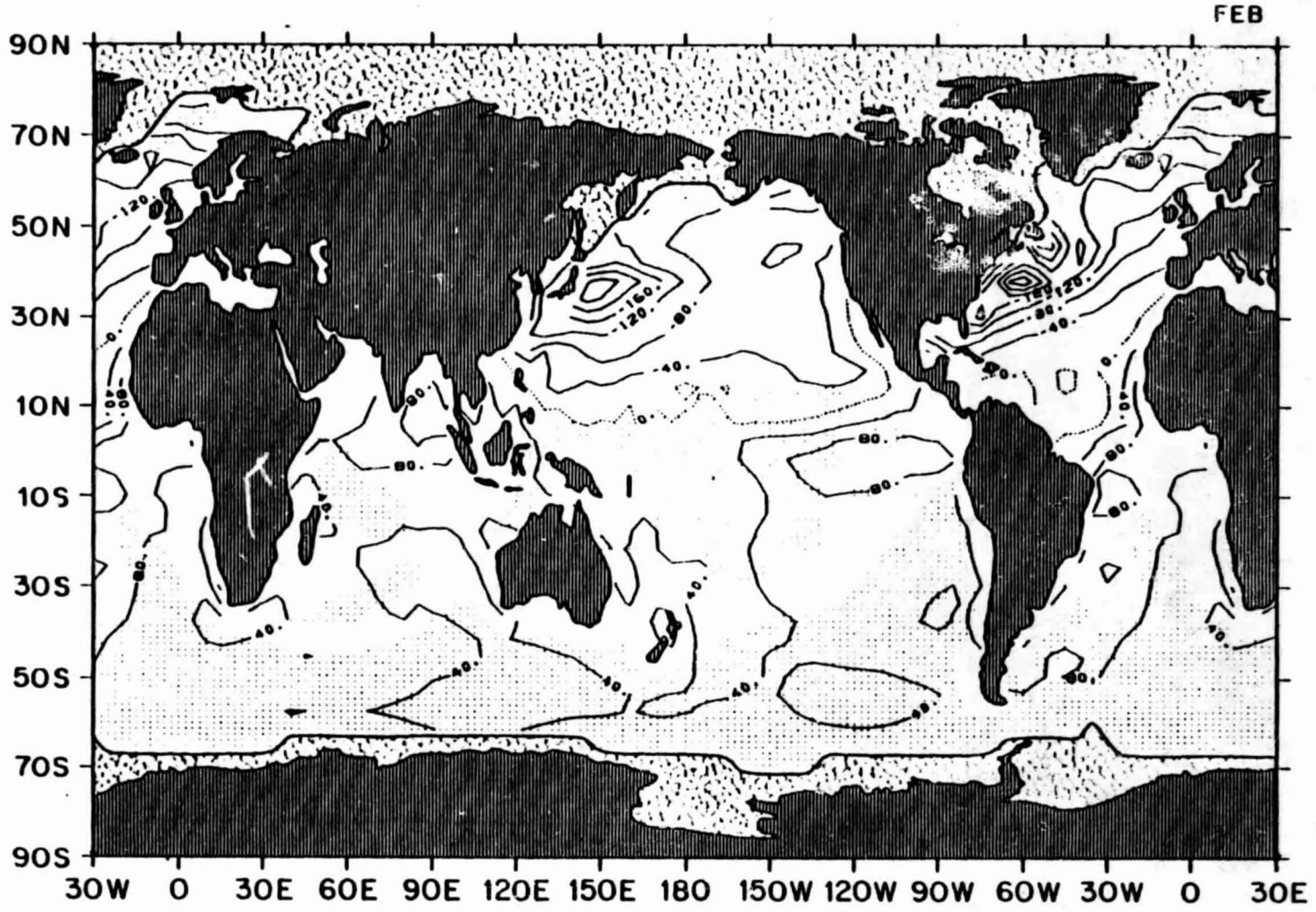

2.68 March mean net downward heat flux (W m^{-2})

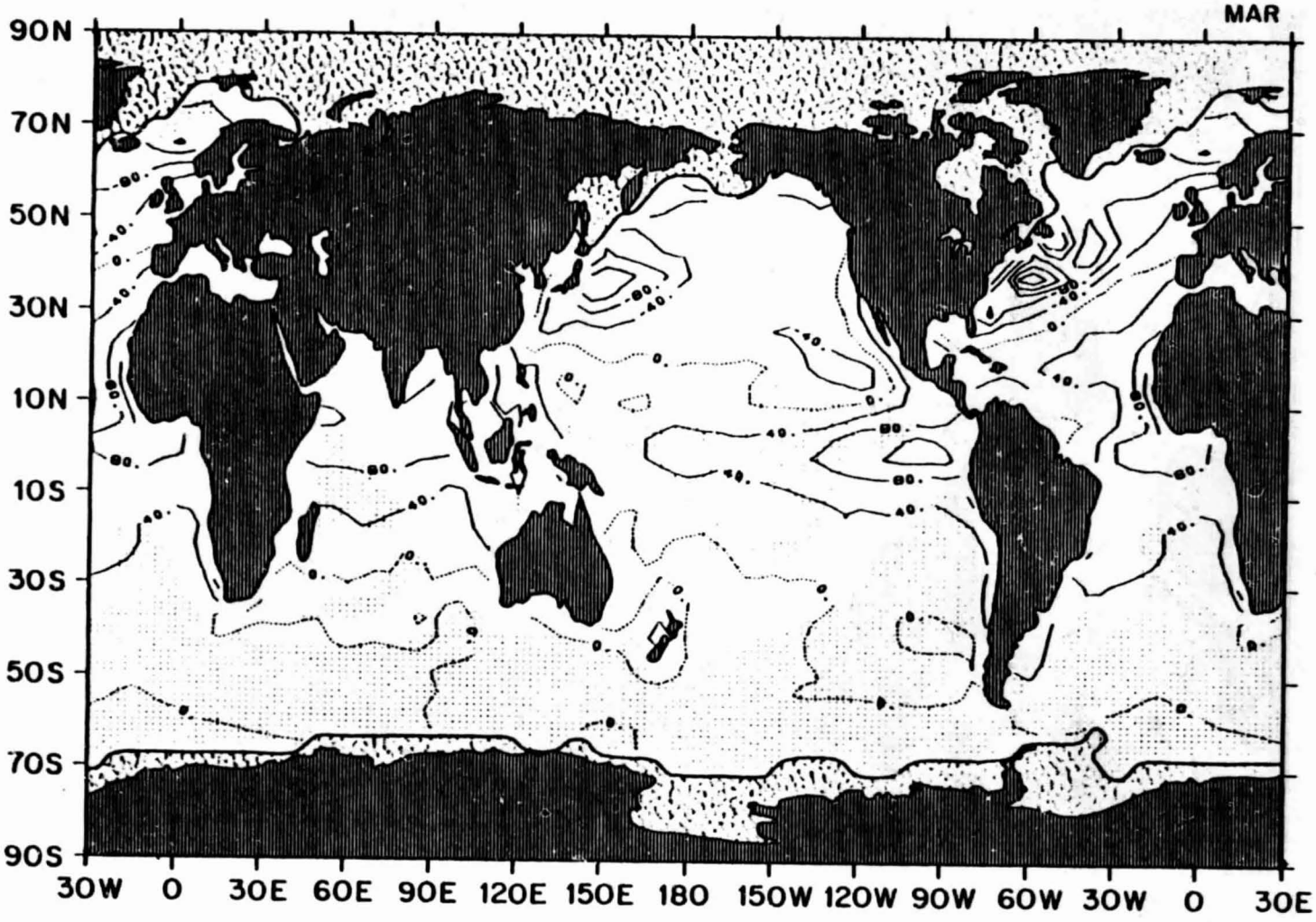

2.69 April mean net downward heat flux (W m^{-2})

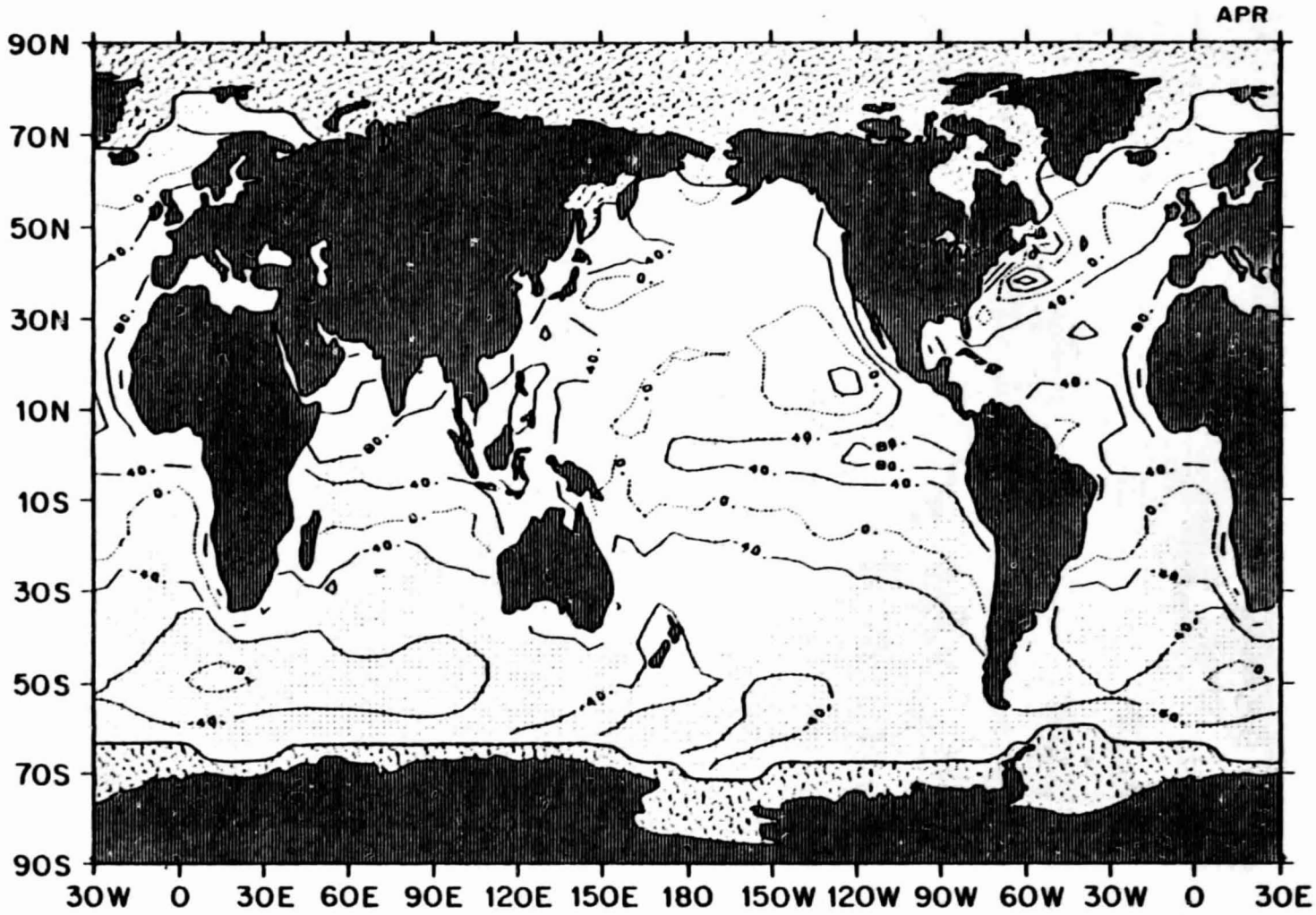

2.70 May mean net downward heat flux (W m^{-2})

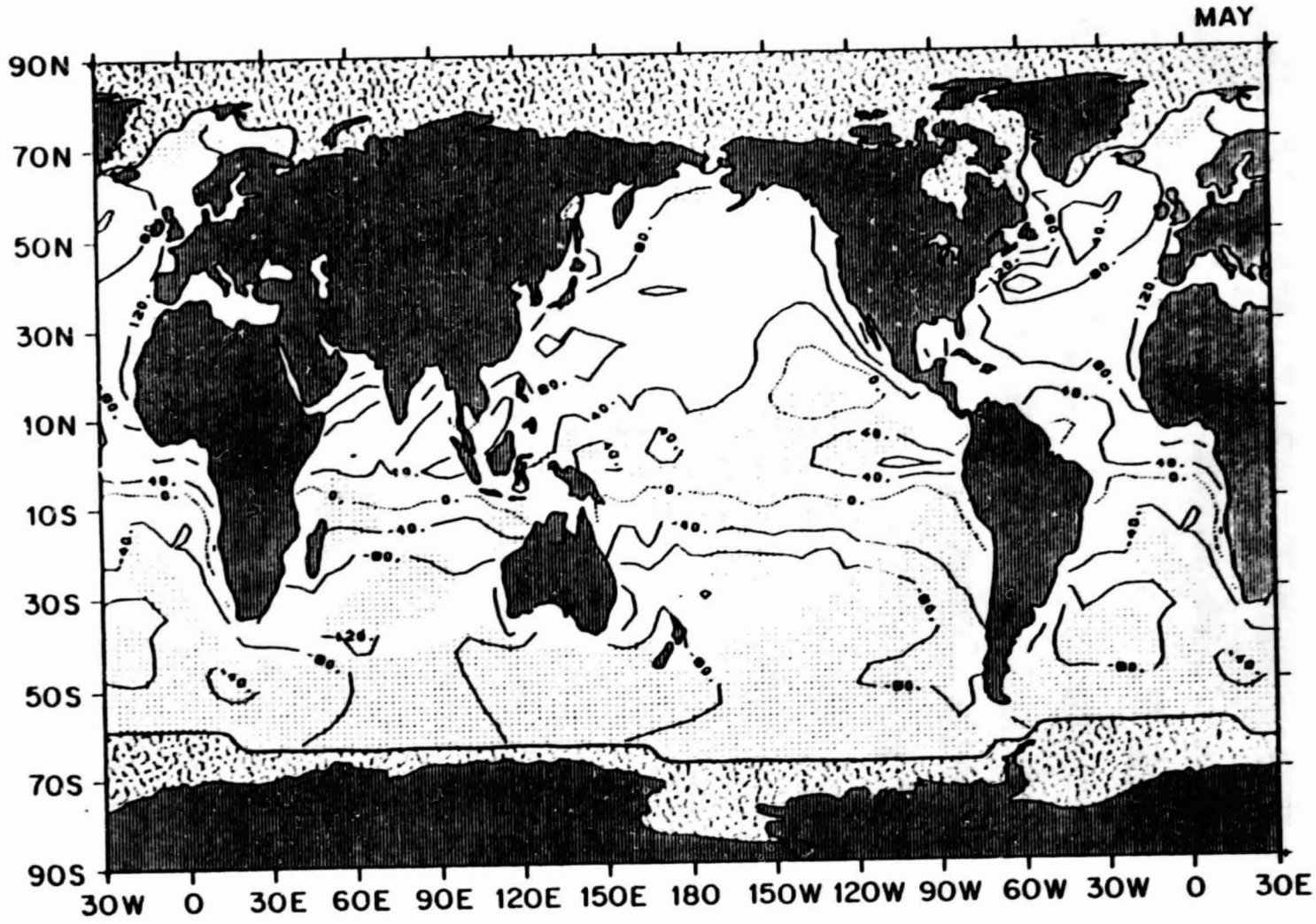

2.71 June mean net downward heat flux (W m^{-2})

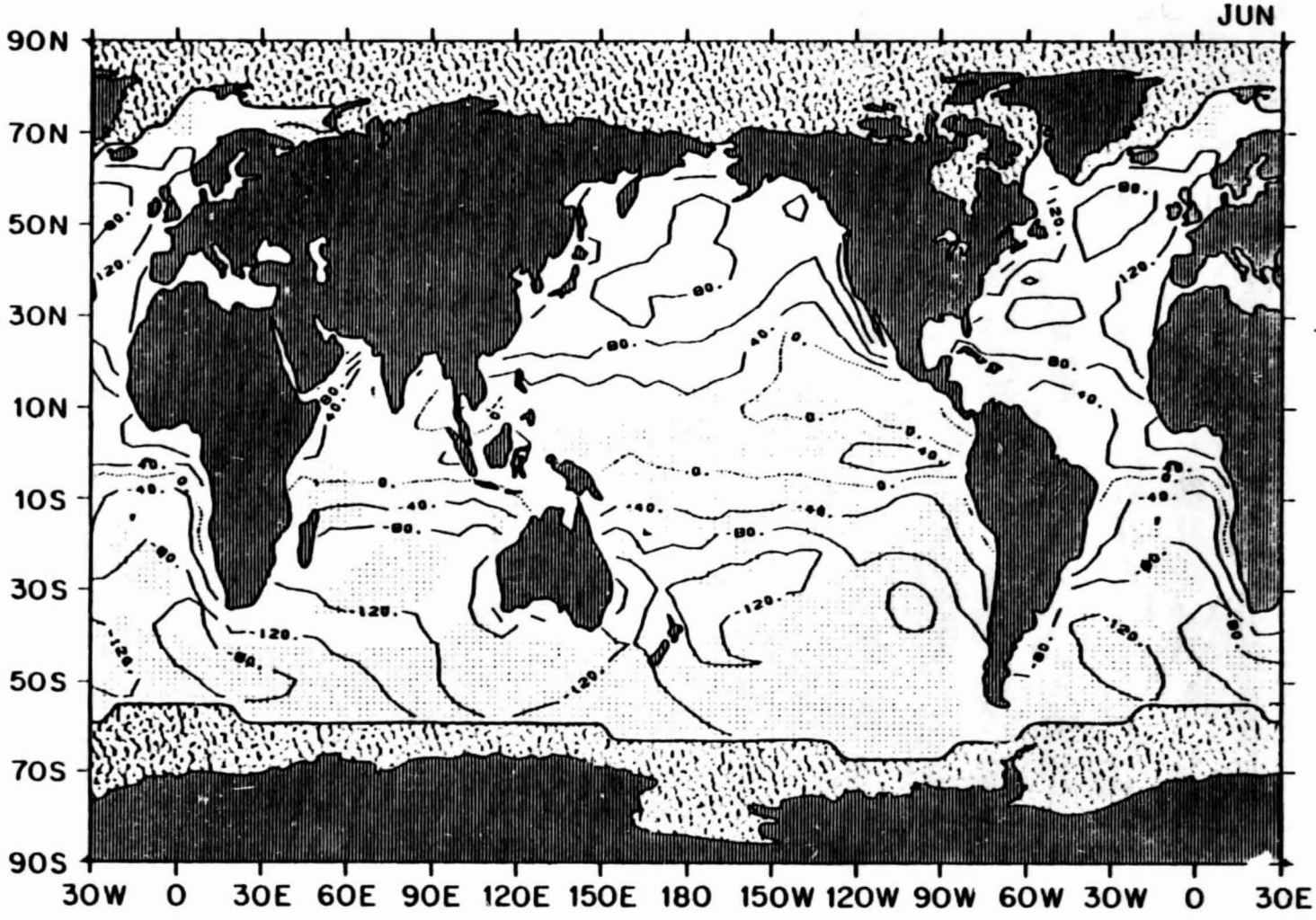

2.72 July mean net downward heat flux (W m^{-2})

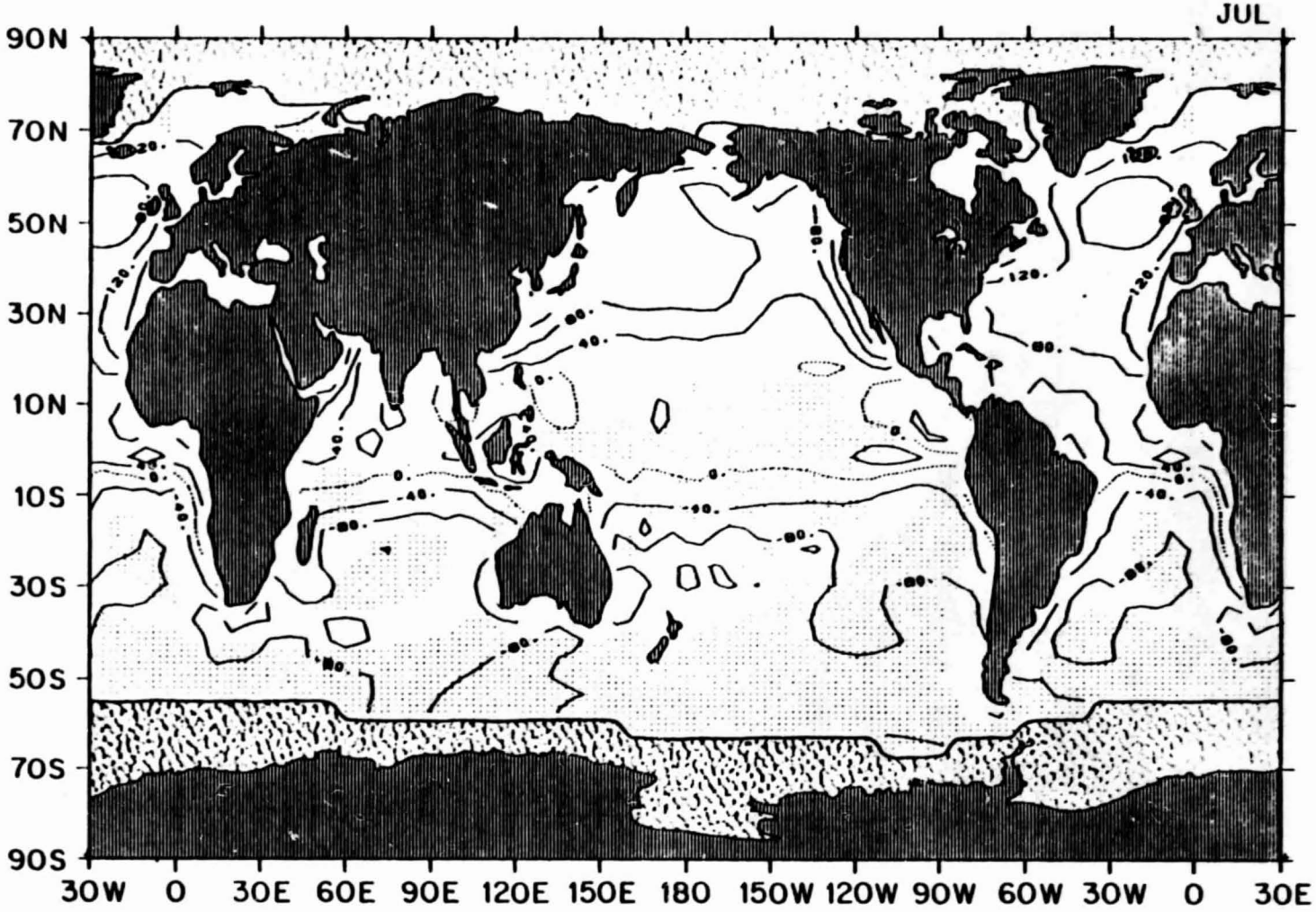

2.73 August mean net downward heat flux (W m^{-2})

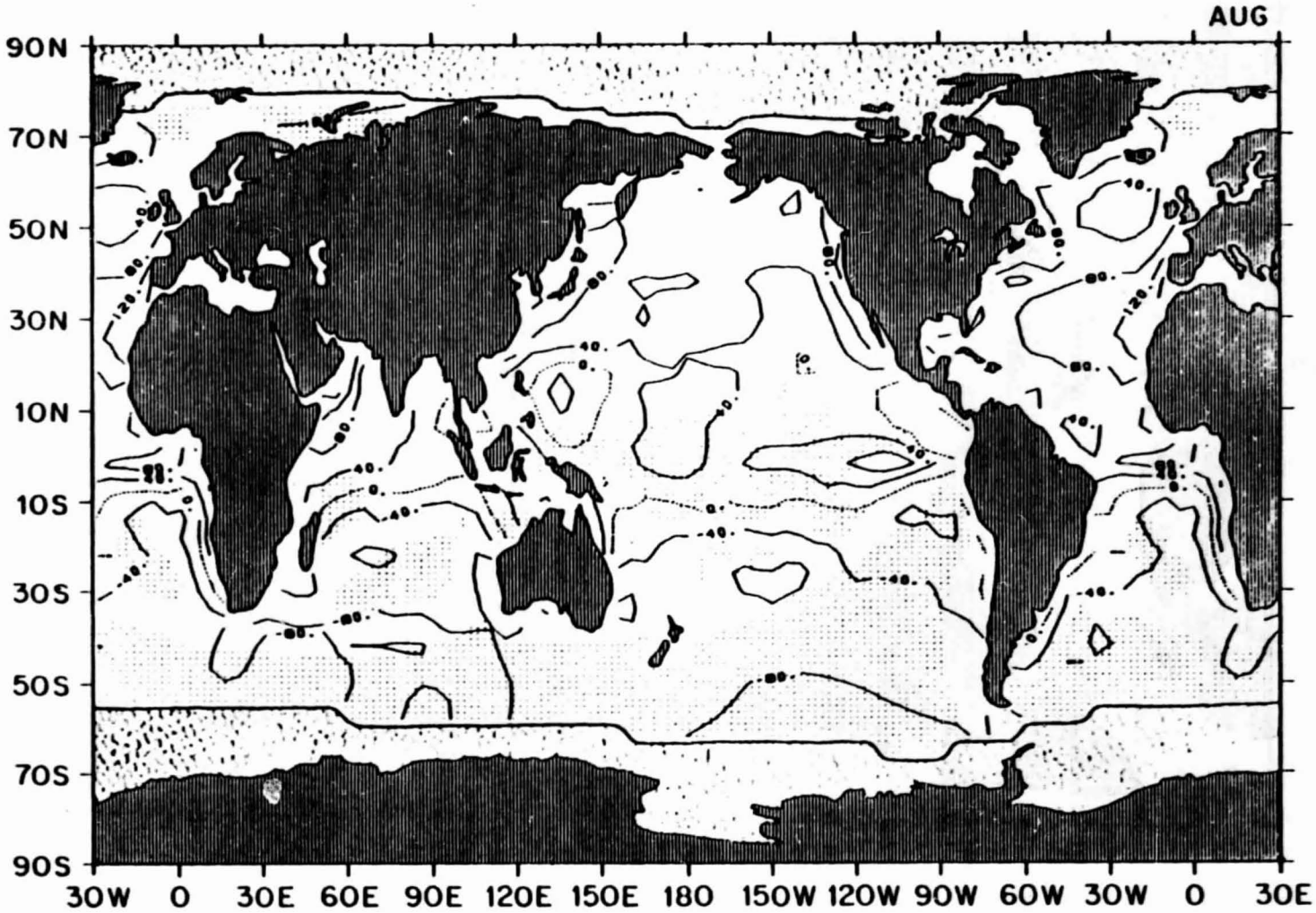

2.74 September mean net downward heat flux (W m^{-2})

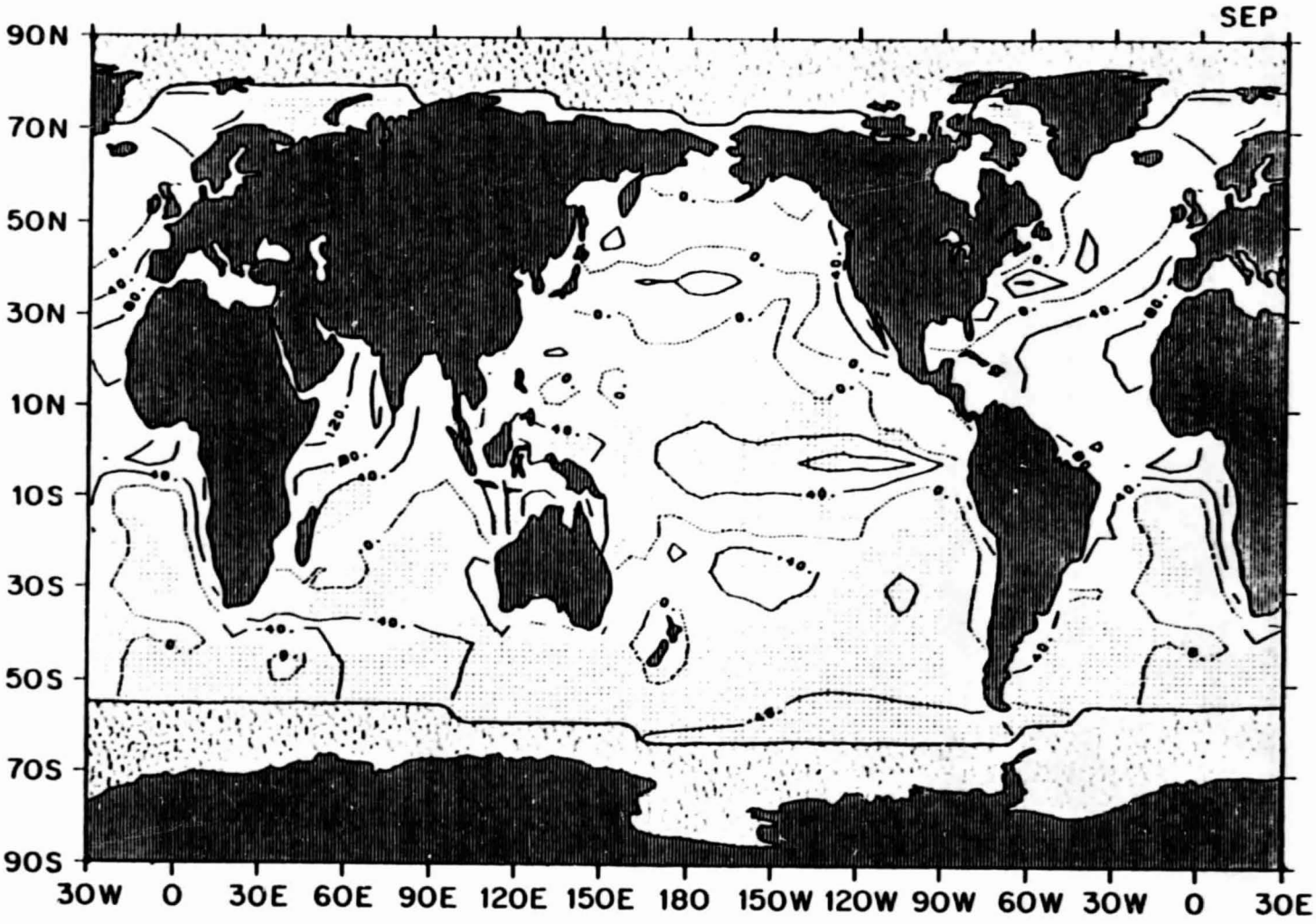

2.75 October mean net downward heat flux (W m^{-2})

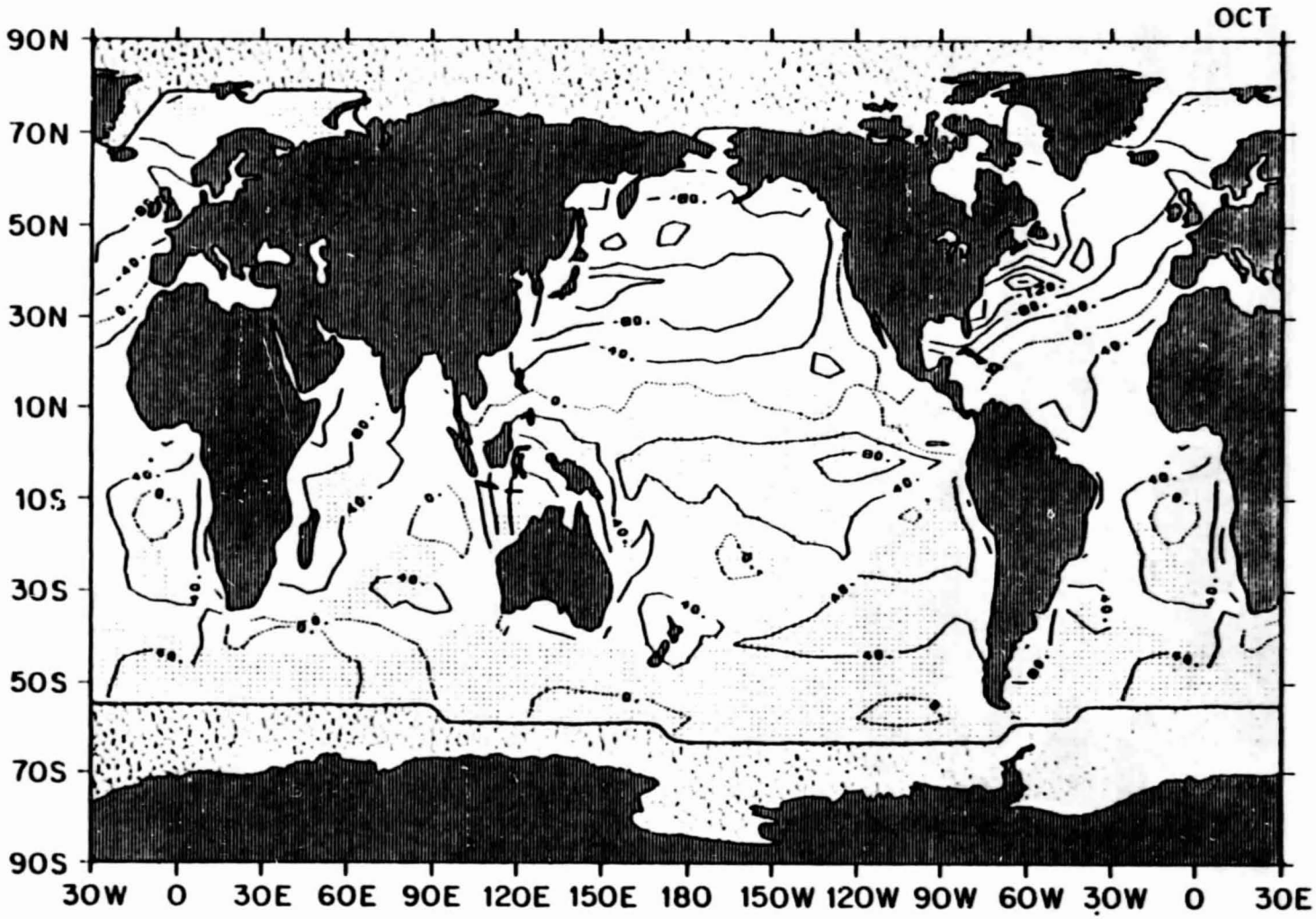

2.76 November mean net downward heat flux (W m^{-2})

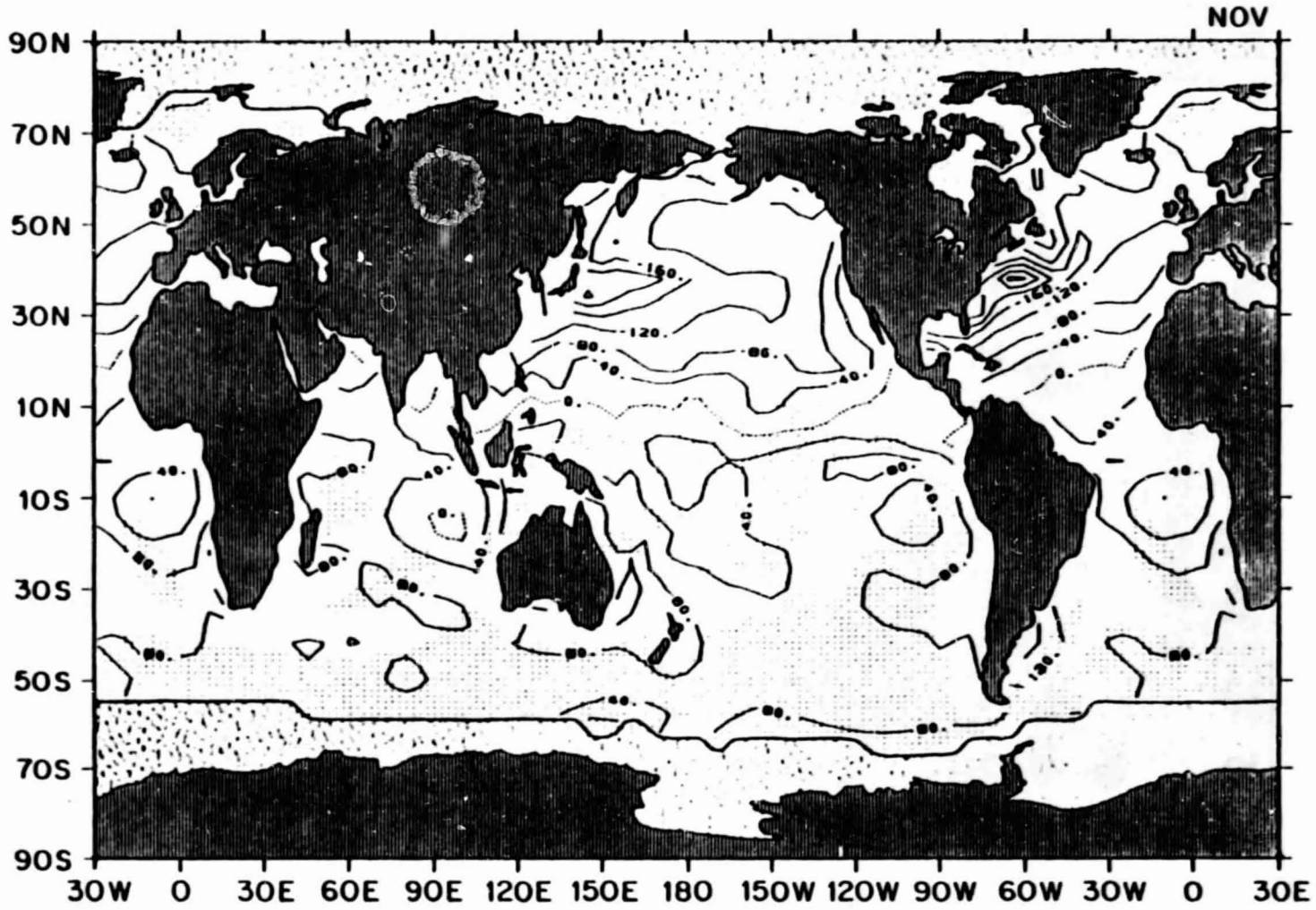

2.77 December mean net downward heat flux (W m^{-2})

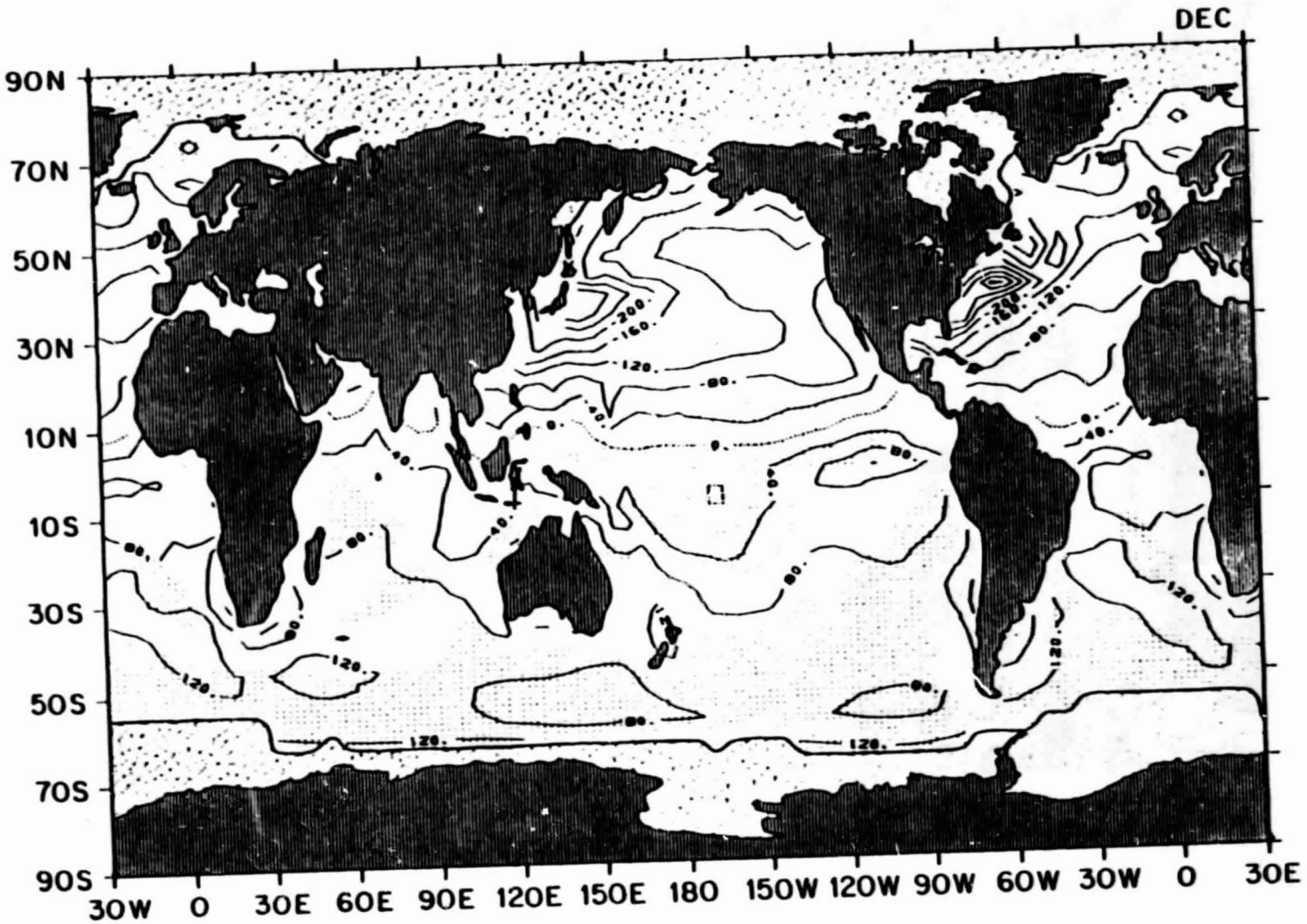

2.78 Annual mean net downward heat flux (W m-2)

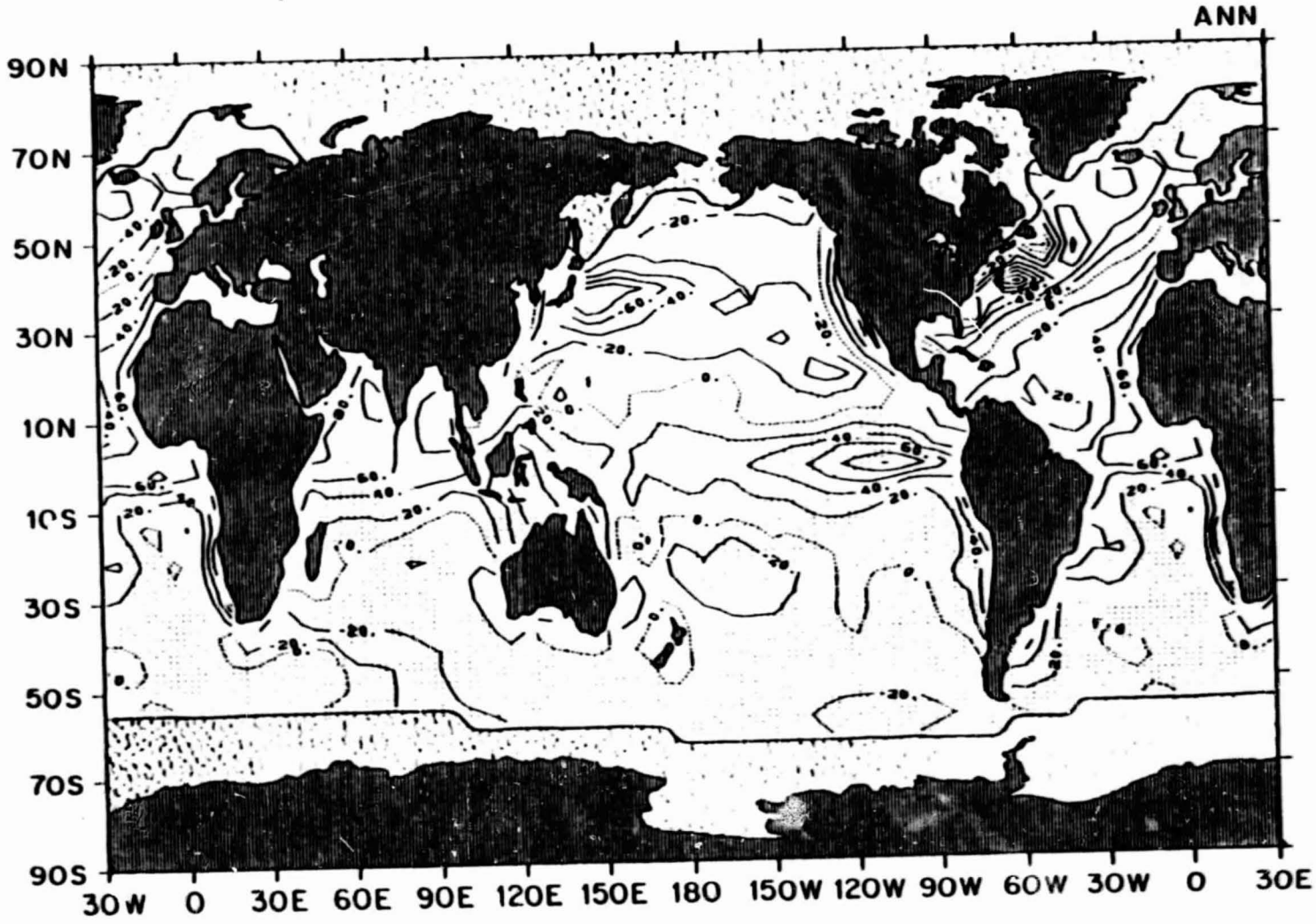

MONTHLY VARIATION OF THE ZONALLY-AVERAGED HEAT BUDGET COMPONENTS

	Chart Number
Available Solar Heat Flux	2.79
New Upward Long-Wave Flux	2.80
Net Downward Radiative Flux	2.81
Latent Heat Flux	2.82
Sensible Heat Flux	2.83
Net Downward Heat Flux	2.84

2.79 Zonal mean available solar flux (W m^{-2})

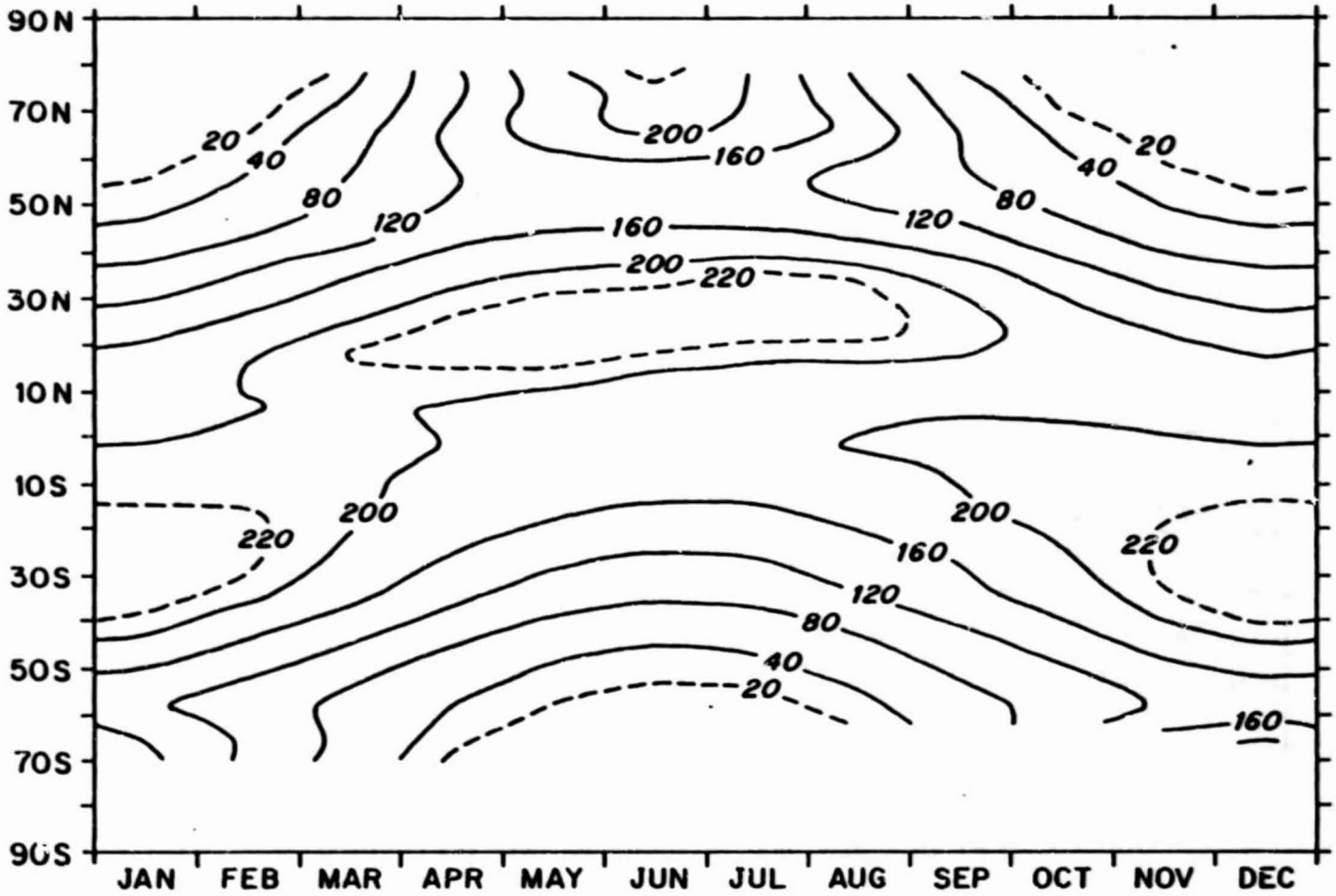

2.80 Zonal mean net upward long-wave flux (W m^{-2})

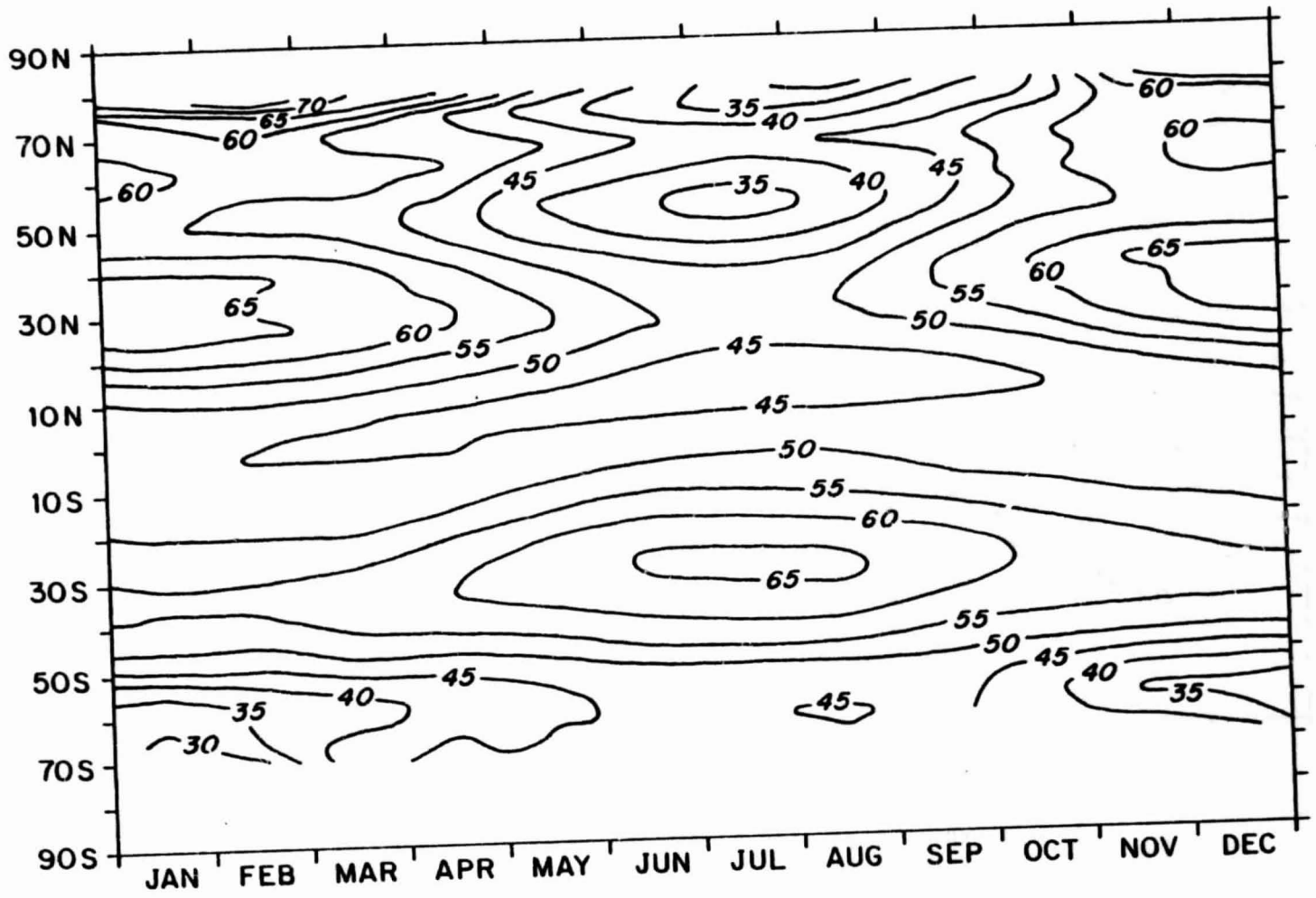

2.81 Zonal mean net downward radiative flux (W m^{-2})

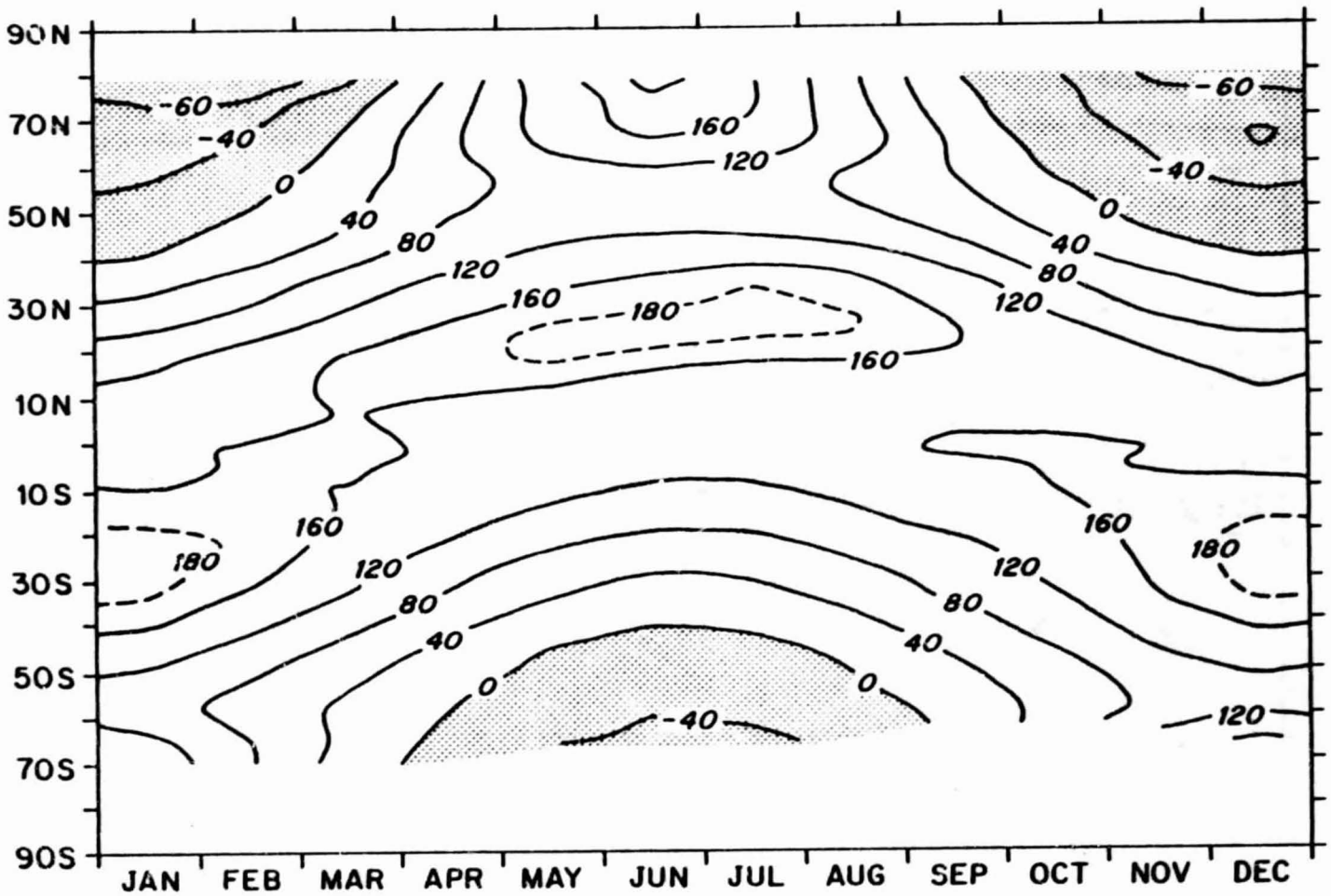

2.82 Zonal mean latent heat flux (W m^{-2})

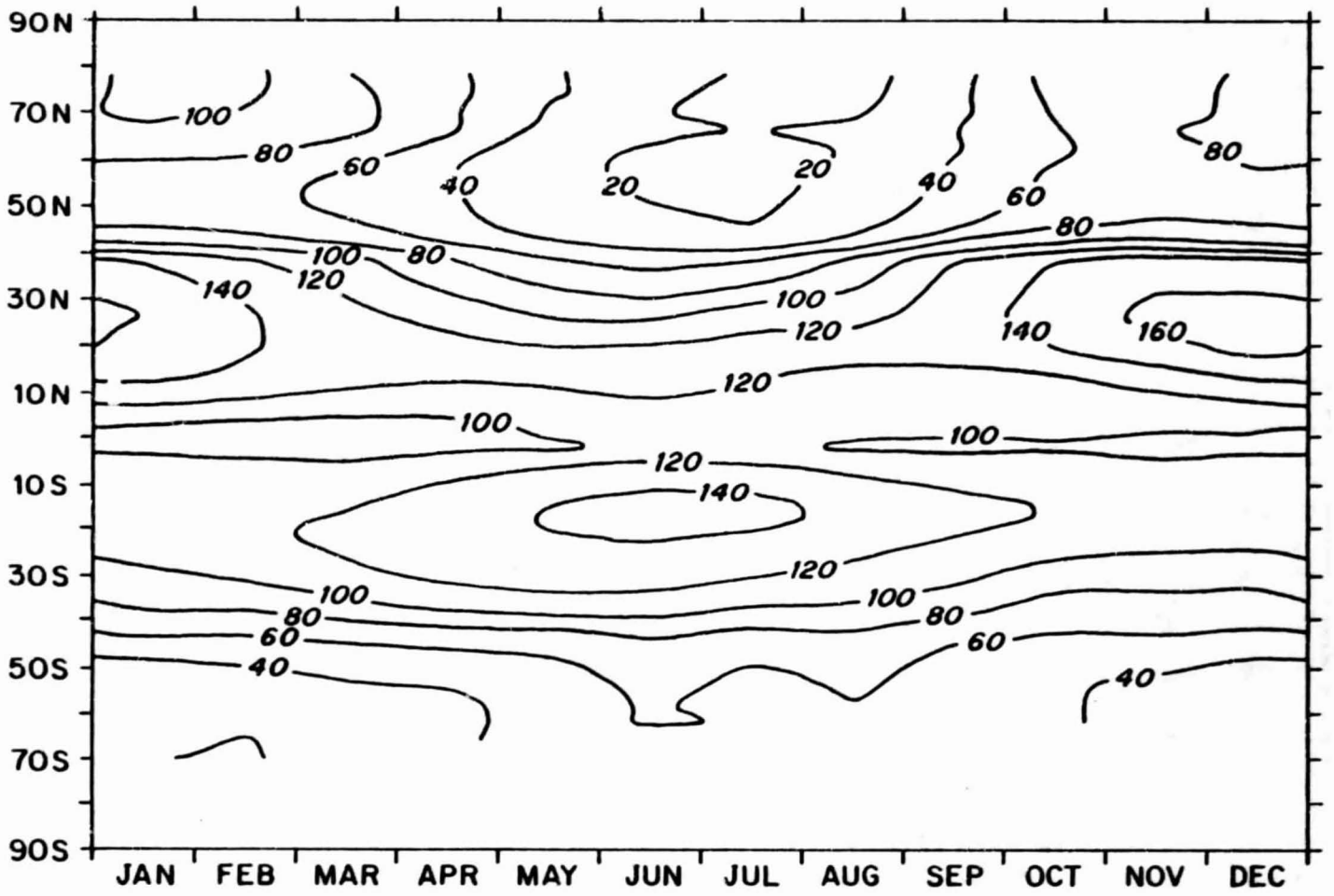

2.83 Zonal mean sensible heat flux (W m^{-2})

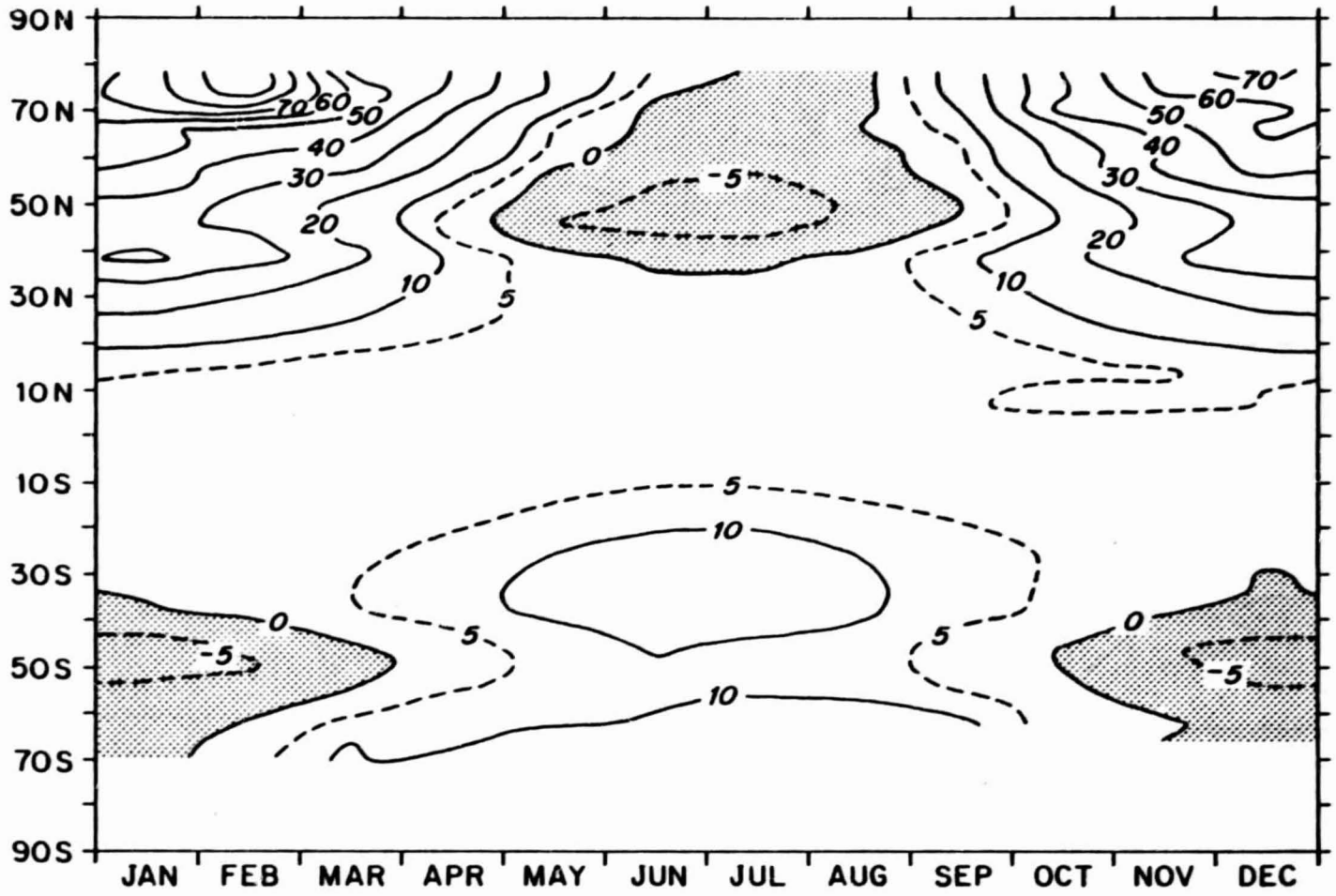

2.84 Zonal mean net downward heat flux (W m^{-2})